

December 2018

Fabrication of Silver-doped Zinc Oxide Thin Films Through Optimized Sol-Gel Deposition and Nanoparticle Wetting Process

Reed T. Heintzkill

University of Wisconsin-Milwaukee

Follow this and additional works at: <https://dc.uwm.edu/etd>

 Part of the [Materials Science and Engineering Commons](#)

Recommended Citation

Heintzkill, Reed T., "Fabrication of Silver-doped Zinc Oxide Thin Films Through Optimized Sol-Gel Deposition and Nanoparticle Wetting Process" (2018). *Theses and Dissertations*. 1993.
<https://dc.uwm.edu/etd/1993>

This Thesis is brought to you for free and open access by UWM Digital Commons. It has been accepted for inclusion in Theses and Dissertations by an authorized administrator of UWM Digital Commons. For more information, please contact open-access@uwm.edu.

FABRICATION OF SILVER-DOPED ZINC OXIDE THIN FILMS
THROUGH OPTIMIZED SOL-GEL DEPOSITION
AND NANOPARTICLE WETTING PROCESS

by

Reed T. Heintzkill

A Thesis Submitted in
Partial Fulfillment of the
Requirements for the Degree of

Master of Science
in Engineering

at

The University of Wisconsin-Milwaukee

December 2018

ABSTRACT

FABRICATION OF SILVER-DOPED ZINC OXIDE THIN FILMS THROUGH OPTIMIZED SOL-GEL DEPOSITION AND NANOPARTICLE WETTING PROCESS

by

Reed T. Heintzkill

The University of Wisconsin-Milwaukee, 2018
Under the Supervision of Professor Nidal Abu-Zahra

Zinc Oxide (ZnO) has been of significant interest as a Transparent Conductive Oxide (TCO) given its sizable direct band-gap, and as a potential substitute for Indium-Tin Oxide for use in optoelectronic and piezo-electric devices, due to its comparatively abundant and nontoxic precursor materials. Sol-gel processing is an easy, low-energy method for fabricating ZnO thin films, and there has been increasing interest in doping the compound such to give it p-type semiconductive character.

This thesis thoroughly investigates sol-gel processing of ZnO thin solid films, with focus on wet-chemistry (sol-gel) methods of doping the material with silver (both as elemental ions and nanoparticles,) in the interest of achieving p-type doped ZnO. From dozens of similar but varying documented procedures, optimal processing methods and parameters for experimentation involving solutions-based doping were investigated and codified into a repeatable standard operating procedure (SOP), confirmed by X-Ray Diffraction results showing preferential (002)-peak, c-axis crystalline orientation. Heretofore unexplored study of the use of organic solvents as wetting agents and introduction of silver nanoparticles in layering processes within the sol-gel processing framework are shown to further improve c-axis orientation. A newly-adapted, quantified method of XRD preferential orientation analysis is implemented alongside UV-Visual bandgap analysis and SEM/AFM

microscopy methods to further confirm improved crystallinity and reduced-diameter nanoscale c-axis oriented crystallites.

These experiments and characterizations are analyzed in the context of structure and properties leading to material performance, with results documented in detailed appendices.

ProQuest Print Index:

Sol-gel processing of Zinc Oxide (ZnO) thin solid films were investigated as a means of synthesizing Transparent Conductive Oxide (TCO) layers for use in optoelectronic and piezo-electric devices, with concentration on wet-chemistry (sol-gel) methods of doping the material with silver, (both as elemental ions and nanoparticles,) in the interest of obtaining p-type doped ZnO. Optimal processing methods and parameters for experimentation involving solutions-based doping were investigated and codified into a codified and repeatable standard operating procedure (SOP), confirmed by XRD results showing preferential (002)-peak, c-axis crystalline orientation. Heretofore unexplored study of the use of organic solvents as wetting agents and introduction of silver nanoparticles in layering processes within sol-gel framework are shown to further improve c-axis orientation. A newly-adapted, quantified method of XRD preferential orientation analysis is implemented alongside UV-Visual bandgap analysis and SEM/AFM microscopy methods to further confirm improved crystallinity and reduced-breadth nanoscale c-axis oriented crystallites.

© Copyright by Reed T. Heintzkill, 2018
All Rights Reserved

To my parents:

Mark and Megan who
never chose for me what was
too much or not enough

TABLE OF CONTENTS

ABSTRACT.....	iii
TABLE OF CONTENTS	ix
LIST OF FIGURES.....	xi
LIST OF TABLES.....	xiii
LIST OF ABBREVIATIONS.....	xv
ACKNOWLEDGEMENTS.....	xvii
1. Chapter 1: Introduction.....	1
1.1. Introduction.....	3
1.2. TCO Application in Opto-electronic Devices.....	3
1.3. Zinc Oxide and Sol-gel Processing.....	5
1.4. ZnO Crystalline Structure, Preferential Orientation, and XRD Characterization	8
1.5. p-type doping of ZnO Thin Films.....	10
1.6. Initial stages and early attempts at synthesis	12
1.7. ZnO Thin Films Optimization, Doping Attempts, and Process Breakthroughs	14
2. Chapter 2: Optimization of Sol-Gel Spin-Coated ZnO Thin Films for Silver Doping.....	17
2.1. Introduction.....	19
2.2. Experimental Narrative and Preliminary Results	23
2.2.1. (Project A/B) – Solution Stabilizer, Aging & Massloss	25
2.2.2. (Projects D & G) – Preliminary Doping Attempts.....	31
2.2.3. (Project F) – Factorial Analysis of Aging and Time/Temperature	37
2.2.4. (Projects J & H) – Additional Heat Processing Parameters	43
2.3. Analysis and Discussion	47
2.3.1. Precursor Solution.....	49
2.3.2. Processing Parameters	57
2.3.3. Conductivity and Surface Morphology	61
2.3.4. Final SOP.....	63
2.4. Conclusion.....	65
3. Chapter 3: Effects of Substrate, Wetting, and Nanoparticle Layering of Silver-doped ZnO Thin Films	67
3.1. Introduction.....	69
3.2. Experimental Narrative: Process, Methods, and Immediate Results	71
3.2.1. (Experiment A) – Incorporation of Silver Nanoparticles and Use of Mica Substrate.....	75
3.2.2. (Experiment B) – Layering and Substrate Parameter Analysis under Inert Atmosphere.....	79
3.2.3. (Experiment C) – Initial Wetting and Layering.....	83
3.2.4. (Experiment D) – Wetting and Layering.....	87

3.2.5.	(Experiment E) – Final Improvements through Modification of Solvent and Wetting.....	91
3.3.	Analysis and Discussion	95
3.3.1.	Degree of Preferential Orientation.....	95
3.3.2.	Band Gap Analysis	99
3.3.3.	Correlation of Crystallinity and Surface Morphology.....	101
3.3.4.	Wetting Processes in ZnO Film Fabrication	102
4.	Conclusions and Future Work.....	105
4.1.	Major Findings	107
4.2.	Additional Findings and Future Work:	107
4.3.	Final Thoughts	109
	REFERENCES.....	111
	Appendix A: Table of chemical systems reviewed by Znaidi in ZnO Sol-gel Review:	115
	Appendix B: X-Ray Diffractograms	117
	Appendix B-2AB: Chapter 2, Experiments A/B.....	117
	Appendix B-2DG: Chapter 2, Experiments D/G.....	123
	Appendix B-2F: Chapter 2, Experiment F.....	126
	Appendix B-2JH: Chapter 2, Experiment J/H.....	130
	Appendix B-3A: Chapter 3, Experiment A.....	135
	Appendix B-3B: Chapter 3, Experiment B	139
	Appendix B-3C: Chapter 3, Experiment C.....	143
	Appendix B-3D: Chapter 3, Experiment D.....	146
	Appendix B-3E: Chapter 3, Experiment E.....	152
	Appendix C: Microscopy	157
	Appendix C-2DG: Experiment 2-DG.....	157
	Appendix C-3A: Experiment 3-A.....	159
	Appendix C-3B: Experiment 3-B	161
	Appendix C-3C: Experiment 3-C.....	164
	Appendix C-3D: Experiment 3-D.....	166
	Appendix C-3E: Experiment 3-E.....	171
	Appendix D: Degree of Preferential Orientation Calculation.....	178
	Appendix E: UV-Visual Spectroscopy	183
	Appendix F: Chemicals Utilized.....	193

LIST OF FIGURES

Figure 1-1. Traditional and Inverted architectures of BHJ OSC devices.....	4
Figure 1-2. Sol-gel process flow chart.....	6
Figure 1-3. ZnO Sol-gel equilibria systems and mechanisms	7
Figure 1-4. ZnO wurtzite unit cell and diagram of z-axis ZnO growth.....	8
Figure 1-5. Formation energies of intrinsic and substitutional defects in ZnO.....	10
Figure 1-6. Extrinsic p-type semiconduction model (electron bonding)	11
Figure 1-7. XRD Spectra illustrating progress through ZnO Thin Films Project.....	13
Figure 2-1. Zinc Oxide Sol-gel process and variables.....	20
Figure 2-2. XRD Spectra from a variety of early-stage experiments.....	23
Figure 2-3. Various Schema of Zinc bridging with ligand stabilizers.....	25
Figure 2-4. XRD spectra of covered MEA- and uncovered DEA-stabilized samples.....	28
Figure 2-5. XRD spectra comparing all solutions, aged 48-hours and 18 hours.....	29
Figure 2-6. XRD spectra of Project D preliminary silver-doped and undoped ZnO films.....	32
Figure 2-7. Comparison of XRD output for varying concentrations of silver-doped ZnO.....	34
Figure 2-8. EDS-detected elemental proportions of silver in doped ZnO thin films	35
Figure 2-9. Appearance of slides produced in Project F.....	39
Figure 2-10. XRD spectra of Project F samples aged 24 hours	40
Figure 2-11. XRD spectra of Project F samples aged 48-hours	41
Figure 2-12. XRD Spectra of Project J Trials aged 24- (top) and 48-hours (bottom)	45
Figure 2-13. Simplified XRD peak intensity of Touam's findings	52
Figure 2-14. Sheet resistivity measurement by four-point probe	61
Figure 3-1. Aberrant surface morphology of Ag-doped ZnO thin films.....	70
Figure 3-2. Electron micrographs of Expt A surface features	77

Figure 3-3. XRD Spectra for Expt. A on glass and Si-wafer substrates	78
Figure 3-4. XRD Spectra from experiment B.....	82
Figure 3-5. Optical micrographs of undoped experiment ‘C’ sample	85
Figure 3-6. Electron micrographs of Expt. C, doped samples at 100X magnification.....	85
Figure 3-7. XRD Spectra from Experiment C.....	86
Figure 3-8. XRD Spectra for Experiment D, Silver-doped, annealed samples	89
Figure 3-9. XRD Spectra of Experiment E	94
Figure 3-10. Calculated Optical Band Gap (E_g).....	100
Figure 3-11. AFM 3D Overlay of PGME/AgNP-treated undoped ethanol-based film	102
Figure 3-12. AFM 3D Overlay of PGME/AgNP-treated silver-doped ethanol-based film.....	103
Figure 3-13. AFM 3D Overlay dry (untreated) undoped ethanol-based film	103

LIST OF TABLES

Table 2-1. Processing variables involved in ZnO thin film fabrication.....	21
Table 2-2. Project A/B matrix of variables	26
Table 2-3. Project G doping concentration table	33
Table 2-4. Project F time and temperature matrix	38
Table 2-5. Variable naming matrix for Projects J & H	43
Table 2-6. Touam's peak intensity ratios calculated.....	52
Table 3-1. Experiment A processing parameters matrix	75
Table 3-2. Experiment B parameters matrix	79
Table 3-3. Experiment C parametric matrix.....	83
Table 3-4. Names and properties of solvents used in experiment D	87
Table 3-5. Experiment D parametric matrix.....	88
Table 3-6. Comparison of EGME/PGME solvents. or review.....	91
Table 3-7. Experiment E parametric matrix	92

LIST OF ABBREVIATIONS

TCO	Transparent Conductive Oxide
LED	Light Emitting Diode
OSC	Organic Solar Cell
MO	Metal Oxide
ETL	Electron-Transport Layer
BHJ	Bulk Heterojunction
OPV	Organic Photovoltaics
HTL	Hole-Transport Layer
ITO	Indium Tin Oxide
E_g	Band Gap Energy
PDF	Powder Diffraction File
XRD	X-ray Diffraction
SOP	Standard Operating Procedure
SZO / Ag:ZnO	Silver-doped Zinc Oxide
ZnAc / ZnOAc	Zinc Acetate Dihydrate
EtOH	Ethanol
r -value	molar ratio of additive to solvent
DEA	Diethanolamine (2,2'-Iminodiethanol)
MEA / EA	Monoethanolamine (2-Aminoethan-1-ol)
DI	deionized water (H_2O)
EDS/EDX	Energy-Dispersive X-ray Spectroscopy
CTE	Coefficient of Thermal Expansion
NP	nanoparticle(s)
AgNP	Silver Nanoparticle/dispersion
EGME / 2-ME	Ethylene glycol monomethyl ether (2-Methoxyethanol)
PGME	Propylene glycol monomethyl ether (1-methoxy-2-propanol)

ACKNOWLEDGEMENTS

My most gracious appreciation goes out to the members of our ‘gang of three,’ the Zinc Oxide Solar Cells group under the care and auspices of Dr. Nidal Abu-Zahra over the past few years: Jon Wolgamott was both a friend in a new place as well as a mentor in the ways of graduate school at UWM; And I can certainly not express enough thanks to Karl Flanagan-Morris, our ever-ready go-to guy for laboratorial – and laborial – scientific and moral support: your dedication, camaraderie, and hard work have been invaluable.

My mentors and professors at UWM, specifically Dr. Nidal Abu-Zahra and Dr. Benjamin Church deserve special recognition as beacons of help and support throughout this process. The lessons I have learned from both of you in finding grace in dealing with bureaucracy and working through the noise – rival even the brilliant instruction and advising on technical and academic work I’ve been lucky enough to receive from each of you. I am grateful to have fine examples to look up to as I progress through my career in Academia.

Thanks too to the staff of the College of Engineering & Applied Sciences’ Advanced Analysis Facility, specifically Dr. Steven Hardcastle, and Dr. Afsaneh Moghadam. You both have been so helpful and insightful, but more importantly, kind and patient. I would also like to express tremendous gratitude to Karen Gebhardt for her unexpected and excellent editing/proofing assistance.

No thanks could be complete without mention of the fantastic instruction I received as a nontraditional student at Northeast Wisconsin Technical College, and then as an undergrad at the University of Wisconsin – Green Bay. I credit the late Dr. Roberta Sulk as my first inspiration toward pursuits in chemistry and higher education: her story of adult struggle to achieve academically catalyzed my resolve to do the same. To all of my instructors and professors at UWGB, and to each and everyone in the Department of Chemistry and College of Natural & Applied Sciences I was lucky enough to come across: I am forever in awe of both the academic fervor and most altruistic efforts to *teach*, and teach *well*. Specific mention is deserved to my long-time advisor, teacher, ‘inspirator’, and friend, Dr. Michael McIntire; as well, my research advisor, Dr. Jeremy Intemann, whose brief but concentrated prophetic interaction with me propelled my interest in current goals and ambitions.

I have been extremely fortunate to have had the opportunity to work with some fantastic individuals at UWM’s Graduate School, including Dean Gajdardziska-Josifovska and many others on Graduate Faculty Committee, such as Associate Dean Tracey Heatherington. Tracey’s work with

Danielle DeVasto in creating the Preparing Future Faculty and Professionals seminars and course was so extremely insightful, inspirational, and helpful in negotiating the various opportunities and hazards of the graduate experience, and the lifestyle of a fledgling academician.

I would also like to shout out to all my fellows in the Shared (esp. Student) Governance groups of UWGB and UWM, whom are too many to be named. It has been my honor to serve with all of you, I am so proud to have known each of you, and to have had the opportunity to work on so many important issues for the greater good of our respective UW schools. Our UWGB advisor, John Landrum, had the unenviable task of focusing my well-kempt outrage into productivity; and the SAPS personnel at UWM were likewise helpful in keeping me even-keeled in governance matters.

Love and gratitude to all the friends I've made inside and outside of school, including my dearest class/lab-partners-turned-friends, Cathy, Janelle, Beth, Swaroop; not to mention the cascading group of friends they've been kind enough to introduce me to and include me with. Love too, to all those who have befriended me in the great city of Milwaukee, most especially Jack & Rachel, and the entire Tuesday Night Shuffleboard crew. Not to mention my wonderful and kind roommates over the years, including Keenan, and all the friends you shared with me from the Geoscience Department. The sum of these friends' collective camaraderie and inclusiveness over my time here has been so appreciated, and I wish you all the best in your lives to come!

Utmost and unfathomable thanks to my extensive extended family, who have been so loving and supportive of my choice to transition from an uninspired life to one of a professional scientist. I couldn't have done this without the constant encouragement of all my family, from our matriarch Mommom, to too many aunts, uncles, and cousins to be counted. Earlier in my life, I never would have dreamt to reach so far, but your unending love and support kept me going throughout. I have faith that Grandpa Tom would be proud.

Finally, inappreciable love and thanks to my parents and siblings. Nothing can describe my appreciation for being fortunate enough to encounter all of you as willing participants in the experiment of our family unit. While my love for all of you transcends words, please know that each of you have individually and explicitly brought me to this place, turned me in to the person I am, and I shall be forever grateful.

Chapter 1:

Introduction

1.1. Introduction

The epoch of functional optoelectronic devices is upon us: throughout our lives, we find ourselves interfacing with touchscreen devices that depend upon interaction between light and electronic response – and this trend is in no danger of faltering. Our now omnipresent *touch* devices’ functionalities rely upon a number of highly-engineered conglomerations of electronic and materials engineering breakthroughs. Although not often considered in the same breath, it ought to be noted that the fields of Materials Science and Electrical Engineering shall be forever intertwined in the realm of digital device fabrication.

One of the most fundamental innovations that led to our ability to fabricate these amazing devices was the discovery of special materials which exhibit both optical transparency and electrical conductivity – a family of materials known as transparent conductors, or more specifically, Transparent Conductive Oxides (TCOs). The use of TCO materials in optoelectronic devices has become ubiquitous and necessary in technological implementations of everyday life. Whether the consumer is aware of these foundational materials’ integral connection with their terminal usage is another question entirely, but there is little doubt that TCO materials play a fundamental role in nearly any modern human-interface device.

1.2. TCO Application in Opto-electronic Devices

Specific applications of TCO materials in devices are many, and include transparent electrodes [1] for various morphologies of solar cell technology [2] and LED devices [3]; photoelectrochemical cells[4]; photodiodes and metal-insulator-semiconductor diodes[3]; and most specifically of interest to our group, as protective buffer layers to prevent degradation of organic solar cells (OSC) [5].

By utilizing a conductive Metal Oxide (MO) as the electron-transport layer (ETL) of a bulk-heterojunction (BHJ) OSC (Figure 1-1, left), improved resistance to oxygen diffusion can be achieved,

leading to increased stability of Organic Photovoltaic (OPV) cells. MO materials such as ZnO, Al₂O₃, TiO₂, and MoO₃ have been shown to be practical buffer layers in OSCs, due to the low diffusion rate of oxygen through MO materials [6]. Zinc Oxide and TCO materials have been studied as n-type semiconductors as far back as a 1957 Bell Labs study, but p-type doping has been historically more difficult, only forthcoming in the last 20-30 years [2]. To act as successful charge-carriers, MO materials used as ETLs must be n-type semiconductors, but an additional p-type TCO material is required for the hole-transport layer (HTL) and transparent MO cathode. In an alternate “inverted” architecture (Figure 1-1, right), the cathode and anode layers are reversed, with a transparent n-type MO anode on the top of the cell, but once again, a p-type material is needed for the cathode HTL. The need for an inexpensive, easily-produced p-type TCO is inescapable.

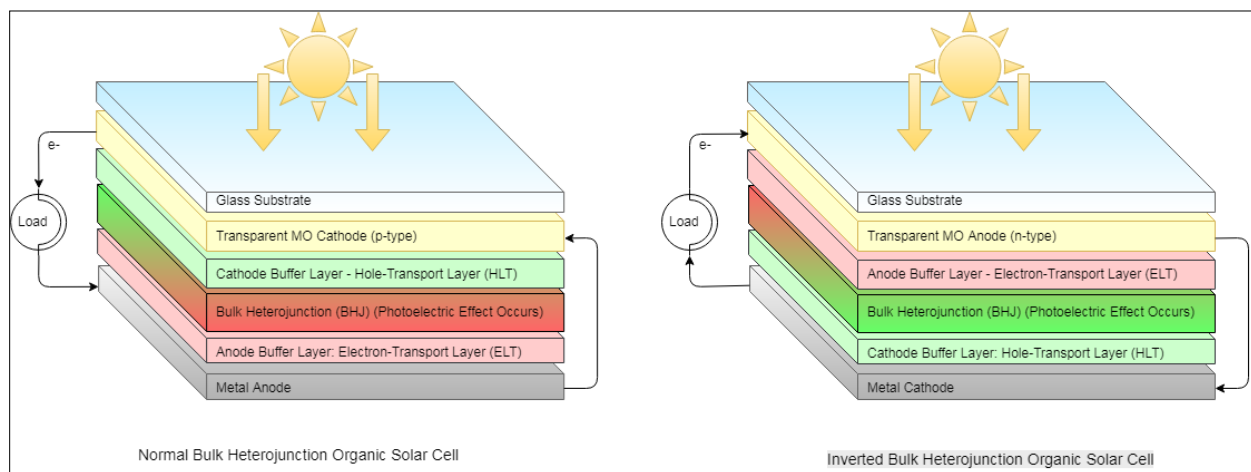


Figure 1-1. Traditional and Inverted architectures of BHJ OSC devices. Left: Normal device with p-type TCO cathode. Right: Inverted design in which n-type TCO is utilized as a transparent anode.

By far, the most widely-used TCO in contemporary devices is Sn-doped In₂O₃, commonly referred to as Indium-Tin Oxide (ITO). While not excessively toxic, ITO has been shown to be harmful to animals and humans [7]. Indium is among the least prevalent elements in the earth’s crust, and is only able to be obtained as a byproduct of zinc smelting [8]. It is therefore a highly energy- and resource-

dependent commodity and is vulnerable to volatile market events. Given these deficiencies, low-cost, low-energy and scalable alternatives to ITO are being actively pursued by industry [9].

1.3. Zinc Oxide and Sol-gel Processing

Zinc oxide offers a particularly desirable set of properties as a candidate for an ITO replacement. Zinc is an abundant element, and is an essential trace mineral with extremely low toxicity to humans [10]. Zinc oxide is a direct band gap (E_g) semiconductor, with an optical band gap energy of $E_g=3.2\text{eV}$ [4], and exciton binding energy of 60 meV [11] at room temperature. While natively an n-type semiconductor like other TCOs, many recent studies have reported success in various methods of p-type doping [1, 4]. Zinc oxide also has the advantage of being easily synthesized at relatively low temperatures by sol-gel chemistry [12], making it ideal for industrial scale-up, such as roll-to-roll processing [13].

Sol-gel chemistry is a low-temperature, solutions-based approach to ceramic MO synthesis (Figure 1-2). Organometal salts are dissolved in an alcohol solution with a stabilizer. The solution is mixed and aged at a set temperature, causing hydrolysis and bimolecular addition of ions. This aged sol is then evenly deposited onto a substrate, at which time the sol is evaporated in a “pre-heat” step to form a xerogel – a network formed via hydroxo- and oxo-ligand dimerization [14]. Finally, the xerogel is exposed to thermal sintering, in which nucleation is followed by crystallite growth. The sintering process also serves to burn off residual organics left in the xerogel network.

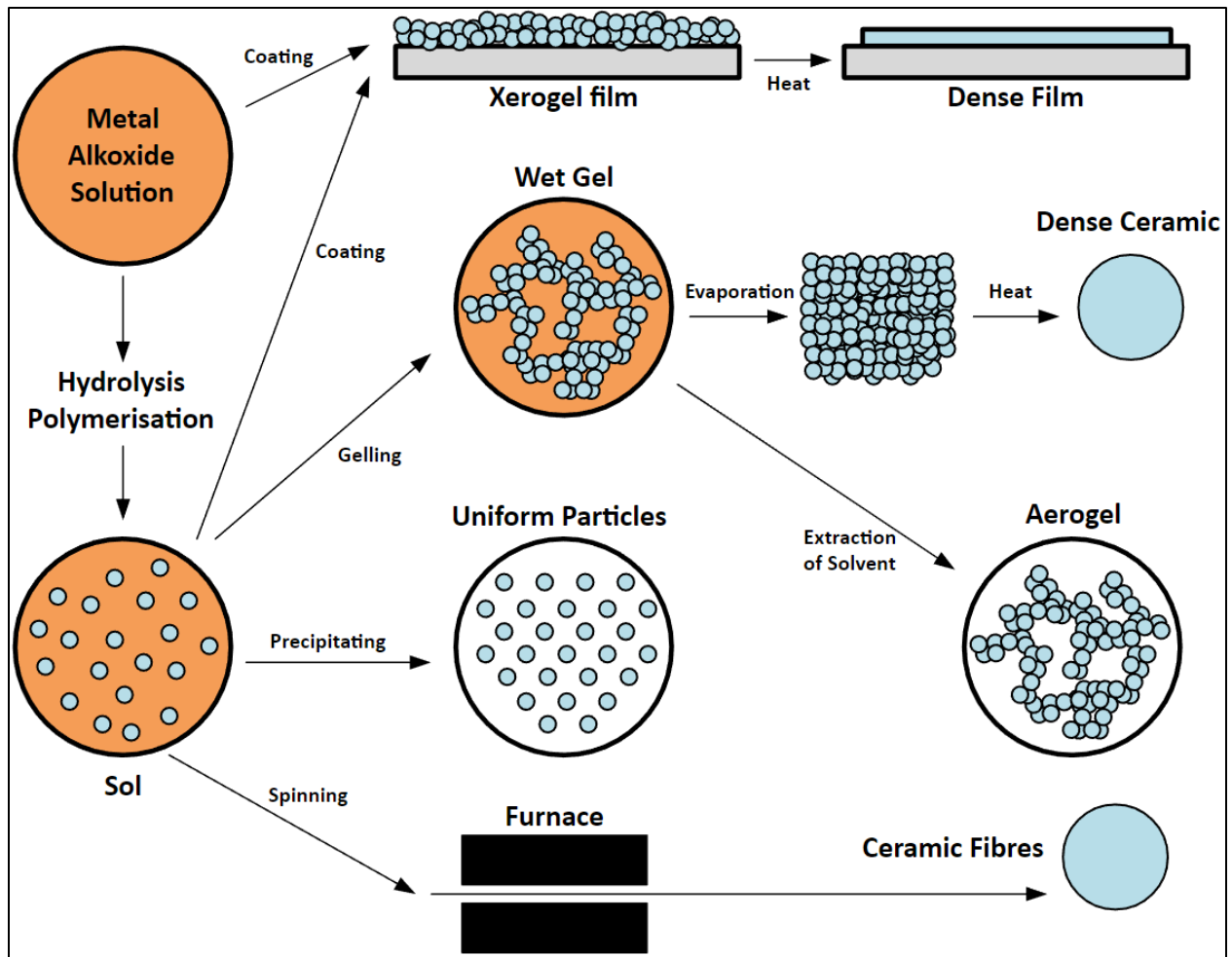


Figure 1-2. Sol-gel process flow chart. Illustrates processing from precursor to intermediate, through final stages. *Source:* by *Claudio* [CC BY-SA 3.0 (<https://creativecommons.org/licenses/by-sa/3.0>) or CC BY-SA 4.0 (<https://creativecommons.org/licenses/by-sa/4.0>)], from Wikimedia Commons.]

One advantage of the sol-gel fabrication method is the ability to tune the nucleation and morphology of the material by manipulation of various parameters in the sol-gel process. For example, preferential c-axis crystal growth may be encouraged by changing the concentration or identity of the precursor salt, or by altering the times and temperatures of the pre-heat and sintering stages. Further, solutions-based fabrication of TCOs allow for precise, even, and homogeneous addition of dopant ions, bypassing the need to resort to high-temperature diffusion processes.

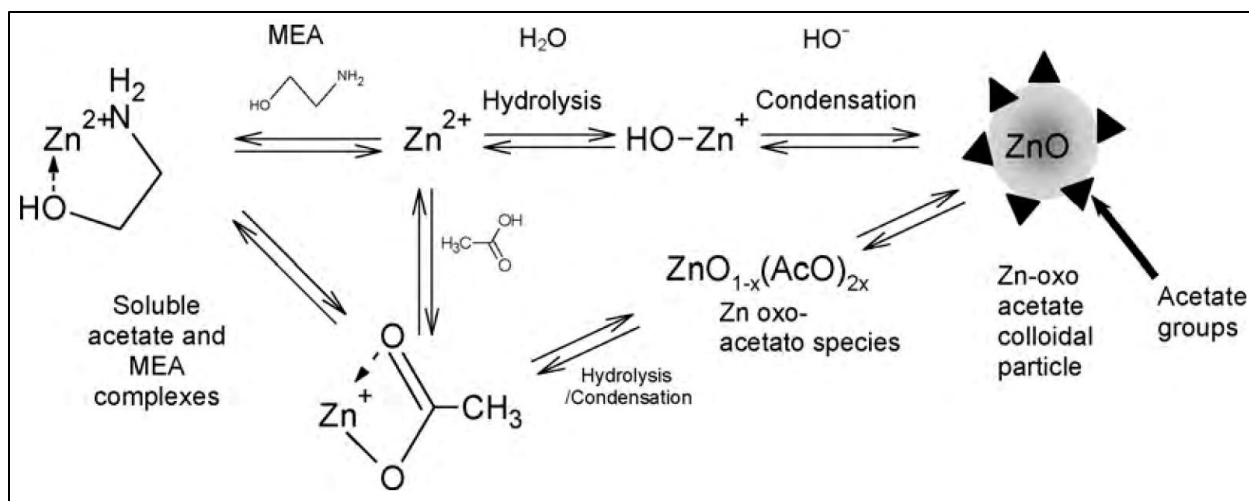


Figure 1-3. ZnO Sol-gel equilibria systems and mechanisms. Starting precursor materials (left) go through multiple interacting equilibria, including complexation with stabilizer, hydrolysis, and condensation to final Zn-oxo-acetate particle (right) before pre-heat treatment evaporates volatile species and post-heat treatment carburates remaining organics and begins crystallization process. *Source: Znaidi et al [15].*

In general, sol-gel chemistry is a well-established and reliable methodology for a variety of solution-solid fabrication scenarios. That said, each unique chemical instance of sol-gel processing possesses distinct and often complicated mechanisms and interactions between its systems of chemical equilibria. A simplified scheme of systems of equilibria in ZnO sol-gel process is shown in Figure 1-3 above, although thorough review the detailed mechanisms involved are beyond the scope of this endeavor.

While sol-gel ZnO thin-film synthesis is a relatively new and novel method of TCO fabrication, it has been well studied and documented. Indeed, throughout our studies, a primary source of technique and methodology was followed at length: Lamia Znaidi of the *Laboratory for High Pressures Materials Engineering at the University of Paris* published a thorough review [16] of sol-gel deposited ZnO thin film studies, citing over 70 individual publications, and summarizing many of the primary parameters utilized by these studies (Appendix A). As thorough and thoughtful as the review was, it was quickly apparent to the UWM team that while detailed methodologies for ZnO sol gel synthesis existed, no clear and concise ‘recipe’ came to light that produced high-quality, useful and dopable ZnO thin films

ideal for our purposes. A major objective of our ongoing research became the optimization of a standard repeatable process in our efforts to produce high-quality TCO thin films.

1.4. ZnO Crystalline Structure, Preferential Orientation, and XRD Characterization

As a stoichiometric oxide in its pristine state, ZnO's crystalline geometry is defined by its atoms' respective radii, their two shared electrons forming the solid into adjacent tetrahedra in a hexagonal close-packed wurtzite structure (Figure 1-4A). An ionic compound, the zinc atom donates its two 4s valence electrons to fill oxygen's 2p orbital band, making it a wide band-gap II-VI semiconductor [17].

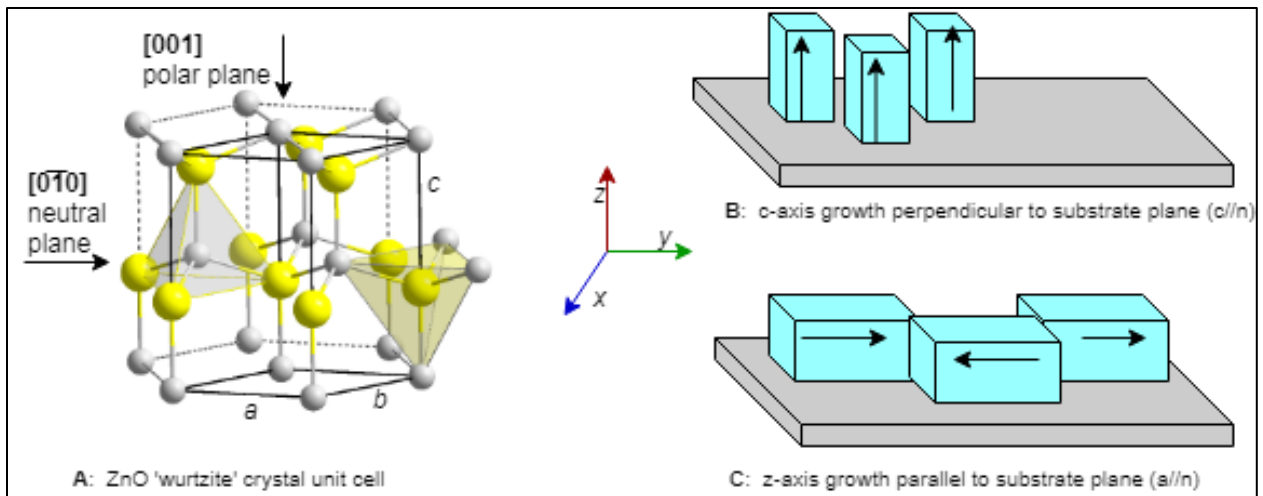


Figure 1-4. ZnO wurtzite unit cell and diagram of z-axis ZnO growth. Unit cell (A) shows two units of stoichiometric ZnO forming dual tetrahedra; B and C show different axial growth methods. *Source: A: public domain; B/C: adapted from Znaidi et al [15].*

It is important to note that the wurtzite unit cell consists of two ZnO formula units, and that depending on how the unit cell is oriented, the [001] plane will consist of either Zn-polar or O-polar faces [18]. The orientation of the ZnO crystal growth in sol-gel thin films is extremely important to their optoelectronic properties:

“Polycrystalline ZnO films usually grow with the c-axes of the crystallites oriented approximately perpendicular to the film plane [117 [19], 118 [20]]. Therefore, the electrical transport in polycrystalline films, which is measured laterally, occurs in almost all cases perpendicular to the c-axes of the crystallites.” – Ellmer, ([1], p. 56)

Early work by Znaidi et al determined that ZnO crystal growth orientation (Figure 1-4 B/C) was tunable through various solution parameters [21]. They later showed that many sol-gel preparations exhibited (002) preferential peak intensity, indicating “c//n” orientation [16]. Because of these characteristics of ZnO thin films, our primary method of determining the quality of our films was based upon the intensity of the (002) X-Ray Diffraction (XRD) peaks, as well as the intensity ratio of (002) compared to other known ZnO crystallographic orientations (esp. (100) and (101) peaks).

A quantifiable method of comparing one preferential peak to others is known as the Texture Coefficient, and has been used by many researchers to compare XRD peaks [22], [23], [24]. It is defined as follows:

$$TC = \frac{\frac{I_{(hkl)}}{I_{0(hkl)}}}{\left(\frac{1}{n}\right) \sum \left[\frac{I_{(hkl)}}{I_{0(hkl)}}\right]}$$

“where $I_{(hkl)}$ and $I_{0(hkl)}$ are the integrated intensities of $(h \ k \ l)$ reflections measured for an experimental specimen and a standard powder sample, respectively, and n is the total number of reflection planes.” [25]. While this method is not utilized in our analyses per se, an adapted version of it was developed for use in analyzing second phase experiments, as laid out in Section 3.3.1. Powder diffraction file (PDF) intensity for naturally-occurring polycrystalline ZnO (zincite) is shown in figure 1-7 (red lines).

1.5. p-type doping of ZnO Thin Films

Early in the exploration stages of this research endeavor, the group's founder and original team leader, Jon Wolgamott, posited that given the relative ease of solutions-based doping methods, the sol-gel process was an ideal avenue for exploring new methods of p-type doping in ZnO. If the sol-gel process relied upon a dissolution of organometallic salts as a basis for the precursor solution, he surmised that it should be a straightforward process to introduce a discrete quantity of dopant atoms as cations in a similar metal salt.

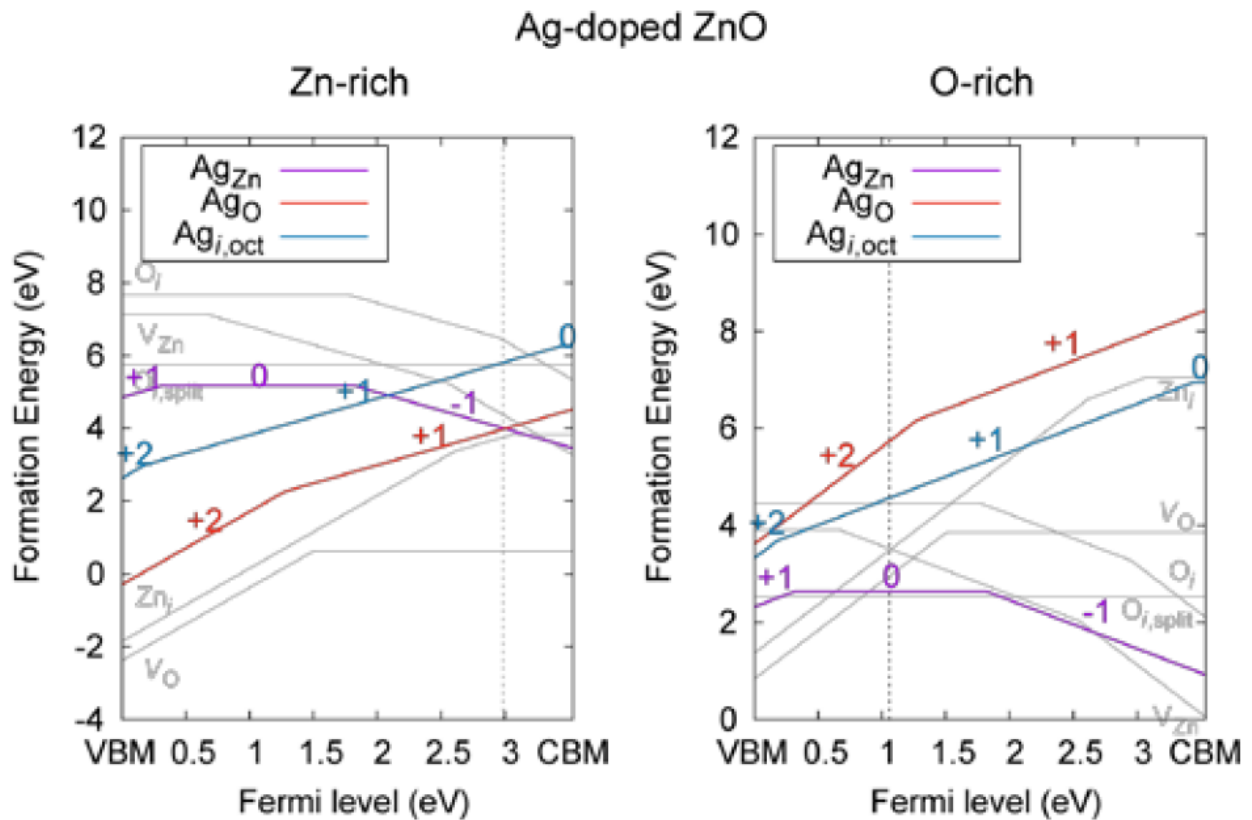


Figure 1-5. Formation energies of intrinsic and substitutional defects in ZnO. Intrinsic defects are shown in grey while silver-doped interstitial and vacancy defect formation energies are shown in color for both Zinc-(left) and Oxygen-rich (right) circumstances. *Source: Yim et al [26].*

In investigating this theory, Wolgamott came across a just-published study by Yim et al at The Research Institute of Advanced Materials at Seoul National University, in which computational methods were utilized to establish a database of theoretical formation energies of dopant atoms in a

ZnO lattice [27]. The database utilized automated first-principles calculations to provide formation energy vs. fermi level diagrams (Figure 1-5) in Zn-rich and O-rich conditions as opposing limits, for periodic elements through row six [26].

Analysis of thermodynamic favorability for defect formation based upon the Yim database led Wolgamott to compare p-type favorable dopants from Group 15(VA): [N, P, As Sb]; Group 1(IA): [Li, Na, K, Rb]; and Group 11(IB): [Cu, Ag, Au]. Elements from both groups 15 and 1 were ultimately dismissed as study candidates based upon various issues of practicality, safety, and compatibility with the sol-gel process. Based partially upon the fundamental p-type extrinsic semiconductor electron bonding model (Figure 1-6), as well as additional first principles calculations from a National Renewable Energy Lab paper [28], Group 11 atoms were identified as the focus of our study.

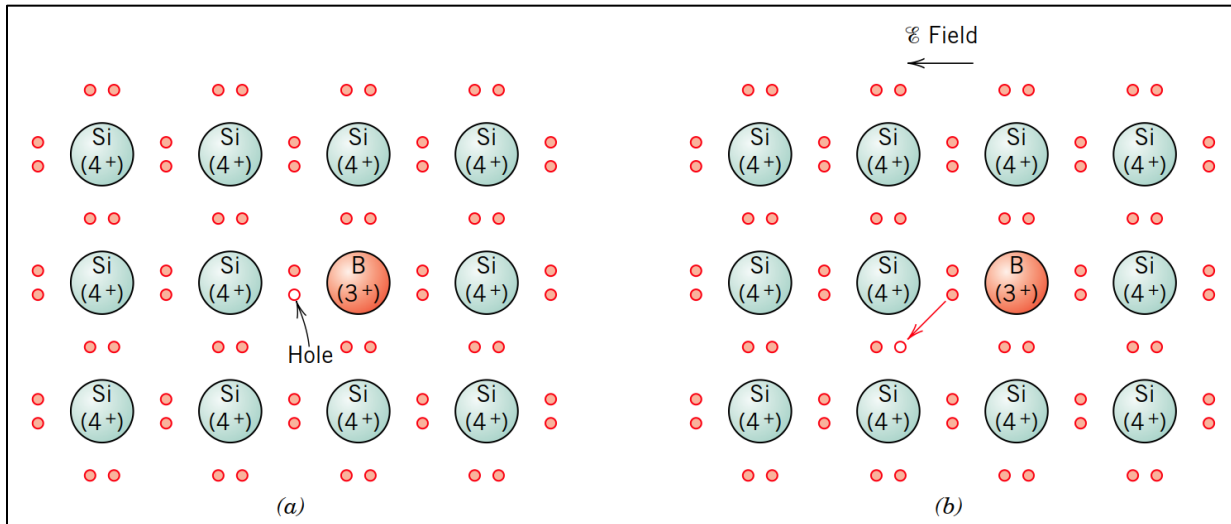


Figure 1-6. Extrinsic p-type semiconductor model (electron bonding). (a) An impurity atom such as boron, having three valence electrons, may substitute for a silicon atom. This results in a deficiency of one valence electron, or a hole associated with the impurity atom. (b) The motion of this hole in response to an electric field. *Source: Callister [29].*

To achieve p-type doping of ZnO with group-IB elements requires both zinc substitution (M_{Zn}) acceptor defects, as well as the suppression of native hole-killer defects such as oxygen vacancies (V_O) and zinc interstitials (Zn_i) [28]. Calculations by Yan et al indicate that given the formation and transition energies of Ag_{Zn} , silver is the ideal Group 11 atom for p-type doping of ZnO, and may in

fact be more effective than N_O substitution [28], which has already been shown to produce p-type ZnO. Silver is also well known to be an excellent conductor, and while a precious metal, the cost of doping on the scale of 1-2 at% was not deemed prohibitive to research. Thus the ZnO Solar research group was established, intent on determining the feasibility of using sol-gel chemistry to dope ZnO with silver as a p-type semiconductor.

1.6. Initial stages and early attempts at synthesis

As discussed, the ZnO sol-gel Review by Znaidi was utilized extensively as a starting point for initial stage experiments, proof of concept, and technique sources. Before a doped ZnO thin film could be attempted, a standard procedure for synthesizing simple ZnO from sol-gel technique was required. The first several iterations of experiments attempted to discern a set of common and repeatable processing steps amid a blur of various documented methods. In general, the processes described in Section 1.3 above were followed, but early trials were stymied simply by unfamiliarity with the chemistry methods. These early efforts were further thwarted by unclear understanding of the dynamics of pre-heat operations on the morphology of ZnO crystal structure, and how the post-heat stage temperature influences decarburization of organics from the sol matrix.

At the infancy of this project, many difficulties were encountered in confirming synthesis of ZnO thin films and powders, stemming largely from unfamiliarity with specific lab procedures and incorrect assumptions in cases wherein literature was not specific. We subsequently developed a fast-paced trial-and-error protocol aimed at successful synthesis, and to determine whether the brown residue found in all the samples was some sort of contaminant or if there was simply something wrong with the process. The XRD output from some of these early attempts are shown in Figure 2-2. After further literature review and experimentation, we discovered that a vital aspect of the sintering/annealing process, in addition to grain formation and crystal growth, was the elimination of

residual organic matter from the initial sol. The precursor materials being alcohol, amine, and acetate, various species of organics and volatiles were present in the sol, which needed to be removed in order to purify the final ZnO product. Longer post-heat treatment time and higher temperatures were called for, but literature describing post-heat treatment protocols varied dramatically (see Appendix A, Post-heat treatment column).

Project Evolution

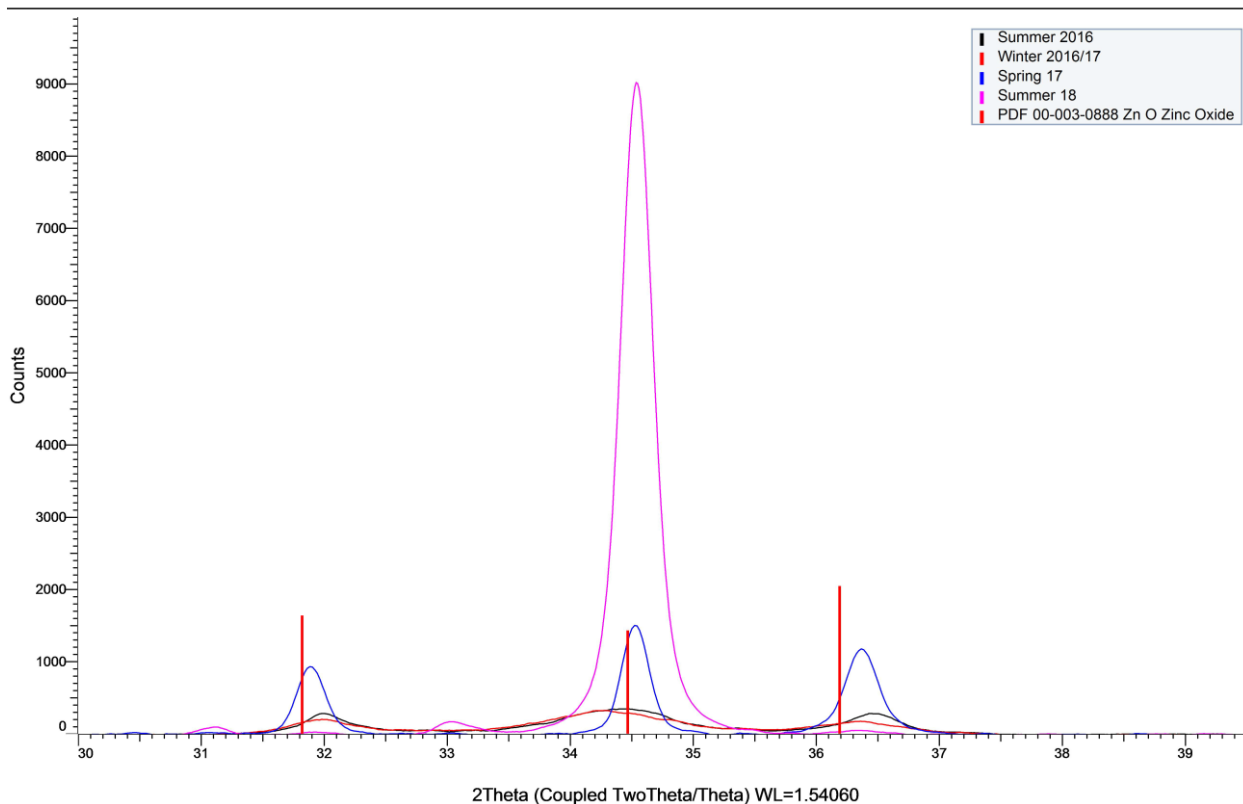


Figure 1-7. XRD Spectra illustrating progress through ZnO Thin Films Project. Examples of peak intensities and orientation ratios can be seen progressing from early stages in 2016 through final stages in 2018.

For several weeks, rapid trial and error experimentation with dramatic variation of parameters involving time and temperature of the various stages of synthesis (mixing, aging, deposition, pre-heat, and post-heat treatments) was undergone. After 17 independent experiments including 35 separate iterations of parameter modification, we were eventually able to achieve successful synthesis of ZnO thin films, as confirmed by XRD analysis (Figure 1-7). Although ZnO peaks were now appearing on XRD spectra, the peaks were short and broad in comparison to literature. Furthermore, the

preferential (002) peak at $\sim 34^\circ 2\theta$, representing c-axis crystal orientation was not dominant compared to (100) and (101) peaks.

1.7. ZnO Thin Films Optimization, Doping Attempts, and Process Breakthroughs

Given the many methods and variables described in the ZnO Sol-gel Review, our initial difficulties synthesizing ZnO at all, and the still less-than-ideal quality of films being produced, it was determined that a more comprehensive and methodological study of processing variables was necessary. Chapter 2, *Optimization of Sol-Gel Spin-Coated ZnO Thin Films for Silver Doping*, is a comprehensive review of over a dozen independent experiments performed over the first-year course of this project, under the direction of Mr. Wolgamott. As experiments were designed and performed, the authors' comprehensive understanding of the sol-gel synthesis process evolved in turn. In some cases, certain experimental parameters that were examined early in the project needed to be reexamined to account for unexpected confounding factors. In other cases, variables identified early in the project and thought to be significant did not prove to be so. A diagram of the ZnO sol-gel process and the variables determined to be applicable can be found in the introductory section of Chapter 2.

With p-type silver doping of ZnO films representing the genesis of this project, throughout the thesis, extra attention is paid toward doping attempts. Indeed, many of the experiments discussed in Chapters 2 and 3 were performed in duplicate with an undoped control group and a second batch of doped product. In this way, confounding parameters to silver doping can be either identified or ruled-out.

Chapter 3 presents late-stage experiments performed after the major parametric analysis had been completed, and after the thesis author had taken charge of the project. Innovative and unconventional layering and wetting techniques were implemented in attempt to improve surface smoothness and

conductivity, some with unexpectedly extraordinary success. These breakthroughs are laid out in careful detail, and theories as to their otherwise unexplained success are discussed.

Chapter 2:

Optimization of Sol-Gel Spin-Coated

ZnO Thin Films for Silver Doping

2.1. Introduction

Incorporation of silver ions in sol-gel fabrication of ZnO thin films has been proposed as a method of achieving p-type semiconduction in ZnO as a Transparent Conductive Oxide. While fabrication methods for sol-gel ZnO thin film synthesis are ample in literature, the exact methods and parameters of the procedures vary significantly from one source to the next. After replication of several distinct analyses' processing parameters for plain sol-gel fabrication and foreign-element doping techniques, best practices for each process were established and optimized. These parameters were then incorporated into combined methodology for silver doping.

Sol-gel fabrication of ZnO thin films via spin-coating consists of several common sequential steps, as illustrated in Figure 2-1. A soluble zinc salt, usually Zinc Acetate dihydrate (ZnAc) is dissolved in an alkyl alcohol with a stoichiometric ratio (γ value) of stabilizer. Generally, this stabilizer is an amine alcohol with a primary hydroxyl group, which both assists in the solvation of ZnAc, and acts as a base in assisting in the complexing of Zn(II) cations [16]. This solution is mixed at an elevated temperature until ZnOAc is fully dissolved, and then aged for a period to allow for hydrolysis of the various zinc and organic species, and to begin the formation of colloids that will later polymerize to form the gel. After aging, the sol is deposited on a spinning substrate in dropwise addition through the use of a spin-coater machine. After applying a coat of sol, the layer is dried and may undergo 'pre-heat' treatment. This deposition and pre-heat treatment is repeated until the desired number of coats have been applied, at which point the coated substrate is subjected to a 'post-heat' sintering step, resulting in the formation of ZnO grains and ultimately crystal growth.

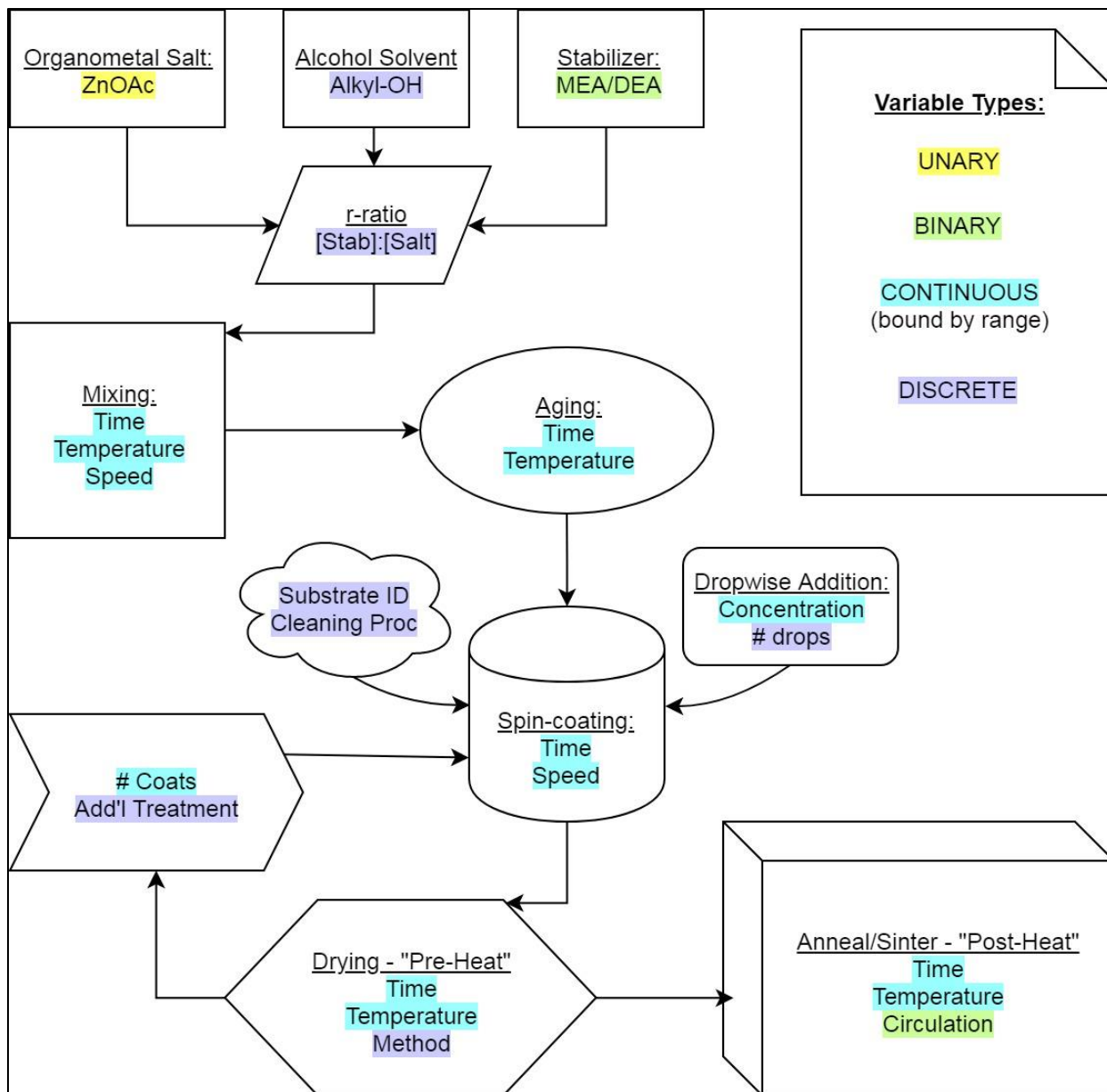


Figure 2-1. Zinc Oxide Sol-gel process and variables. Each step in the process may involve one or more variable methods. These variables are color-coded in the “Variable Types” key in the upper-right.

Each step in the sol gel synthesis and spin-coating fabrication process is the subject of a number of variables, as further illustrated in Figure 2-1. Over the course of this study, many of these variables were identified, examined, researched, and methodologically adjusted to optimize these values for our specific application. A detailed review of undoped ZnO synthesis methods was consulted, as discussed in Chapter 1, as well as several other research studies. These variables are identified in

Table 2-1, where their default literature values are compared to the range of values explored in our experiments.

Process	Variable	(1)Literature; (2)Znaidi Review; (3)Physical Limit	Bounds of UWM Study
Solution	Salt	(2) mostly ZnOAc, few exceptions	ZnOAc
	Alcohol	(2) Alkyl Alcohols, Glycols	Ethanol, Propylene glycol, Propylene glycol methyl ether
	Concentration	(2) 0.02 – ~2 mol/L	0.25 – 1.5 mol/L
	Additive	(2) Primary amines, glycerol, acids and bases	MEA/DEA
	pH	(1) 6.4 – 10.6	not investigated
	r-ratio	(2) 0 – 2	0.75 - 2.0
Mixing	Time	(3) 0 – unbound	60 min
	Temperature	(3) (-114) – 173° C	50-60 C
	Speed	(3) 0 – max RPM	300-400
Aging	Time	(3) unbound	0-96 hrs
	Temperature	(2) 25, 60	25
	Add'l Variable	(1) none found	density, viscosity, mass loss
Substrate	Identity	(2) many	Soda Glass, ITO, Silicon, Quartz
	Cleaning Process	(2) many	Indexed per expt.
Spin-coating and Addition Method	Sol Concentration	(2) 0.02 – 2M	0.25 – 0.75M
	Drops	(2) many	1-10
	Time	(2) many	30, 60s
	Speed	(2) many	3000
	Coat Count	(1) 5–20	1–10
Drying ("pre-heat")	Time	-	0–15
	Temperature	(2) 40-500	0-200
	Action	(1) various	Air-circulated oven, Ambient Furnace, Conduction Hotplate
Anneal/Sinter ("post-heat")	Time	-	60-240
	Temperature	(2) 150-900	250-500
	Other	-	Air-circulated oven, Ambient Furnace, Conduction Hotplate
Other per-layer Treatment	Substrate temperature before deposition	-	200, 220, 300

Table 2-1. Processing variables involved in ZnO thin film fabrication. The middle column describes the bounds of some variables as found in literature, compared to the bounds undertaken by this study (right column).

Experimental Narrative and Sequence of Labeling

In the interest of clarity, experimental narrative has been divided into major classifications representing separate subchapters herein, based upon experiments performed and variables examined. Each subchapter will outlay experimental procedure and summary results, plus immediate implications leading to the subsequent subchapter; intensive examination of results, discussion, and conclusions for the summation of experimental procedures are addressed collectively at the end of the chapter.

Within each subchapter's 'experimental' section, a matrix summarizing the experimental variables is presented to clarify the methodology of the experiment. In some cases, these tables will also include the sample identification codes that were used in the experimental process. While these codes are not necessarily valuable to the reader, they may help in identifying applicable results, and illustrate the thought process involved in the design of experiment. In general, each individual experiment was coded with a sequential alphabetical prefix, followed by additional numerals to identify variables tested and replicated samples.

2.2. Experimental Narrative and Preliminary Results

Early proof of concept experiments focused on successful replication of established sol-gel methods, mostly following Znaidi's ZnO Sol-gel Review document [16], choosing parameter values essentially arbitrarily, based on methods perceived as most common. A series of rapid trial-and-error experiments eventually led to an initial formulation of sols which, when heat-processed, produced films that indicated presence of ZnO by XRD characterization. However, the XRD peaks obtained from these early trials were short and broad (Figure 2-2,) indicating lower-than-ideal crystallinity, and the slides appeared opaque and discolored. In order to achieve a standard formulation for experimental doping, significant improvement upon these early trial procedures was necessary, and a series of more careful and methodological optimization experiments were undertaken.

Early Attempts

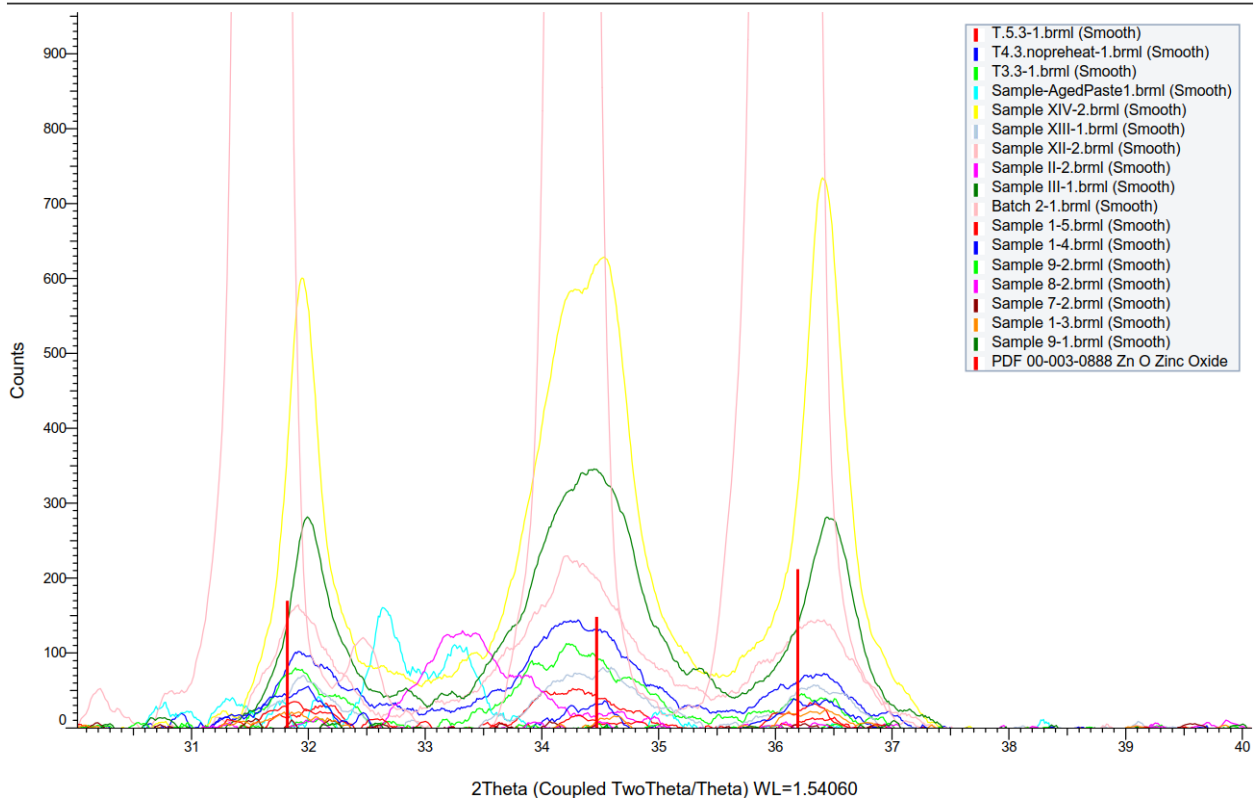


Figure 2-2. XRD Spectra from a variety of early-stage experiments carried out prior to those documented in Chapter 2. Early attempts yielded low-intensity, broad peaks indicating low-crystallinity and sometimes outright failure to achieve the desired ZnO product.

As soon as successful ZnO film synthesis could be confirmed, attempts to implement silver doping became a priority, as outlined in Section 2.2.2. As it happened, this doping process was a rather simple and straightforward matter, discussed in Section 2.2.3 (Experiments D & G,) but optimized ZnO film fabrication remained wrought with difficulty. Much of the remaining work in this phase (indeed, all that is reported in this Experimental section) focused on continued optimization of the sol-gel process, and the establishment of a Standard Operating Procedure (SOP) for future doping attempts.

In addition to the experiments documented in this section, dozens of other less formal trials were conducted over the course of 2016-17, addressing such issues as film porosity and crystallinity, and how those relate to film conductivity. Unfortunately, lack or loss of documentation and poor training of lab personnel during times of turnover rendered much of these experiments' data useless, as mentioned in Section 2.2.4. While these trials are not useful in documenting our study, many of the lessons learned from these trials led to minor improvements in technique, and contributed in terms of improving our general knowledge and experience with this science. Furthermore, negative findings are findings nonetheless, and helped steer us away from further unnecessary or inapplicable experiments.

Unless otherwise indicated, all samples were characterized by X-Ray Diffraction (XRD) on a Bruker D8-Discover instrument, using a $\text{CuK}\alpha 1$ source at 40kV and 40mA, with a wavelength of $\lambda=1.54\text{\AA}$, scanning between $30 - 40^\circ 2\theta$ to examine primary ZnO (100), (002), and (101) orientation peaks (Figure 1-6). Electron microscopy and Energy-Dispersive X-ray Spectroscopy (EDS) were carried out with a JEOL JSM-6460 LV scanning electron microscope.

2.2.1. (Project A/B) – Solution Stabilizer, Aging & Massloss

This experiment was designed to simultaneously determine an ideal stabilizing agent, and to better understand the role of solution aging in the sol-gel process. Literature indicated that a stabilizer chemical with a primary amine group (a terminal NH_2) was an important additive, “act(ing)... as a base and a complexing agent”[16]. It was observed early in the project that the additive also significantly aided in dissolution of the zinc salt in alcohol solutions. Initial trials used diethanolamine (DEA) as stabilizer, but Znaidi’s review suggested monoethanolamine (MEA) may be sterically preferable as a bidentate ligand both in chelating (Figure 2-3a) the Zn ions and bridging (Figure 2-3b,c) them to one another in the initial formation of the gel colloid. All solutions in this experiment were made in duplicate, one with DEA as stabilizer, the other at higher concentration of ZnAc with MEA as stabilizer.

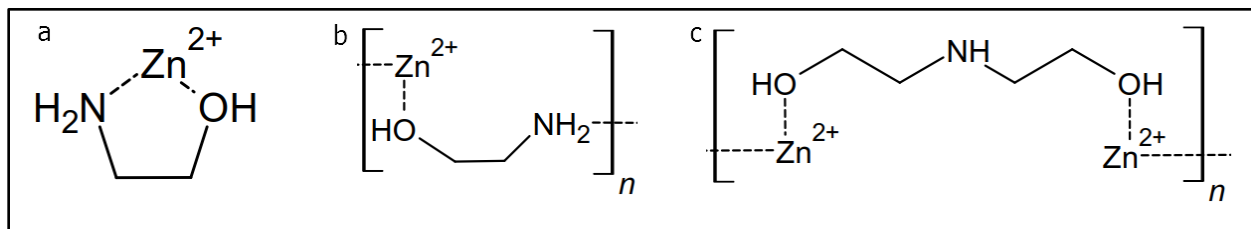


Figure 2-3. Various schema of zinc bridging with ligand stabilizers. a) MEA chelating zinc ion as a bidentate ligand. b) MEA acting as a bridging ligand in the partial polymerization of the gel. c) DEA likewise acts as a bridging ligand but is sterically hindered from chelating with a single zinc ion.

The precise mechanism of gel formation is not completely agreed upon in literature [15, 20], owing largely to the fact that many distinct hydrolysis, condensation, chelation, and complexing reactions are occurring simultaneously in both equilibrium and competition with one another [31]. At this early stage, it was unclear to the group exactly how the aging process affected the final quality of thin films, and whether gelation could be caused by evaporation of solvent in the forming Zn matrix. Early attempts at sol-gel synthesis indicated viscosity of the precursor solution may play a role in the thickness of deposited layers, which in turn may affect the quality of the final film.

The protocol devised for this experiment tested evaporation of solvent by allowing one solution to age covered only by a permeable tissue paper, one control solution sealed with parafilm, and one solution sealed for 24 hours, then uncovered and allowed to evaporate. Each solution was then deposited onto glass slides after 18, 24, 42, and 48 hours, as shown in Table 2-2.

Experimental

Aged	DEA-Stabilized			MEA-Stabilized		
	Covered	Uncovered	Covered for 24-hours	Covered	Uncovered	Covered for 24-hours
18 hrs	A.1.1	A.2.1	–	B.1.1	B.2.1	–
24 hrs	A.1.2	A.2.2	–	B.1.2	B.2.2	–
42 hrs	A.1.3	A.2.3	A.3.3	B.1.3	B.2.3	B.3.3
48 hrs	A.1.4	A.2.4	A.3.4	B.1.4	B.2.4	B.3.4
>48 hrs	A.1.5	A.2.5	A.3.5	B.1.5	B.2.5	B.3.5

Table 2-2. Project A/B matrix of variables. Two major trials consisting of different stabilizers (A & B) are treated identically by aging time and how they are covered.

DEA-stabilized precursor solution was prepared by dissolving ZnAc ($\text{Zn}(\text{CH}_3\text{COO})_2 \cdot 2\text{H}_2\text{O}$; Sigma-Aldrich) in anhydrous ethanol ($\text{C}_2\text{H}_5\text{OH}$; Sigma-Aldrich) to a concentration of [0.5M], stirred magnetically while DEA was added dropwise until ZnAc fully dissolved, yielding a ratio of stabilizer to salt (γ value, defined as $[\text{additive}]/[\text{Zn}^{2+}]$), at approximately 1. MEA-stabilized solution was prepared identically, using MEA instead of DEA, and at a Zinc concentration of [0.75M]. Solutions were covered and mixed for 1 hour on a 60°C hot plate. Solutions were then each split into three ~15mL aliquots, weight of each recorded, covered as described above, and aged 18 hours at room temperature.

The first batch of 18-hr aged slides were processed by dropping 1-3 drops of each solution on a respective 1x1 inch glass microscope slide, cleaned with detergent and DI water. Each sample was placed directly into a 250°C tube furnace for 1 hour, then removed and allowed to air cool. Subsequent samples were made by repeating this process at 24, 42, and 48 hours of aging. Sample

flasks were weighted before and after each deposition event to track evaporation of solvent as mass loss, adjusted to account for mass loss from drop-coat.

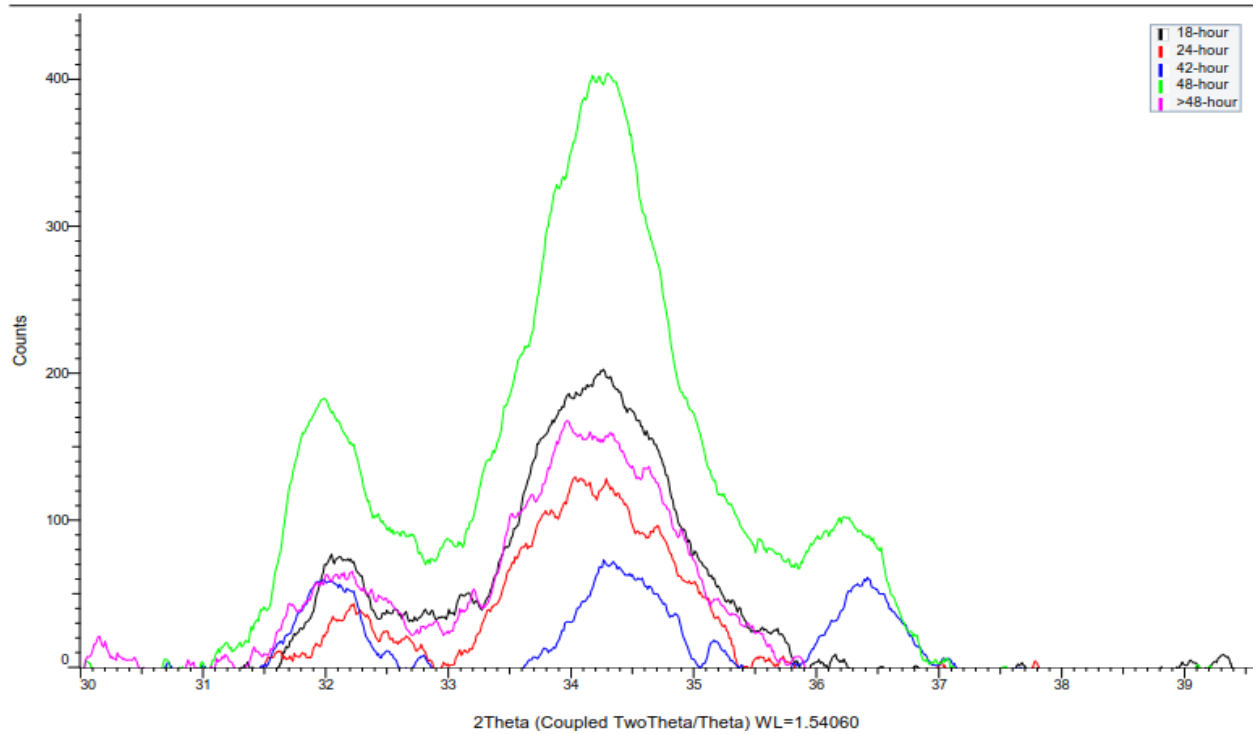
Results

Processed slides appeared cloudy with brown and yellow discoloration. At the time of the experiment, our analysis of XRD spectra was somewhat qualitative and subjective, focused on finding improvement in intensity and narrowing of peaks. Given the preliminary nature of this experiment, extensive and rigorous analysis has not been carried out, instead screening for commonalities and correlation between shared variables.

Comparing DEA- and MEA-stabilized solutions, we tend to see more consistent (002) preferential peak intensity in MEA-stabilized samples (Figure 2-4, top), with (002) peak generally twice as intense as (100) and (101). In contrast, samples from the DEA-stabilized solutions were inconsistent in peak-intensity and ratios, rarely showing (002) preference, sometimes exhibiting approximately equal peak intensities or ratios more closely matching powder diffraction ratios (Figure 2-4, bottom).

In comparing samples by aging time, some correlation in peak intensity and preferential orientation ratio was observed between each of the stabilizers' solutions separately. For DEA-stabilized samples, both covered and uncovered solutions' samples found the 18-hour aged trials to be superior in intensity and (002) preference (Figure 2-5, bottom), while MEA-stabilized samples indicated 48-hour aging to be superior in intensity and preferential peak ratio (Figure 2-5, top).

MEA Covered



DEA Uncovered

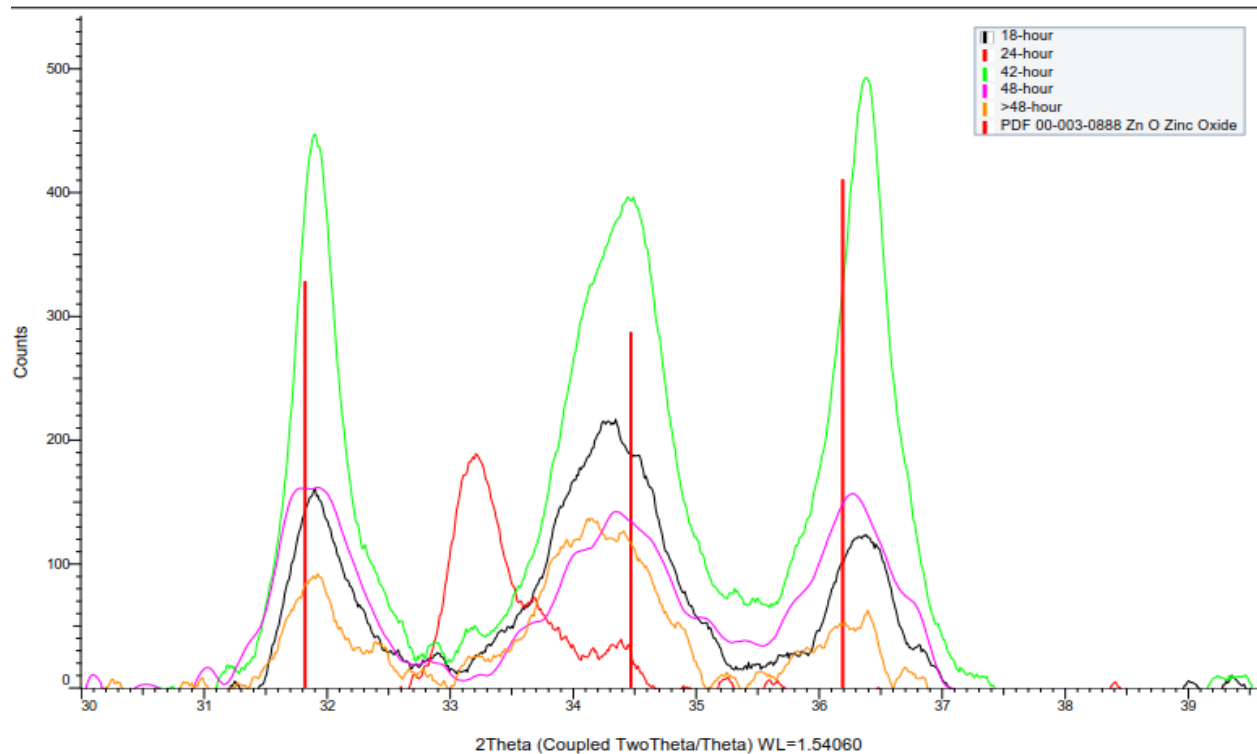
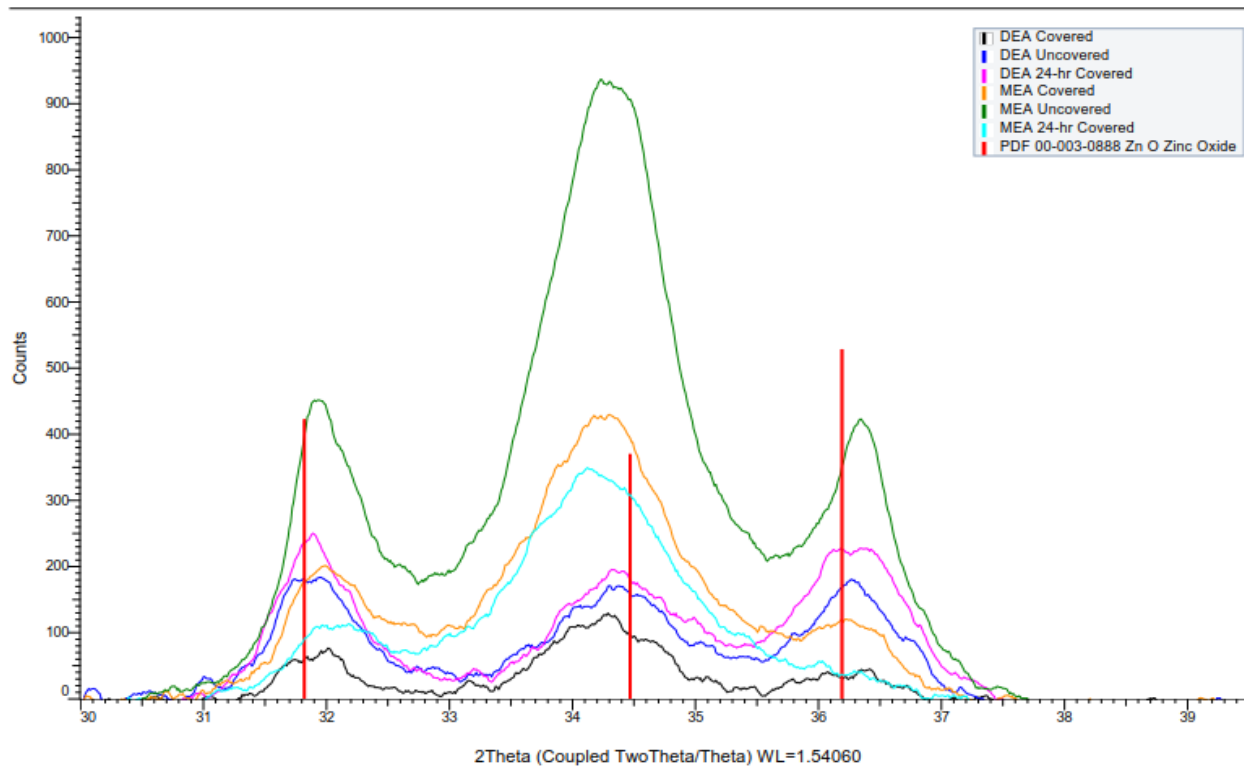


Figure 2-4. XRD spectra of covered MEA- and uncovered DEA-stabilized samples. MEA-stabilized (top) samples show superior 002-peak orientation to DEA-stabilized samples (bottom).

48-hour Aged Samples



18-hour Aged Samples

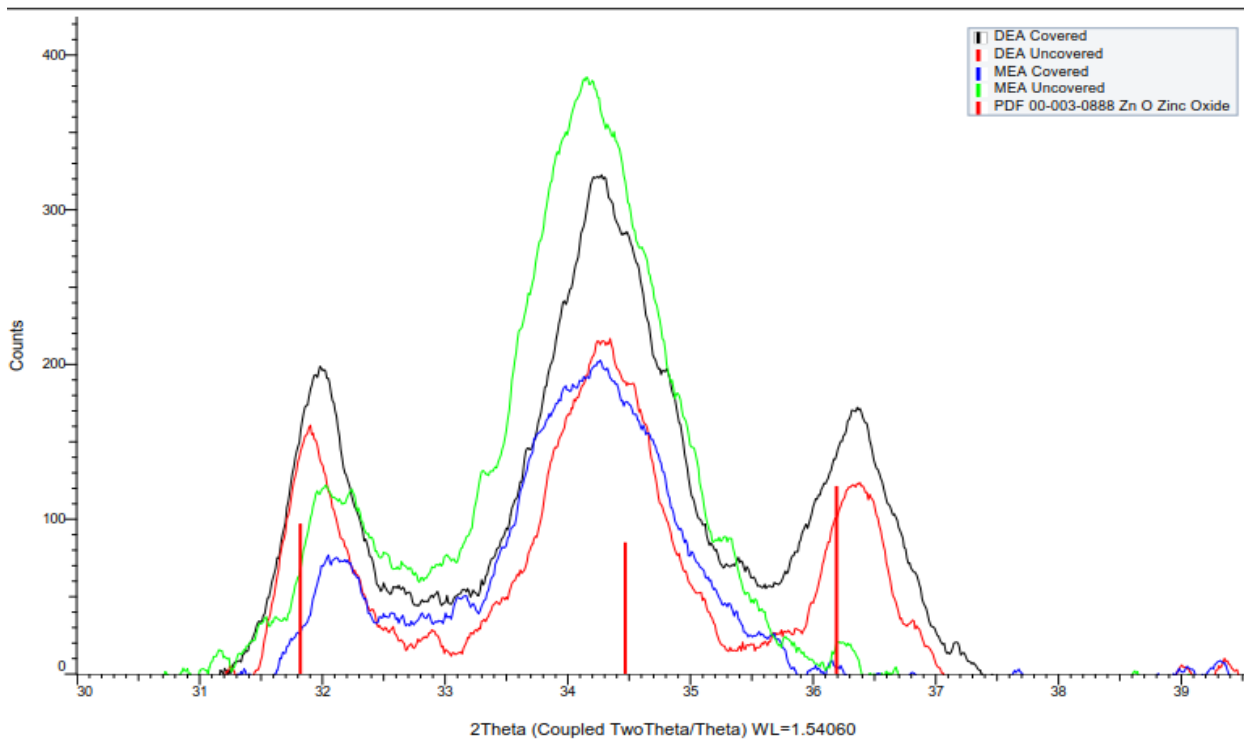


Figure 2-5. XRD spectra comparing all solutions, aged 48-hours and 18 hours. In general, we see improvement to peak intensity in 48-hour aged samples (top), but generally better (002)-ratio in 18-hour aged (bottom) samples.

2.2.2. (Projects D & G) – Preliminary Doping Attempts

While the precise processing parameters for fabricating ZnO thin films had not been optimized to ideal specifications at this point, the major encumbrances to successful ZnO synthesis had been remedied, and attention shifted to achieving proof-of-concept in doping. Having identified silver as the preferred dopant element, the next milestone was to determine a solutions-chemistry method of incorporating silver into the sol-gel process.

Continued literature review revealed successful attempts to achieve silver-doped ZnO thin films by Touam et al [32], and our first doping efforts focused on replicating this work. Touam's method relied upon the use of silver nitrate (AgNO_3) as the dopant salt, to be incorporated stoichiometrically into the ZnAc solution. Silver compounds are notoriously insoluble, with the exception of its nitrate and acetate salts, so only cursory efforts were made to investigate alternative elemental sources of silver. Given the complex systems of equilibria (Figure 1-3) involved in the sol-gel process, it initially seemed intuitive to utilize silver acetate as a precursor, if only to limit the mere quantity of species involved and to reduce more complex equilibria interactions. However, in consideration of silver's dubious solubility in water, let alone our nonaqueous ethanol solvent, we determined that the risk of insolubility from the common-ion effect was less desirable than the inclusion of the additional nitrate species.

An initial experiment was contrived in which two solutions – undoped 1.5M ZnAc; and 4 at% Ag-doped (1.5M metal salt) – were deposited by spin-coating 12 layers on to 200°C glass slides, then annealed at 500°C for 1hr. XRD analysis for these samples confirmed ZnO as per previous trials (Figure 2-5). The doped sample shows broader, less intense peaks which are uniformly right-shifted by less than $0.1^\circ 2\theta$.

Preliminary Doping Attempts

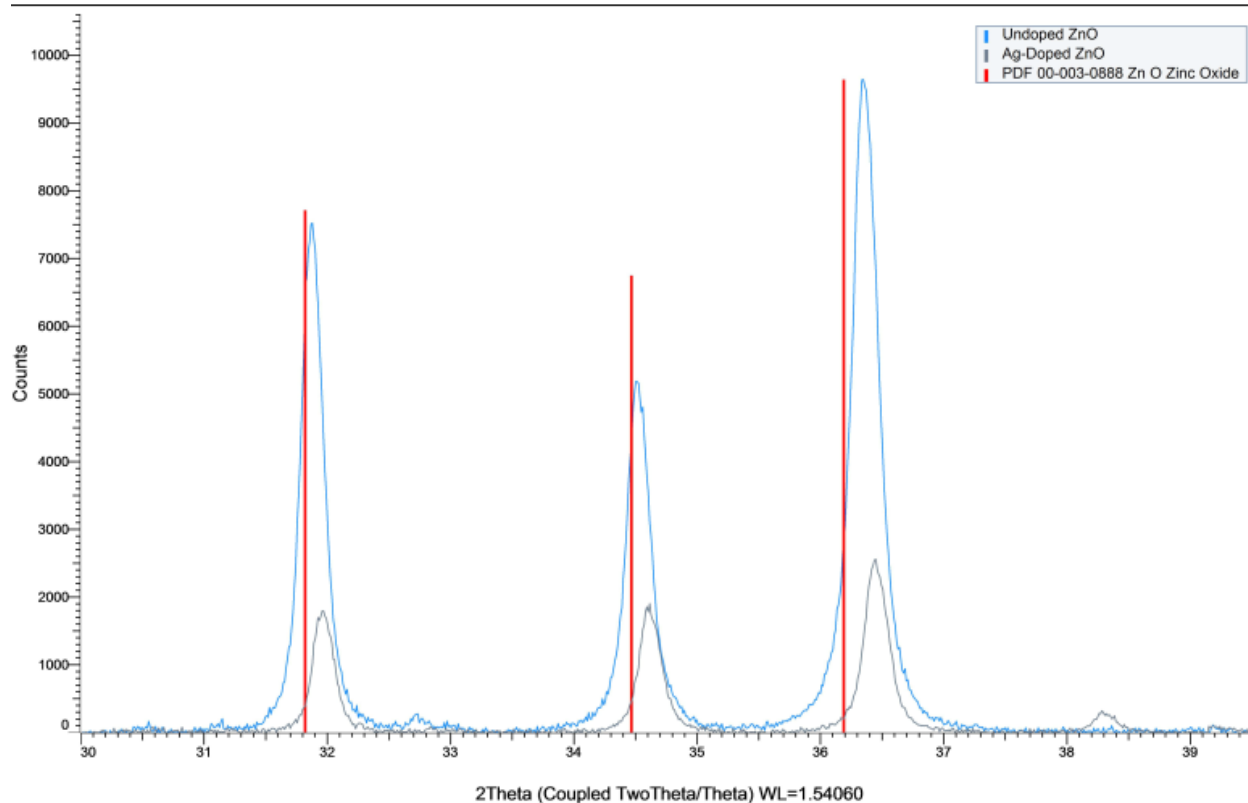


Figure 2-6. XRD spectra of Project D preliminary silver-doped and undoped ZnO films. Doped films (black line) tend to exhibit lower intensity and slight shift to the right compared to undoped ZnO films (blue line), although this formulation has resulted in less (002)-preference than other experiments.

The apparent success of this initial doped solution offered proof of concept that AgNO_3 could be incorporated into ZnAc solutions to yield ZnO thin films. The composition of the solution was known to include elemental silver, so no attempts were made at this point to quantitatively verify the silver concentration. Encouraged by this success, a more rigorous doping protocol was envisioned, continuing in the effort to replicate the Touam findings by adjusting dopant concentration as the primary variable. Table 2-3 illustrates four solutions that were formulated, representing 1-4 at% silver concentration. No additional undoped control sample was prepared in this case, as an undoped batch had just been produced and characterized.

Experimental:

In the interest of focusing on consistency of silver dopant concentration above precise ZnAc molarity, this experiment was initially formulated with a standard AgNO₃ solution, volumetrically separated, and ZnAc added gravimetrically to each sample subsequently, in proportional concentrations indicated on Table 2-3, above. MEA stabilizer was added dropwise to each solution separately, measured by recording each solution's mass change, and yielding r-values between 0.87 – 0.98. Solutions were covered and stirred with magnetic spinvane on a hotplate at 60°C for 1 hour, then transferred to lab drawer for 24 hour aging.

Solution ID (5mL aliquots)	mol AgNO ₃	mol Zn	at% Ag:Zn	Combined salt [SZO] M
G1	3.850E ⁻⁰⁵	3.718 E ⁻⁰³	1.035%	0.751
G2	7.700E ⁻⁰⁵	3.684 E ⁻⁰³	2.090%	0.752
G3	1.155E ⁻⁰⁴	3.647 E ⁻⁰³	3.167%	0.753
G4	1.540 E ⁻⁰⁴	3.611 E ⁻⁰³	4.265%	0.753

Table 2-3. Project G doping concentration table. Generally, the same molar ratio of zinc atoms ('mol Zn' column) are mixed with differing concentrations of silver (mol AgNO₃ column) to yield different silver-zinc atomic ratios but nearly identical total metal salt molar ratio.

Triplicate slide samples were engraved, cleaned with soap and water, bathed in dilute nitric acid, rinsed with DI water and ethanol, then dried in furnace at 200°C for 10 minutes. Slides were removed from furnace and spin-coated (3000RPM, 30s) with 4 drops of solution per spin, then returned to furnace for appx. 10 mins. Spin-coat deposition was repeated 4 times per slide, then samples were transferred to 500°C furnace, annealed for 2-3 hours, and quenched in ambient air.

Results:

While the intention of triplicating samples was to verify reproducibility, logistical issues in transferring so many samples between a heat-plate and small tube-furnace resulted in inconsistencies in annealing time/temperature variables. The slides produced were mostly transparent, with moderate

cloudiness throughout the surface. Unlike previously fabricated samples, these doped samples also had light blue-black discoloration throughout the film, observed to be darker and more prominent as dopant concentration increased. This discoloration is understandable, as silver compounds are known to be a highly photoactive, and silver nitrate itself is commonly used to stain biological and organic samples. Indeed, throughout the project, the silver staining was helpful in identifying doped samples, and in confirming that silver was present in the samples. Due to other inconsistencies mentioned, samples for XRD and EDS characterization were selected based on optimal visual appearance and transparency.

X-ray Diffraction confirmed the presence of ZnO as identified by the three ‘signature’ peaks between $30-40^\circ 2\theta$. As discussed in the previous chapter, the middle (002) peak represents the preferred orientation, and the ratio of (002) to other peaks is seen to decrease with increased silver concentration (Figure 2-7).

Ag-doped ZnO by Dopant Atomic Percent

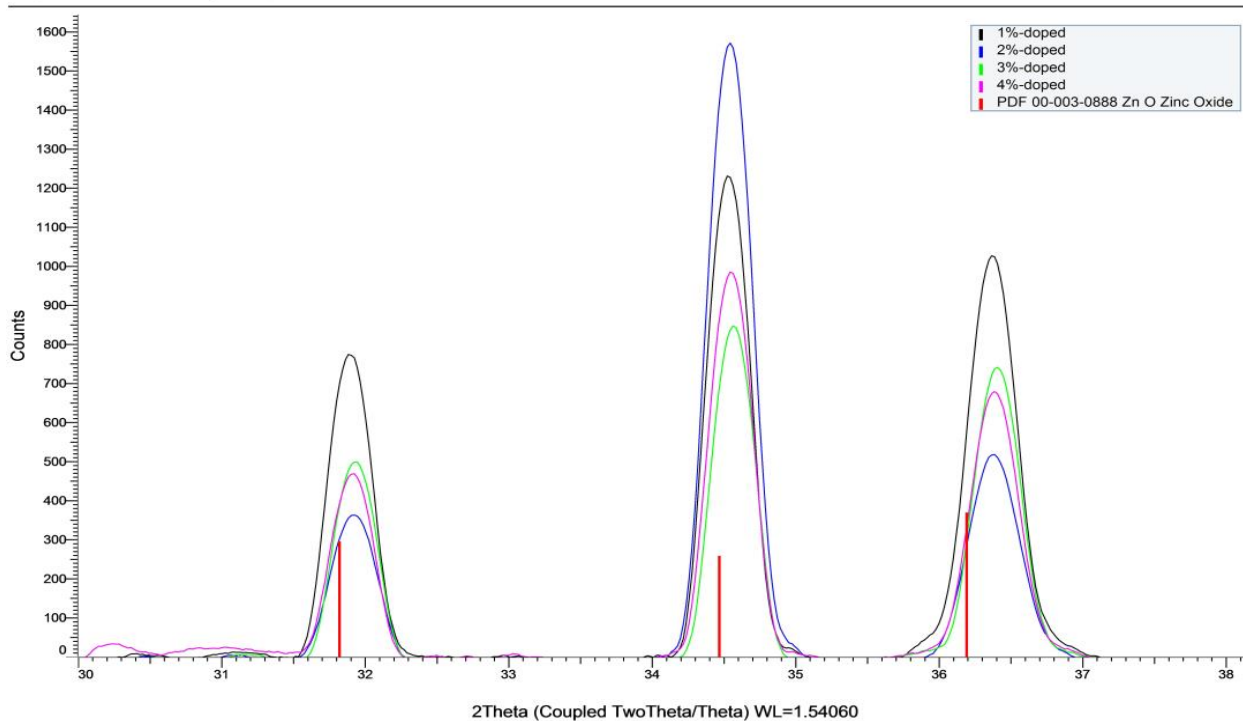


Figure 2-7. Comparison of XRD output for varying concentrations of silver-doped ZnO. Dopant concentration increases by appx 1% from bottom (black line, 1%) to top (green line, 4%).

EDS (Energy-Dispersive X-Ray Spectroscopy) characterization was performed to verify existence of elemental silver, and to confirm the stoichiometric ratios. While the EDS output did generally confirm increasing silver concentration within the samples, the calculated atomic percent did not align with theoretical dopant concentration, as shown in Figure 2-8. This is partially due to EDS detecting elements from within the glass substrate, and partially due to the miniscule quantity of silver in the sample to begin with. The 1%-doped solution, for example, is conceivably below the instrument's detection limit.

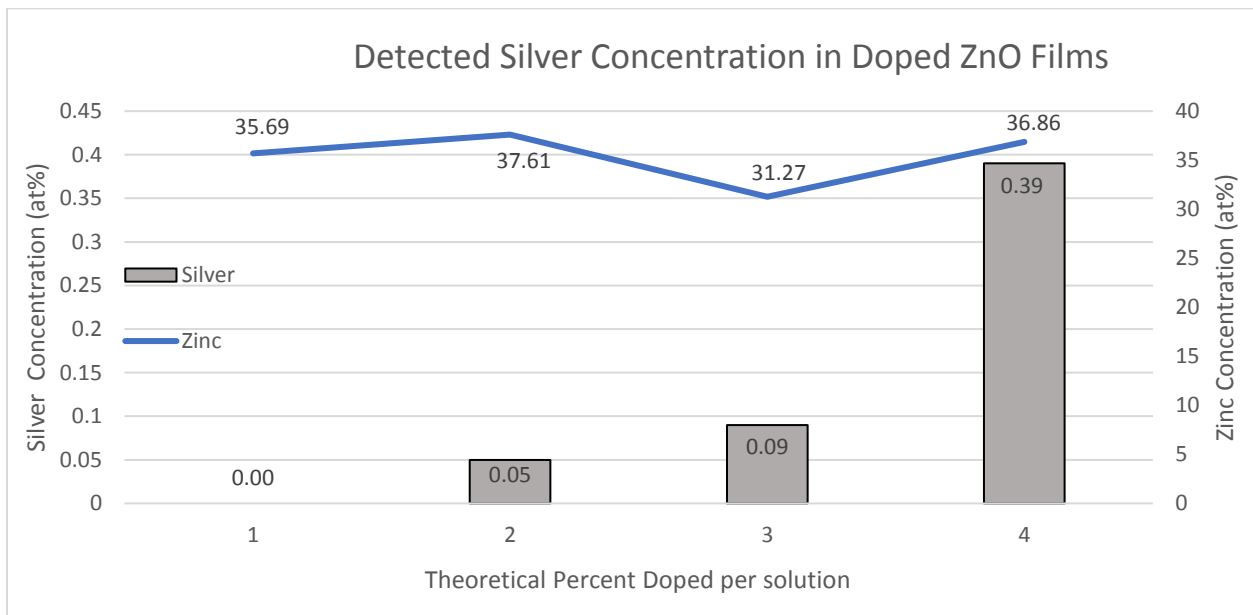


Figure 2-8. EDS-detected elemental proportions of silver in doped ZnO thin films. Blue line indicates EDS-calculated concentration of Zinc, indicating approximate error range.

2.2.3. (Project F) – Factorial Analysis of Aging and Time/Temperature

Having successfully replicated a silver-doping method and confirming the feasibility of the project's endeavor, we returned focus toward optimization of processing parameters for our ZnO films. Initial attempts discussed in Section 2.2 determined that MEA was a preferable stabilizer to DEA, and that the solutions should rest at least 24 hours before deposition, but thermal processing variables of temperature and time were still poorly understood and not well documented in literature. The Znaidi review reports 'pre-heat' temperature ranges from room temperature up to 500°C, and 'post-heat' treatments ranging from 150-900°C.

Beyond simply determining the ideal times and temperatures for our process, we also sought to examine any causal factors that could correlate time/temperature variables with film properties. To this end, a 'high/low' factorial analysis was devised to examine the roles of solution aging once again, pre-heat time and temperature, and post-heat time. Given the limitations of our furnace at the time, we were unable to perform the post-heat processing at temperatures greater than 350°C. (Sequentially, this experiment was performed prior to the doping experiment reported in the previous section, in which a furnace with higher temperature threshold was able to be used.) We have since determined higher post-heat processing temperatures to be the most important variable in fabrication of high-quality films but were unfortunately unable to factor that into this experiment.

A single standard solution would be made up, and eight samples prepared after solution aged 24 and 48 hours. Each iteration would test low and high values for pre-heat temperatures (220, 280°C), pre-heat time (30, 90 minutes), and post-heat processing (1, 3 hours) at 350°C. Once again, in retrospect, broader ranges would likely have returned more significant and actionable data.

Experimental:

Sample ID	Sol Age (hours)	Pre-heat Temperature (°C)	Pre-heat time (minutes)	Post-heat time (hours)	Sample ID	Sol Age (hours)	Pre-heat Temperature (°C)	Pre-heat time (minutes)	Post-heat time (hour)
F24.LL.L	24	220	30	1	F48.LL.L	48	220	30	1
F24.HL.L	24	280	30	1	F48.HL.L	48	280	30	1
F24.LL.H	24	220	30	3	F48.LL.H	48	220	30	3
F24.HL.H	24	280	30	3	F48.HL.H	48	280	30	3
F24.LH.L	24	220	90	1	F48.LH.L	48	220	90	1
F24.HH.L	24	280	90	1	F48.HH.L	48	280	90	1
F24.LH.H	24	220	90	3	F48.LH.H	48	220	90	3
F24.HH.H	24	280	90	3	F48.HH.H	48	280	90	3

Table 2-4. Project F time and temperature matrix. Sample coding sequentially indicates aging time, whether pre-heat temperature and time will be “hi or low”, and whether post-heat time will be high or low.

Solution was prepared to our current SOP, 0.72M ZnAc in ethanol with an MEA r-ratio of 0.8, stirred at 60°C for 1 hour, then aged in the lab drawer. Slides bathed in dilute nitric acid, washed with DI water, and rinsed with ethanol were dried at 220°C for 15 minutes, and spin-coated at 3000RPM for 30 seconds with 5-10 drops solution per coat. Slides were transferred to 220°C and 275-300°C ovens respectively for approximately 10 minutes between each of five coats, then left in their respective ovens for 30 or 90 minutes per table 2-4, above. Samples were removed from pre-heat furnaces and allowed to cool to room temperature, while post-heat furnace ramped to 350°C. Samples were annealed for 1 hour at 350°C, then 1-hour samples were removed, and oven was mistakenly turned off, with the second set cooling-down with the oven. These samples that should have been treated for a full 3 hours were re-annealed the next day for 3 hours at 350°C and air-quenched.

After the solution had aged 48 hours, the above process was repeated exactly as above, except that 3-hour post-heat samples were removed after 3 hours and air-quenched. Appearance of processed films is displayed in Figure 2-9, below:

Results:

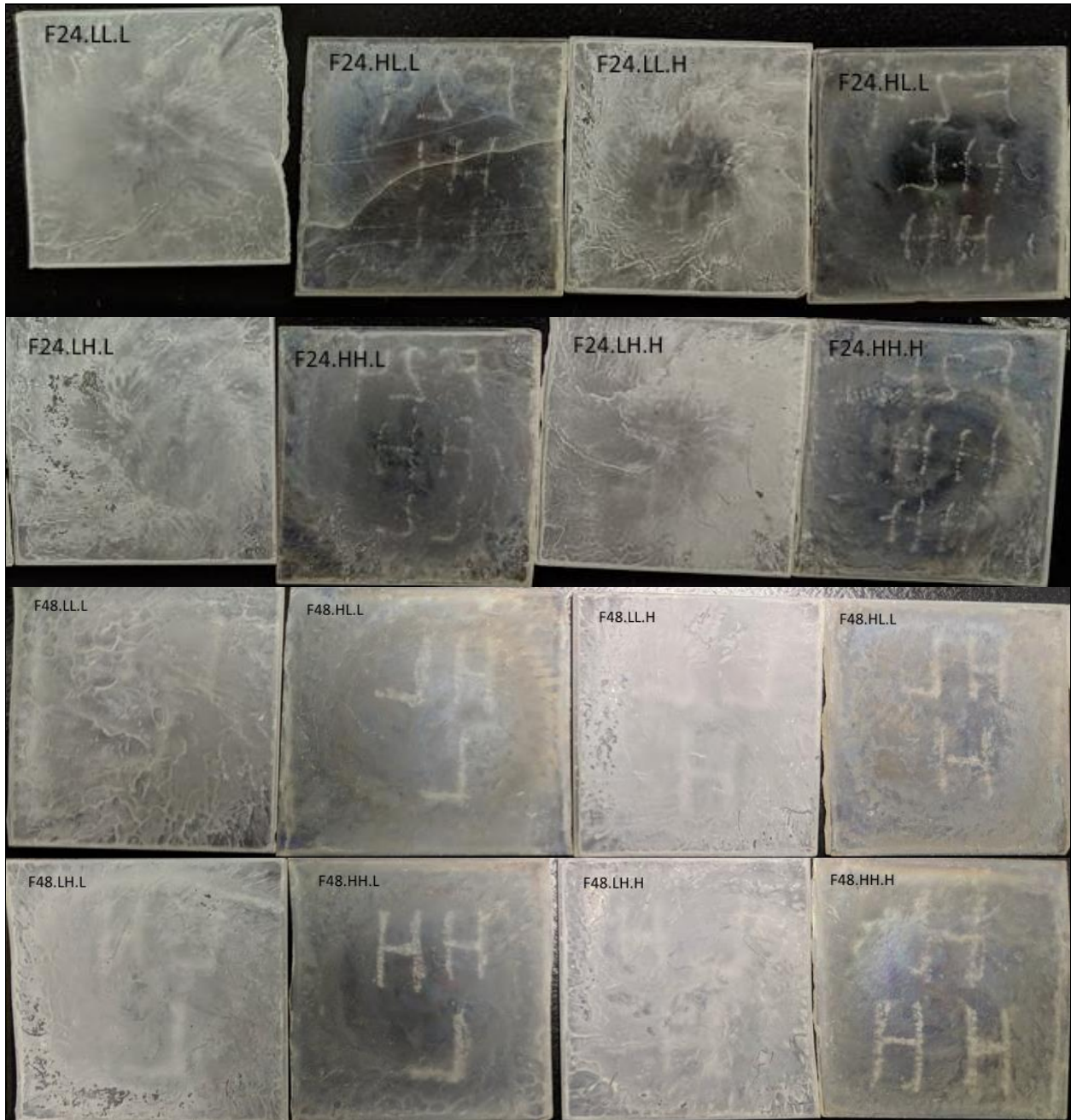


Figure 2-9. Appearance of slides produced in Project F. Increased opacity is observed in longer-aged samples, but generally improved transparency for samples exposed initially to higher pre-heat processing.

Processed films were generally cloudier than past trials, although the yellow discoloration observed in many prior experiments was mostly absent from these samples, with the exception of those aged 48-hours and pre-treated at 275-300°C. Photographs of the output slides are shown in Figure 2-8.

XRD analysis returned a host of complicated, seemingly counterintuitive and contrary results, which are analyzed and discussed at length in Chapter 2.7. In general, samples aged 24 hours and initially dried at higher temperatures showed greater peak intensity and preferential orientation (figure 2-10), whereas 48-hour aged samples tended to have lower intensity and poorer (002)-ratio (figure 2-11).

24-hour Aged

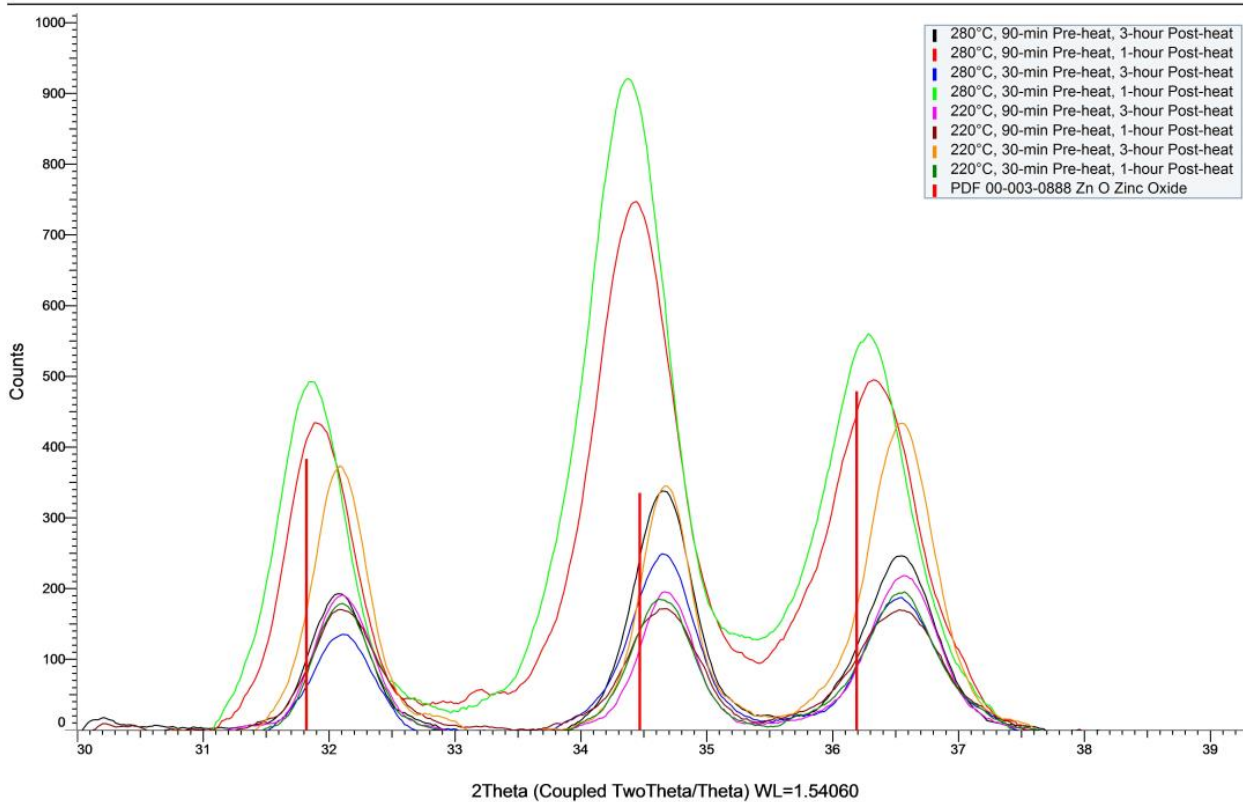


Figure 2-10. XRD spectra of Project F samples aged 24 hours. Greater peak intensity and 002-preferential orientation are observed in these samples than 48-hour samples, and those with higher initial pre-heat temperature also seem to be preferable.

48-hour Aged

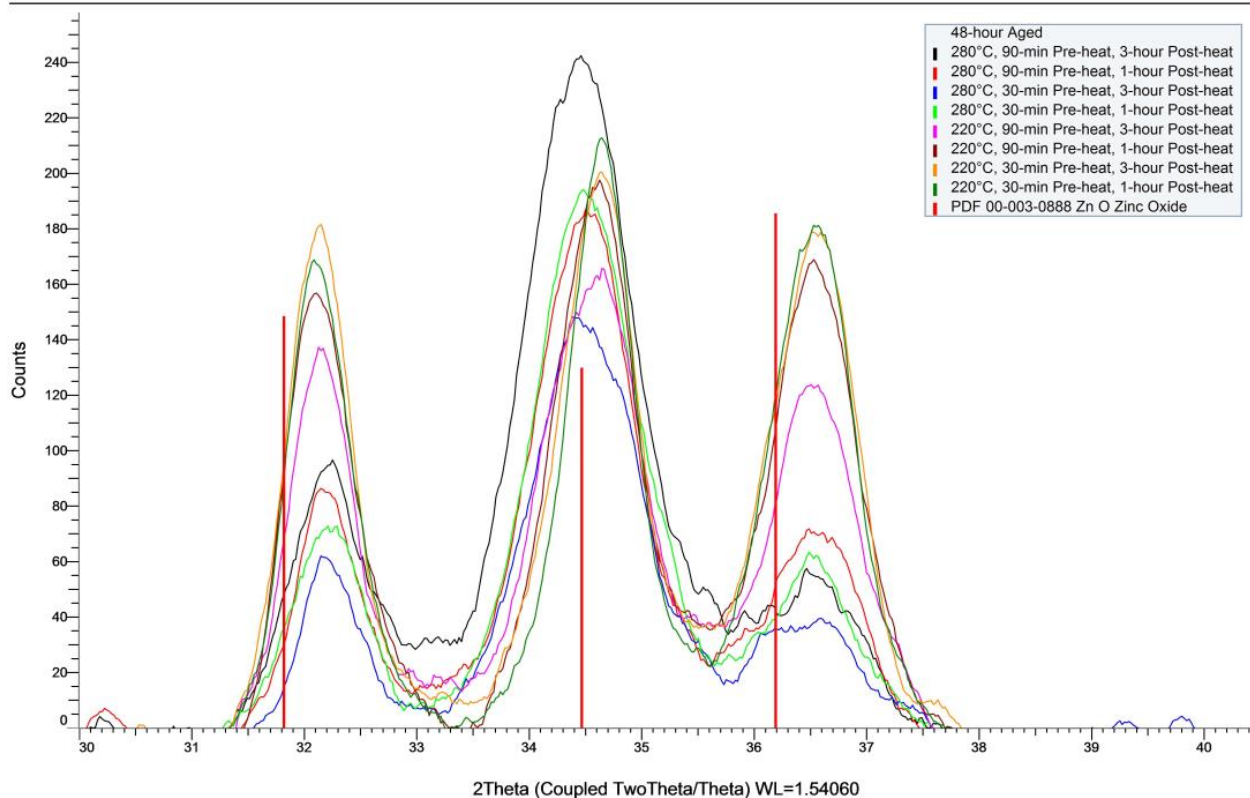


Figure 2-11. XRD spectra of Project F samples aged 48-hours. These samples show generally less peak intensity and unequal (002)-peak preferential orientation.

2.2.4. (Projects J & H) – Additional Heat Processing Parameters

While Project F's parametric analysis attempted to decode the causal factors behind time and temperature variation in the aging, pre-heat and post-heat processing of ZnO sol-gel, the results were inconsistent and inconclusive. Owing partly to equipment limitations, the 'high/low' factorial method did not have range enough to offer much useful information leading to a standardized SOP.

Having seen marked improvements in the quality of films produced when annealed in our new furnace capable of higher temperatures, our next trial focused on the pre-heat (drying) temperature while also further addressing solution aging as an interaction. An additional procedure was carried out in an attempt to replicate findings by Natsume & Sakata [33], in which films were subjected to thermal annealing between each deposition layer, rather than a single annealing after all coats had dried under normal pre-heat conditions, as shown in Table 2-5.

Experimental

Age	Expt. J				Expt. H
	70°C	100°C	150°C	200°C	80°C
24-hour Aged	J.1.1-1	J.1.2-1	J.1.3-1	J.1.4-1	–
	J.1.1-2	J.1.2-2	J.1.3-2	J.1.4-2	
48-hour Aged	J.2.1-1	J.2.2-1	J.2.3-1	J.2.4-1	H.2.1-1
	J.2.1-1	J.2.2-2	J.2.3-2	J.2.4-2	H.2.1-2

Table 2-5. Variable naming matrix for Projects J & H. Additional experiments were carried-out but were not accurately recorded.

Solution J was prepared per SOP to a ZnAc concentration of 0.75M and r-ratio around 1, mixed at 60°C for one hour, then aged. Slides were washed in dilute nitric acid, rinsed with ethanol, and dried at 100°C for 10 minutes. Deposition of 3-4 drops on spin-coater at 3000RPM for 30 seconds, then pre-heat treated at the temperatures above for 10 minutes, then repeated for total of four coats. All slides were then annealed together at 500°C for one hour.

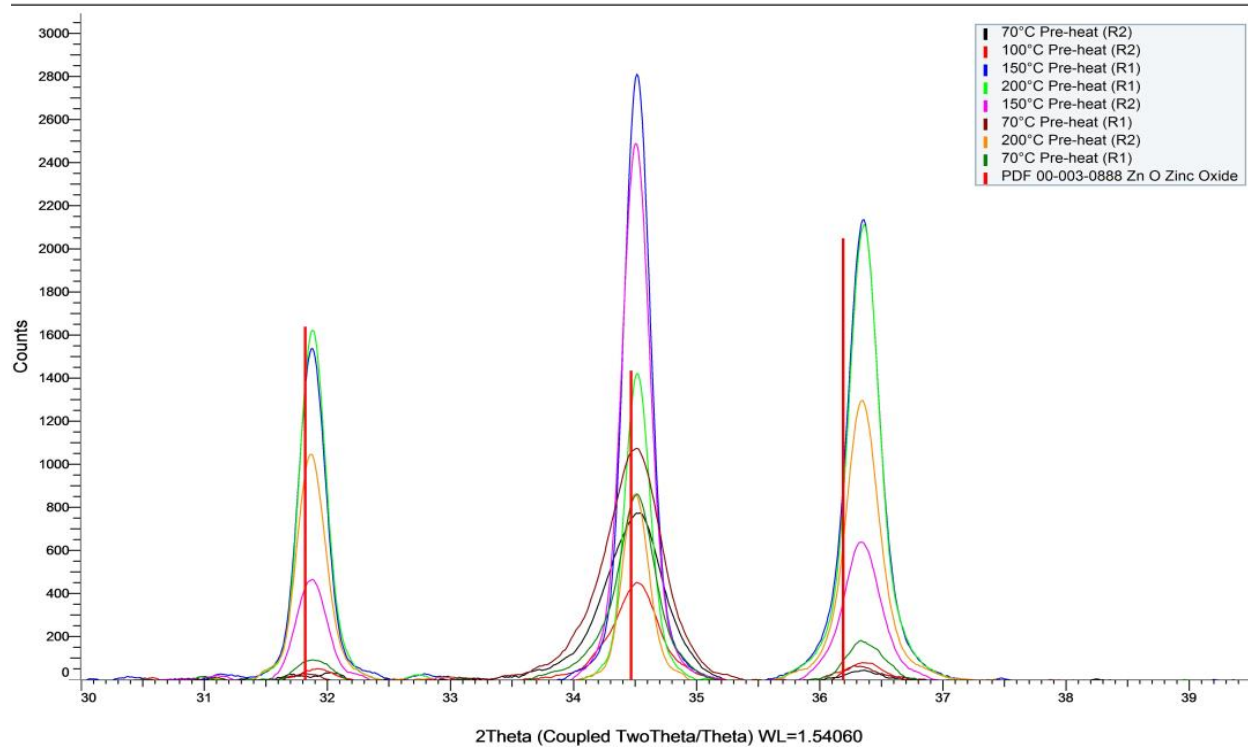
Solution H was likewise prepared per SOP to ZnAc concentration of 0.75M and r-ratio of approximately 1.2, stirred one hour at 60°C and aged covered in lab drawer for 48hours. These samples were prepared as above, but dried and pre-heat treated at 80°C for 10 minutes and annealed at 500°C for 20 minutes between each coat, for a total of five coats. Although it appears that samples identified as H.1.1 through H.1.7 were also fabricated, records of what these trials represented were lost, so the only valid data are for the two samples noted above.

Results

In general, solutions aged 24-hours demonstrated superior preferred (002)-orientation ratio compared to 48-hour aged samples (Figure 2-12). Of these 24-hour aged solution samples, those treated at 150°C showed highest peak intensities and (002)-preferred orientation, where samples aged at 200°C seemed to mirror PDF peak-ratios. Solutions aged at lower temperatures also have significantly-reduced (100) and (101) peaks, although their overall intensities are greatly diminished.

Samples from Project H yielded intense peaks and preferential peak ratios, indicating annealing between coats may be effective, but with no control sample or documentation of early trials, little can be positively deduced. Findings from this experiment are further analyzed later in this chapter, and the method of annealing between coats is re-examined in Section 3.2.4.

24-hour Aged



48-hour Aged

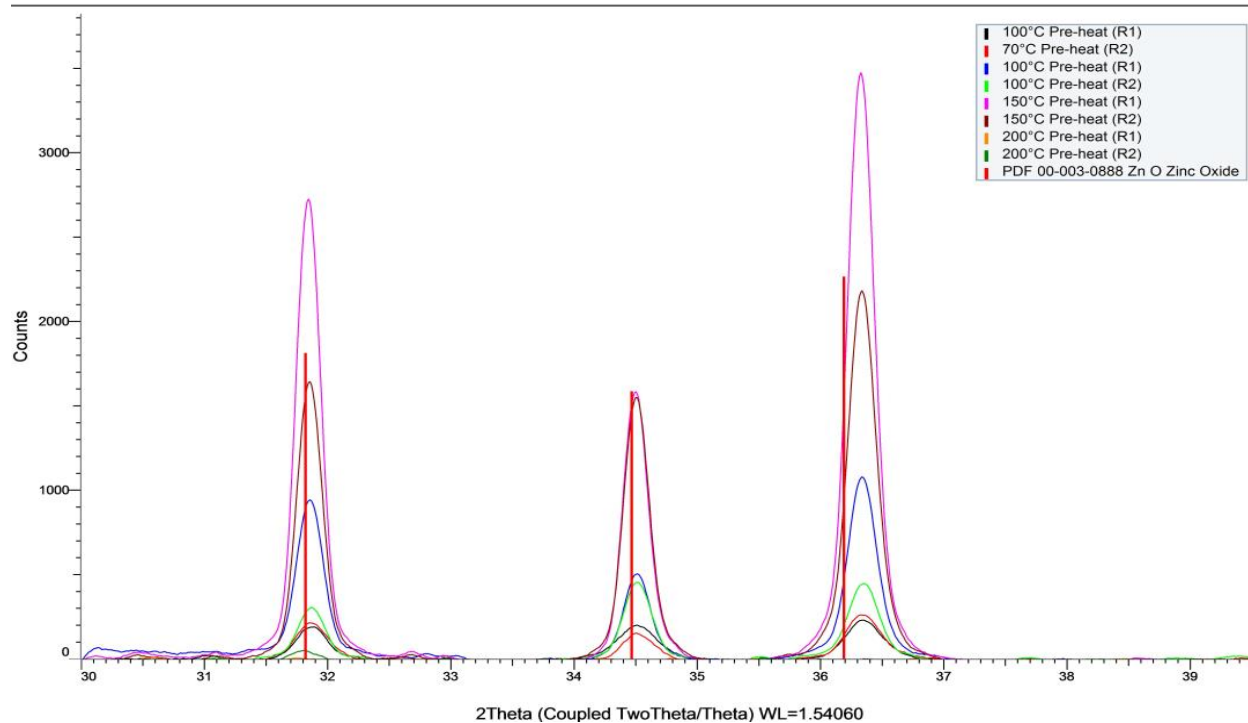


Figure 2-12. XRD Spectra of Project J Trials aged 24- (top) and 48-hours (bottom). Of solution aged 24-hours, samples pre-heat treated at 150°C (blue and pink lines) show preferred (002)-peak ratio compared to samples treated at higher and lower temperatures.

2.3. Analysis and Discussion

The experiments described in this chapter are representative of a profound and rather unique learning process that our working group was embarking upon, in a field of wet-chemistry processing that none of us were familiar with, and we had few sources of experiential knowledge other than literature review. While many masters' research projects are performed under the strict control and direction of a faculty advisor, Dr. Abu-Zahra gave us wide berth in choosing the subjects, methods, and direction of our research. This academic freedom has been subjectively greatly beneficial as a pedagogical approach for learning research methods such as scientific process, experimental design, project management, and countless other lessons, although the tradeoff for this style of advising was that we did not have access to a subject-matter expert, and therefore had no easy way to debug stalled or failed experimental obstacles.

Given this lack of experience and know-how, many of the hard-won conclusions and answered questions of the first half of this project were later found to be answered in extant literature. While this portion of the project did not, in fact, produce much by way of new findings or novel results, many of our experimental results may now serve to confirm previous findings, and more importantly, have given us the experience to establish a standard operating procedure of best practices for our application, from which further experimental activities have been based.

In the interest of completeness, comparative X-ray Diffractograms for all experiments discussed in Section 2.2 have been included in Appendix B. They may be referenced in the discussion herein but are generally not re-printed.

2.3.1. Precursor Solution

Solvent

The use of alcohol solvents (defined as organics whose primary functional group is one or more terminal hydroxide, e.g. R-OH,) in ZnO sol-gel chemistry has been widely discussed, both by the Znaidi review and countless other studies which do not warrant specific reference. In general, primary alcohols' most important attribute in sol-gel solubility is its dielectric constant, which is largely dependent on the number of carbons in its organic chain. Given the ubiquity and low-toxicity of ethanol compared to methanol, it is by far the most used solvent, and generally considered the most optimum for use in this sol-gel chemistry. The only other solvent reported in the review was 2-methoxyethanol, also called ethylene glycol monomethyl ether (EGME, Table 3-6), which is not generally used because of its high toxicity [16]. In Section 3.2.5, we report on the use of propylene glycol methyl ether (PGME,) an alternative to EGME proposed by Tseng et al [34]. Meanwhile, the results of our experiments in Chapter 2 give us no reason to propose a solvent other than ethanol for use in our SOP.

Stabilizer / Ligand

The Znaidi review also goes in to significant detail concerning the use of amine ligands as stabilizers in the systems of equilibria that take place within the sol. While the review does mention some publications in which other additives are used to modify the pH of the solutions, by far the most common additives used were DEA and MEA amine ligands (see Figure 2-3), and these were the only additives investigated in our experiments.

Project "A/B" discussed in Section 2.2.1 is the only applicable experiment to our determination of utilizing MEA exclusively as our stabilizing ligand. As shown in Appendix B: Experiments A/B,

comparison of XRD output from samples treated with equal molar ratio of DEA and MEA, those treated with MEA showed significantly improved (002)-peak ratio to other crystal reflection planes, where DEA samples generally showed peak ratios equal to the PDF literature data. These findings remain consistent despite aging and covering (evaporation, mass-loss) treatments, which demonstrated changes in peak intensity, but not preferred orientation ratios throughout the study.

Our findings are consistent with Znaidi's previous work and summary conclusions in the review document, and our SOP has been adjusted to include the use of MEA as stabilizing ligand.

The molar ratio (so-called '*r*-value') of the amine ligands to Zn(II) ions is broadly reported between 0-2 in the review. While one Znaidi publication reports unsurprising improvement in (002)-orientation by increasing MEA *r*-ratio from 0 to 1 [15], another notes that (002)-face dominates XRD spectra as the *r* value is moved toward 2:1 MEA to zinc. Intuitively, we can consider that in a perfect solution system, MEA would act 50% as a bidentate ligand with a 1:1 zinc partnership, and 50% as a bridging ligand between two zinc ions (see Figure 2-3). Imagining a Boltzmann distribution of such a system, we would see the peak at around 1.5 MEA to Zinc. Additionally, as amines are generally basic in nature, solution pH tends to increase with *r*, which was shown by Sagar et al to inhibit uncontrolled hydrolysis reactions and promote ZnO formation [35]. While nearly all experiments in this study utilized a 1:1 *r*-value, we propose that a value between 1.5-2 is more appropriate for future SOPs.

Doping

As we approached early attempts at doping, including Experiment D (Section 2.2.2), we were unaware of any previous attempts to implement silver doping in sol-gel chemistry. However, continued literature review showed us that Touam et al had apparently achieved success in using sol-gel to synthesize silver doped ZnO (SZO) thin films in atomic concentrations from 1-5%, but chose to focus on the effects of doping on resistivity of films, rather than p-type character [32]. The Touam paper identified a number of other studies that carried-out silver doping in ZnO through sol-gel processing, although none of them confirmed p-type character either [36]–[38]. Touam’s justification for focusing on resistivity rather than p-type character was explained by indicating that the studies, incorporating various SZO fabrication methods[36]–[56], all tended to focus on p-type character, although closer inspection of these papers indicate only four studies attempting to confirm p-type conductivity [37], [39], [42], [51], with only one study making a compelling case that it was achieved [51].

In Project G’s effort to replicate the Touam findings, dopant concentrations of 1, 2, 3, and 4 atomic percent silver to zinc were attempted. As shown in Figure 2-7, samples doped with 2 at% silver showed highest peak intensity and (002)-ratio. This finding conflicts with Touam’s observation that, “peak intensities of the Ag-doped ZnO thin films increase when silver content were increased from 1 to 5 at%.” Since Touam’s actual XRD values are not available, a simplified peak height comparison was performed by approximating baselines for each XRD signal, then measuring peak height (in pixels) for (002) and (102) peaks, as shown in Figure 2-13. These peak intensities are tabulated and compared in Table 2-6, and degree of preferred orientation calculated per the Lotgering method [57]. Essentially, the proportion by which the (002) peak intensity is greater than the sum of all crystalline peaks (in this case, only (002) and (102), as the (100) cannot be discerned,) are compared

to the “Pure ZnO” intensities. This method of quantification paints a very different picture than Touam’s explanation, indicating 2at% silver doping offers the greatest improvement in crystallinity and preferred orientation, and in agreement with our findings.

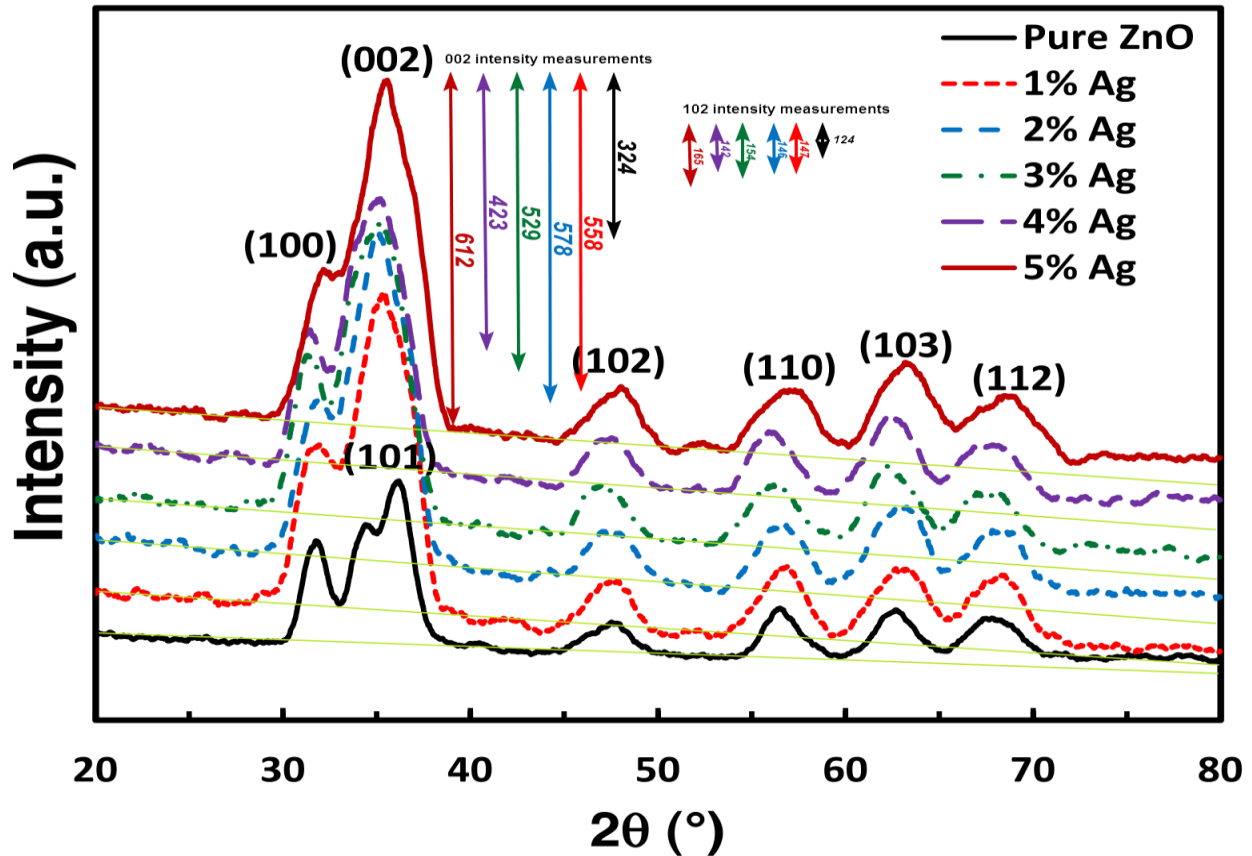


Figure 2-13. Simplified XRD peak intensity of Touam’s findings. Yellow baselines were drawn and arrows marked “002 intensity measurements” were drawn from (002) peak to baseline for each XRD spectra shown. (102)-peaks were measured similarly and evaluated in Table 2-6.

	102 peak intensity (pixels)	102 peak %relative intensity	002 peak intensity (pixels)	002 peak %relative intensity	Proportion 002 intensity	Degree of 002 orientation
Pure ZnO (standard)	124	100%	324	100%	0.723214	0%
1% Ag	147	119%	558	172%	0.791489	25%
2% Ag	146	118%	578	178%	0.798343	27%
3% Ag	154	124%	529	163%	0.774524	19%
4% Ag	142	115%	423	131%	0.748673	9%
5% Ag	165	133%	612	189%	0.787645	23%

Table 2-6. Touam’s peak intensity ratios calculated by intensity rather than area under curve, but otherwise following the formula laid out in Section 3.3.1.

During the experimental period of this phase of the project, attention was placed on rapid development of our SOP, utilizing the quick and simple process of XRD evaluation to make decisions on how to proceed – all with the assumption that more rigorous characterization procedures would be developed as the project progressed. Those more advanced characterizations have indeed taken place as we've moved to the later phase (Chapter 3), but given the advances made in the later stage, we have not considered it necessary to go back and characterize early doping attempts further. Given the relative ease with which silver was added to sols, and our process's conformation to literature on the subject, we consider the procedure discussed in Section 2.2.2 to be successful in its doping endeavor. Chapter 3 further addresses p-type conductivity, so that aspect is considered beyond the scope of this optimization effort.

Concentration

Concentration of the precursor salt in the sol is suggested by the Znaidi review to be highly influential on the degree of c-axis orientation, although values reported in it range from 0.02 – ~2 mol/L; most literature report using 0.75M. While the review generally shows concentrations between 0.3 – 0.6M to cause preferential c-axis orientation and higher (~1.3M) concentrations to yield a-axis (100) orientations, these reports are significantly confounded by solution aging variables [16].

Experiments performed after A/B stabilizer trials and baseline doping (expt. D) were all set to 0.75M precursor salt concentration, allowing the majority of experiments in this chapter to be compared to one-another, independent of the concentration variable. Later-stage literature review ultimately drove us to modifying the SOP toward lower starting concentrations[58], also discussed in Chapter 3.

Aging

Among all of the experimental variables examined, solution aging parameters were the most difficult to individuate from other parameters or determine as concrete causal factors in film quality and are also the least understood in literature. For better or worse, solution aging was considered as a factor in many of our studies, although this is partially a matter of logistics: there is a limit to the number of samples that can be deposited and treated in one day, so many of our studies took place over more than one day. In these cases, solution aging time was considered not so much as a causal factor, but a relevant changed variable to be considered.

The Znaidi review identifies a number of studies in which conflicting information is reported on the effects of aging on the preferential axis of deposited films, although in some cases these conflicting findings come from studies using significantly different chemical systems than the ZnAc/MEA/Ethanol system we prefer. In Znaidi's own studies, preferential c-axis orientation was observed in most concentrated and dilute systems, but when dilute (0.05M) solutions reached 72-hour age, (100)-peak reflection took over and individual square crystals were observed on the surface of films [15], [21].

The two primary experiments we conducted that focus on solution age as a significant factor in film quality are A/B (Section 2.2.1,) in which aging is contrasted with stabilizer identity, and experiment F (2.2.3,) in which aging is considered alongside heat-processing parameters, discussed below. Diffractograms from experiment A/B are compared by aging time in Appendix B-2AB, pages 4-6. Comparison of these graphs show (002)-preferred growth at 18-hours, followed by less intense, but still generally improved (002) ratio at 24 hours. The solutions aged 42 hours seem to revert to peak ratios more closely matching PDF values, while solutions aged 48 hours and more then display (002)-preferential peaks and greater intensity. The discrepancy in the 42-hour sample may be related

to systemic experimental error at that stage of the experiment, or it may speak to reaction kinetics in the sol aging process. Further comparison of 24- to 48-hour aged solutions can be seen in Appendix B-2F, page 1, where all heat treatment variables are compared on separate graphs. Since successful c-axis oriented films have been repeatedly produced using solutions aged from 24-72 hours in these and other experiments, and literature does not seem to definitively indicate aging being of greater importance than stabilizer and solvent concentration, no further attention shall be paid to this factor, other than to include in the SOP that solutions be aged at least 24 hours prior to deposition, and be used no later than 72 hours after.

Other

Finally, the only other solution-related variables that were considered in this phase of the project were viscosity and mass loss in Project A/B. Given the low viscosity of organic solvents and our knowledge at the time of the gelation mechanism of the sol-gel, it seemed intuitive that the change in viscosity of the sol during the aging process may be a factor in its ability to adhere to the substrate, ultimately effecting the quality of the films. With no easy way of measuring the viscosity of a solution before deposition, we recorded the change in mass of covered and uncovered solutions in order to track evaporation of solvent. Analysis of the XRD spectra from this experiment (Appendix B-2AB) does not reveal correlation between covered and uncovered solutions, and preferential orientation or film quality: in some cases, uncovered solutions seem to have improved certain samples, while other cases seem to cause deleterious effects in XRD peaks (e.g. 24-hour aged Uncovered DEA treatment). Later attempts to thicken sols with viscous but presumably miscible alcohols such as ethylene glycol resulted in poorly-formed films, and this line of inquiry was terminated. SOP has since been to keep solution flasks covered while storing and aging.

2.3.2. Processing Parameters

Spin-coating

Spin-coating of material precursor onto substrate media is a simple and easy deposition method used ubiquitously in thin films fabrication. While other processes such as dip-coating and spray methods are also used, they tend to be more effective in scaled application and industrial use, where spin-coating allows rapid application and process progression. The two major variables in spin-coat processing are RPM of the spinning chuck, and duration of the spin process. While manipulation of these variables was attempted in early trials, continued literature review indicated that spin conditions of 3000 RPM and 30s spin times were nearly universal in ZnO sol-gel processing. The only pertinent factor in modification of spin parameters is the relation between film thickness (t) and the angular momentum (ω) of the spinning substrate, $t \propto (\sqrt{\omega})^{-1}$ [59]. We concluded that our SOP would use the parameters above in all trials and experiments unless film thickness was to be modified.

Slide Cleaning

While not the subject of a specific experiment, slide cleaning procedure developed as the project progressed, from simple soap and water cleaning to acid bath and various drying techniques. One significant discovery was that slides physically scrubbed with just gloved fingers in Alconox soap-water prior to acid wash and drying delivered significantly improved film clarity and overall quality. Additionally, slides dried at around 200°C either in an oven or on a hot-plate, and then coated immediately at this elevated temperature also tended to result in improved film quality.

Pre-Heat Treatment

As discussed in Section 2.2.3, heat processing steps were initially a source of great confusion, given the wide temperature ranges reported. Znaidi points out a fundamental maxim that pre-heat (drying)

temperatures need to be above the BP of the solvent, and suggests that pre-heat treatment at 300°C is appropriate for 2-methoxyethanol (BP: 124°C) solutions [16]. In a set of experiments with isopropanol as a solvent (BP: 82.6°C), Raoufi and Raoufi point out that the thermal decomposition of ZnAc occurs at 240°C, and therefore use 250°C as their pre-heat temperature [60]. Similarly, Kim et al. showed optimum (002) ratio at 275°C pre-heating with 650°C post-heat conditions [61]. Ethanol has a significantly lower BP (78.37°C), indicating that temperatures above 100°C but below 300°C may be appropriate.

The technical deficiencies of experiment F was discussed in Section 2.2.3, and while not all of the experiment's results are useful, examination of the samples pre-treated at 280°C generally show greater peak intensity and better (002)-ratio than those treated at 220°C (Appendix B-2F, page 2). No significant differences in film quality can be seen between the samples treated for 90 minutes versus 30 minutes (Appendix B-2F, page 3,) which makes sense when considering that the pre-heat treatment is intended to remove by evaporation or decomposition, solvents and organics in the deposited layer: glass substrates and thin films will reach equilibrium temperature with the oven or heat plate within minutes of exposure to the heat source, and additional time at this comparatively low temperature will not result in any further improvement. While higher pre-heat temperatures may be advisable, a 200°C hot plate was found to be sufficient to evaporate solvent in the majority of our experiments and continued to yield high-quality samples in later-stage experimentation.

Post-Heat Treatment (Annealing)

Continuing on the analysis of Experiment F, we find that the limitation of our furnace at that time essentially renders experimental findings on this subject useless. Literature review and subsequent experiment has revealed that higher-temperature processing steps are almost always preferable. (N.b. *sintering*, *annealing* and *carburizing*, are terms sometimes used interchangeably in the context of sol-gel

post-heat processing, although other sources identify them as distinct and separate processes [34].) The majority of studies cited as most similar to our process reported optimized (002)-orientation at 500°C, including the Raoufi study that showed film quality declining at 600°C and above [32], [34], [60], [62]–[64]. In subsequent experiments, certain substrates were found to deform at temperatures above 550°C, so the SOP generally calls for post-heat treatment between 500-550°C.

2.3.3. Conductivity and Surface Morphology

Throughout this phase of the project, our ultimate goal was to synthesize conductive ZnO thin films, and to achieve p-type conductivity in doped samples. While some electron microscopy was carried out in the course of this part of the project, examination of films' surface features and morphology was not yet part of the research paradigm, and only surfaced as a topic of interest as conductivity was explored. Beyond what is published herein, many months' work of characterization efforts and subsequent experimental trials were devoted to film conductivity, including informal multimeter probing, 4-point probe testing, and modification inclusion of conductive elements into film fabrication techniques. None of these efforts achieved their purpose in confirming p-type character, or in showing our films to be conductive at all.

Our primary method of testing films was with a 4-point probe (Figure 2-14,) in which two outer electrodes apply a voltage between them, causing a current to flow within the sheet surface. The two inner probes measure voltage being passed between them, by which sheet resistivity is calculated as a function of these voltage and current measurements between electrodes [65].

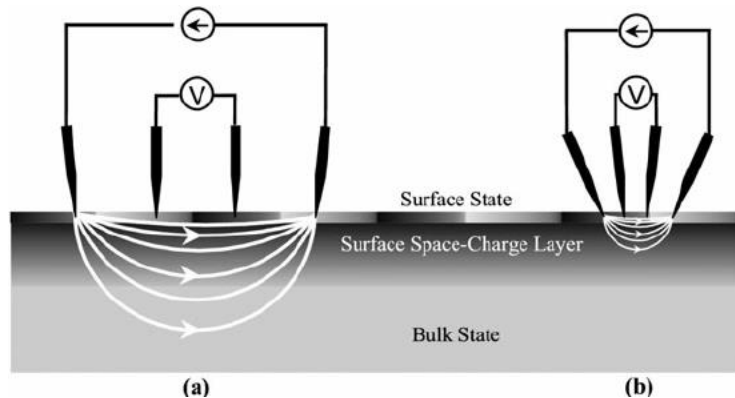


Figure 2-14. Sheet resistivity measurement by four-point probe. As described above, potential is measured across a line between which current is already being passed (a), a more compact apparatus is shown (b). *Source: Hasegama [66]*

While 4-point measurement is generally considered a sound method for quantifying sheet resistivity, it measures current laterally across the film. As discussed in Section 1.4, conduction in ZnO occurs through the c-axis, which is oriented perpendicular to the substrate plane. It may be that

surface conductivity is simply the wrong method for quantifying the conductivity of c-axis oriented ZnO thin films. Additionally, ZnO is an intrinsic wide-gap semiconductor: its native character should more closely resemble an insulator, and theoretically, it would not be conductive unless assembled into a p-n junction. Despite these considerations, Touam's study – one we repeatedly sought to replicate – reported successfully 4-point measurements below $0.05 \Omega \cdot \text{cm}$ on doped and undoped ZnO thin films.

With our inexperience in electronic characterization techniques and only superficial input from electrical engineers during this project, it is possible or even likely that our failure to confirm conductivity in our samples was due to a trivial but fundamental error in our characterization efforts. Indeed, with so many other indications that our synthesis technique was working, it seems unlikely that we were somehow able to fabricate films that have all of the characteristics of ample ZnO thin films in literature, with our films' lack of conductivity being the *only* nonconforming property.

These failures led us to investigate other potential sources causing the films to be non-conducting, and ultimately to our observation of cracking, peeling, and other surface features revealed by SEM analysis. Remediation of these surface features became the main impetus behind the processes and breakthroughs of Chapter 3.

2.3.4. Final SOP

The SOP was developed as an ongoing process through all the experiments and analyses discussed in this chapter and was, therefore, a 'living document' through much of the process. The following represents the version of the SOP at the time of this final analysis, so subsequent chapters may not have followed this procedure exactly. This final procedure combines confirmed findings from the analysis of experiments carried out in Chapter 2, from literature review, and from learned best practices. While this particular SOP is scaled toward small-volume (5-10mL) solutions, it is easily scaled with simple stoichiometry and larger glassware. For example, larger solutions would be necessary to accurately measure silver nitrate for exact dopant concentrations, as single milligram portions are difficult to work with.

Solution: All lab glassware is cleaned with Alconox, rinsed with DI water, and dried with acetone. Generally, 25-mL Erlenmyer flasks are used as the reaction vessels, to which 5mL 200-proof ethanol is added volumetrically. To this, 0.823g zinc acetate dihydrate is added to a concentration of 0.75M*. Reaction flask is placed on balance and tared, then MEA is added dropwise to appx 0.45g, (r -ratio ≈ 1.5). A magnetic spinvane is added, and if solution is to be doped, appx 0.001g silver nitrate is added (appx 1.5at% silver:zinc), then flask wrapped in foil to prevent light exposure. Flask is capped and placed on 60°C heatplate for 1 hour under magnetic stirring. Solution is transferred to a room-temperature lab drawer for aging at least 24 hours.

Substrate: Soda-lime glass slides (or other substrate) are cut, engraved, washed and scrubbed by hand with Alconox solution, rinsed with DI water, then placed in appx 3M nitric acid bath overnight. Slides are carefully removed from acid bath and rinsed in DI water with gloved fingers. Slides are then picked up with tweezers and rinsed first with cleaning-grade ethanol or isopropanol, then acetone. Slides are arranged deposition side up on a freshly foil-covered hot plate at 200°C for 15 minutes.

Spin-coating: Slide is carefully placed on spin-coater with clean tweezers and vacuum turned on. Spin coater is started at 3000rpm for 35 seconds, and no more than 1-2 drops are dropped appx 2cm above spinning substrate at $t=5s$. Slide is carefully removed and immediately returned to hot plate, at which point additional samples may be run. After at least 10 minutes have passed since first slide was returned to hot plate, deposition process is repeated to 6 total coats (or as determined by experiment).

Post-heat Treatment: Upon completion of appropriate number of coats, slides are transferred from aluminum foil boat to furnace-safe ceramic plate and placed in 500°C furnace for 2 hours or as long as prescribed by experiment. At the end of annealing time, furnace is switched off and allowed to cool to ambient temperature with slides inside.

* Subsequent literature review [58] has led us to favor 0.25M concentration for optimal (002)-orientation.

2.4. Conclusion

Through meticulous experimentation, trial-and-error, and extensive literature review, best practices and optimized Standard Operating Procedure for sol-gel synthesis of ZnO thin films were established, and fine-tuned for use in doping experimentation. While many experiments were flawed, and some altogether unsuccessful, the process of working through them and analyzing their results was ultimately instructive in familiarizing our group with procedural practices and pitfalls.

While silver doping was achieved and confirmed, p-type character and film conductivity were never successfully confirmed and remain a point of continued interest. Analysis and manipulation of films' unusual surface features are proposed for future study.

Although no fundamentally new or novel findings were documented, confirmation and findings contrary to other researchers' conclusions may be helpful and worthwhile in academic interest.

Chapter 3:

Effects of Substrate, Wetting, and Nanoparticle Layering on Preferred Orientation of Silver-doped ZnO Thin Films

3.1. Introduction

An optimized methodology for synthesis of silver-doped ZnO thin films through sol-gel processing has been established in Chapter 2. However, in comparison to undoped control samples, doped films produced by this process developed unexpected morphological features believed to contribute to unexpectedly high sheet resistivity. In addition to exploring the role of substrate identity in preferential crystal formation, improvised fabrication techniques were developed in efforts to improve preferred c-axis orientation of doped and undoped ZnO films. Heretofore unexplored surface wetting and layering techniques – and the incorporation of silver nanoparticles (AgNP) in these layering processes – were attempted, resulting in extraordinary improvement in the preferred (002) crystal orientation to expected polycrystalline peak ratios.

As progress was made in the optimization of doped and undoped film fabrication methods discussed in Chapter 2, results became more standard and repeated. Two major trends in surface morphology were observed from electron micrographs: ripples (Figure 3-1, Left), and ‘cracking’ discontinuities (Figure 3-1, Right). These aberrant features were observed in both doped and undoped samples but seemed to be more prevalent in doped samples. Concurrently, samples’ XRD spectra continued to return relatively short, broad peaks, indicating less-than-ideal crystallinity, and extempore 4-point tests suggested much higher sheet resistivity than expected. It was hypothesized that these unexpected morphologies may have been contributing to the unsatisfactory characterization results, and efforts were undertaken to mitigate their occurrence.

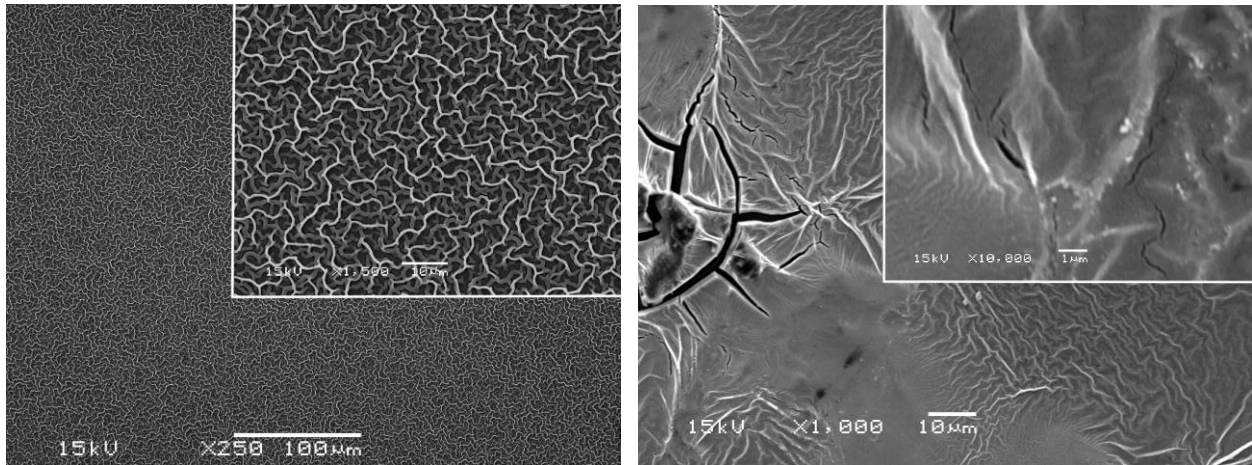


Figure 3-1. Aberrant surface morphology of Ag-doped ZnO thin films. (Left) Electron micrograph of continuous ‘rippling’ throughout sample at 250X and 1500X (inset). (Right) Discontinuous rippling, areas of smooth continuous surface, and visible cracks seen in certain areas (1000X) of other films.

As these morphologies were investigated both experimentally and in literature review, improved understanding of the causes of these surface features was revealed, including the revelation that the ‘rippling’ shown above is a common occurrence, sometimes cited as being beneficial to film conductivity, but also disruptive to semiconductor properties as discussed in Section 3.3.3.

These efforts to reduce cracking and discontinuities resulted in the development of new and heretofore unreported surface wetting techniques that have made dramatic improvements in film crystallinity and c-axis preferential orientation.

3.2. Experimental Narrative: Process, Methods, and Immediate Results

In following with the previous phase of this project outlined in Chapter 2, each major experiment was assigned a letter to distinguish its process and results from other experiments. This system was reset at “A,” and each iteration is generally now referred to as an “Experiment” rather than “Project” for this second phase of the project.

The cracked and rippled appearance of these unexpected surface features evokes images of dried riverbeds and the concept of rapid or uneven drying: the unequal contraction of one surface over another. In earlier experiments, exhaustive attention had been given to drying and cooling variables, taking into consideration times, temperature ramps, atmosphere, and various other factors that ultimately failed to show any significance in the quality of films produced. A factor that had not been considered was the thermal expansion differential between the ZnO film and substrate material. Although the Znaidi review indicated some variation in substrate identity from one study to another, the primary property addressed was crystallinity of the substrate itself, leading to epitaxial growth in films. Therefore, little attention had been paid to the substrate’s Coefficient of Thermal Expansion (CTE) in literature, and we felt this warranted study.

Visible cracks on the film are obvious impediments to electron mobility, and the ripples, we supposed, might also serve to interrupt, or at least extend the electron free path, leading to increased resistivity. As another possible mitigation measure, we devised to incorporate silver nanoparticles (AgNP) within the sol, expecting that particles of an appropriate size to fill the ‘gaps’ between cracks or ripples may serve to improve electrical conductivity of the films. The Experiment A, examining use of mica substrate and investigating proof of concept for the incorporation of AgNP into thin films is described in Section 3.2.1.

Following the apparent success of the AgNP ‘layered’ deposition process between ZnAc coats and observation of significant changes in morphology on differing substrates, further experimentation was required to confirm these findings. Additional substrate media, including low-CTE Borosilicate glass were acquired to more thoroughly investigate the effects of substrate identity on surface morphology. Given the purpose of this Experiment B in confirming previous findings, and in an effort to curb confounding externalities, the fabrication SOP was modified to more stringent processing parameters, including processing in a glovebox under inert atmosphere, along with a greater number of deposition coats with a lower-concentration of precursor solution, detailed in Section 3.2.2.

Having shown that application of AgNP dispersion between ZnAc precursor sol coats had a beneficial effect on both preferential orientation and sheet resistivity – as well as reducing cracking and rippling surface features – it was necessary to determine whether the presence of inter-layer nanoparticles was the causal determinant in improvement, or if the ethanol-diluted dispersion was merely acting as a wetting agent, ‘smoothing’ each coat between sol layers. Experiment C in Section 3.2.3 describes a protocol comparing controlled deposition of doped and undoped sol in untreated coats versus inter-layer deposition of both dilute NP dispersion and plain ethanol between coats.

In yet another effort to confirm layering and wetting process findings, an additional experiment was devised to examine the effects of inter-layer wetting by solvents of varying viscosities and polarities. Given these solvents’ differing properties, additional post-heating trials were introduced to observe the effects, if any, of high-temperature annealing between deposited layers. Experiment D, explained in Section 3.2.4, once again confirmed the positive effect of AgNP deposited between precursor coats, and offers further insight into the dynamics of wetting, drying, and annealing in ZnO sol-gel synthesis.

Finally, Experiment E was envisioned late in the writing stages of this project to investigate one further solvent, and to use factorial analysis to confirm the effects of the novel wetting method, described in Section 3.2.5.

Unless otherwise indicated, all samples were characterized by X-Ray Diffraction (XRD) using a Bruker D-8 Discovery instrument, using a $\text{CuK}\alpha 1$ source at 40kV and 40mA, with a wavelength of $\lambda=1.54\text{nm}$, scanning between $30 - 40^\circ 2\theta$ to examine primary ZnO (100), (002), and (101) orientation peaks, as defined by Powder Diffraction File (PDF) 00-003-0888, and generally included in diffractograms. Electron microscopy was carried out with JEOL JSM-6460 LV scanning electron microscope, and UV-Visual Spectroscopy was performed with OceanOptics SD2000 spectrometer, and Spectragryph software[67].

3.2.1. (Experiment A) – Incorporation of Silver Nanoparticles and Use of Mica Substrate

The goals of the initial experiment were to determine whether the coefficient of thermal expansion (CTE) of the substrate affected surface features of the final film, as well as to incorporate silver nanoparticles into the sol-gel matrix and determine what, if any effect this would have on surface morphology. As control substrate, soda-lime glass was used, and experimental substrates were silicon metal wafer and mica slide. Mica is a glassy silicate mineral with a linear CTE of appx. 3×10^6 m/(m·K)[68], which is relatively close to that of ZnO ($4.3 - 5.6 \times 10^6$ m/(m·K) [69]).

While five different sol-gel treatments were devised for each substrate, only four were used, as shown in Table 3-1 below: undoped ZnAc solution as control group; silver-doped ZnAc solution; undoped ZnAc solution mixed with silver nanoparticles; alternately-layered undoped ZnAc solution and diluted nanoparticle dispersion.

Experimental:

Experiment A: Treatments:	Solution / Treatment Description (per coat):	Substrates (each treatment)
1 – Control	Undoped [0.75]ZnO solution	Soda-lime glass;
2 – Silver-doped	2at%Ag-doped [0.75]ZnO solution	
4 – Zn-AgNP	Undoped [0.75]ZnO mixed with AgNP, added to 0.0032 mg/mL NP concentration	Mica;
5 - Layered	Undoped [0.75]ZnO deposition, followed by 0.004mg/mL AgNP deposition	Si-wafer (2 replicates)

Table 3-1. Experiment A processing parameters matrix. Four treatments (first column) are implemented on three substrate media.

Undoped control solution (1) was prepared per established optimized SOP. Zinc Acetate Dihydrate ($Zn(CH_3COO)_2 \cdot 2H_2O$; Sigma-Aldrich) was dissolved in 200-proof anhydrous ethanol (C_2H_5OH ; Sigma-Aldrich) to a concentration of [0.75M]. MEA (Sigma-Aldrich) was added dropwise gravimetrically to achieve a ratio of 2:1 MEA:ZnAc. The solution was covered and stirred magnetically at 60°C for one hour, then returned to the drawer to rest for 24 hours. Silver-doped solution (2) was

made identically but for the addition of silver nitrate (AgNO_3 ; Sigma-Aldrich) to ZnAc salt at an atomic ratio of 0.02Ag : 1Zn. Aliquots of 5mL undoped solution (1) were separated and 1.25mL silver nanoparticle solution (60nm particle size dispersion, 0.02mg/mL; Sigma-Aldrich) was added to solution (4), yielding a AgNP concentration of 0.0032 mg/mL.

Given the probationary nature of this experiment and considering the expense of the new substrates, sample slides were cut into smaller sizes than usual (1-inch square and circular slides split in four to yield appx 0.5 sq. inch glass and mica slides, and similarly small quarter-circle mica slides). Five slides each of soda-lime glass, mica, and silicon wafer, were etched on reverse to identify, then left in ~3M nitric acid solution overnight. Slides were removed from acid bath and rinsed with DI water and ethanol, then dried in ~170°C oven on aluminum boat for appx. 10 minutes. Boat was removed and allowed to cool to ambient temperature.

Precursor solutions were deposited onto substrates by spin-coating (4-5 drops, 3000 rpm, 35s), and placed in 170°C oven for 10 minutes to dry between coats. Spin-coating / drying process was repeated for total of five coats per sample. “Layered” samples were prepared by spin-coat deposition of undoped (0) solution and drying as described above, followed by spin-coat addition of ethanol-diluted (1:4) AgNP dispersion (final AgNP concentration: 0.004 mg/mL,) and dried between ZnAc coats (treatment “5”). All samples were then post-heat treated in 400°C furnace for 1 hour, then allowed to cool in furnace at a rate of -1°C/min.

Initial Results:

Annealed samples generally showed splotchy, irregular formation of translucent white ZnO layer on transparent (glass, mica) slides, appearing whitish and iridescent on mica slides (Figure 3-2, left). Microscopic evaluation showed continued presence of problematic morphological features, including cracks and rippling, bubbles and holes in film surface (Figure 3-2).

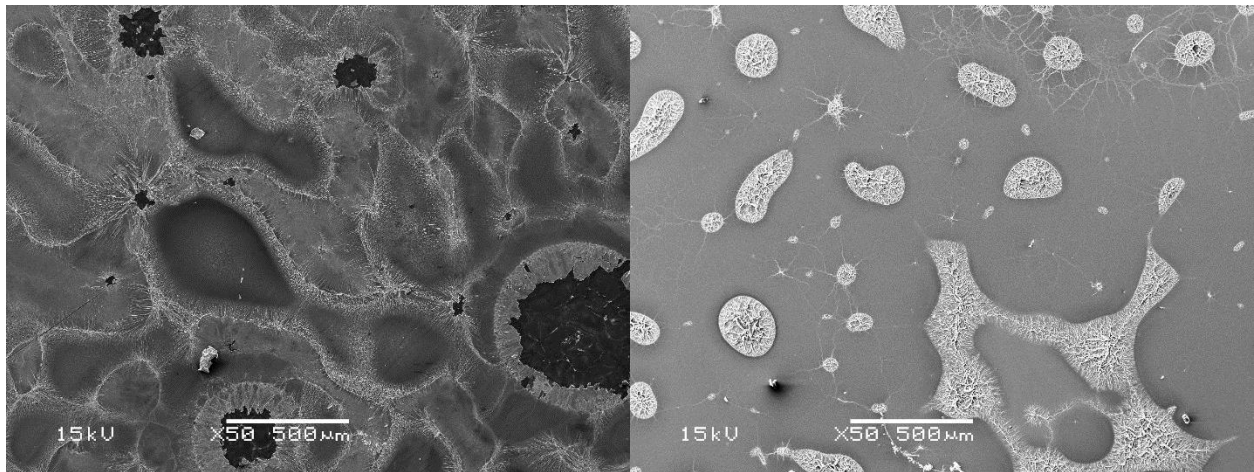
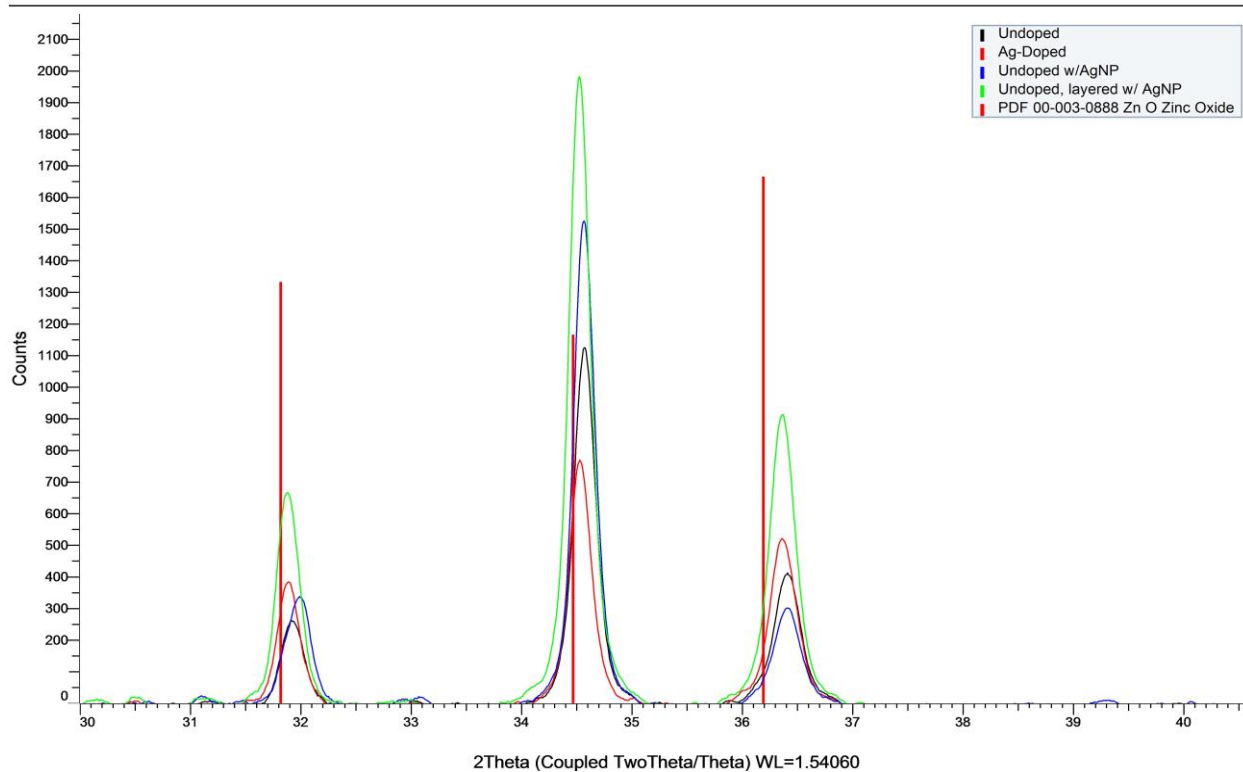


Figure 3-2. Electron micrographs of Expt A surface features. Surface features include cracks and bubbles (silver-doped, mica substrate, left) as well as aggregated 2D nanostructures (undoped, glass substrate, right).

While XRD spectra for glass and silicon substrates delivered results useful for analysis, output from mica slides showed such peak splitting and shifting as to render these spectra inconclusive for ZnO crystallites. This finding did serve to confirm that substrate material does influence crystal formation, although background signal from the substrate itself could not be ruled out as a confounding factor. Examining the useful glass and silicon XRD output, samples treated with AgNP (both mixed with precursor solution and layered between precursor layers) showed significantly increased peak intensity and (002) preferential orientation compared to doped and undoped samples not treated with NP (Figure 3-3).

Anecdotal sheet resistivity measurements also indicated significant improvement in conductivity for NP-treated films, but given the inconsistent surface morphology, no formal analyses of electrical properties were conducted. With evidence to suggest positive effects of nanoparticle treatment on ZnO thin films, an expanded and more meticulous analysis was warranted.

Soda-lime Glass Substrate



Si-wafer Substrate

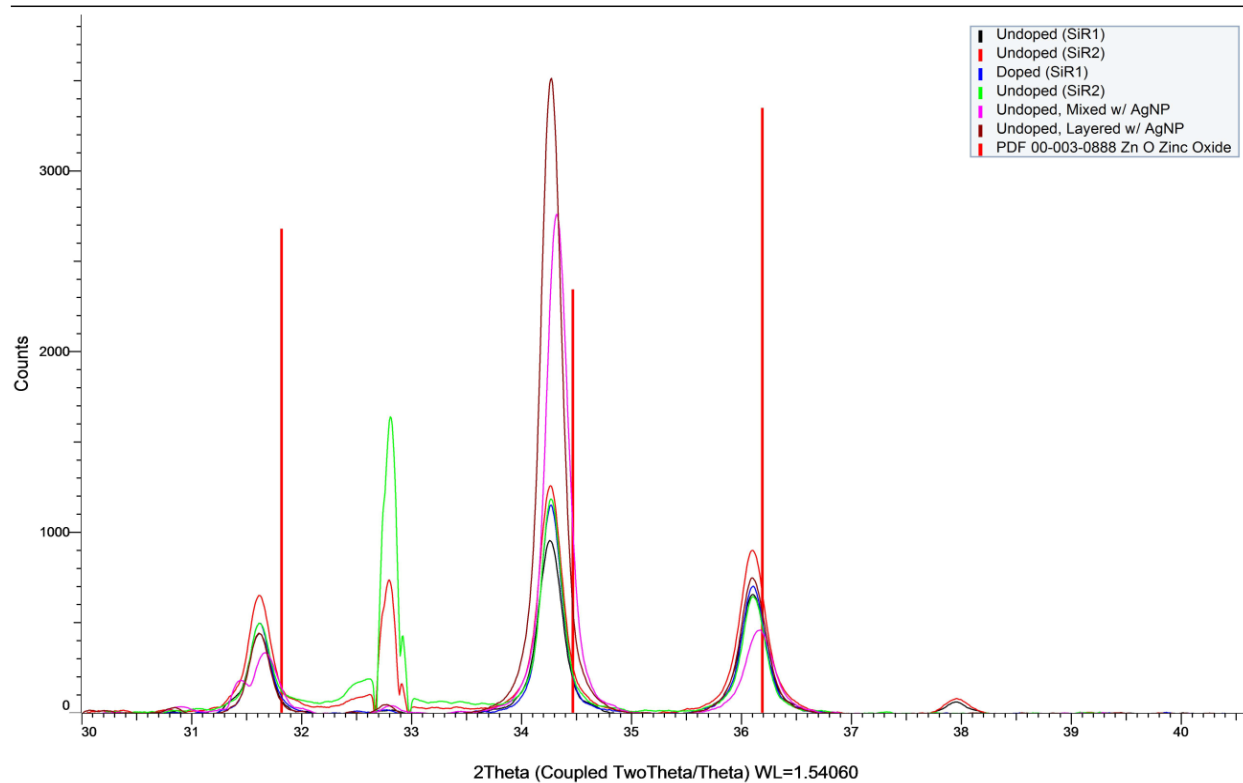


Figure 3-3. XRD Spectra for Expt. A on glass and Si-wafer substrates (upper, lower, respectively). Samples treated with AgNP show significantly improved intensity and preferred orientation.

3.2.2. (Experiment B) – Layering and Substrate Parameter Analysis under Inert Atmosphere

Following promising findings in exploratory attempts to incorporate AgNP into ZnO films, a more deliberate and rigorous parameter analysis was devised to confirm previous findings, expand understanding of the effect substrate has on morphology of films, and to further refine the SOP for successful film fabrication. In this experiment, substrates were expanded to include quartz and borosilicate glass in addition to silicon, mica, and sodalime glass utilized in previous trials.

A number of minor alterations to existing SOP were made based upon ongoing literature review of successful ZnO sol-gel fabrication techniques. Findings showing that lower precursor concentration resulted in greater preferential crystal orientation [58], led us to increase the number of coats applied per sample while reducing the solution concentration. In an effort to reduce surface feature interruptions caused by dust and other foreign inclusions, this set of experiments was performed within a glovebox under inert gas (nitrogen) pressure. Zinc to stabilizer (*r*-ratio) was set to 1 and slide cleaning procedure was modified slightly to align with procedures followed by Tseng et al. [34] in their aluminum-doping attempts.

Experimental:

Experiment B: Treatments:	Solution / Treatment Description (per coat):	Substrate IDs: (each treatment)
0 – Control	Undoped [0.25]ZnO solution	0 – Glass
1 – Silver-doped	1.5at%Ag-doped [0.25]ZnO solution	1 – Mica
2 - Layered	Undoped [0.25]ZnO deposition, followed by 0.004mg/mL AgNP deposition	2 – Borosilicate glass 3 – Si-wafer 4 – Quartz

Table 3-2. Experiment B parameters matrix. Three treatment methods (first column) are performed on five substrates.

Both doped and undoped precursor solutions were made following established SOP with alterations as mentioned above. Zinc Acetate Dihydrate and MEA were mixed at a 1:1 molar ratio into absolute ethanol at a concentration of 0.25mol salt to L solvent. For the doped solution, AgNO₃

was dissolved with ZnAc, resulting in a dopant concentration of 1.5at%. Precursor solutions were stirred at 60°C for one hour, then covered and placed in cabinet at room temperature, aging 48 hours. Silver nanoparticle dispersion was diluted in ethanol at a ratio of 4:1, yielding final concentration of 0.004 mg/mL.

Sample slides were cut to 1x1 inch squares (1-in circular disk for Si wafers), notched in corners to identify, washed with Alconox and rinsed in DI water, then left in ~3M Nitric acid bath overnight. Within the glove box, slides were removed from acid, rinsed in acetone and isopropanol, then dried on a 200°C heat plate for 10 minutes before spin coating. Doped and undoped solutions were samples were placed on spin-coater and spun at 3000 rpm for 35 seconds, with 1-2 drops deposited per coat. After each coat, slides were returned to heat plate to dry. This process was repeated to 10 total coats per sample. For 'layered' samples, dried substrate slide was placed on spin coater and 1-2 drops undoped solution deposited at 3000rpm, spun for 30 seconds. Substrates were placed back on heat plate to dry for 10-20 then returned to spin-coater and nanoparticle dispersion was dropped (1-2 drops) at same speed and time settings, then returned to hot plate. This procedure was repeated to 10 coats of nanoparticles between 10 coats of precursor solution. All samples were then transferred to room temperature furnace, which was ramped to 500°C over two hours, maintained at 500°C for four hours, then furnace was shut off and samples cooled to room temperature in furnace.

Initial Results:

See Appendix C-3B: Appearance of films was generally improved from past trials. Surface defects such as spots and spreading lines were most visible on mica and silicon slides, and doped samples tended to display more cloudiness and discoloration. Glass and quartz samples showed the best transparency, while borosilicate glass was generally cloudier, but appeared smooth with fewer

noticeable abrupt defects. In most cases, spreading lines were most visible toward the outside edges of the slides.

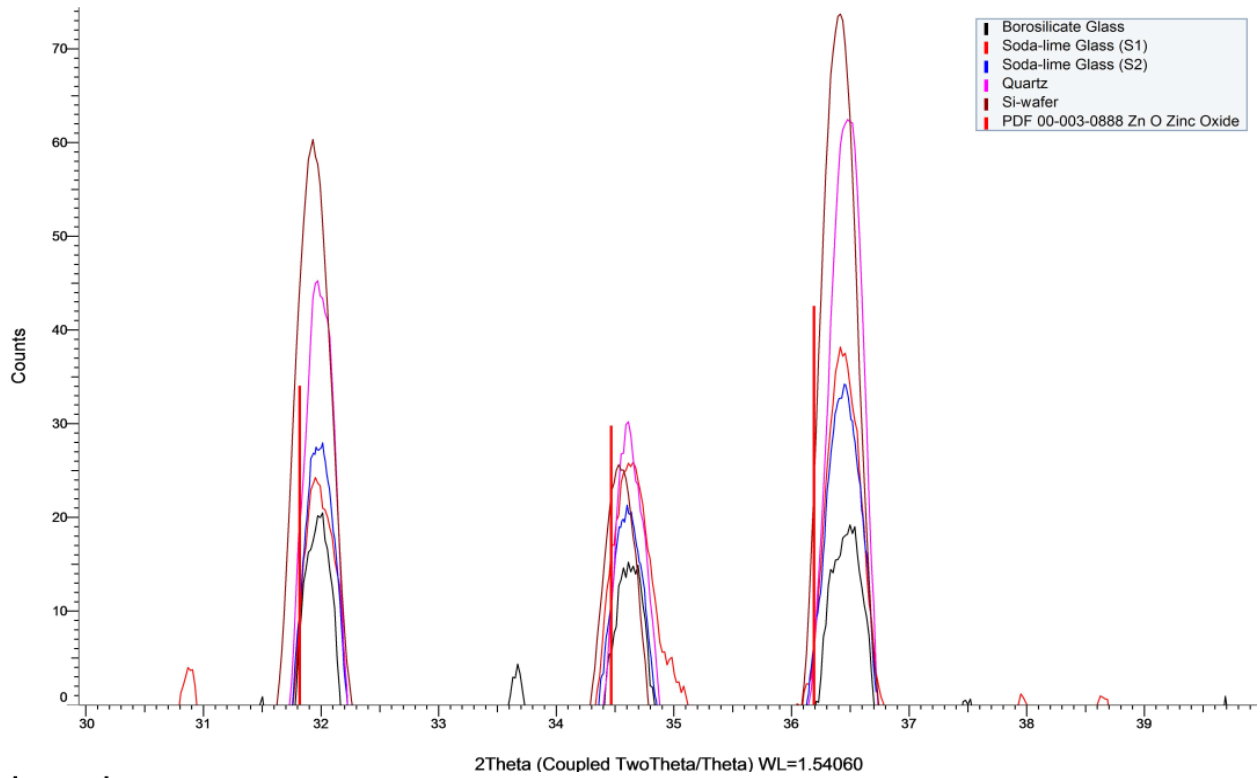
XRD Spectra were processed with Bruker DIFFRAC.EVA v3.0 software for more thorough analysis than in previous experiments, in preparation for quantitative analysis per section 3.3.1 below. Software automatically removed background, and smoothed spectra with a 0.614 smooth factor, using default (non-Gaussian) algorithm.

In general, XRD spectra for this experiment has shown taller, narrower peaks than in any previous trials, indicating changes in SOP processing parameters were likely beneficial. Comparison of XRD charts stacked by precursor/treatment shows crystal orientation at ratios similar to theoretical standards for non-NP treated doped and undoped (Figure 3-4, top) samples, while NP-layered samples (Figure 3-5, bottom) show significantly improved (002) preferential orientation.

Silicon samples tend to dominate peak intensity comparisons for all treatments, but comparative intensities of other substrates vary from one treatment to the other. In all trials, mica samples once again returned shifted and split peaks, resulting in inconclusive findings with regard to ZnO crystallinity, and mica spectra were removed from subsequent analyses.

Once again, samples treated with silver nanoparticles displayed significant improvement in both intensity and preferential peak ratio, adding confirmation to previous findings.

Undoped



Layered

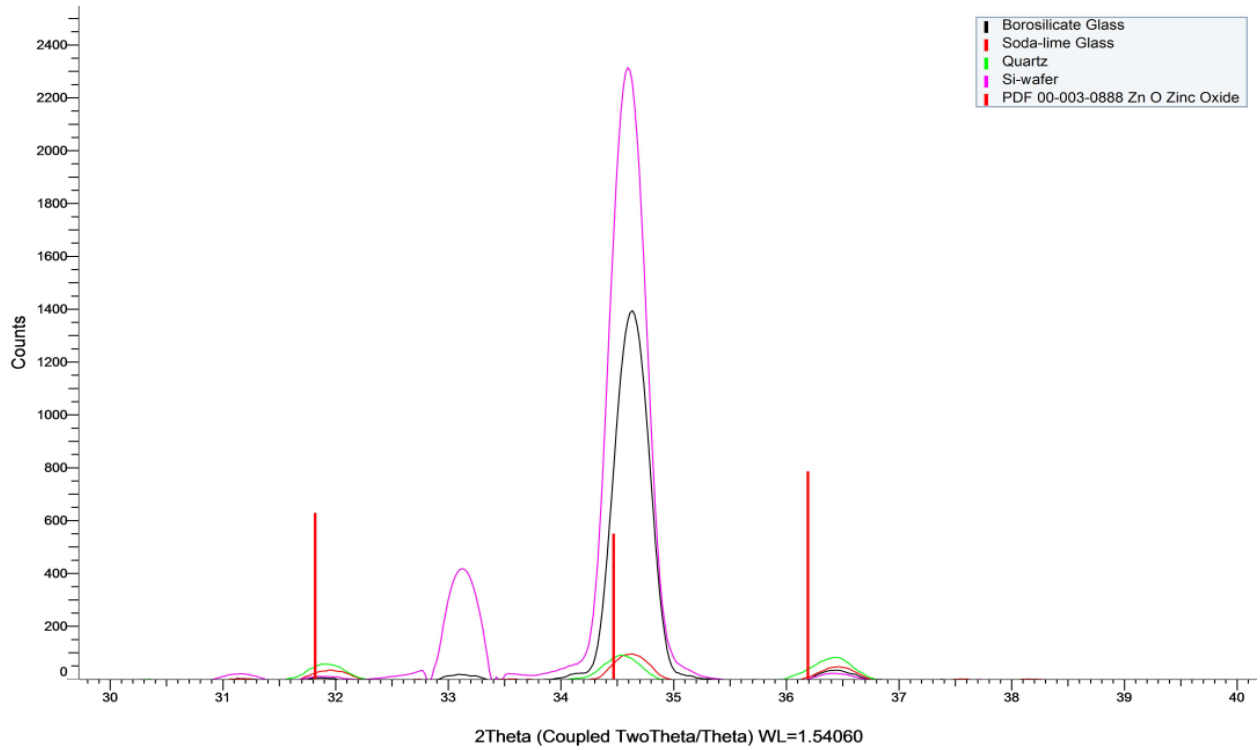


Figure 3-4. XRD Spectra from experiment B: Undoped (top) vs. layered process (bottom). Layered samples show staggeringly improved intensity and 002-peak ratio preference.

3.2.3. (Experiment C) – Initial Wetting and Layering

Previous findings indicated that a layering process, by which silver nanoparticles dispersed in an aqueous/alcohol medium were deposited between dried layers of ZnO precursor solution resulted in significant improvement in both ZnO crystallinity by peak intensity, and preferential crystallinity about the (002) orientation. Given the dramatic ‘smoothing’ effect this layering process seemed to have on film surfaces by microscopic evaluation, and the relatively low concentration of nanoparticles in the dispersion (4ppm), it was necessary to determine whether the improved surface morphology was caused by the presence of silver nanoparticles, or if the improvement was due to a wetting process between each layer.

In this iteration of the study, both doped and undoped precursor solutions would be tested with no treatment (control), as well as layered with nanoparticle dispersion and pure ethanol between each coat. This experiment utilized only borosilicate glass as substrate per last experiment’s findings.

Experimental:

Experiment C: Treatments:	Treatment Description (repeated x10):	Solutions/Treatments
D – Dry Control	Simple deposition of solution, no wetting or layering between coats.	0 - Undoped [0.25]ZnO
E – Ethanol	Solution deposited, dried, wetted with ethanol, dried, repeat.	1 - 1.5at%Ag-doped [0.25]ZnO solution
S – Sandwiched NP layer	Solution deposition, dried, treated with NP dispersion, dried, repeat.	2 – Undoped, no pre-heat treatment

Table 3-3. Experiment C parametric matrix. Three treatments (first column) are made using doped and undoped solutions.

Undoped & doped precursor solutions, ethanol-diluted silver dispersion were prepared identically to the previous experiment (Section 3.2.2). Borosilicate slides prepared, cleaned and dried identically. Control group slides were placed on spin coater and spun for 35 seconds at 3000RPM, applying 1-2 drops undoped or doped precursor (respectively) to either slide, then returned to 200°C hot plate for at least 10 minutes between coats, repeated to 10 coats. Ethanol-layered samples were

likewise deposited with precursor solutions, dried, then returned to spin-coater and 1-2 drops ethanol applied to dried surface between each coat and dried again on hot plate. This deposition of precursor, drying, ethanol, drying, was repeated 10 times. Similarly, the AgNP samples were treated with undoped and doped precursor solutions respectively, dried, and then treated with diluted silver dispersion (1-2 drops) between each coat for a total of 10 applications of precursors and 10 applications of nanoparticles per slide. Finally, a third batch of undoped dry, ethanol, and NP-layered samples were fabricated as described above, but without any pre-heat annealing, they simply air-dried at 25°C before post-heat treatment, which was carried out on all nine samples by placing them in a cold furnace, temperature-ramped furnace to 500°C as described in Section 3.4, above.

Initial Results:

A complete collection of recorded images for this experiment may be found in Appendix C-3C. For undoped films, surface feature ripples and cracking were once again observed in the untreated control sample (Figure 3-5, left), though not to the extent as had previously been recorded. These surface features seemed to be diminished in ethanol-layered sample (Figure 3-5, mid), resulting in generally smooth film. The AgNP-treated sample showed severe cracking and tearing unlike we had ever seen before (Figure 3-5, right), and it is supposed that this occurred as the result of some anomalous error, although no replicates were fabricated in this experiment that could verify this assumption.

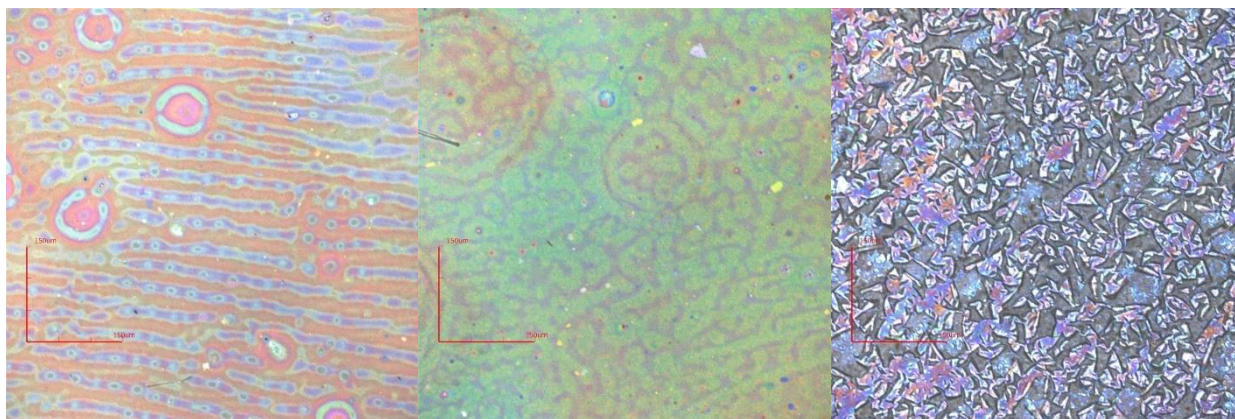


Figure 3-5. Optical micrographs of undoped experiment 'C' sample. 20X magnification for untreated (left), ethanol-wetted (middle,) and NP-layered (right) samples.

Contrary to expectations, doped samples showed far fewer surface imperfections in all treatments (Figure 3-6), and significant discontinuities were not observed in the control or ethanol-treated samples until a zoom factor of 10,000. At this level of magnification, the SEM was unable to focus on the NP-treated sample.

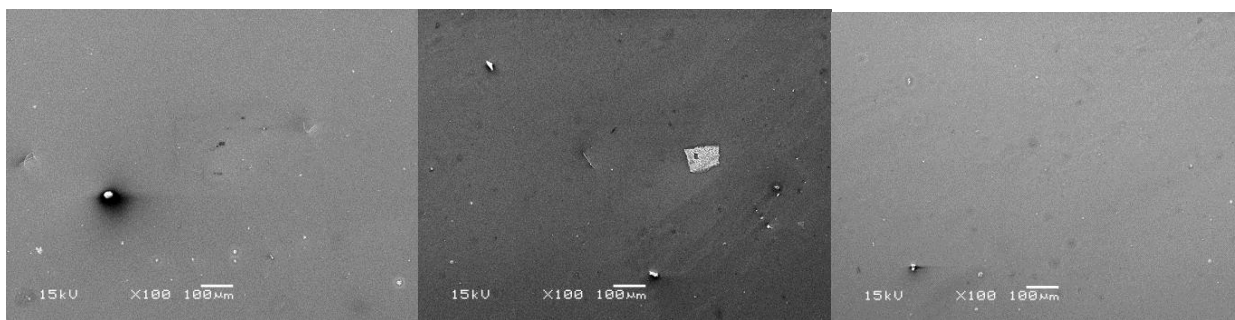
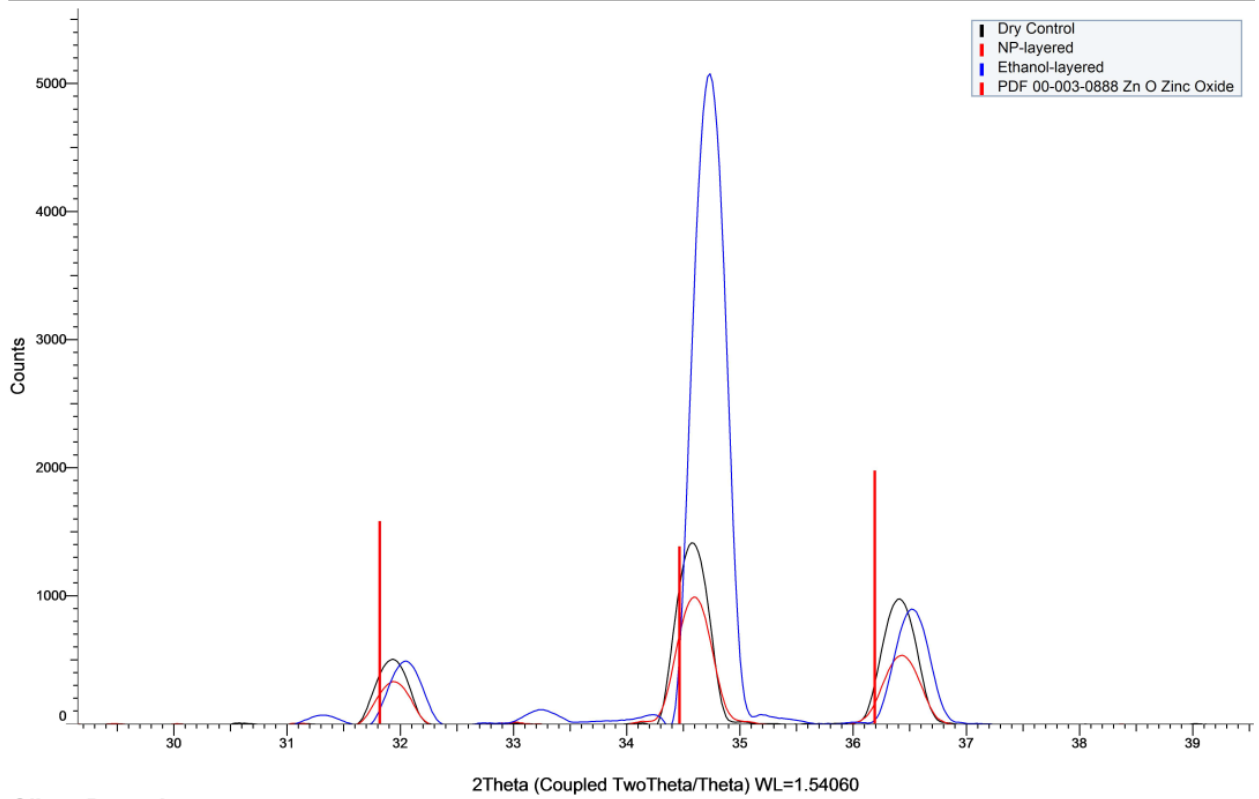


Figure 3-6. Electron micrographs of Expt. C, doped samples at 100X magnification. Dry control (left,) ethanol-wetted (middle,) and NP-layered (right) samples shown.

XRD spectra also demonstrated significantly different findings between undoped and doped samples. In undoped samples, the ethanol-treated film showed significantly higher intensity and 002-peak preference (figure 3-7, top). However, in doped samples, the ethanol- and nanoparticle-treated samples showed much higher peak intensity and preferential orientation compared to the untreated sample (figure 3-7, bottom). The three samples that were not pre-heat treated showed very low intensity, but the NP-layered sample had better 002-orientation than other treatments. See Appendix B-3C.

Undoped



Silver Doped

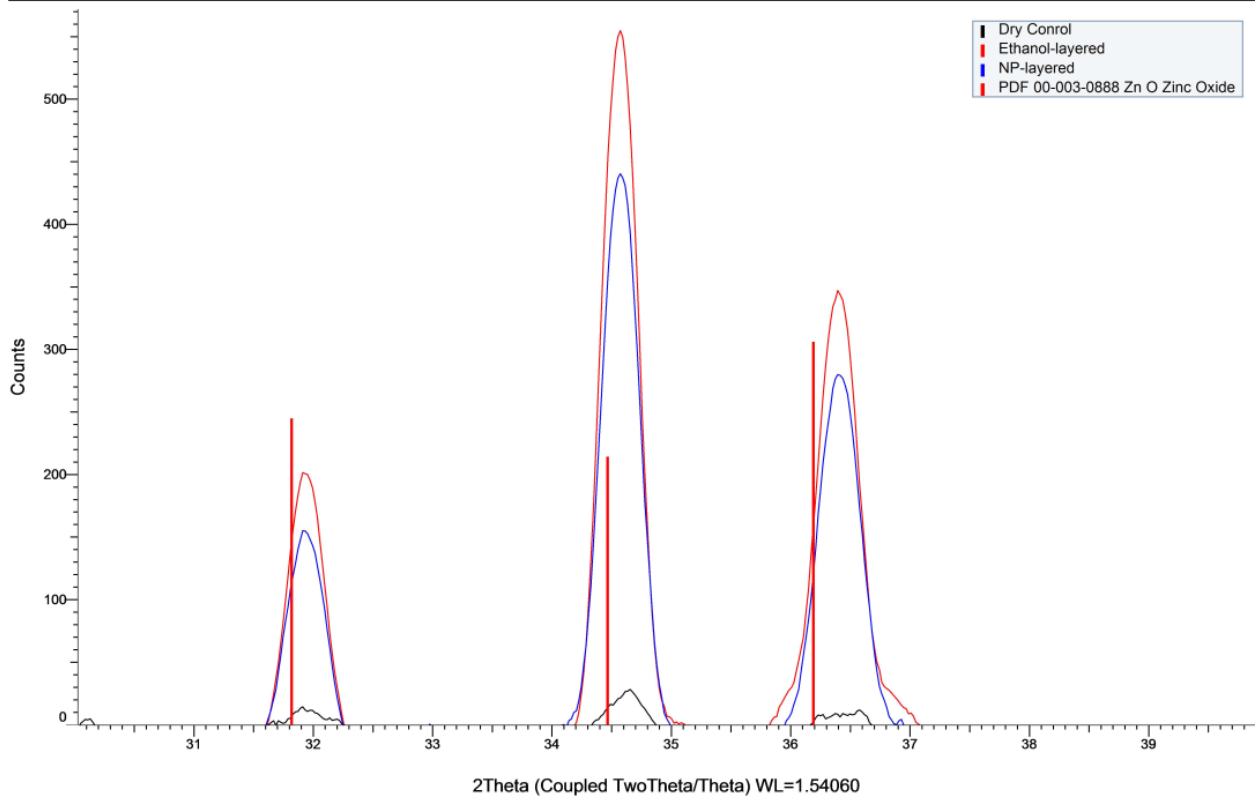


Figure 3-7. XRD Spectra from Experiment C: undoped (top,) and silver-doped (bottom.)

3.2.4. (Experiment D) – Wetting and Layering

Although the results from section 3.2.3 continue to show improvement in crystallinity, preferred orientation, and conductivity of doped films, the underlying question concerning whether the cause of improvement lies in the presence of nanoparticles or the wetting process in layering, was not conclusively answered. This experiment also seeks to further investigate the relationship between nanoparticle interaction and surface wetting by introducing additional solvents of varying polarities and viscosities (Table 3-4,) as wetting agents to determine what, if any relationship exists between surface wetting and film morphology. Additionally, all replicates of the doped and undoped samples were exposed to post-heat annealing temperatures between each coating, in an attempt to validate the theory initially investigated in Chapter 2's Experiment H.

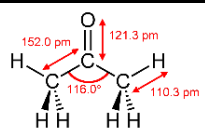
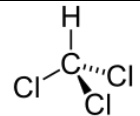
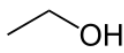
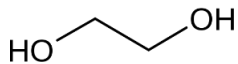
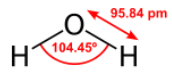
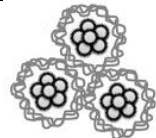
Common Name	Abbr.	Structure	IUPAC Name, formula	Relevant Properties	Viscosity (mPa*s)	Dielectric Constant
Acetone	Acetone		Propanone, (CH ₃) ₂ CO	Polar, aprotic solvent	0.295	20.7
Chloroform	CHCl ₃		Trichloromethane CHCl ₃	Slightly polar, aprotic solvent	0.563	4.8
Ethyl Alcohol	EtOH		Ethanol CH ₃ CH ₂ OH	Primary alcohol	1.2	24.3
Ethylene Glycol	EG		Ethane-1,2-diol (CH ₂ OH) ₂	Polar, protic Ether, Primary alcohol,	16.1	37
DI Water	H ₂ O		Water H ₂ O	Deionized water suitable for solutions chemistry	0.89	29.3
Silver Dispersion	AgNP		Silver Nanoparticle dispersion in aqueous buffer	Diluted with absolute ethanol to 0.004mg/mL	~1	unk.

Table 3-4. Names and properties of solvents used in experiment D. Viscosity and dielectric constant are among properties that may contribute to a solvent's wetting efficacy.

Experimental:

Experiment D: Treatments:	Treatment Description (repeated x5):	Wetting Solvents:
0 - Undoped	[0.25] ZnO Undoped solution, wetted and dried but not annealed between coats	A – Acetone C – Chloroform
1 – Silver-doped	3at%Ag-doped [0.25]ZnO solution, wetted and dried but not annealed between coats	D – Dry (not wetted) E – Ethanol
D – Doped, annealed	3at%Ag-doped [0.25]ZnO solution, wetted, dried, and thermally annealed between layers	G – Ethylene Glycol H – DI Water
U – Undoped, annealed	[0.25] ZnO Undoped solution, wetted, dried, and thermally annealed between coats	N – AgNP dispersion

Table 3-5. Experiment D parametric matrix Treatment solutions (first column,) are implemented with various wetting solvents.

Undoped and Doped solutions were made according to existing SOP at precursor concentration of [0.25M] and r-value of 1. Doped solution was formulated to 3at% silver. Solutions were covered, mixed for 1 hour at 60°C and aged for 48 hours. Borosilicate slides were cleaned and dried identical to prior procedure.

Trial **0** (undoped) and **1** (doped) samples were treated identically, with a layer of precursor sol deposited by spin coating 3 drops at 3000rpm for 35 seconds, then returning sample to 200°C heatplate. After at least 10 minutes of drying, samples were returned to the spin coater one at a time and each treated with one of the solvents listed in table 3-1, above. Additionally, one ‘dry’ control sample from each trial was not treated with any solvent. The process was repeated for 5 coats each of precursor and solvent treatment. Trials **D** (doped, annealed between layers) and **U** (undoped, annealed between layers) were treated identically to 0 and 1 above, but were placed in 500°C furnace for appx 20 minutes after each solvent coat. These trials were also subjected to 5 coats each of precursor and solvent treatment. All samples were then transferred to 600°C furnace for 4 hours, then furnace shut off and allowed to cool with samples inside.

Initial Results:

To the naked eye, samples appeared to be generally more transparent than past experiments' samples, with fewer signs of spreading lines and discontinuities, but closer inspection did reveal cracking and rippling features on some samples, as shown in Appendix C-3D and discussed in subsequent chapter sections.

Once again, XRD results in general showed significantly more intense peaks than in previous experiments, especially for samples treated with nanoparticles. Silver-doped samples, annealed between each layer show greatest intensity and preferential orientation (Figure 3-8). In general, samples treated with silver nanoparticles showed most desirable peak intensity and orientation.

Doped, Annealed

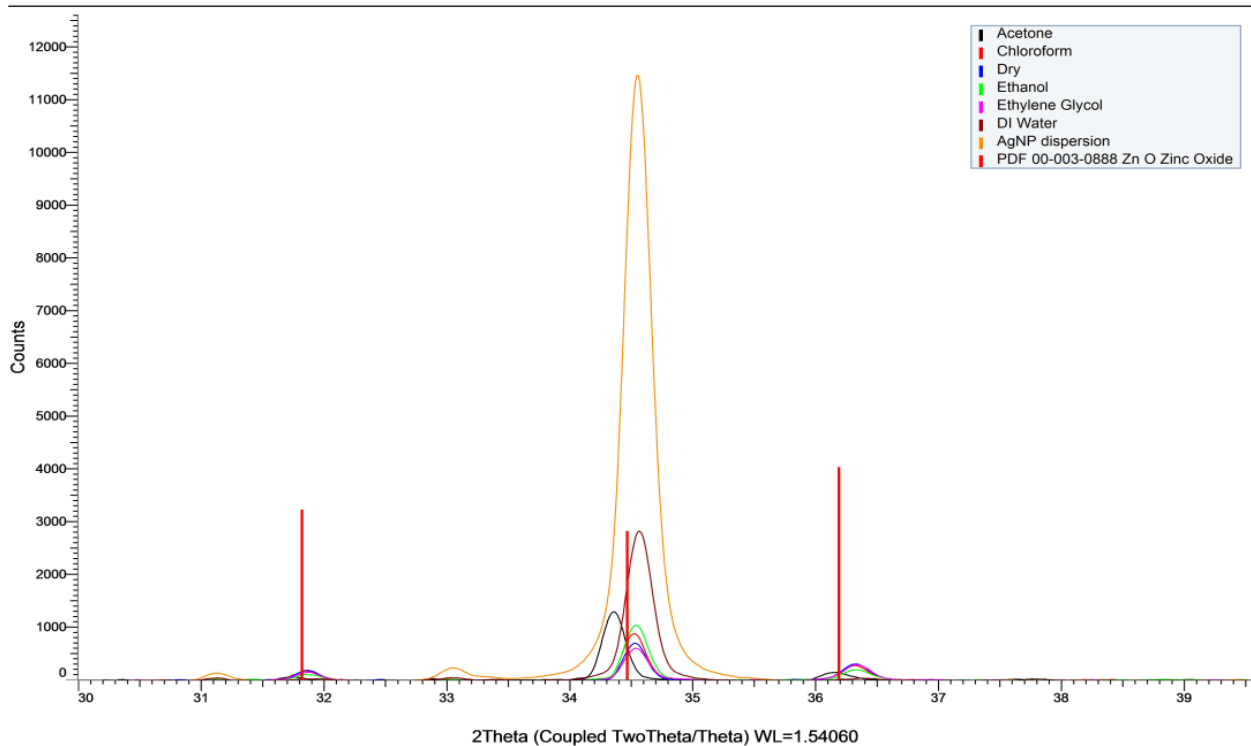


Figure 3-8. XRD Spectra for Experiment D, Silver-doped, annealed samples. Yellow line shows solution with nanoparticle dispersion.

3.2.5. (Experiment E) – Final Improvements through Modification of Solvent and Wetting

Through the process of compiling the acquired knowledge and experience, and composing the narrative of this two-year project, additional loose-ends were identified, and confirmations were desired in the explanation of some of the determined conclusions. This final experiment represents the capstone of the project, testing one final synthesis and processing solvent, and verifying the results of the newfound layering and wetting process in thin film synthesis.

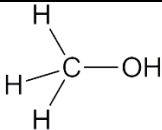
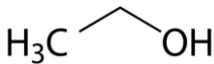
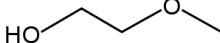
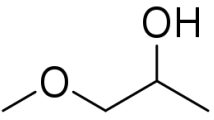
Common Name	Methanol Methyl Alcohol	Ethanol Ethyl Alcohol	Ethylene Glycol Monomethyl Ether (EGME) 2-methoxyethanol	Propylene Glycol Monomethyl Ether (PGME) 1-methoxy-2- propanol
Structure:				
(Dielectric Constant @ 20 °C) / (BP (°C))	32.35 / 64.7	25.0 / 78.3	16.93 / 124.6	12.3 / 120
Toxicity:	Moderately toxic	Low toxicity	Toxic, carcinogenic	Low toxicity

Table 3-6. Comparison of common sol-gel solvents. Solvents with relatively high dielectric constants and short carbon chains are better at dissolving salts.

A review of literature pertaining to ZnO sol-gel doping processing brought back to our attention the work of Tseng et al [34] and their group's use of propylene glycol monoethyl ether (PGME) as an effective solvent in sol-gel processing. While the Tseng group's purpose in utilizing PGME was primarily as a safer substitute to its significantly hazardous and less-stable cousin, 2-methoxyethanol, they also reported improved quality of thin films, owing to the solvent's physical attributes. A comparison of EGME vs PGME is shown in Table 3-6 above, and comparison with other solvents is found in Appendix F. Although our group had before considered the properties of viscosity and surface tension as potential factors in sol deposition, we had theretofore been unable to identify enough suitable viscous solvents nor confirmational data to warrant an experimental iteration. The

Tseng paper provided both the identity of a proven solvent and evidence of successful use in sol-gel processing to warrant additional study. Given our breakthroughs in wetting and layering processes, PGME was a perfect candidate solvent both to investigate in its own right, and to use as an unknown new material with which to put our processing techniques to the test.

Experimental:

Starting solutions 0-3 were prepared identically with the exception of the identity of their solvent (Ethanol for 0, 1; PGME for 2, 3) according to our most recent SOP: ZnAc salt and MEA stabilizer were measured gravimetrically and mixed with 5 mL solvent to a final Zn concentration of 0.25M; r-ratio of 1. For doped solutions, AgNO₃ was added gravimetrically to Ag:Zn ratio of 1.5at%. These solutions were covered and magnetically stirred on a 100°C hotplate for 1 hour, then transferred to cabinet to age 48 hours. Additional NP solutions were made by combining 1 mL AgNP dispersion (0.02 mg/mL) with 4mL PGME or Ethanol to final NP concentration of 0.004 mg/mL.

Experiment E: Solutions:	Solution Description:	Wetting Solvents:
0 – Undoped Ethanol	[0.25] ZnO Undoped EtOH-solution, wetted and dried between coats	D – Dry (untreated)
1 – Silver-doped Ethanol	1.5at%Ag-doped [0.25]ZnO EtOH-solution, wetted and dried between coats	E - Ethanol G – PGME
2 – Undoped PGME	[0.25] ZnO Undoped PGME-solution, wetted and dried between coats	O – Ethanol/AgNP
3 – Silver-doped PGME	1.5at%Ag-doped [0.25]ZnO PGME-solution, wetted and dried between layers	P – PGME/AgNP

Table 3-7. Experiment E parametric matrix Four solutions from two different solvents (first column) were used to factorially examine wetting treatments by PGME and Ethanol, as well as NP treatment.

Soda lime glass slides were etched, washed with Alconox soap and DI water, then left in a dilute (~3M) Nitric Acid bath overnight. Slides were removed, rinsed with acetone then ethanol, and placed on 200°C hotplate for at least 15 minutes before coating.

Samples were first coated with respective solutions 0-3 above, via spin-coating at 3000RPM for 35s, then returned to hotplate. Samples were then subsequently treated with respective wetting solvent per Table 3-6 above by identical spin-coating process and returned to hotplate. This process was repeated for 6 coats of both precursor sol and wetting solvents.

Samples were then thermally annealed at 500°C for two hours, then furnace turned off, and samples allowed to return to ambient temperature as furnace cooled.

Initial Results:

Annealed slides were among the clearest to date, and while silver discoloration was apparent, it was not as prominent as observed in previous trials. While certain zones of “streaking” could be observed, fewer surface discontinuities were apparent than ever previously. All samples were inspected by optical and electron microscopy (Appendix C-3E).

While XRD Spectra do indicate that PGME is an effective starting solvent, the most intense 002 peaks and ratios came from doped and undoped ethanol precursor solutions that were subsequently treated with NP-containing solutions (Figure 3-9).

Indeed, the XRD peaks for ethanol- and PGME-based NP dispersions are nearly identical on undoped ethanol samples, although PGME-based NP dispersion is superior in doped ethanol samples, as shown in Appendix B-3E and discussed later in this chapter. In general, samples wetted with PGME/AgNP solutions showed drastically improved intensity and (002)-peak ratio.

Undoped Ethanol-based

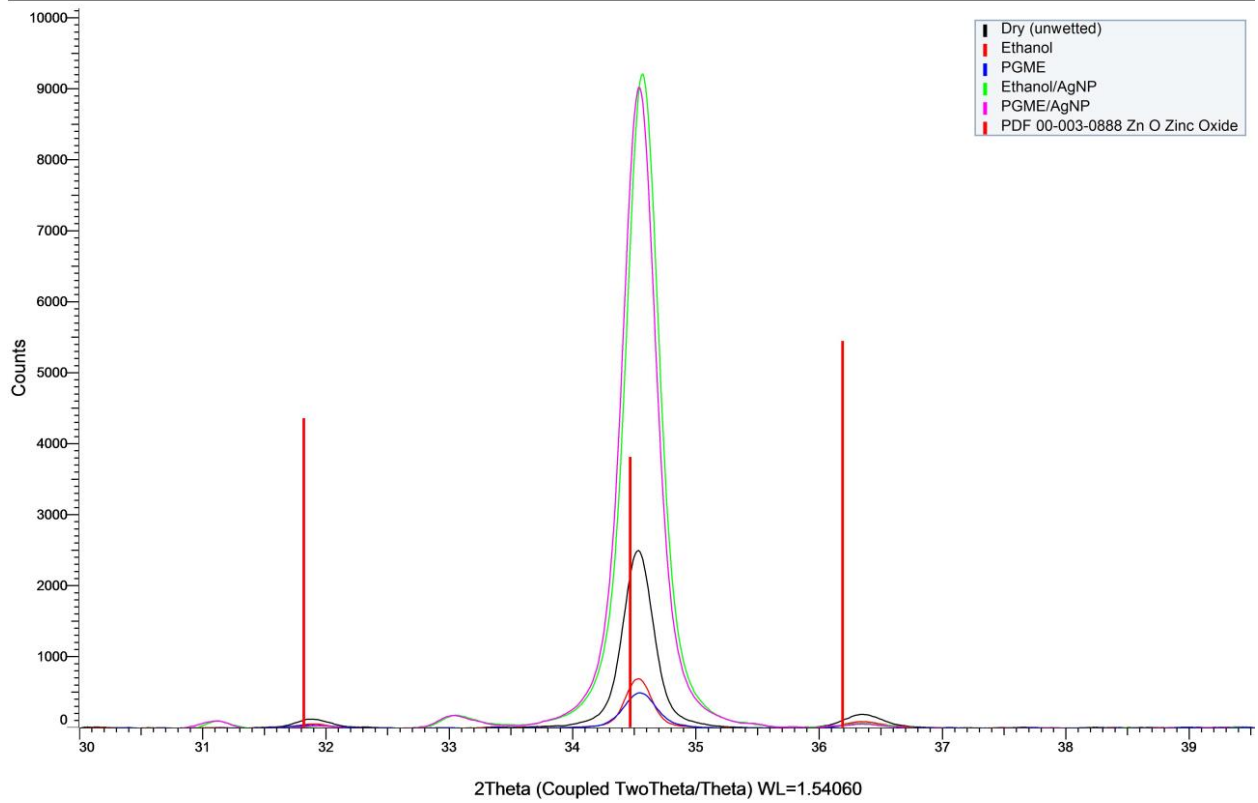


Figure 3-9. XRD Spectra of Experiment E: undoped ethanol samples with various wetting treatments. Samples treated with AgNP dispersion showed significantly enhanced (002) peaks.

3.3. Analysis and Discussion

Speaking broadly, the second phase of this project represented more deliberate, logically-planned and organized experimental procedure, given our significant experiential advancements in Chapter 2. Perhaps not-unrelatedly, this phase was endowed with unexplained luck, unexpectedly extraordinary success in experimental attempts, and breakthroughs of significance to the sol-gel film processing community of research and industry.

The experimental process in this phase understandably took a slower pace given that personnel resources were reduced to half that of early-phase (Chapter 2) rapid trial-and-error processing. This more planned and deliberate pace allowed for more appropriate pre-trial literature review and incisive experimental design, yielding significantly improved results.

Given the respective successes of this phase, more rigorous and intentional, publication-worthy data analysis processes and methods were required. Spontaneous and subjective XRD comparisons were supplanted with quantitative methodologies; uniform and consistent imaging processes and surface-texture analysis methods were (gradually) implemented; difficulties with electronic characterization (i.e. conductivity measurement problems,) were addressed with alternative and literature-endorsed optical band-gap analyses.

3.3.1. Degree of Preferential Orientation

Over the course of this project, (e.g. throughout Chapter 2,) qualitative comparison of XRD spectra was used as the primary guide in determining relative success or failure of given samples and trials, and in the decision-making process for further experimental design. However, in final analysis, a more quantified method was required to compare relative success and failure from one experiment to the next. A method for calculating the degree of preferential orientation (also referred to as texture coefficient) was adapted from methods used by Znaidi [62] and Chakrabarti [70], (referencing Barrett

[71] and Lotgering [57] respectively), in which measured intensity of preferential peak over theoretical intensity (from powder diffraction file) is divided by theoretical proportion of preferential peak intensity to sum of all peak intensities, yielding a decimal between -1 to 1 representing the degree of preferential orientation calculated.

Calculation Method:

These methods are adapted to compare integrated areas under peaks rather than mere peak intensity, and to utilize our own standard as theoretical sample, rather than powder diffraction file.

Our calculation of preferred (002) orientation, $f_{(002)}$, is described as:

$$f_n(002) = \frac{P_n - P_0}{1 - P_0} \quad (1) \quad \text{where:}$$

$$P_{002} = \frac{A_n(002)}{\sum A_n(hkl)} \quad (2) \quad \text{and:}$$

$$P_S = \frac{A_0(002)}{\sum A_0(hkl)} \quad (3),$$

in which $A_n(002)$ is the integrated area under the (002) peak of the sample, $\sum A_n(hkl)$ are the sum of areas under the (100), (002), and (101) peaks between 30 - 40° 2 θ of the sample; and $A_0(002)$ is the area under the (002) peak of our standard, with $\sum A_0(hkl)$ the sum of areas under the (100), (002), and (101) peaks between 30 - 40° 2 θ of our standard.

The standard was fabricated using our established SOP, at a precursor concentration of [0.75M] and r-ratio of approximately 1. After mixing and aging for 24 hours, sol was deposited via spin-coat (5-drops per coat) on borosilicate glass slide then dried on 200°C hot plate for ten minutes between coats, for a total of eight coats, then annealed for 100 hours at 650°C.

As elaborated in Section 1.4 and detailed throughout Section 2.3, X-Ray Diffraction was relied-upon as the first and primary means of characterization of films. This new Degree of Preferential

Orientation methodology was used to quantitatively analyze XRD findings from each this chapter's experiments, the plots presented in Appendix D as matrices of bar graphs based on the factorial analysis parameters of each experiment.

Results:

Results concerning substrate identity, Experiments A & B, are confounded by the interference of mica on XRD spectra, rendering the negative calculated crystallinity of mica samples to likely be incorrect. However, given the improvements in crystallinity through the use of AgNP dispersion in treating samples from both experiments A & B, the investigation into substrate identity was mostly abandoned in favor of exploring wetting processes.

Although the 'no pre-heat,' ambient-temperature dried samples in Experiment C do show greater degree of (002) orientation, the samples themselves were highly clouded and had so many defects observable to the naked eye, they were discarded from further analysis.

This degree of preferential orientation calculation proved most useful in comparing the films produced by Experiments D & E. They indicate that our processing parameters for these experiments universally create better-oriented films than the process used for fabricating the standard (in these experiments, the common significant modified variable was the lower concentration of starting solutions,) and also suggest that nearly all solvents used in intra-layer wetting were beneficial to preferential orientation. Chloroform and Acetone are notably the least effective wetting solvents, while ethanol and even simple deionized water showed significant improvement, and the silver nanoparticle dispersion created films with nearly 100% improved preferential orientation across both experiments.

3.3.2. Band Gap Analysis

As we know from basic physics, wavelength and energy are related by the Planck-Einstein relation, $E = \frac{hc}{\lambda} \leftrightarrow \lambda = \frac{hc}{E}$. Thus, shifts of the optical band edge toward longer wavelengths (right, or red-shifts,) result in shifts of the associated energy to the left (lower energy). The optical band edge can be used to calculate band gap, as explained by Wang et al., "...a sharp absorption edge is generally observed in the transmittance spectra of direct band gap semiconductor films... (this) edge in the transmittance spectra may result in a sharp peak in the plot of $dT/d\lambda$ vs. λ ..." [72].

The final experiments with publishable results (D & E,) were characterized with Ocean Optics SD200 Ultraviolet/Visible (UV-Vis) Spectrometer in the interest of analyzing optical properties such as total and average optical transmission, absorption edge, and optical band gap. In following with the Touam experimental process, in which several other papers [72]–[74] are referenced using the first derivative of the transmission spectra noted above, with wavelength converted to energy, we calculated these band gaps using Spectragryph optical spectroscopy software [67]. These optical spectra, derivative plots, and graphs comparing calculated band gaps are recorded in Appendix E.

Faj and Shah suggest that doped ZnO films tend to exhibit the Burstein-Moss effect, in which the band gap is widened due to excess free electrons filling energies above the conduction band, but note that this effect occurs to a critical limit, at which point band gap narrowing is observed as free electrons begin to cause the donor and conduction bands to merge [75]. Given that explanation of band gap variance, it is important to note that Touam's paper also cites conflicting sources on whether silver doping of ZnO causes band gap widening or narrowing. Touam's own experimental findings suggest band widening up to 4at% silver doping through sol-gel wet processing, which tends to match the findings of Xue et al [43], who synthesized their films with magnetron sputtering. Another interesting observation of ours was that a paper often-cited for reporting decreased band-gap with

increasing silver concentration, in fact mistakenly referred to red-shifted absorption peaks as narrowing band gap, when they likely meant to suggest the opposite [45].

Despite the sometimes-conflicting experimental findings on the effect of silver doping on band gap, the calculated values of our experiments' band gap values between 3.2-3.3eV (Figure 3-10) aligns with Touam and many other similar studies [41], [43], [76]–[79]. Furthermore, comparison of ΔE_g (see bottom pages of [Appendix E](#),) within our experiments suggests that silver doping with intra-layer annealing (Experiment D), as well as solutions treated with intralayer PGME wetting (Experiment E), both result in relative increase in band gap for all test conditions.

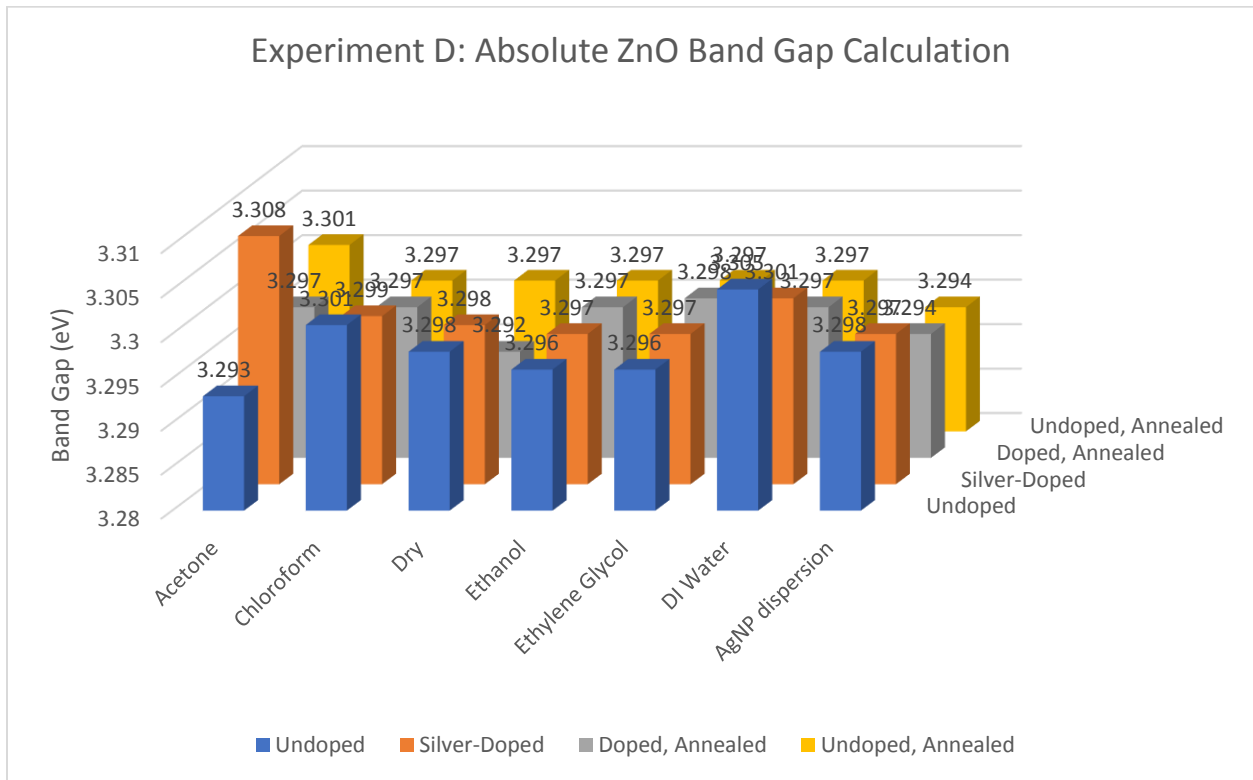


Figure 3-10. Calculated Optical Band Gap (E_g) for Experiment D.

3.3.3. Correlation of Crystallinity and Surface Morphology

Throughout our examination, much emphasis has been placed on the crystallinity of fabricated films, their preferential orientation, and surface features and morphology. While we were unable to successfully carry out direct performance characterization such as conductivity/resistivity testing (see Section 2.3.3), we are able to correlate many of our observed property enhancement to performance metrics.

For example, an article we only recently became aware of in Nature Communications [80] brings together many aspects of our own study in its report on the effects of EGME and MEA as interfacial layers on ZnO layers actually incorporated into inverted polymer LEDs (iPLEDs). In this case, the rippled nanostructures we observed early in our work are reported to improve efficiency of iPLED devices by improving electron-hole recombination. Given that OPV cells are essentially the exact inverse of LED devices, and recombination is what we try to *prevent* in solar cells, we can infer from Lee's findings that reduction in rippling surface features may lead to diminished recombination, and more efficient photocells. The same authors further showed that the surface treatment with EGME and MEA leads to dipolar polarization, improving electron transport mobility and recombination in polymer solar cells [81]. Our own processing using superior solvents has shown to improve smoothness and crystallinity, suggesting application in real devices may surpass the improvements shown by Lee et al.

Another study by Duta et al. specifically examined the effect of surfactant addition on the rippling and "2D coherent structures" and dendritic morphology of ZnO films produced through spray pyrolysis [82]. The surface features shown and described by Duta are remarkably similar to many such features observed throughout our analyses, and their analysis further related lower frequency and stark contrast of these features with reduced surface roughness and increased surface energy. Furthermore,

their comparison of crystallite sizes suggests that lower crystallinity results in higher disorder and greater microstrain on the surface.

3.3.4. Wetting Processes in ZnO Film Fabrication

The processing parameters developed in this study, specifically in later-stage experiments involving wetting solvents and nanoparticle inclusion have shown significant improvement in 002-preferential orientation and in the smoothness of surfaces observed in microscopy. To further validate our processes' effectiveness, a few samples showing the best improvement in crystallinity were analyzed by Atomic Force Microscopy (AFM) with an Agilent Technologies model 5420 instrument to obtain RMS surface roughness measurements, as shown in figures 3-10 through 3-12, below.

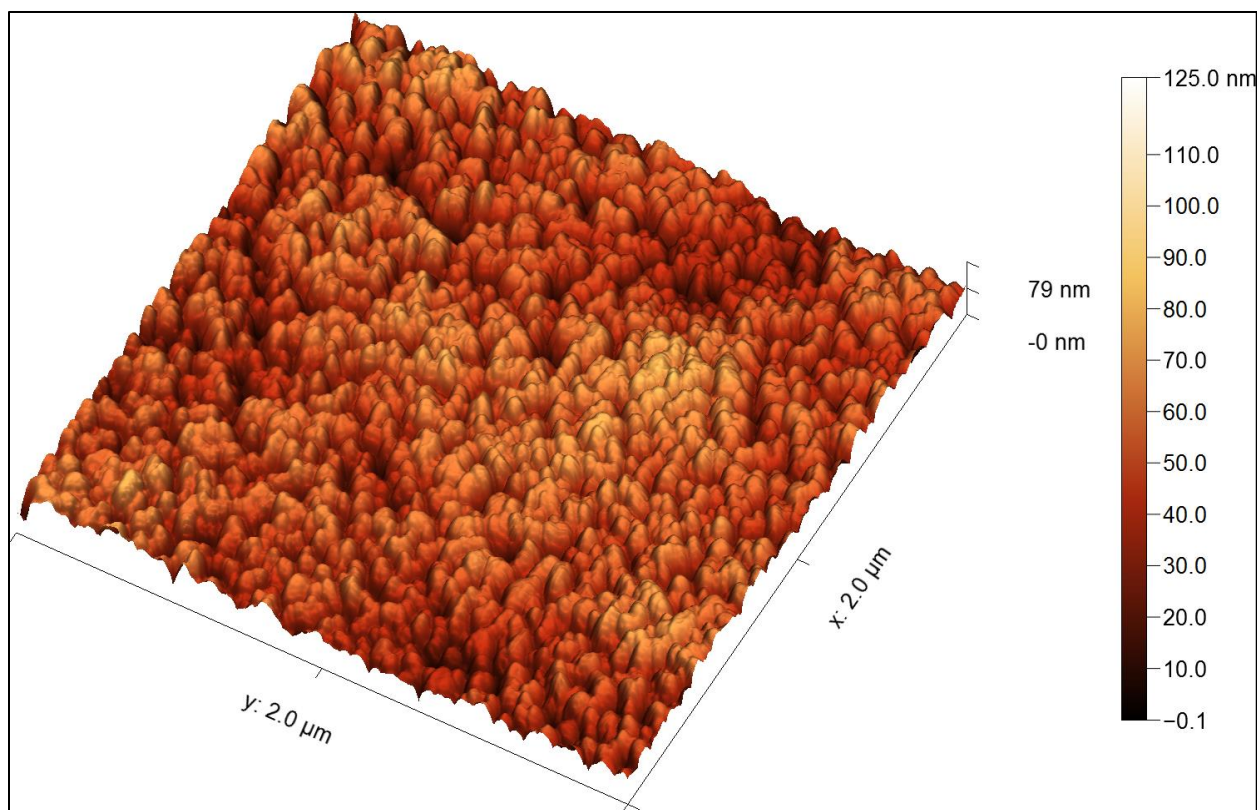


Figure 3-11. AFM 3D Overlay of PGME/AgNP-treated undoped ethanol-based film. RMS roughness (Sq): 10.45nm.

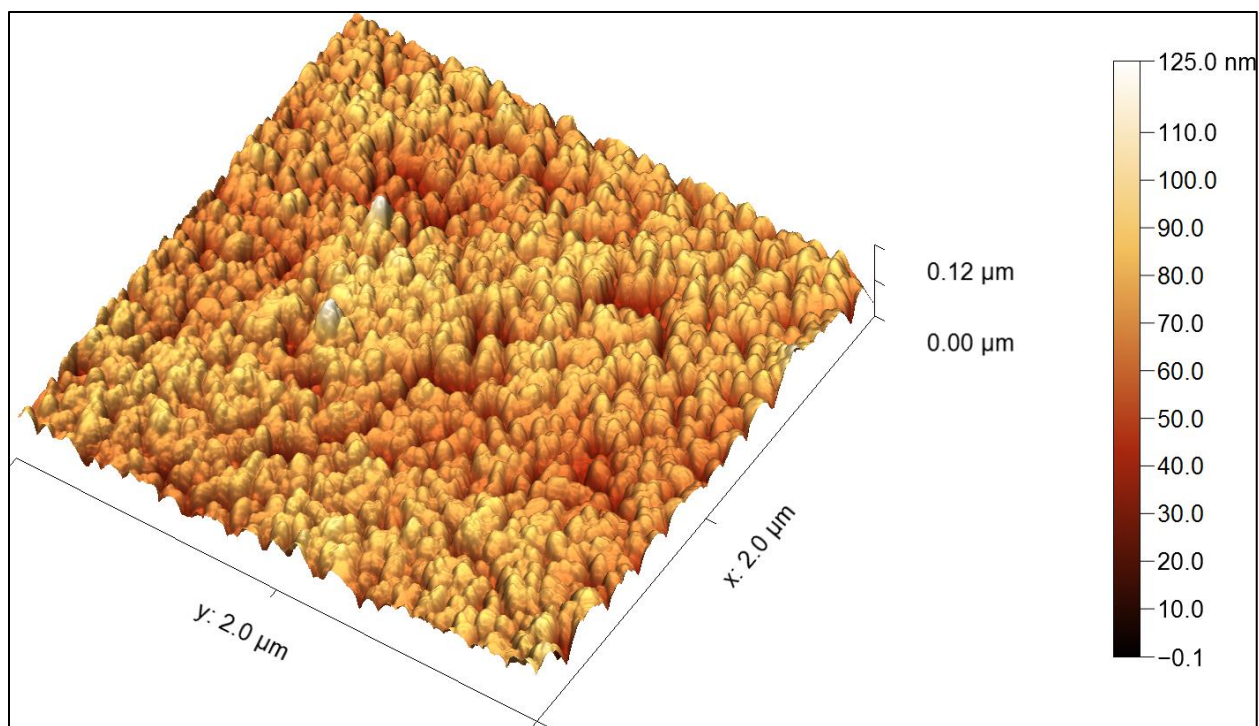


Figure 3-12. AFM 3D Overlay of PGME/AgNP-treated silver-doped ethanol-based film. RMS roughness (S_q): 10.81nm.

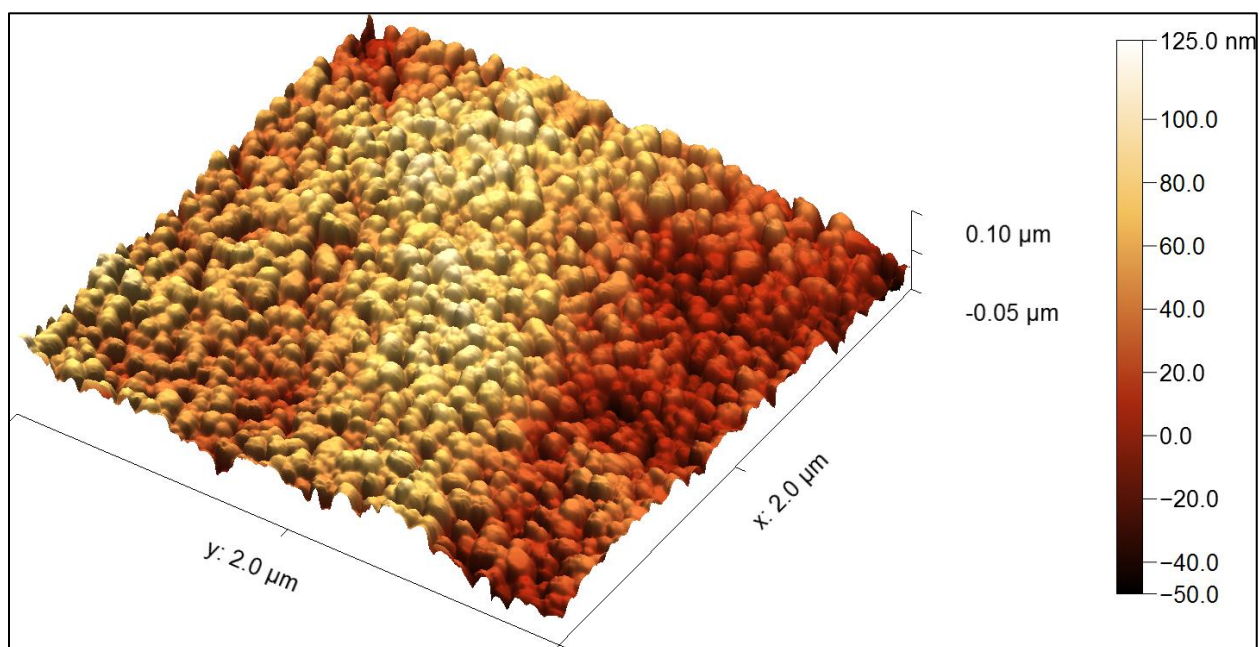


Figure 3-13. AFM 3D Overlay dry (untreated) undoped ethanol-based film. RMS roughness (S_q): 13.54nm.

As seen in these images, both PGME/AgNP-treated, doped and undoped samples show reduced roughness and finer crystallite size compared to the untreated undoped sample.

Use of AgNP, PGME & MEA

Although our study did not utilize EGME as described in Section 3.2.5, we did find some improvement in using PGME as a starting solvent, but more importantly, as the alcohol mixed with the AgNP dispersion during wetting coats. Indeed, PGME/AgNP solution used as a wetting layer between ethanol-based precursor solution performed better than PGME-based precursor solutions, or Ethanol/AgNP wetting solutions, although all wetting treatments containing silver nanoparticles showed significant improvement in 002-crystallinity. While it is well-documented that silver doping of ZnO generally leads to improvement in 002-orientation ratio [32], [36], [41], the mechanism explaining this improvement often deals with silver atoms interstitially replacing zinc, so this explanation is not adequate to explain why larger nanoparticles would also improve crystallinity. The use of AgNP in ZnO thin films to improve conductivity and other parameters has been reported [53], [55], [56], but again, there is little to explain the improvement shown by our particular combination of solvents and treatments.

Nonetheless, the improvements to surface roughness, crystallinity, and c-axis orientation through our wetting and NP processing parameters result in improved surface morphology that we believe will ultimately lead to improved performance in optoelectronic applications.

Chapter 4:
Concluding Thoughts
and Future Work

4.1. Major Findings

A simple, repeatable SOP was established for use in experimental trials of doping and processing treatments of ZnO thin films. This procedure was then utilized to systematically investigate different processing parameters, ultimately leading to breakthroughs in the use of wetting solvents and nanoparticles in thin film fabrication.

We have shown that intra-layer surface wetting of the ZnO film after pre-heat treatment, with nearly any solvent, leads to improved surface features, crystallinity, and smoothness. We further confirm the viability of using PGME rather than EGME as a precursor solvent, that it performs generally as well as ethanol in this regard, and in most cases is superior in silver-doped samples.

Finally, we have demonstrated that the incorporation of silver nanoparticles into surface wetting treatments further improves the film quality by significant margins.

4.2. Additional Findings and Future Work:

While the wetting and nanoparticle processing techniques are the most exciting findings of this project, a few other parameters were investigated throughout Chapter 3 that are worth discussion and follow-up

Substrate Identity

As mentioned, investigation into the use of mica as a substrate due to its similar CTE to ZnO was investigated, but the interference on XRD interference was too great to be useful, and other techniques were showing progress. That said, Experiment B did suggest that borosilicate glass acted as a much better substrate than soda-lime glass for our NP-layered applications, and it was used through Experiment D, although the only slides that could be sourced were extremely thin (less than 1mm) and tended to warp during annealing. Ample literature exists on epitaxial ZnO growth on various

substrate media, so no further investigation was made on this subject at the time, although additional review of existing literature may suggest further study is warranted.

Intra-layer annealing, temperature

In addition to Chapter 2's poorly-documented Project H, intra-layer annealing was reexamined in this stage, Experiment D. No clear trend was observable in XRD preferential crystallinity analysis, as certain samples showed improvement and others detriment to intra-layer annealing, but microscopy seems to indicate smoother films rendered by annealing between each layer. A more detailed experimental analysis, removing some of the confounding parameters present in our experiment, might yield additional findings on this subject, as such a practice is rarely indicated in literature.

Atmosphere and Cleaning Procedures

Experiments B & C sought to eliminate certain externalities from the experimental procedure by implementing more rigorous slide-cleaning procedures and performing deposition and pre-heat treatment under a nitrogen atmosphere. While these procedural improvements did generally seem to improve quality of films, the burden of working in the confines of a glove box proved too much to be worth what little improvement in film quality could be observed.

Given that traditional doping practices involve pressurized gaseous diffusion, investigation into high-pressure sol gel fabrication techniques might be warranted. More thorough understanding of doping methods would be beneficial to such investigations.

4.3. Final Thoughts

Given that one of the primary improvements revolved around the use of PGME over EGME as prescribed by another study, a side-by-side comparison of the two solvents in similar experimental paradigm is certainly warranted. As well, the comparative use of amine bases including ethylene diamine, following the Lee findings can be carried out immediately.

While these breakthrough findings are impressive and exciting in their own regard, and attempts have been made to explain the relationships between structure, properties, and performance of these new processing methods, more rigorous theoretical models need to be developed before additional long-term experimentation. For example, the quantum size effects of material interactions within a solar device should be well-understood and mapped-out in future iterations of this project.

As well, more reliable and quantifiable performance-based characterization methods such as photo- and cathodo-luminescence characterization, and proper, verifiable electrical resistivity measurements are needed to verify assumptions about material properties and performance.

Finally, incorporation of these experimental process findings into real prototypical devices will be required to fully verify these findings.

REFERENCES

- [1] K. Ellmer, Andreas Klein Dr, and B. Rech, *Transparent conductive zinc oxide: basics and applications in thin film solar cells* / Klaus Ellmer, Andreas Klein, Bernd Rech, editors. Berlin: Springer, 2008.
- [2] T. Minami, "Transparent conducting oxide semiconductors for transparent electrodes," *Semiconductor Science and Technology*, vol. 20, no. 4, pp. S35–S44, Apr. 2005.
- [3] ü. Özgür et al., "A comprehensive review of ZnO materials and devices," *Journal of Applied Physics*, vol. 98, no. 4, p. 041301, Aug. 2005.
- [4] S. S. Alias and A. A. Mohamad, *Synthesis of Zinc Oxide by Sol–Gel Method for Photoelectrochemical Cells*. Singapore: Springer Singapore, 2014.
- [5] K. Kawano, R. Pacios, D. Poplavskyy, J. Nelson, D. D. C. Bradley, and J. R. Durrant, "Degradation of organic solar cells due to air exposure," *Solar Energy Materials and Solar Cells*, vol. 90, no. 20, pp. 3520–3530, Dec. 2006.
- [6] H. Cao et al., "Recent progress in degradation and stabilization of organic solar cells," *Journal of Power Sources*, vol. 264, pp. 168–183, Oct. 2014.
- [7] A. Tanaka et al., "Review of pulmonary toxicity of indium compounds to animals and humans," *Thin Solid Films*, vol. 518, no. 11, pp. 2934–2936, Mar. 2010.
- [8] Polinares - EU policy on Natural Resources, "Fact Sheet: Indium," *European Commission Socio-economic Sciences & Humanities*, 2012.
- [9] D. Angmo and F. C. Krebs, "Flexible ITO-free polymer solar cells," *Journal of Applied Polymer Science*, vol. 129, no. 1, pp. 1–14, Jul. 2013.
- [10] G. J. Fosmire, "Zinc toxicity," *Am J Clin Nutr*, vol. 51, no. 2, pp. 225–227, Feb. 1990.
- [11] V. A. Coleman and C. Jagadish, "Chapter 1 - Basic Properties and Applications of ZnO," in *Zinc Oxide Bulk, Thin Films and Nanostructures*, Oxford: Elsevier Science Ltd, 2006, pp. 1–20.
- [12] S. O'Brien, L. H. K. Koh, and G. M. Crean, "ZnO thin films prepared by a single step sol–gel process," *Thin Solid Films*, vol. 516, no. 7, pp. 1391–1395, Feb. 2008.
- [13] D. Angmo and F. C. Krebs, "Over 2 Years of Outdoor Operational and Storage Stability of ITO-Free, Fully Roll-to-Roll Fabricated Polymer Solar Cell Modules," *Energy Technology*, vol. 3, no. 7, pp. 774–783, Jul. 2015.
- [14] A. C. Pierre, *Introduction to sol-gel processing*. Boston: Kluwer Academic Publishers, 1998.
- [15] L. Znaidi, G. J. A. A. Soler Illia, S. Benyahia, C. Sanchez, and A. V. Kanaev, "Oriented ZnO thin films synthesis by sol–gel process for laser application," *Thin Solid Films*, vol. 428, no. 1–2, pp. 257–262, Mar. 2003.
- [16] L. Znaidi, "Sol–gel-deposited ZnO thin films: A review," *Materials Science and Engineering: B*, vol. 174, no. 1–3, pp. 18–30, Oct. 2010.
- [17] R. E. Hummel, "Electrical Properties of Polymers, Ceramics, Dielectrics, and Amorphous Materials," in *Electronic Properties of Materials*, 4th ed., New York, NY: Springer Science+Business Media, LLC, 2011, pp. 181–211.
- [18] R. Gu et al., "Substrate polarity and surface pretreatment temperature dependence of ZnO homoepitaxy," *Applied Surface Science*, vol. 361, pp. 33–40, Jan. 2016.
- [19] N. F. Foster and G. A. Rozgonyi, "ZINC OXIDE FILM TRANSDUCERS," *Appl. Phys. Lett.*, vol. 8, no. 9, pp. 221–223, May 1966.
- [20] N. F. Foster, "Crystallographic Orientation of Zinc Oxide Films Deposited by Triode Sputtering," *Journal of Vacuum Science and Technology*, vol. 6, no. 1, pp. 111–114, Jan. 1969.
- [21] L. Znaidi, G. S. Illia, R. Le Guennic, C. Sanchez, and A. Kanaev, "Elaboration of ZnO thin films with preferential orientation by a soft chemistry route," *Journal of Sol-Gel Science and Technology*, vol. 26, no. 1–3, pp. 817–821, 2003.
- [22] M. Zhao et al., "Influence of water content in mixed solvent on surface morphology, wettability, and photoconductivity of ZnO thin films," *Nanoscale Res Lett*, vol. 9, no. 1, p. 485, Sep. 2014.

- [23] S. Lemlikchi, S. Abdelli-Messaci, S. Lafane, T. Kerdja, A. Guittoum, and M. Saad, "Study of structural and optical properties of ZnO films grown by pulsed laser deposition," *Applied Surface Science*, vol. 256, no. 18, pp. 5650–5655, Jul. 2010.
- [24] S. Zhang, D. Sun, and X. L. Bui, "MAGNETRON SPUTTERED HARD AND YET TOUGH NANOCOMPOSITE COATINGS WITH CASE STUDIES: NANOCRYSTALLINE TiN EMBEDDED IN AMORPHOUS SiN_x," in *Nanocomposite Thin Films and Coatings*, PUBLISHED BY IMPERIAL COLLEGE PRESS AND DISTRIBUTED BY WORLD SCIENTIFIC PUBLISHING CO., 2007, pp. 1–110.
- [25] D. NYUNG, "A model for development of orientation of vapour deposits," p. 2.
- [26] K. Yim et al., "Property database for single-element doping in ZnO obtained by automated first-principles calculations (Supplement)," *Scientific Reports*, vol. 7, p. 40907, Jan. 2017.
- [27] K. Yim et al., "Property database for single-element doping in ZnO obtained by automated first-principles calculations," *Scientific Reports*, vol. 7, p. 40907, Jan. 2017.
- [28] Y. Yan, M. M. Al-Jassim, and S.-H. Wei, "Doping of ZnO by group-IB elements," *Applied Physics Letters*, vol. 89, no. 18, p. 181912, Oct. 2006.
- [29] William D. Callister and D. G. Rethwisch, *Materials Science and Engineering: An Introduction*, 8th ed. Wiley, 2009.
- [30] M. S. Tokumoto, S. H. Pulcinelli, C. V. Santilli, and V. Briois, "Catalysis and Temperature Dependence on the Formation of ZnO Nanoparticles and of Zinc Acetate Derivatives Prepared by the Sol–Gel Route," *The Journal of Physical Chemistry B*, vol. 107, no. 2, pp. 568–574, Jan. 2003.
- [31] L. Spanhel, "Colloidal ZnO nanostructures and functional coatings: A survey," *Journal of Sol-Gel Science and Technology*, vol. 39, no. 1, pp. 7–24, Jul. 2006.
- [32] T. Touam et al., "Effect of silver doping on the structural, morphological, optical and electrical properties of sol–gel deposited nanostructured ZnO thin films," *Optik - International Journal for Light and Electron Optics*, vol. 126, no. 24, pp. 5548–5552, Dec. 2015.
- [33] Y. Natsume and H. Sakata, "Zinc oxide films prepared by sol-gel spin-coating," *Thin Solid Films*, vol. 372, no. 1–2, pp. 30–36, Sep. 2000.
- [34] Y.-K. Tseng, G.-J. Gao, and S.-C. Chien, "Synthesis of c-axis preferred orientation ZnO:Al transparent conductive thin films using a novel solvent method," *Thin Solid Films*, vol. 518, no. 22, pp. 6259–6263, Sep. 2010.
- [35] P. Sagar, P. K. Shishodia, and R. M. Mehra, "Influence of pH value on the quality of sol–gel derived ZnO films," *Applied Surface Science*, vol. 253, no. 12, pp. 5419–5424, Apr. 2007.
- [36] F. Xian, K. Miao, X. Bai, Y. Ji, F. Chen, and X. Li, "Characteraction of Ag-doped ZnO thin film synthesized by sol–gel method and its using in thin film solar cells," *Optik - International Journal for Light and Electron Optics*, vol. 124, no. 21, pp. 4876–4879, Nov. 2013.
- [37] X. Jin, Z. Zi-Yu, Z. Yang, L. Bi-Xia, and F. Zhu-Xi, "Effect of Ag Doping on Optical and Electrical Properties of ZnO Thin Films," *Chinese Physics Letters*, vol. 22, no. 8, pp. 2031–2034, Aug. 2005.
- [38] A. Chelouche, D. Djouadi, H. Merzouk, and A. Aksas, "Influence of Ag doping on structural and optical properties of ZnO thin films synthesized by the sol–gel technique," *Applied Physics A*, vol. 115, no. 2, pp. 613–616, May 2014.
- [39] M. A. Myers, L. Joon Hwan, B. Zhenxing, and M. Haiyan, "High quality p-type Ag-doped ZnO thin films achieved under elevated growth temperatures," *Journal of Physics: Condensed Matter*, vol. 24, no. 22, p. 229501, Jun. 2012.
- [40] M. E. Koleva, A. O. Dikovska, N. N. Nedyalkov, P. A. Atanasov, and I. A. Bliznakova, "Enhancement of ZnO photoluminescence by laser nanostructuring of Ag underlayer," *Applied Surface Science*, vol. 258, no. 23, pp. 9181–9185, Sep. 2012.
- [41] Y. Chen, X. L. Xu, G. H. Zhang, H. Xue, and S. Y. Ma, "A comparative study of the microstructures and optical properties of Cu- and Ag-doped ZnO thin films," *Physica B: Condensed Matter*, vol. 404, no. 20, pp. 3645–3649, Nov. 2009.
- [42] W. J. Li et al., "Electrical properties and Raman scattering investigation of Ag doped ZnO thin films," *Solid State Communications*, vol. 152, no. 2, pp. 147–150, Jan. 2012.

- [43] H. Xue, X. L. Xu, Y. Chen, G. H. Zhang, and S. Y. Ma, "Influence of Ag-doping on the optical properties of ZnO films," *Applied Surface Science*, vol. 255, no. 5, pp. 1806–1810, Dec. 2008.
- [44] X. B. Wang, C. Song, K. W. Geng, F. Zeng, and F. Pan, "Luminescence and Raman scattering properties of Ag-doped ZnO films," *Journal of Physics D: Applied Physics*, vol. 39, no. 23, pp. 4992–4996, Dec. 2006.
- [45] D. R. Sahu, "Studies on the properties of sputter-deposited Ag-doped ZnO films," *Microelectronics Journal*, vol. 38, no. 12, pp. 1252–1256, Dec. 2007.
- [46] K. Liu et al., "Effect of Ag doping on the photoluminescence properties of ZnO films," *Journal of Luminescence*, vol. 129, no. 9, pp. 969–972, Sep. 2009.
- [47] K. Liu et al., "Strong room-temperature ultraviolet emission from nanocrystalline ZnO and ZnO:Ag films grown by ultrasonic spray pyrolysis," *Applied Surface Science*, vol. 255, no. 5, pp. 2052–2056, Dec. 2008.
- [48] R. Chen, C. Zou, J. Bian, A. Sandhu, and W. Gao, "Microstructure and optical properties of Ag-doped ZnO nanostructures prepared by a wet oxidation doping process," *Nanotechnology*, vol. 22, no. 10, p. 105706, Mar. 2011.
- [49] X. Li and Y. Wang, "Structure and photoluminescence properties of Ag-coated ZnO nano-needles," *Journal of Alloys and Compounds*, vol. 509, no. 19, pp. 5765–5768, May 2011.
- [50] Y.-W. Song, K. Kim, and S. Y. Lee, "Morphology transition of Ag-doped ZnO nanostructures in hot-walled pulsed laser deposition," *Thin Solid Films*, vol. 518, no. 4, pp. 1318–1322, Dec. 2009.
- [51] Y.-W. Song, K. Kim, J. P. Ahn, G.-E. Jang, and S. Y. Lee, "Physically processed Ag-doped ZnO nanowires for all-ZnO p–n diodes," *Nanotechnology*, vol. 20, no. 27, p. 275606, Jul. 2009.
- [52] D. R. Sahu, S.-Y. Lin, and J.-L. Huang, "Study on the electrical and optical properties of Ag/Al-doped ZnO coatings deposited by electron beam evaporation," *Applied Surface Science*, vol. 253, no. 11, pp. 4886–4890, Mar. 2007.
- [53] X. D. Zhou, X. H. Xiao, J. X. Xu, G. X. Cai, F. Ren, and C. Z. Jiang, "Mechanism of the enhancement and quenching of ZnO photoluminescence by ZnO-Ag coupling," *EPL (Europhysics Letters)*, vol. 93, no. 5, p. 57009, Mar. 2011.
- [54] Y. Wei et al., "Enhanced photoelectrochemical water-splitting effect with a bent ZnO nanorod photoanode decorated with Ag nanoparticles," *Nanotechnology*, vol. 23, no. 23, p. 235401, Jun. 2012.
- [55] C.-S. Hong, H.-H. Park, H.-H. Park, and H. J. Chang, "Optical and electrical properties of ZnO thin film containing nano-sized Ag particles," *Journal of Electroceramics*, vol. 22, no. 4, pp. 353–356, Jun. 2009.
- [56] M. H. Habibi and R. Sheibani, "Preparation and characterization of nanocomposite ZnO–Ag thin film containing nano-sized Ag particles: influence of preheating, annealing temperature and silver content on characteristics," *Journal of Sol-Gel Science and Technology*, vol. 54, no. 2, pp. 195–202, May 2010.
- [57] F. K. Lotgering, "Topotactical reactions with ferrimagnetic oxides having hexagonal crystal structures—I," *Journal of Inorganic and Nuclear Chemistry*, vol. 9, no. 2, pp. 113–123, Feb. 1959.
- [58] Ossila Ltd, "Spin Coating: A Guide to Theory and Techniques."
- [59] D. Raoufi and T. Raoufi, "The effect of heat treatment on the physical properties of sol–gel derived ZnO thin films," *Applied Surface Science*, vol. 255, no. 11, pp. 5812–5817, Mar. 2009.
- [60] Y.-S. Kim, W.-P. Tai, and S.-J. Shu, "Effect of preheating temperature on structural and optical properties of ZnO thin films by sol–gel process," *Thin Solid Films*, vol. 491, no. 1–2, pp. 153–160, Nov. 2005.
- [61] L. Znaidi et al., "AZO Thin Films by Sol-Gel Process for Integrated Optics," *Coatings*, vol. 3, no. 4, pp. 126–139, Jul. 2013.
- [62] N. Nagarani, "Structural and Optical Characterization of ZnO thin films by Sol- Gel Method," p. 3, 2013.
- [63] J. Wang, Y. Qi, Z. Zhi, J. Guo, M. Li, and Y. Zhang, "A self-assembly mechanism for sol–gel derived ZnO thin films," *Smart Materials and Structures*, vol. 16, no. 6, pp. 2673–2679, Dec. 2007.
- [64] M. B. Heaney, "Electrical Conductivity and Resistivity," *Signal Processing*, p. 14, 2004.
- [65] S. Hasegawa et al., "Direct measurement of surface-state conductance by microscopic four-point probe method," *Journal of Physics: Condensed Matter*, vol. 14, no. 35, pp. 8379–8392, Sep. 2002.

- [66] "Engineering ToolBox, (2003). Coefficients of Linear Thermal Expansion. [online] Available at: https://www.engineeringtoolbox.com/linear-expansion-coefficients-d_95.html [Accessed 8 Nov. 2017]."
- [67] N. Yamamoto, H. Makino, and T. Yamamoto, "Young's Modulus and Coefficient of Linear Thermal Expansion of ZnO Conductive and Transparent Ultra-Thin Films," *Advances in Materials Science and Engineering*, vol. 2011, pp. 1–10, 2011.
- [68] L. Znaidi et al., "Textured ZnO thin films by sol–gel process: Synthesis and characterizations," *Thin Solid Films*, vol. 617, pp. 156–160, Oct. 2016.
- [69] S. Chakrabarti, D. Ganguli, and S. Chaudhuri, "Substrate dependence of preferred orientation in sol–gel-derived zinc oxide films," *Materials Letters*, vol. 58, no. 30, pp. 3952–3957, Dec. 2004.
- [70] C. Barrett, *Structure of Metals: Crystallographic Methods, Principles, and Data*, 1st ed. McGraw-Hill Book Company, Inc., 1943.
- [71] M. Wang et al., "Optical and structural properties of sol–gel prepared MgZnO alloy thin films," *Thin Solid Films*, vol. 516, no. 6, pp. 1124–1129, Jan. 2008.
- [72] R. Viswanatha, S. Chakraborty, S. Basu, and D. D. Sarma, "Blue-Emitting Copper-Doped Zinc Oxide Nanocrystals," *The Journal of Physical Chemistry B*, vol. 110, no. 45, pp. 22310–22312, Nov. 2006.
- [73] C. A. Parker et al., "Optical band gap dependence on composition and thickness of $\text{In}_x\text{Ga}_{1-x}\text{N}$ ($0 < x < 0.25$) grown on GaN," *Applied Physics Letters*, vol. 75, no. 17, pp. 2566–2568, Oct. 1999.
- [74] Friedrich Menges, Spectragryph v1.2.9. Optical spectroscopy software. .
- [75] S. Fay and A. Shah, "Zinc Oxide Grown by CVD Process as Transparent Contact for Thin Film Solar Cell Applications," in *Transparent Conductive Zinc Oxide: Basics and Applications in Thin Film Solar Cells*, .
- [76] R. E. Marotti, P. Giorgi, G. Machado, and E. A. Dalchiele, "Crystallite size dependence of band gap energy for electrodeposited ZnO grown at different temperatures," *Solar Energy Materials and Solar Cells*, vol. 90, no. 15, pp. 2356–2361, Sep. 2006.
- [77] S. Khosravi-Gandomani, R. Yousefi, F. Jamali-Sheini, and N. M. Huang, "Optical and electrical properties of p-type Ag-doped ZnO nanostructures," *Ceramics International*, vol. 40, no. 6, pp. 7957–7963, Jul. 2014.
- [78] S. Benramache, O. Belahssen, A. Arif, and A. Guettaf, "A correlation for crystallite size of undoped ZnO thin film with the band gap energy – precursor molarity – substrate temperature," *Optik - International Journal for Light and Electron Optics*, vol. 125, no. 3, pp. 1303–1306, Feb. 2014.
- [79] S. M. Hosseini, I. A. Sarsari, P. Kameli, and H. Salamati, "Effect of Ag doping on structural, optical, and photocatalytic properties of ZnO nanoparticles," *Journal of Alloys and Compounds*, vol. 640, pp. 408–415, Aug. 2015.
- [80] B. R. Lee et al., "Highly efficient inverted polymer light-emitting diodes using surface modifications of ZnO layer," *Nature Communications*, vol. 5, no. 1, Dec. 2014.
- [81] B. R. Lee et al., "Amine-Based Polar Solvent Treatment for Highly Efficient Inverted Polymer Solar Cells," *Advanced Materials*, vol. 26, no. 3, pp. 494–500, Jan. 2014.
- [82] M. Duta, D. Perniu, and A. Duta, "Photocatalytic zinc oxide thin films obtained by surfactant assisted spray pyrolysis deposition," *Applied Surface Science*, vol. 306, pp. 80–88, Jul. 2014.

Appendix A: Table of chemical systems reviewed by Znaidi in ZnO Sol-gel Review:

References	Precursor (mol L ⁻¹)	Alcohol	Additive (r)	H ₂ O (h)	Aging time	Substrate	Pre-heat treatment (°C)	Post-heat treatment (°C)	Thickness (nm)	Crystallographic orientation
Natsume and Sakata [61]	ZAD (0.02)	MeOH	-	-	-	Pyrex	80	500-575	160-230	(002)
González et al. [62]	ZAD (0.59)	MeOH	-	-	24 h	Corning glass	50	300, 450	35-204	(100)(002)(101) (100)(002)(101)
Santos et al. [63,64]	ZAD ^a	MeOH	-	-	-	Glass	120	350	(18L) ^a	(002)
Sagar et al. [65,66]	ZAD (0.6)	MeOH	MEA (0-1)	-	48 h	Corning glass	300	400-600	180-190	(002)
Liu et al. [67,68]	ZAD (0.6)	EtOH, PEG (14 g/L)	DEA (1)	(2)	-	Glass	100	500	220 (6L)	(100)(002)(101)
Wang et al. [69]	ZAD (0.5)	EtOH	DEA (1)	-	-	Quartz	400	400-800	300 (6L)	(100)(002)(101)
Kumar et al. [70]	ZAD (0.2)	EtOH	DEA (1)	-	48 h	p-Si(100)	250	350-450	~250	(100)(002)(101)
Shaoqiang et al. [4]	ZAD (0.46)	EtOH	-	-	-	n- and p-type Silicon	40	500 (directly)	200	(002)
Znaidi et al. [47,48]	ZAD (0.05)	EtOH	MEA (2)	-	72 h	Glass	100-135	500 (Gradually)	-	(100)(002)(101) (100)
Wang et al. [71]	ZAD (1.8)	EtOH	MEA (1.5)	-	72 h	Glass	300	350-600	(5L) ^a	(100)(002)(101)
Wang et al. [72]	ZAD (0.19)	EtOH	Ac. Ac. (0.35)	(11.1)	24 h	Glass	100	450	-	(100)
Bao et al. [46]	ZAD (0.4)	EtOH	Lactic Ac.	-	2 h	Quartz	300	500, 550	300 (6L)	Amorphous film (002)
Bole and Patil [73]	ZAD ^a	EtOH	Lactic Ac.	-	-	Glass	300	300-425	375-275	(100)(002)(101)
Kavanagh and Cameron [74]	ZAD ^a	EtOH	Lactic Ac.	(2)	-	Silicon	240	700	-	(100)(002)(101)
Bahadur and Rao [75]	ZAD ^a	EtOH	LiOH-H ₂ O	-	-	F:SnO ₂	80	400	800 (5L)	(100)(002)(101)
Brenier and Ortéga [76]	ZAD (0.15)	1-PrOH	TMAH	-	4 weeks	Silicon	80	250 (O ₂)	20-60	(100)(002)(101)
Peterson et al. [77]	ZAD (0.3)	1-PrOH	Glycerol	-	-	Si(100), quartz	300	700	180 (4L)	(100)(002)(101)
Raoufi et al. [78]	ZAD (0.3)	1-PrOH	MEA (1)	-	-	Glass	250	300-500	500 (8L)	(100)(002)(101)
O'Brien et al. [79] and Rao et al. [80]	ZAD (0.3-0.7) (1.3)	2-PrOH	MEA (1)	-	24 h	UV fused silica	60	450-650	84-437	(100)(002)(101)
Kim et al. [3]	ZAD (0.3-0.5) (0.7) (1-1.3)	2-PrOH	MEA (1)	-	24 h	Corning glass	250	650	-	(100)(002)(101) Amorphous film
Lin and Kim [81]	ZAD (0.5)	2-PrOH	DEA (1)	-	24 h	Si(100), Glass	300	450-550	280 (7L)	(100)(002)(101) (101) ^b
Aslan et al. [82]	ZAD (0.4)	2-PrOH	DEA (1)	(0.5)	-	Si(100) Glass	250	700, 800	1000-1600 (10-15L)	(100)(002)(101) (100)(002)(101)
Chakrabarti et al. [83]	ZAD (0.24)	2-PrOH	DEA (0.006)	-	-	Glass p-Si(100), Soda-lime, quartz, alumina	100	550	-	(002) (100)(002)(101)
Jiwei et al. [84]	ZAD (0.4)	2-PrOH	DEA (1)	(2)	-	SiO ₂ /Si(111), fused-quartz	200 (O ₂)	300-650 (O ₂)	230-350	(100)(002)(101)
Wang et al. [85]	ZAD (0.32)	2-PrOH	DEA (1)	-	-	Si/SiO ₂ /Ti/Pt	300-450	550-800	500 (6L)	(100)(002)(101)
Bae and Choi [86]	ZAD (0.25)	2-PrOH	DEA (1.5)	-	-	Alumina	300	400-900	125-240 (3-6L)	(100)(002) (101) ^b
Ohya et al. [44,87] and Takahashi et al. [88]	ZAD (0.25/0.5)	2-PrOH	DEA (1)	(2)	-	Glass	110	350-600	13-33/L	(100)(002)(101)
Mridha and Basak [89]	ZAD (0.1)	2-PrOH	DEA	-	-	Glass	120	550	260	(100)(002)(101)
Dutta et al. [90]	ZAD (0.03-0.1)	2-PrOH	DEA	-	-	Glass	350	550	36-247	(100)(002)(101)
Basak et al. [91]	ZAD (0.6)	2-PrOH	DMA	-	-	Sapphire	120	550	300 (10L)	(100)(002)(101)
Ghosh et al. [6,92,93]	ZAD (0.6)	2-PrOH	DMA	-	-	Quartz Glass, Si/SiO ₂	120	550	400 (10L)	(100)(002)(101) (100)(002)(101)
Zhang et al. [94]	ZAD (0.3)	PVA	-	-	-	GaN	120	600	434	(002) (100)(002)(101)
Pal and Sharon [95]	ZA (<0.03)	2-PrOH	NaOH (1)	-	-	Si(100) Glass	-	400	5-6L ^a	(100)(002)(101)
Abdel Aal et al. [96]	ZAD ^a	2-PrOH	NaOH	-	-	Glass	-	550	(6L) ^a	(002)
Caglar et al. [97]	ZAD (1)	2-ME	MEA (1)	-	-	p-type single crystal Si	300, 450	550-750	(10L) ^a	(100)(002)(101)
Ohyama et al. [98]	ZAD (0.75)	2-ME	MEA (1)	-	-	Silica	300	600	100-260	(002)
Li et al. [99,100]	ZAD (0.75)	2-ME	MEA (1)	-	-	Silica	300	600	300 (7L)	(002)
Zhu et al. [101]	ZAD (0.75)	2-ME	MEA (1)	-	-	Glass	60	400-550	(4L) ^a	(100)(002)(101)
Fujihara et al. [102]	ZAD (0.75)	2-ME	MEA (1.1)	-	-	Glass	400-500	400-500	200 (5L)	(002)
Znaidi et al. [47,48]	ZAD (0.75)	2-ME	MEA (2)	-	-	Glass	300	500-550	76 (3L)	(002)
Ohyama et al. [45]	ZAD (0.6)	2-ME	MEA (1)	-	-	Silica	500	500	-	(002) (100)(002) (101) ^b

References	Precursor (mol L ⁻¹)	Alcohol	Additive (r)	H ₂ O (h)	Aging time	Substrate	Pre-heat treatment (°C)	Post-heat treatment (°C)	Thickness (nm)	Crystallographic orientation
Nagase et al. [103]	ZAD (0.6)	2-ME	MEA (1)	-	-	Quartz	200	Laser irradiation 600-900	35-190	(002)
Hsieh et al. [104,105]	ZAD (0.6)	2-ME	MEA (1)	-	-	SiO ₂ /Si	270		-	(100)(002)(101)
Yoon et al. [106]	ZAD (0.5)	2-ME	MEA (1) DEA (1)	-	72 h	SiN _x /Si, Pt(111)/Si SiN _x /Si	300	700	140 (5L)	(002) (100)(002) (101) ^b (002) (002)
Choi et al. [107]	ZAD (0.5)	2-ME	MEA (1)	-	-	Pt/TiO ₂ /SiO ₂ /Si	300	400-700	180	(002)
Srinivasan et al. [108-110]	ZAD (0.5)	2-ME	MEA (1)	-	-	Glass, quartz (001) sapphire	350 100, 400	500 450-600	(8L) ^a 530 (10L)	(100)(002)(101) (100)(002)(101)
Kokubun et al. [111]	ZAD (0.45)	2-ME	MEA (1)	-	-	Silica	90/300	500/600	150	(100)(002)(101)
Lee et al. [112]	ZAD (0.35)	2-ME	MEA (1)	-	48 h	Corning glass	350	600	200	(002)
Xue et al. [113]	ZAD (0.35)	2-ME	MEA (1)	-	24 h	Fused silica	300	500	800 (12L)	(100)(002)(101)
Castanedo-Pérez et al. [114]	ZAD (1.14)	EG, 1-PrOH	Glycerol, TEA	(0.31)	30 h	Soda-lime glass, silicon	100	450	160	(100)(002)(101)
Delgado et al. [115]	ZAD ^a	EG, 1-PrOH	Glycerol, TEA	-	24 h	Glass	100	200-600	450 (5L)	(100)(002)(101)
Kamalasanan and Chandra [116]	ZAD (<1.98)	EG, 1-PrOH	Glycerol, TEA	-	-	Soda glass, silicon	-	450	200/L	(100)(002)(101)
Chatterjee et al. [117]	ZNH ^a	PVA	-	-	-	Silicon	-	700-850	~1000	(100)(002)(101)
Toyoda et al. [118]	ZNH ^a	2-ME	-	-	-	Platinized Si	25	250-450 600	^a	(002) (100)(002)(101)
Okamura et al. [43,119]	Zn(OEt) ₂ ^a	1-BuOH	Acac	-	-	p-Si(111)	-	700 (O ₂)	20/L	(100)(002) (101) ^b
Ohya et al. [44,87]	Zn(OPr ⁿ) ₂ (0.2/0.5)	2-PrOH	DEA (1)	(2)	-	Glass	110	600	11-33/L	(100)(002)(101)

Abbreviations (Abbrev.):

Abbrev.	Product name	Chemical formula	Abbrev.	Product name	Chemical formula
ZAD	Zinc acetate dihydrate	[Zn(CH ₃ COO) ₂ ·2H ₂ O]	MeOH	Methanol	CH ₃ OH
ZA	Zinc acetate anhydrous	[Zn(CH ₃ COO) ₂]	EtOH	Ethanol	C ₂ H ₅ OH
ZNH	Zinc nitrate hexahydrate	[Zn(NO ₃) ₂ ·6H ₂ O]	1-PrOH	1-Propanol	C ₃ H ₇ OH
MEA	Monoethanolamine	(HOCH ₂ CH ₂)NH ₂	2-PrOH	2-Propanol	(CH ₃) ₂ CHOH
DEA	Diethanolamine	(HOCH ₂ CH ₂) ₂ NH	1-BuOH	1-Butanol	C ₄ H ₉ OH
TEA	Triethanolamine	(HOCH ₂ CH ₂) ₃ N	2-ME	2-Methoxyethanol	CH ₃ O(CH ₂) ₂ OH
DMA	Dimethylamine	(CH ₃) ₂ NH	EG	Ethylene glycol	HO(CH ₂) ₂ OH
PVA	Polyvinyl alcohol	[-CH ₂ CH(OH)-] _n	PEG	Polyethylene glycol	H(OCH ₂ CH ₂) _n OH
TMAH	Tetramethylammonium hydroxide	(CH ₃) ₄ N(OH)	Ac. Ac.	Acetic Acid	CH ₃ COOH
Acac	Acetylacetonate	CH ₃ COCH ₂ COCH ₃	Lactic Ac.	Lactic Acid	CH ₃ CHOHCOOH

In the thickness column: L: layer. The numbers between brackets for additive and water columns correspond to *r* and *h* values, respectively where:

$r = [\text{additive}]/[\text{Zn}^{2+}]$, $h = [\text{H}_2\text{O}]/[\text{Zn}^{2+}]$.

In the crystallographic orientation column: diffraction peak indicated in bold corresponds to highly oriented films according to one of three main orientations.

^a The precursor concentration in the chemical system and thickness are indicated only when they are mentioned in the corresponding reference.

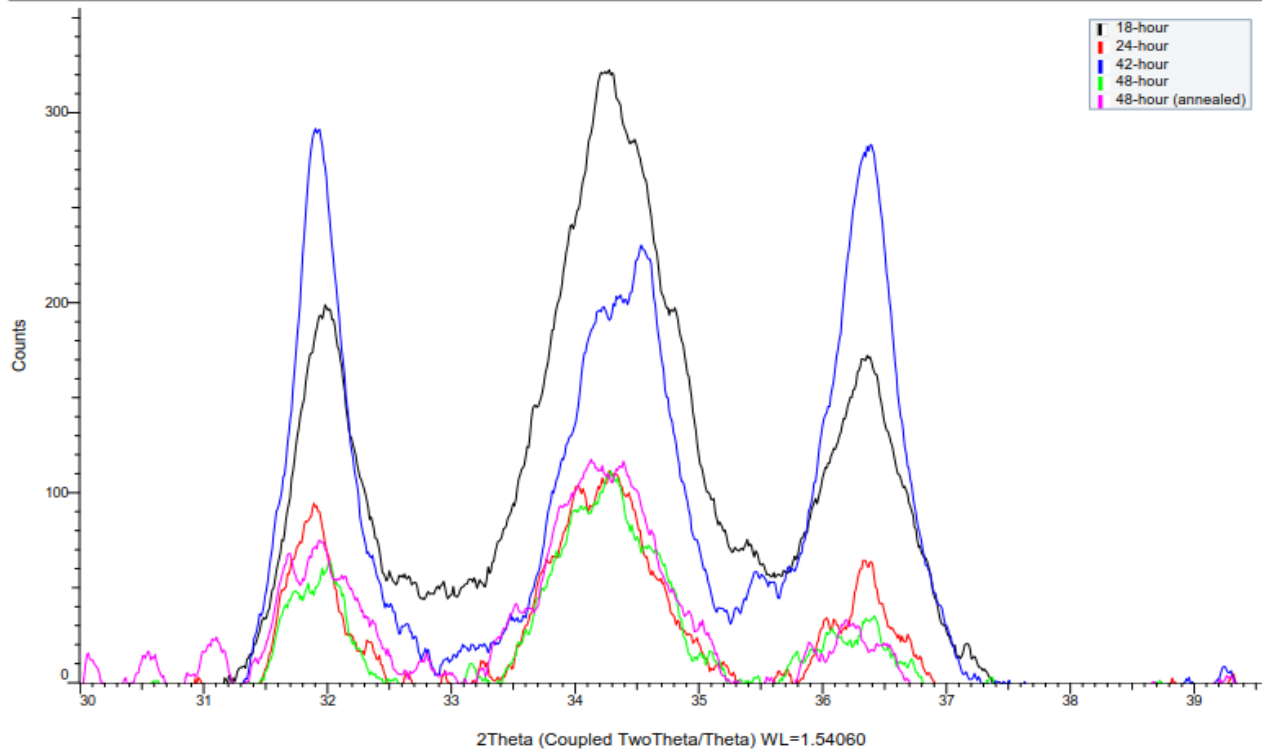
^b The peaks intensities are very close.

Source: L. Znaidi, "Sol-gel-deposited ZnO thin films: A review," Materials Science and Engineering: B, vol. 174, no. 1-3, pp. 18-30, Oct. 2010.

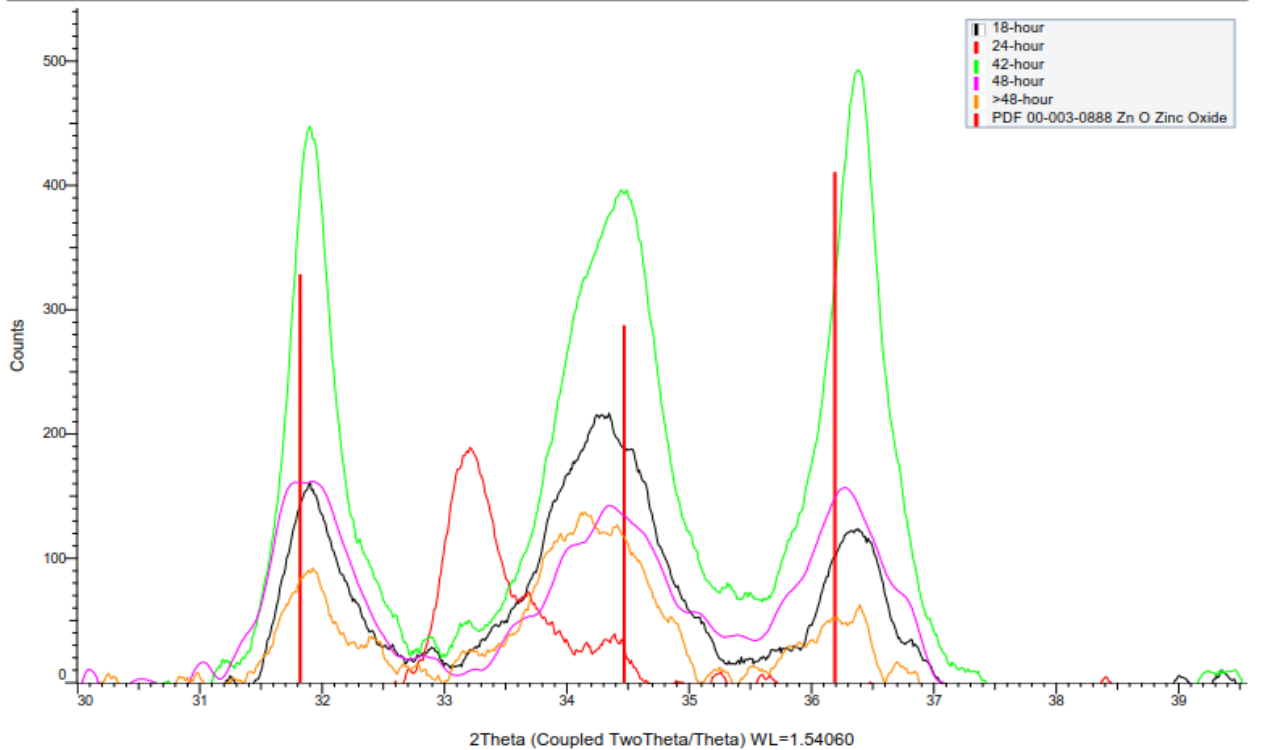
Appendix B: X-Ray Diffractograms

Appendix B-2AB: Chapter 2, Experiments A/B(p. 1/6)

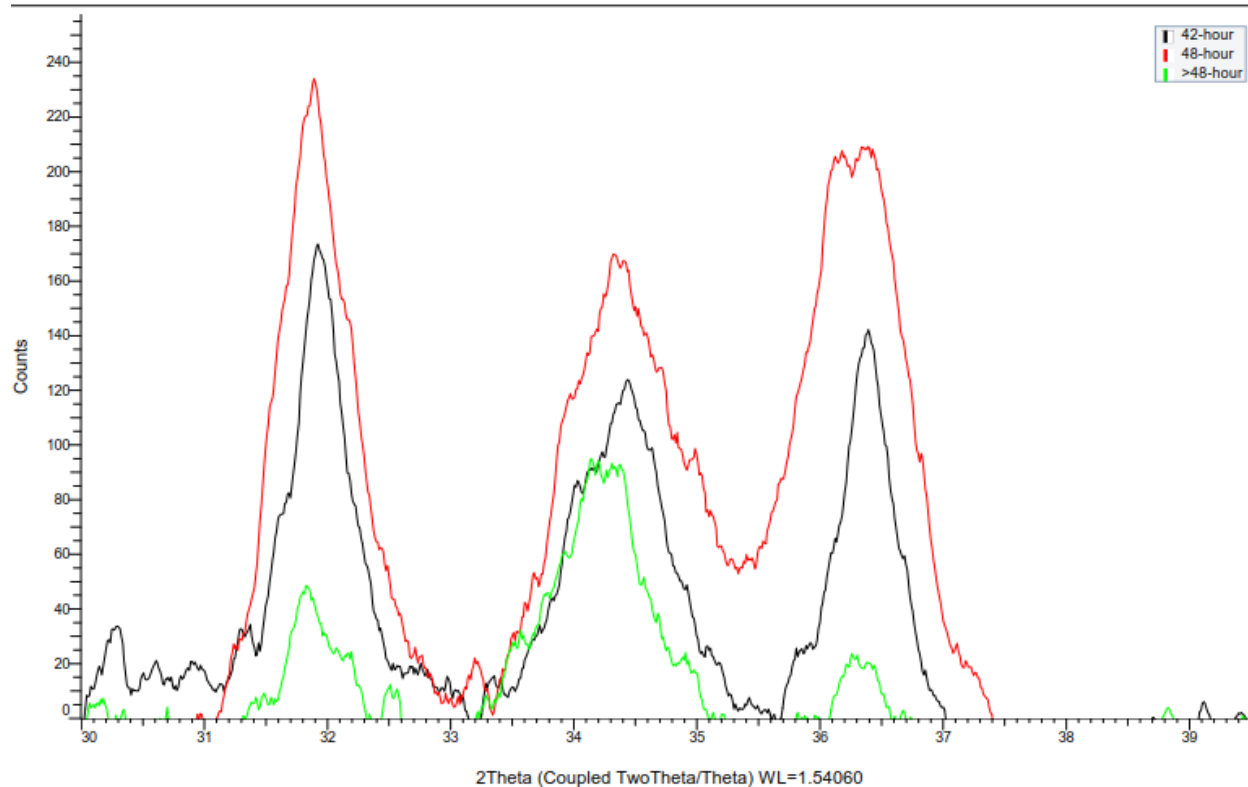
DEA Covered



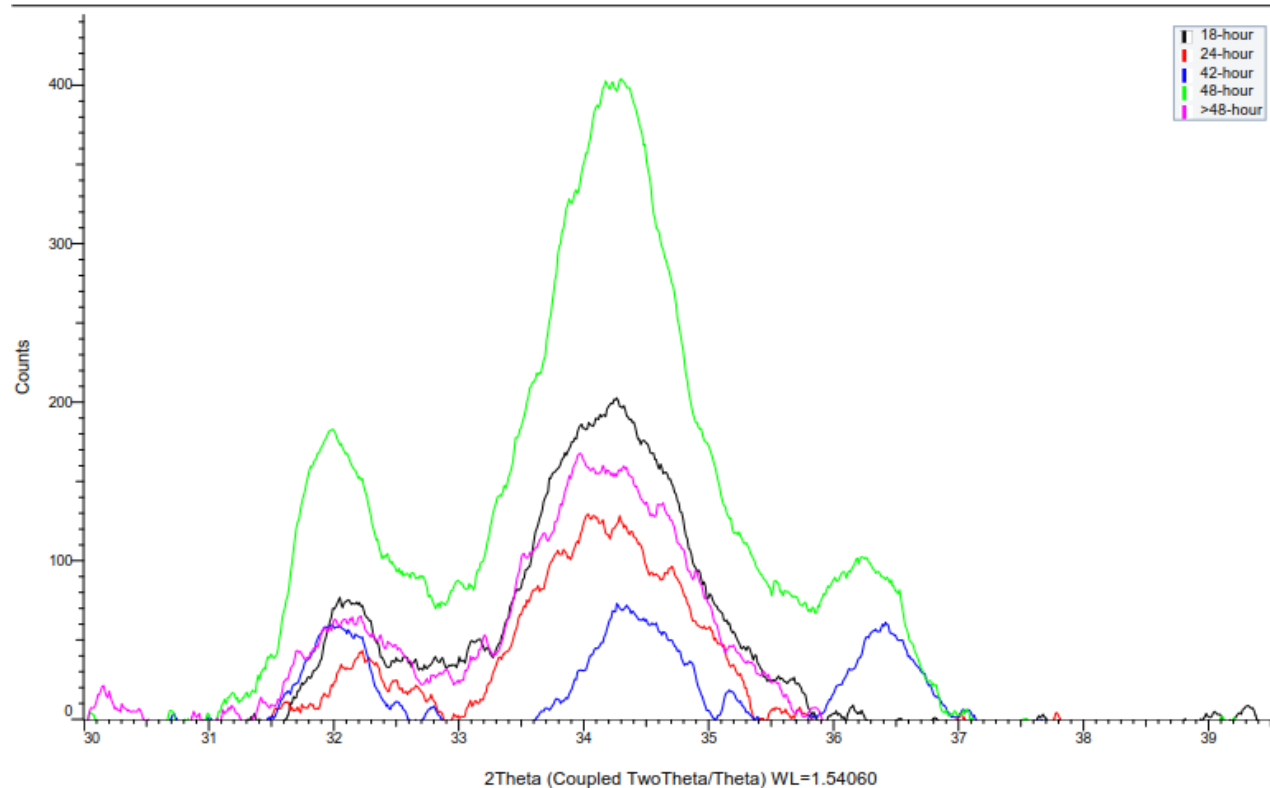
DEA Uncovered



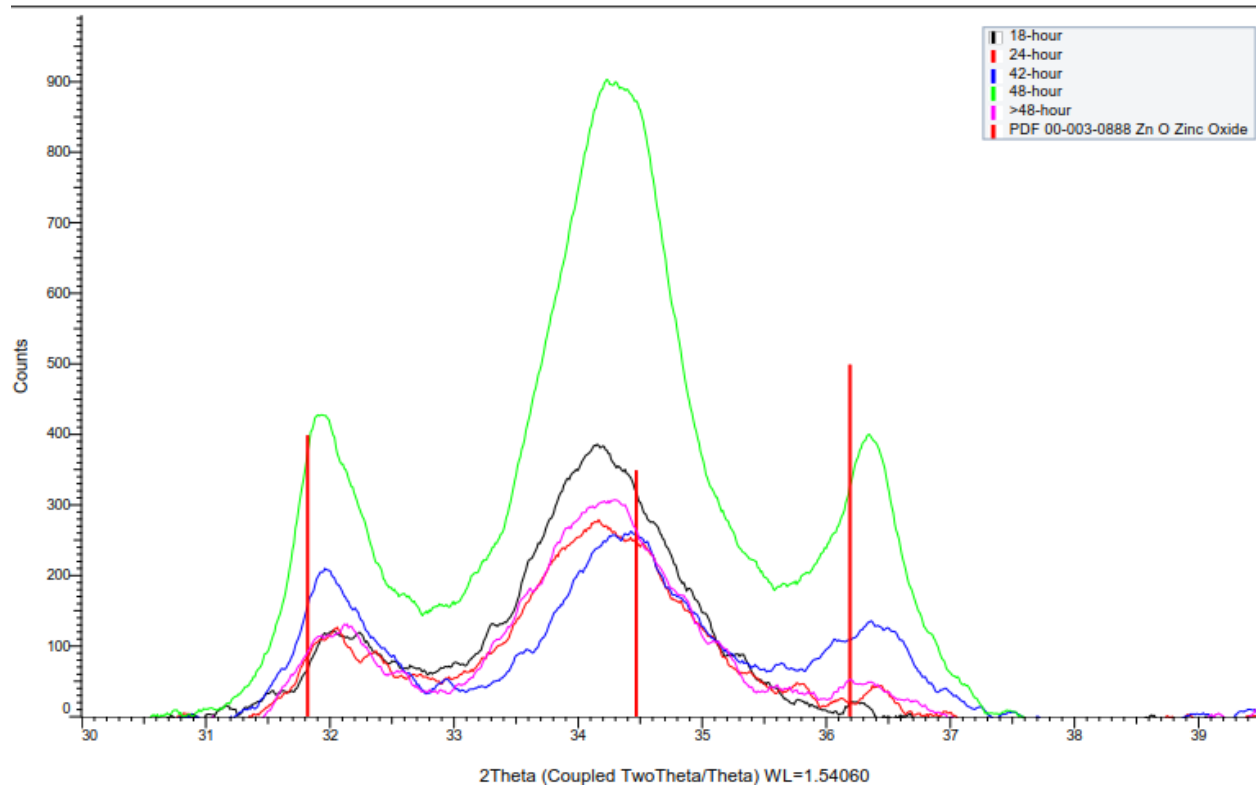
DEA 24-hr Covered



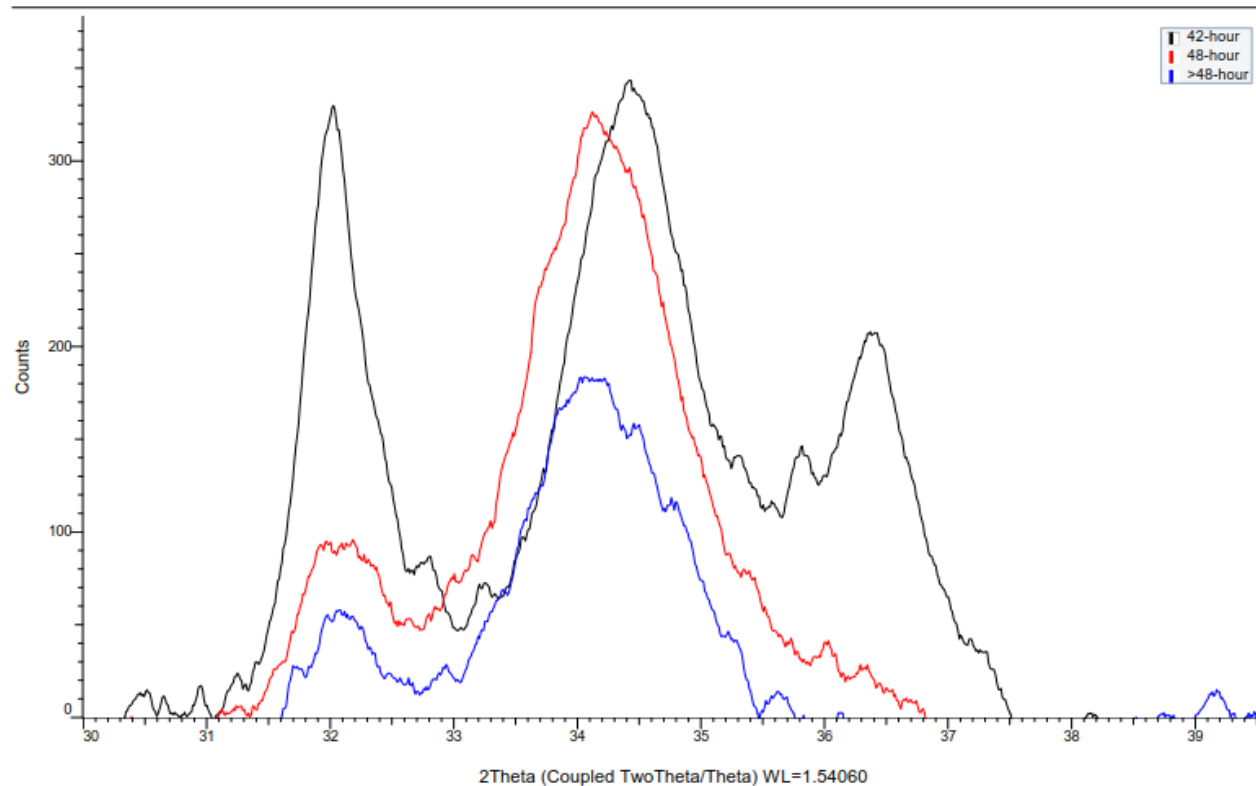
MEA Covered



MEA Uncovered

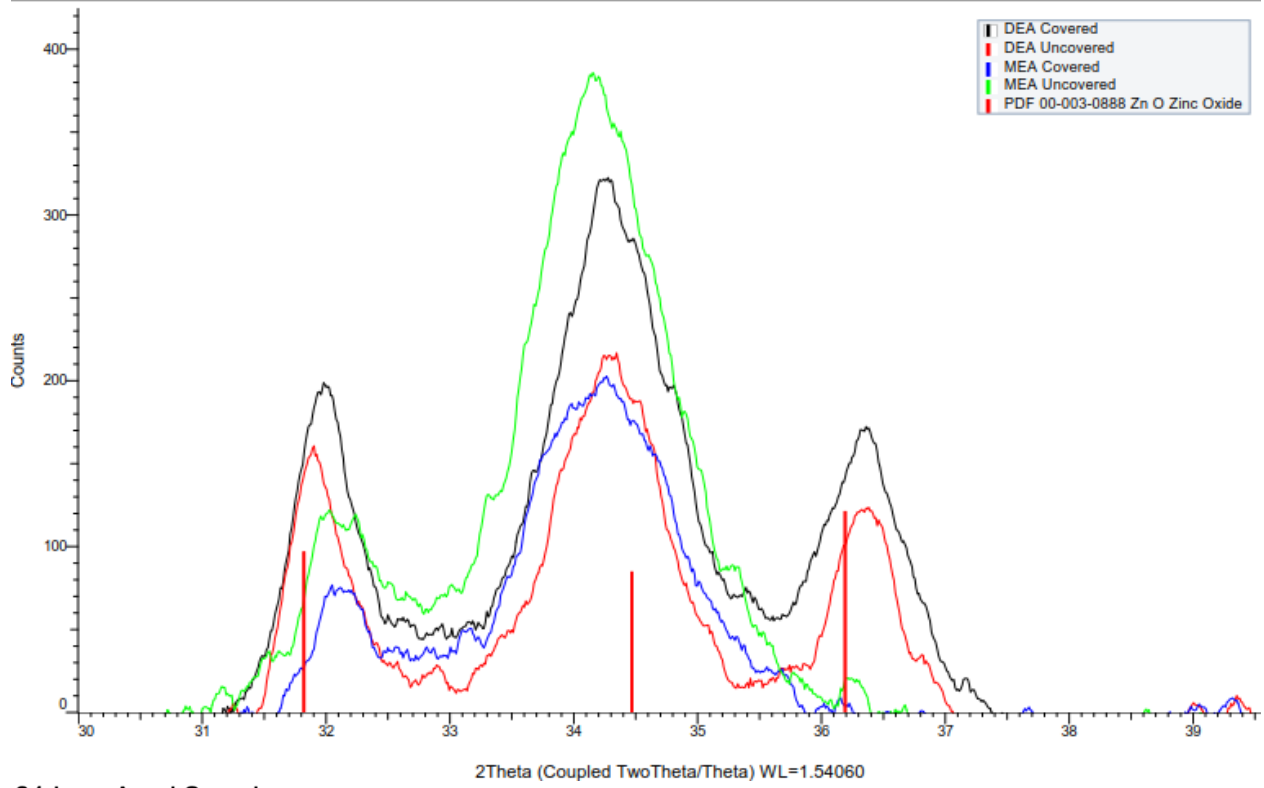


MEA 24-hr Covered

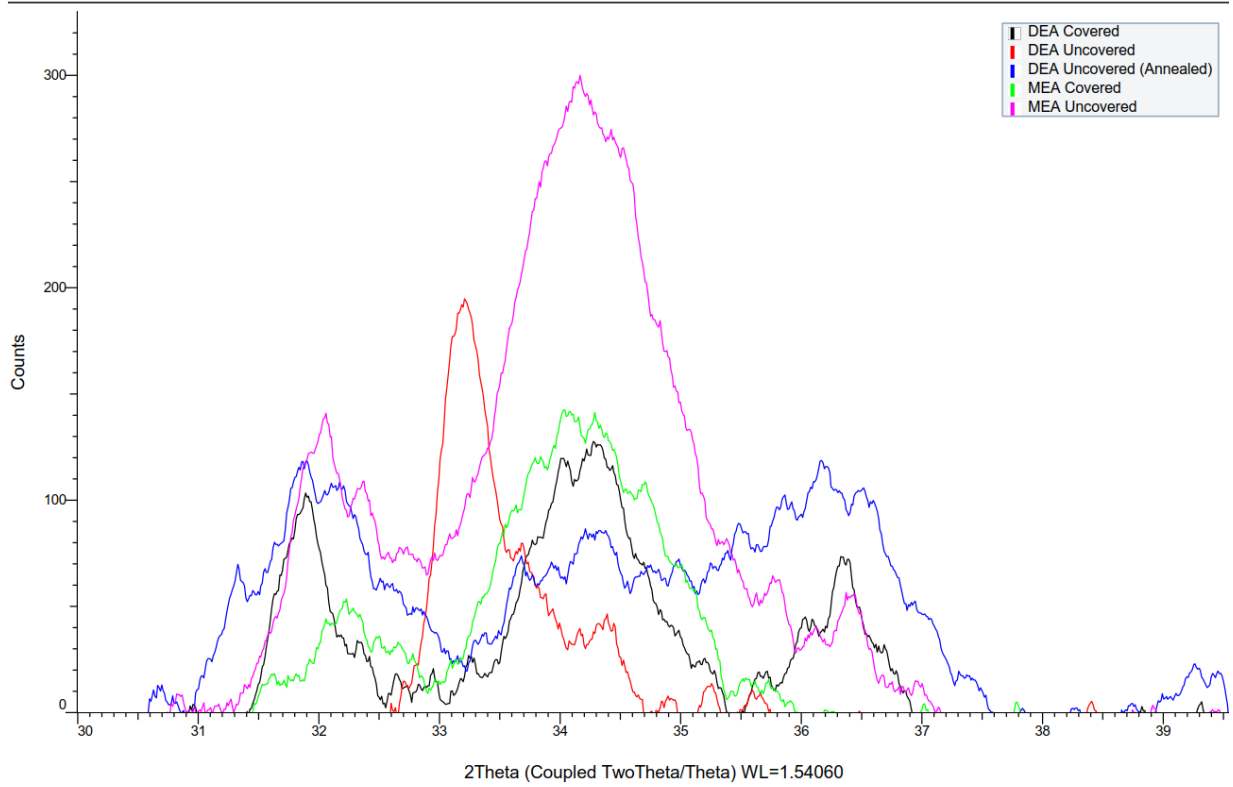


Appendix B: Chapter 2, Experiments A/B (4/6)

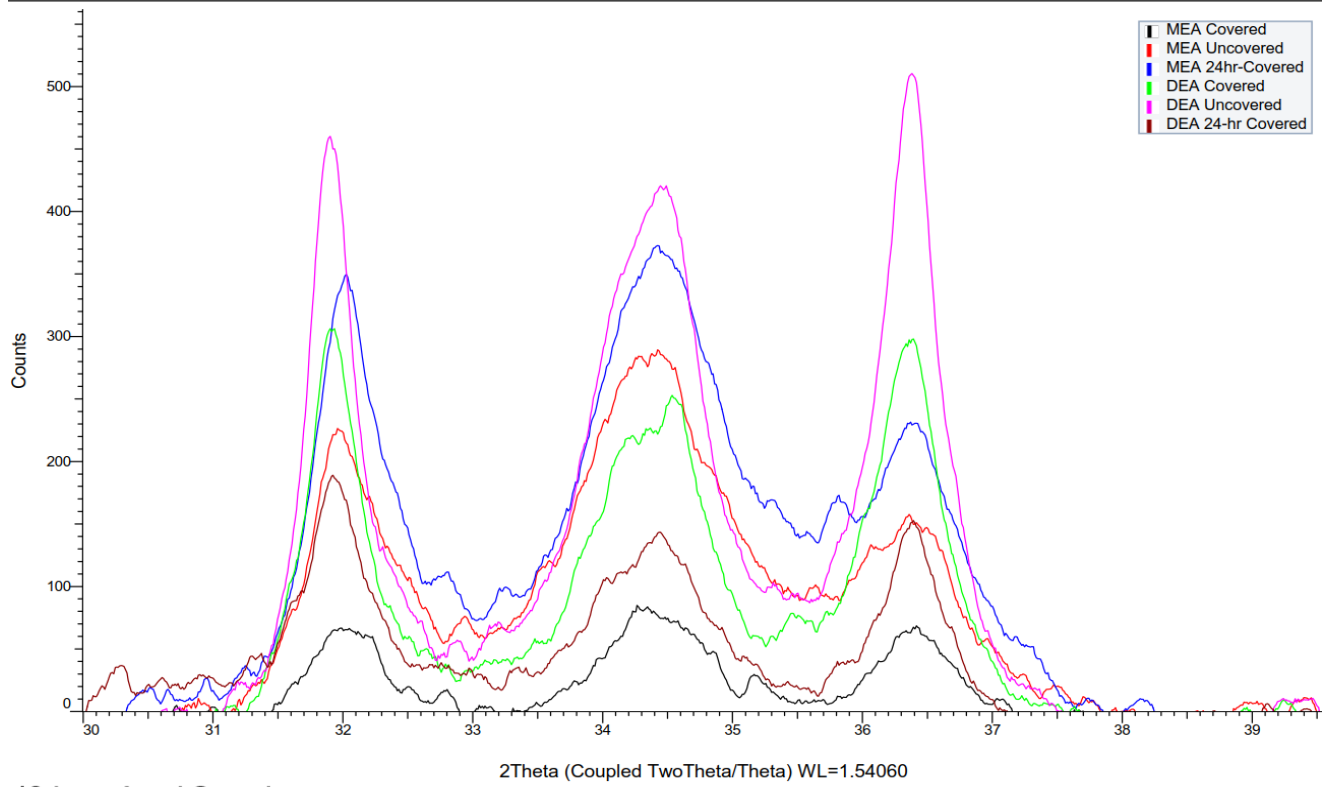
18-hour Aged Samples



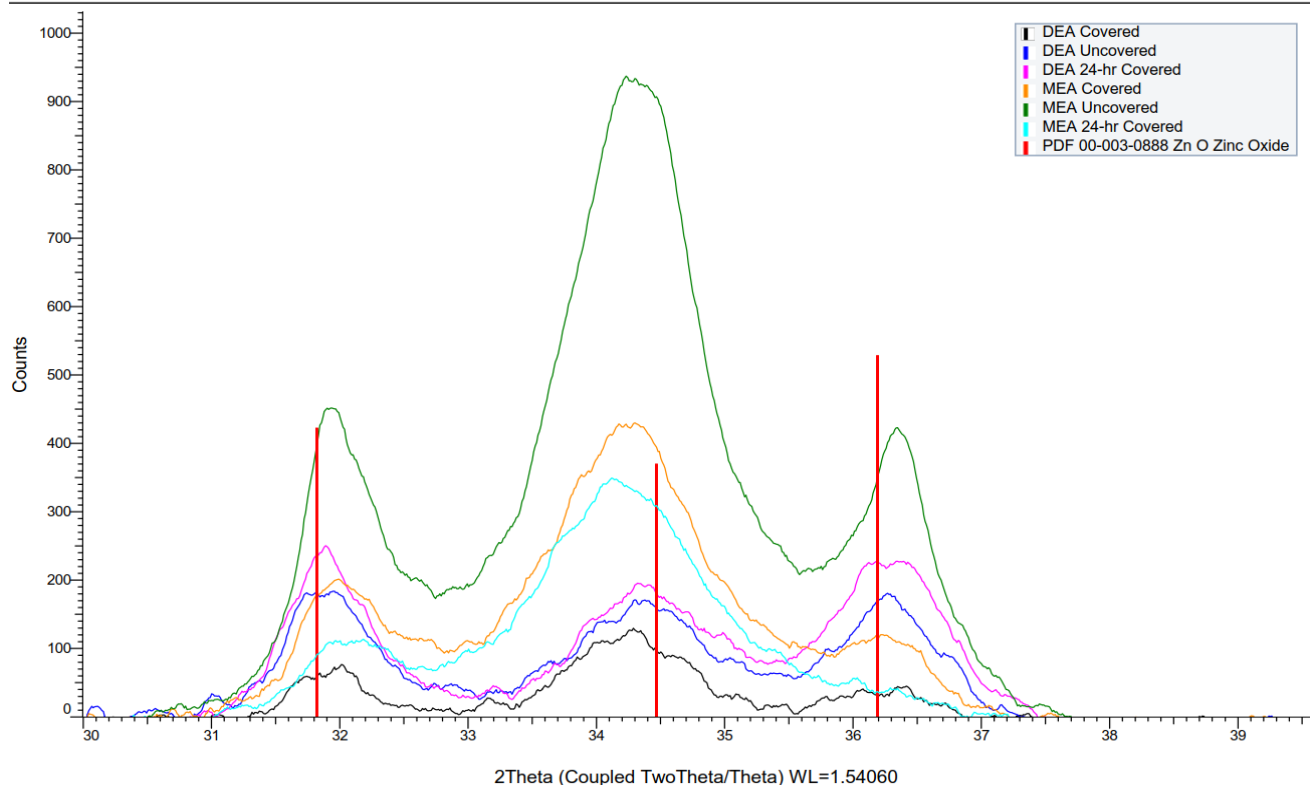
24-hour Aged Samples



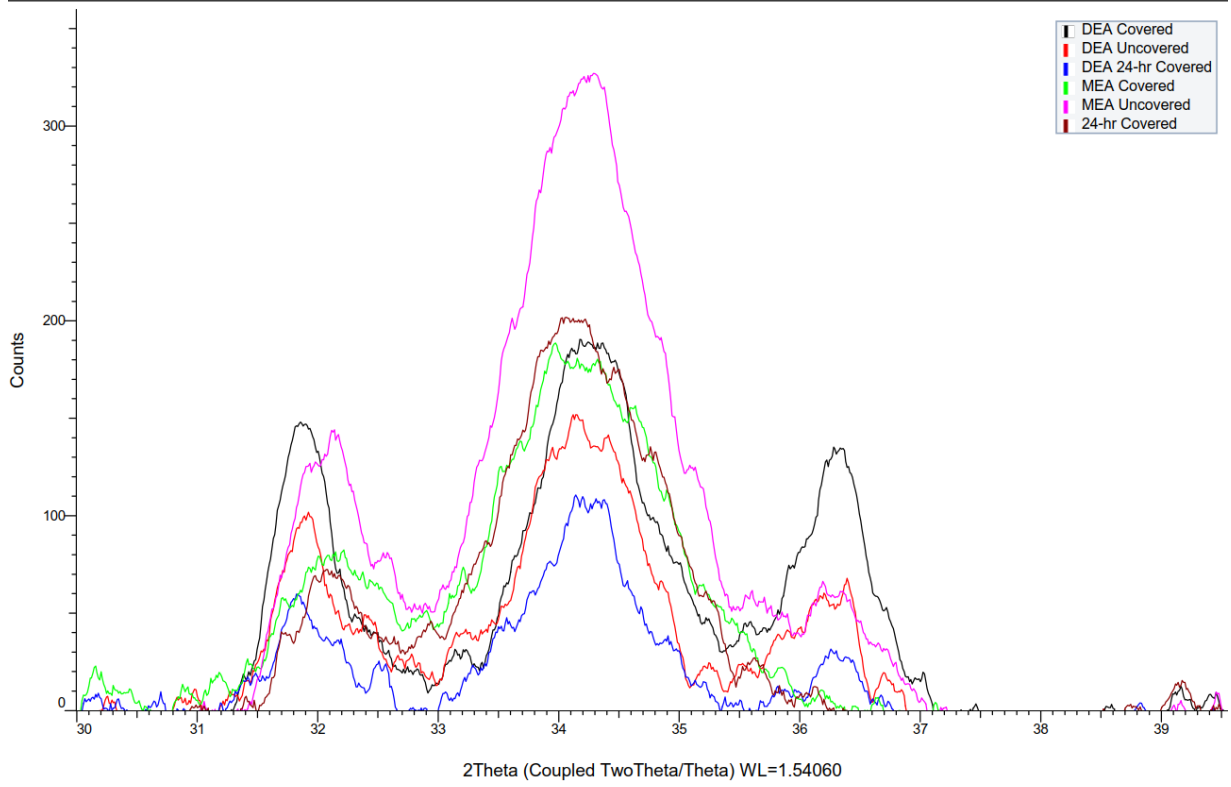
42-hour Aged Samples



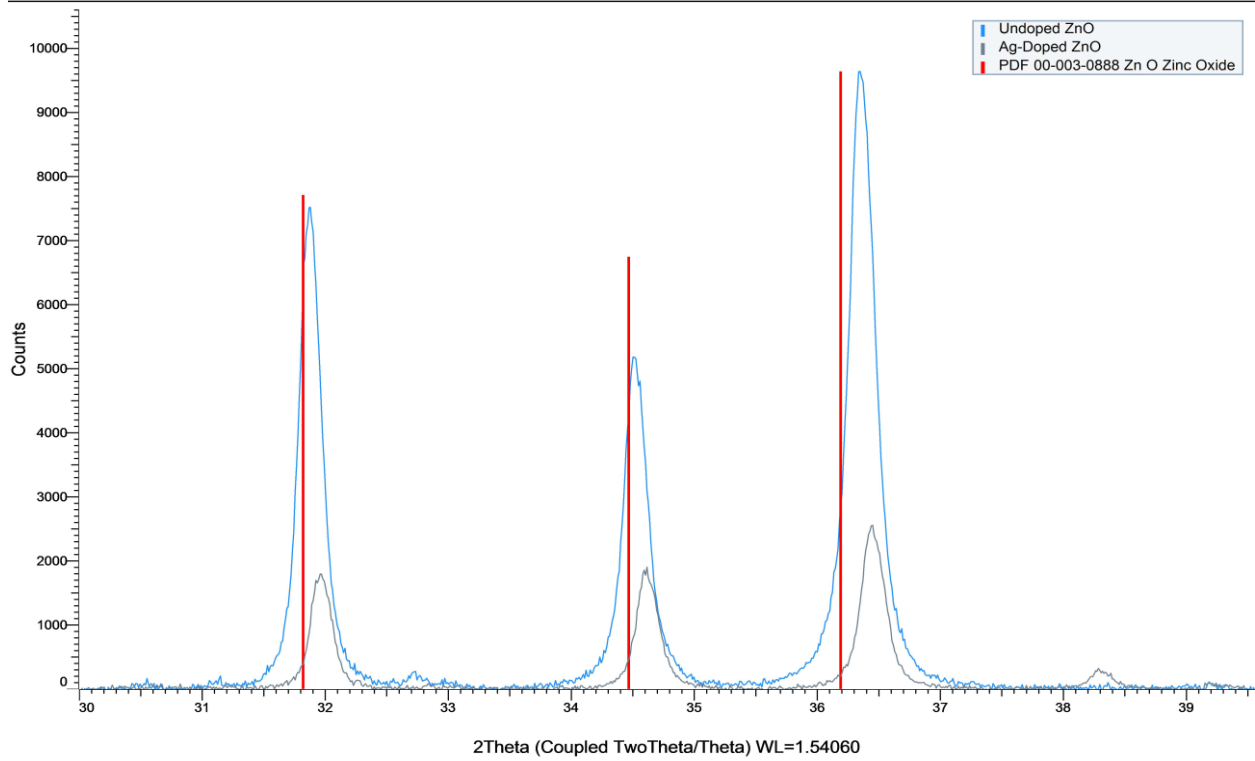
48-hour Aged Samples



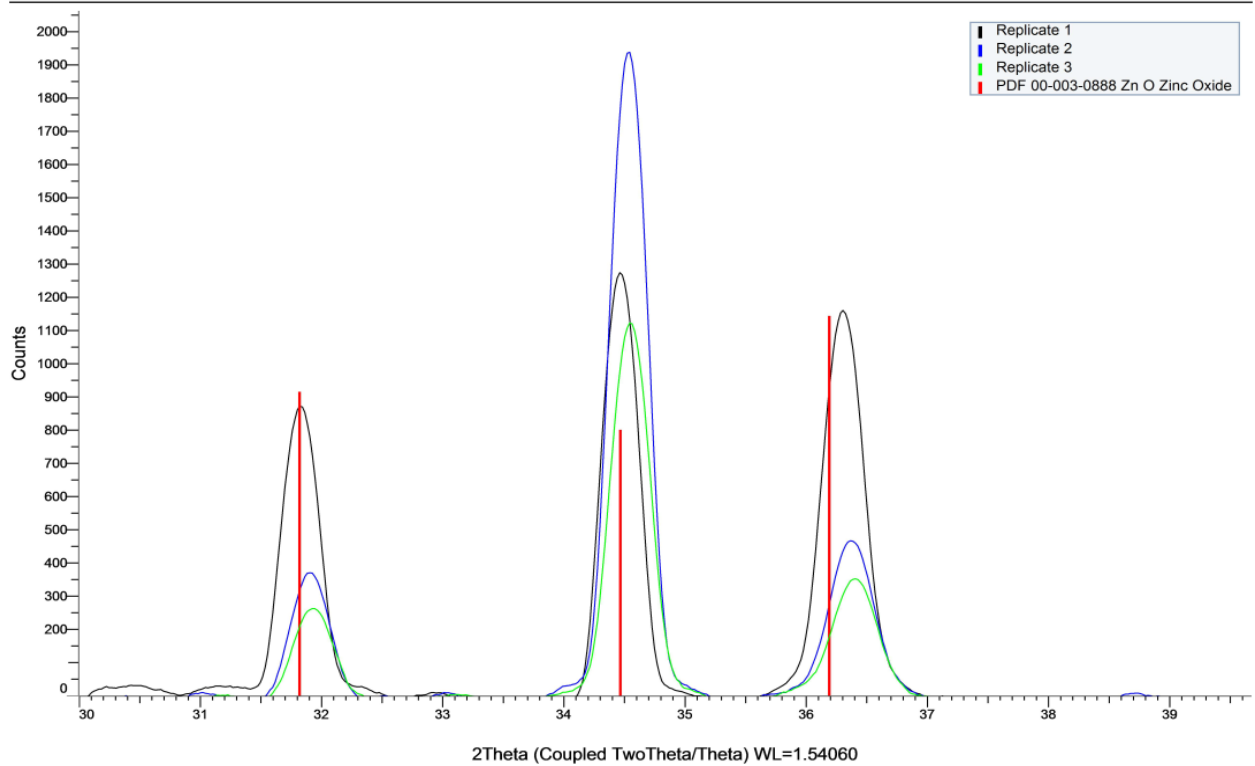
>48-hour Aged Samples



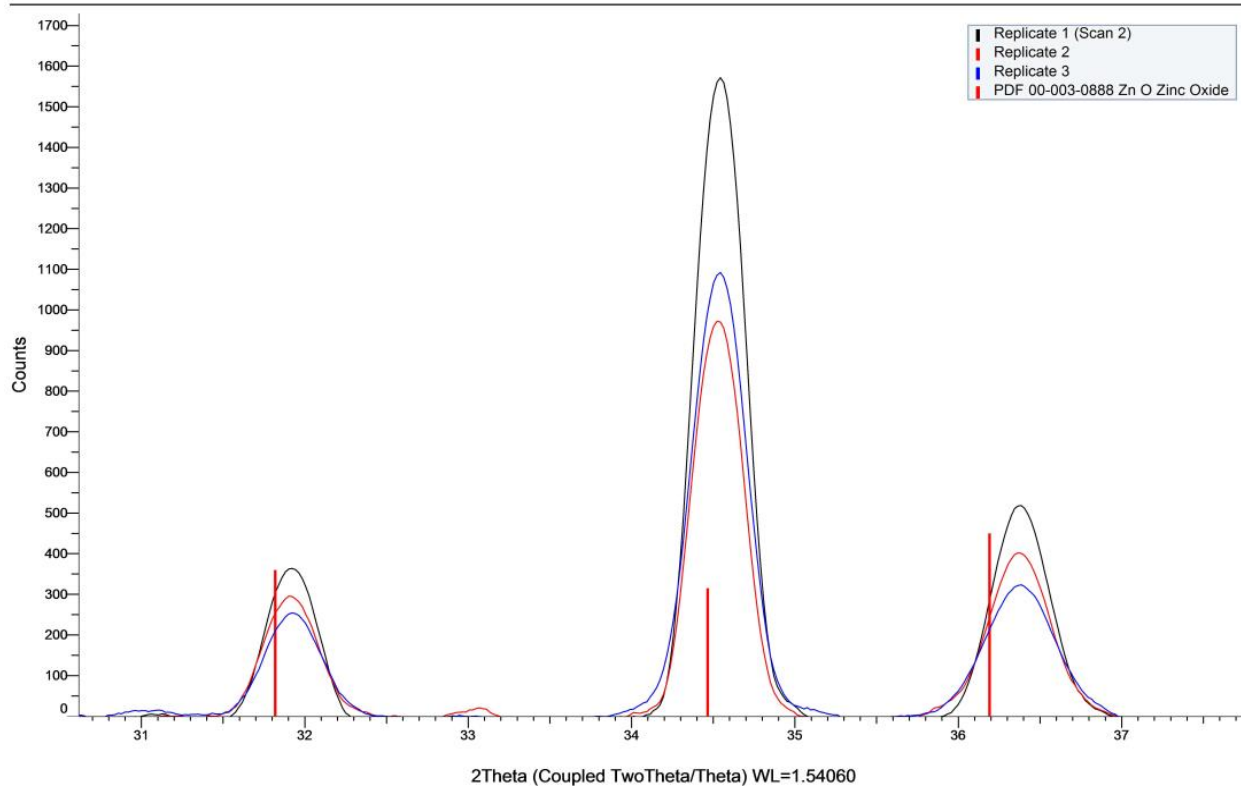
Preliminary Doping Attempts



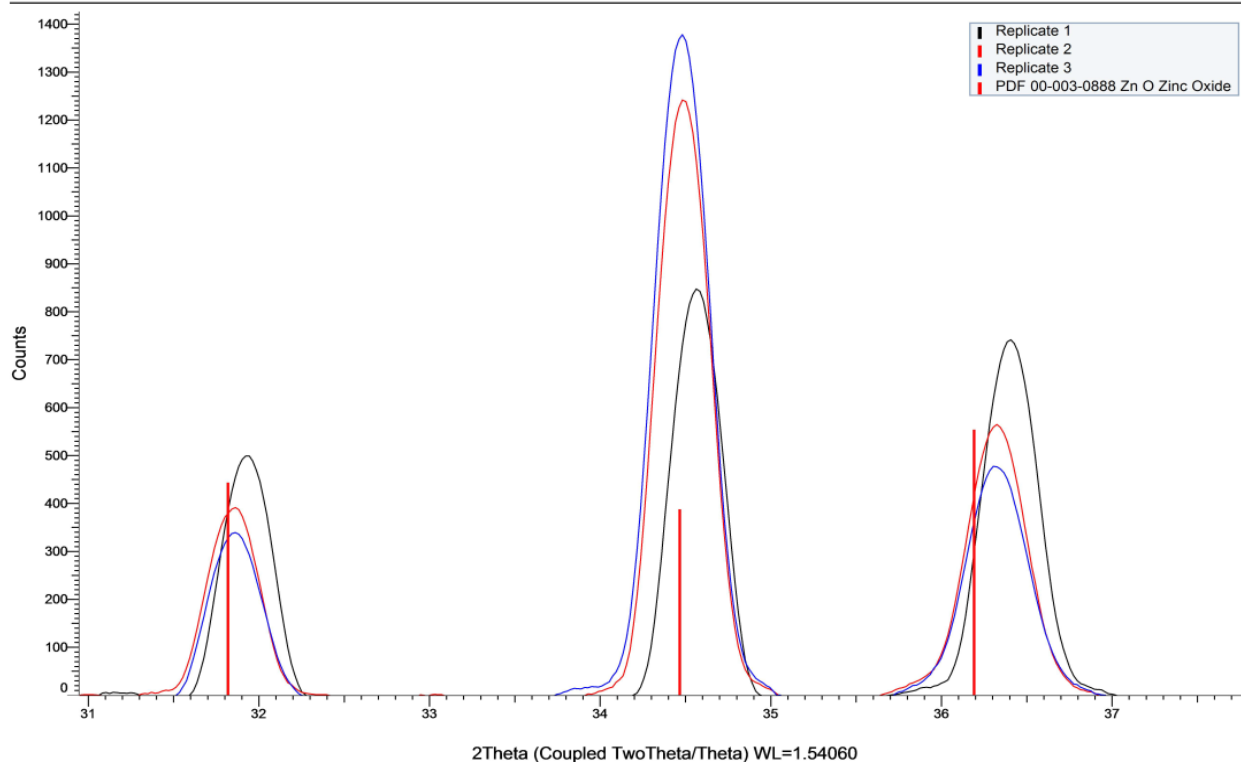
1% Ag-doped ZnO



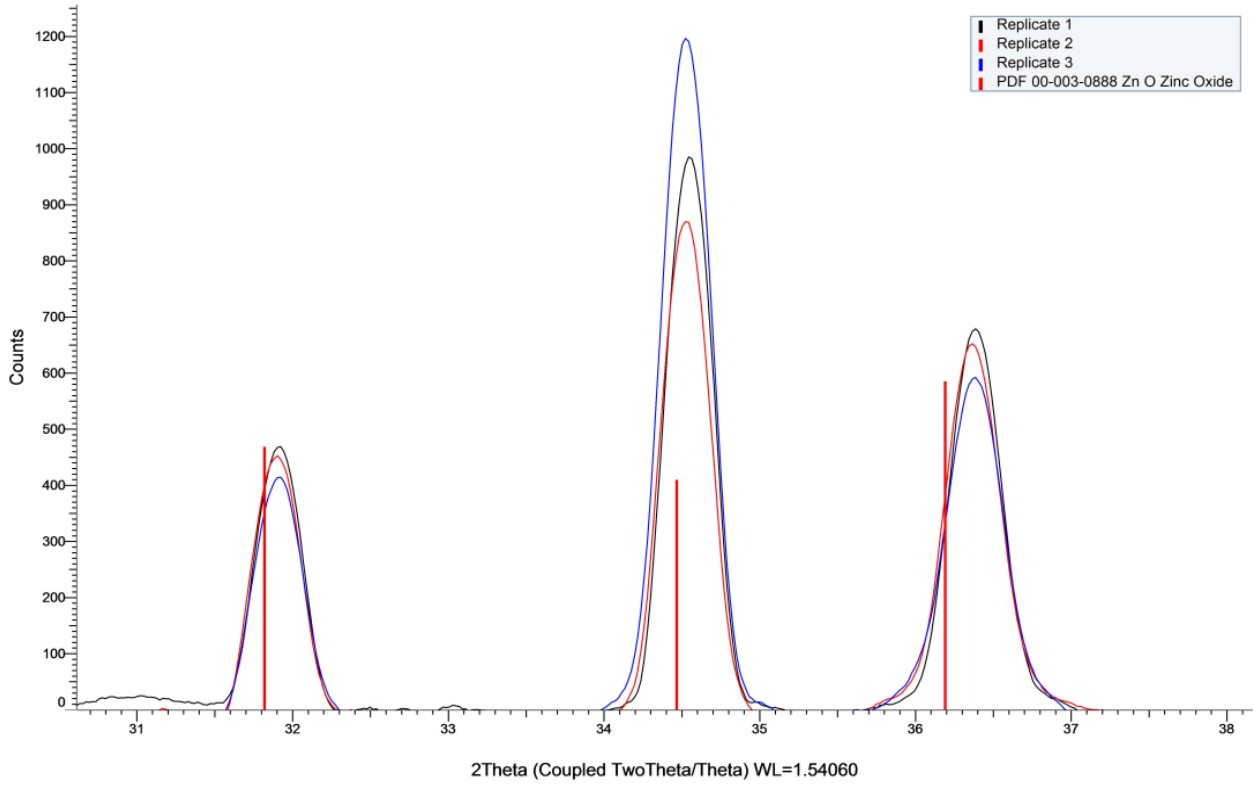
2% Ag-doped ZnO



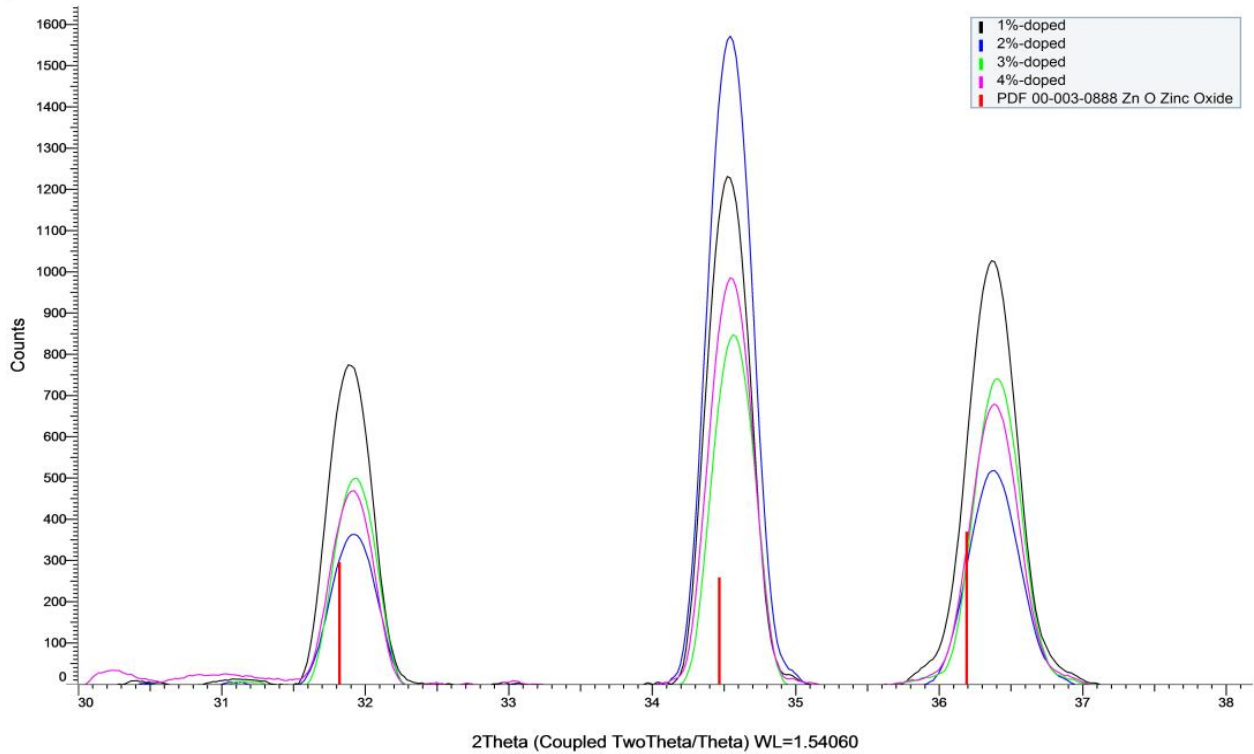
3% Ag-doped ZnO



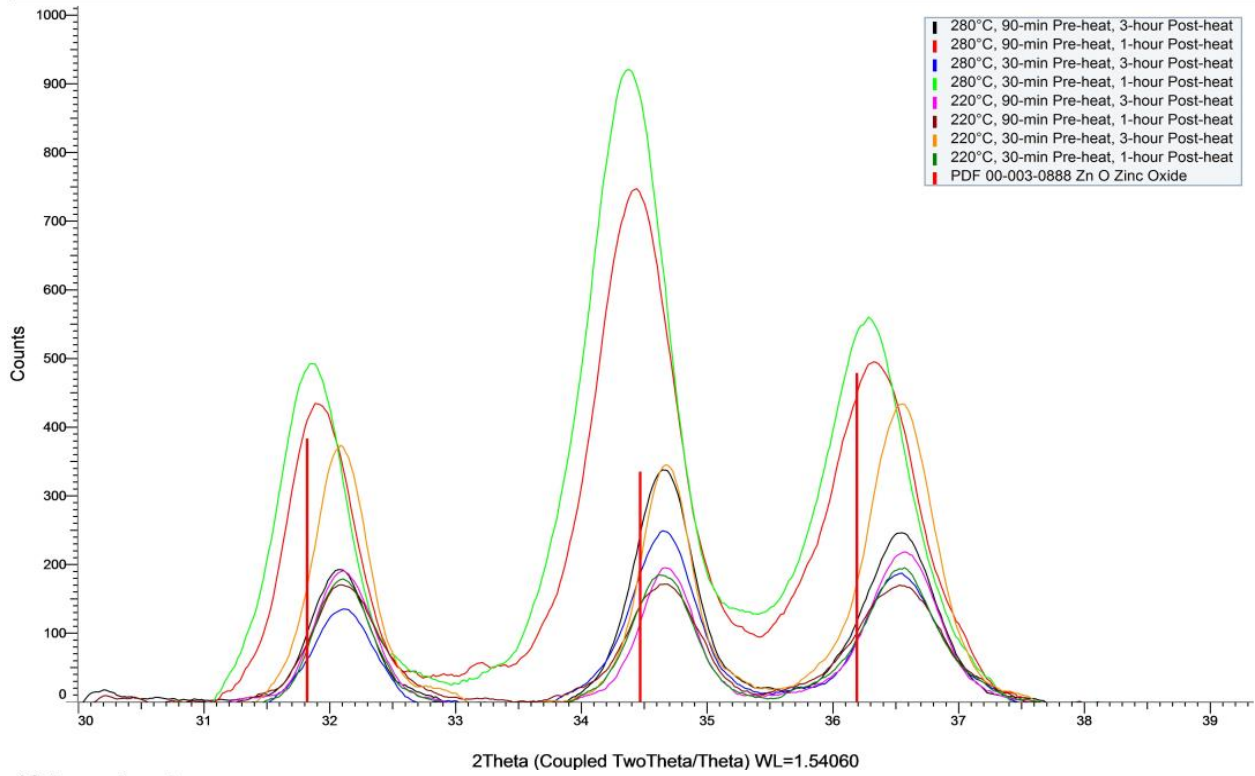
4% Ag-doped ZnO



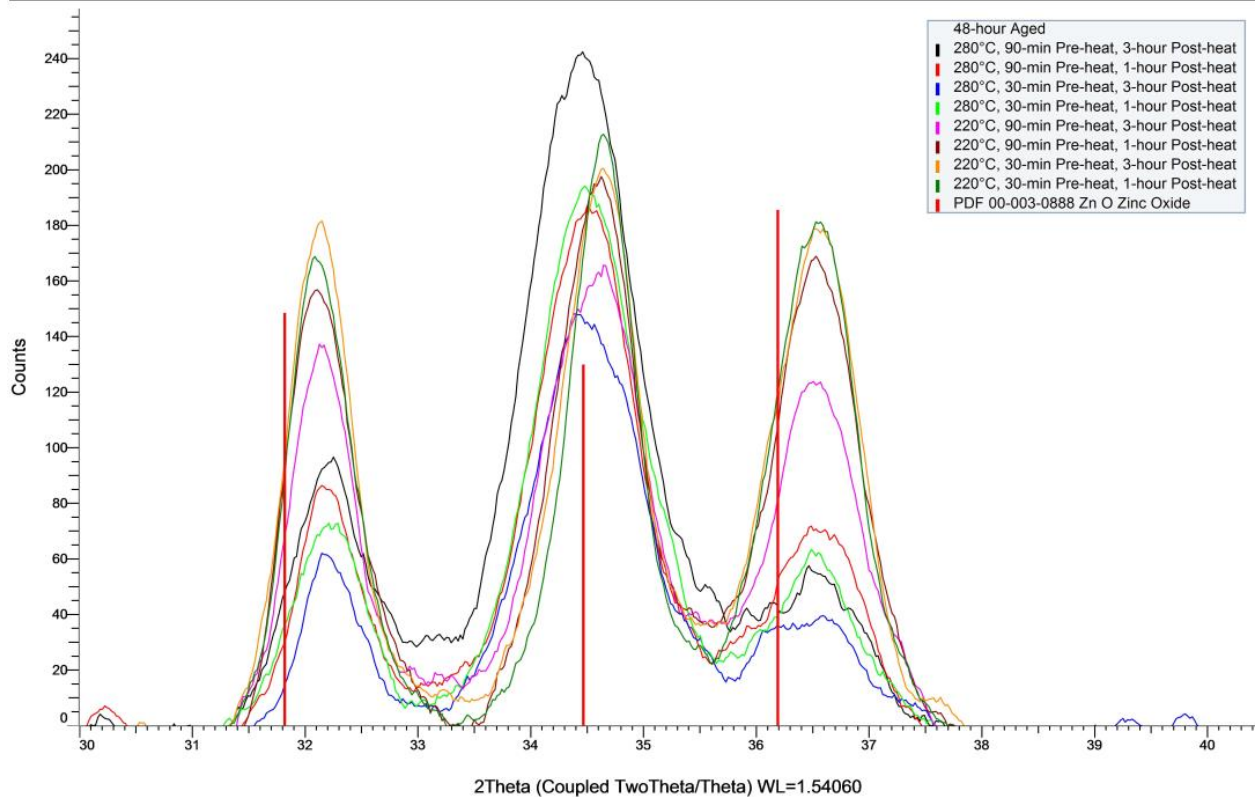
Ag-doped ZnO by Dopant Atomic Percent



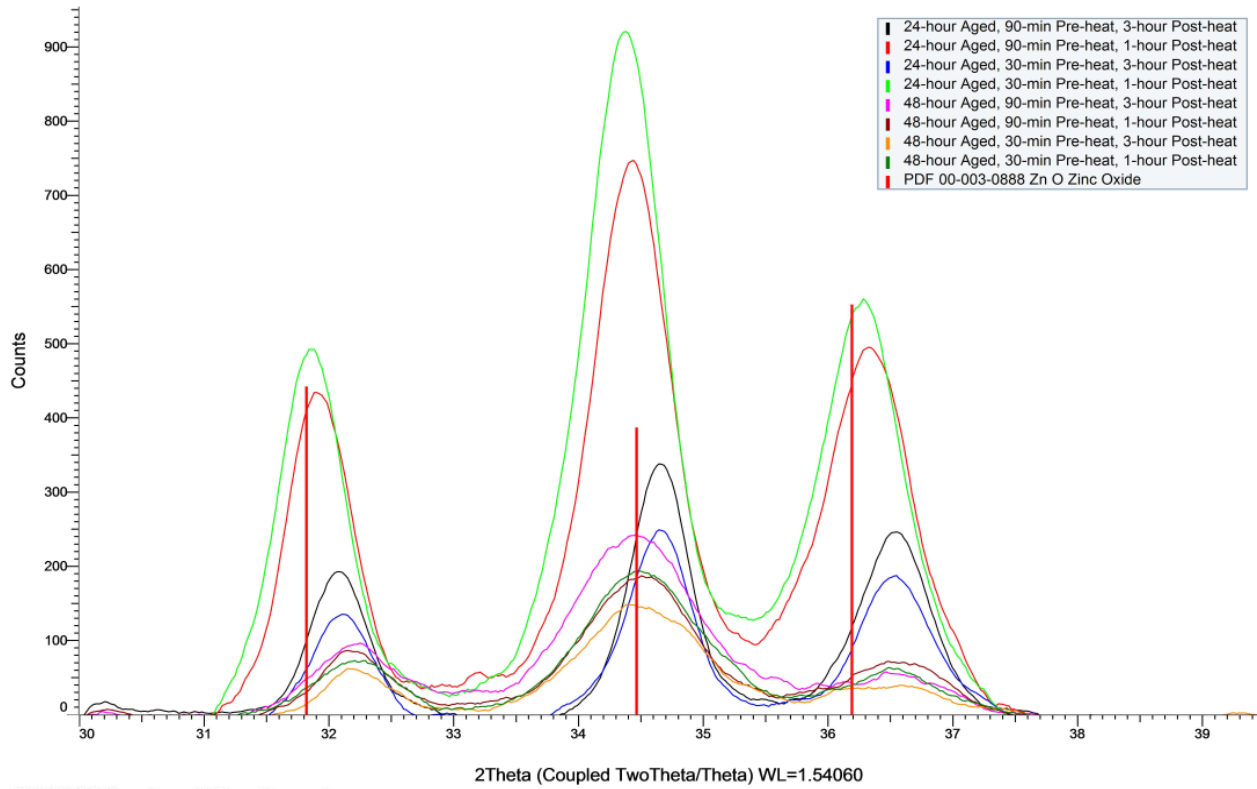
24-hour Aged



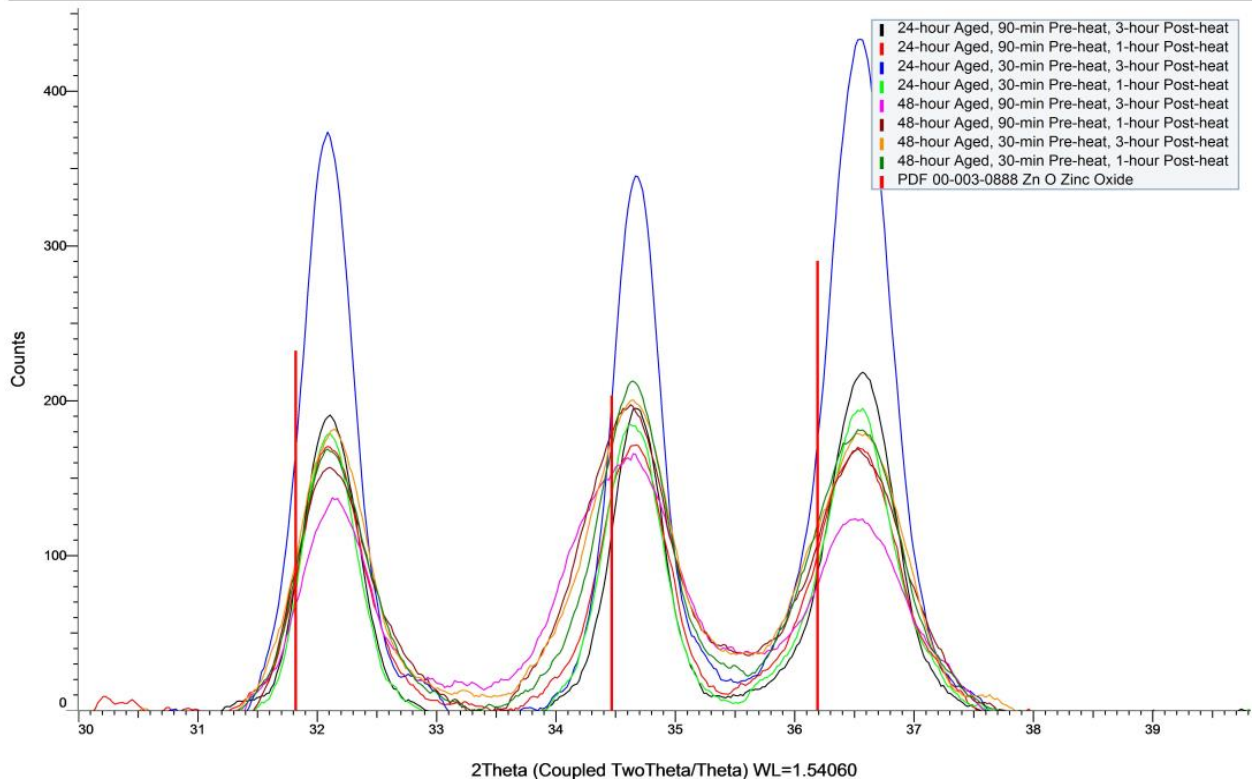
48-hour Aged



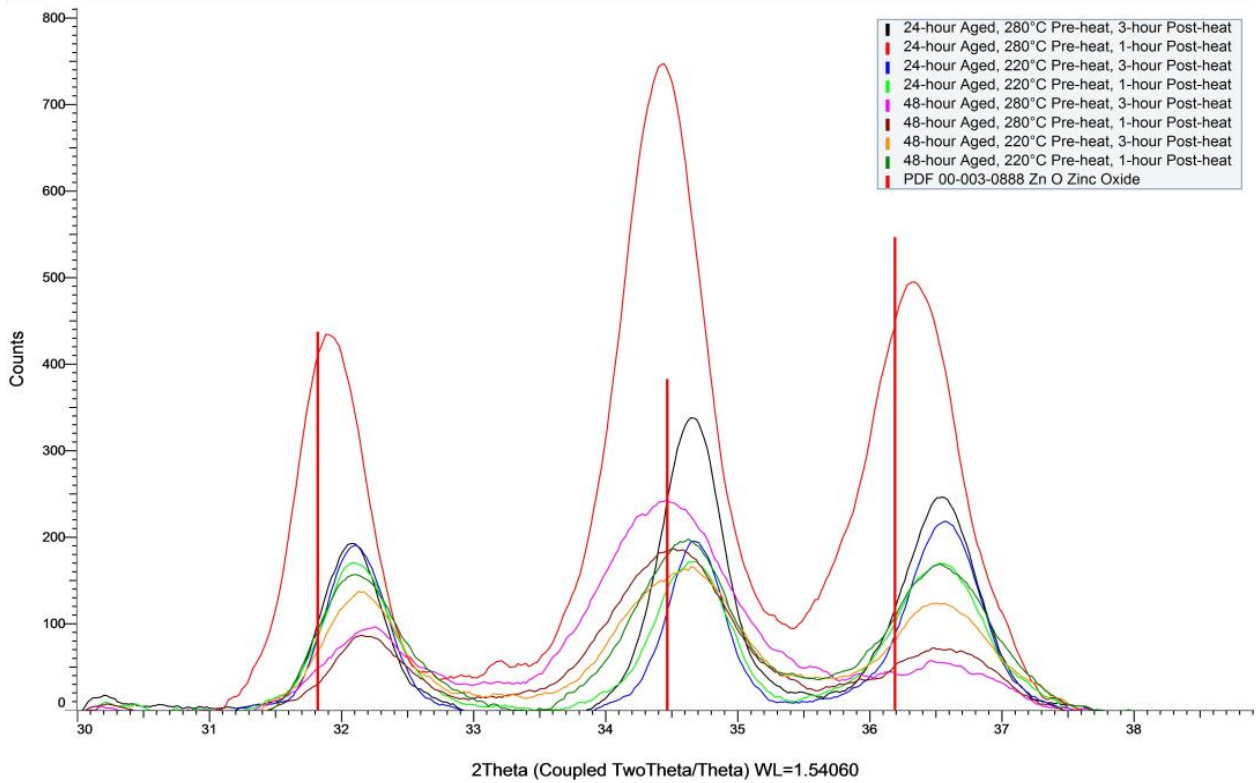
280°C Pre-heat Treatment



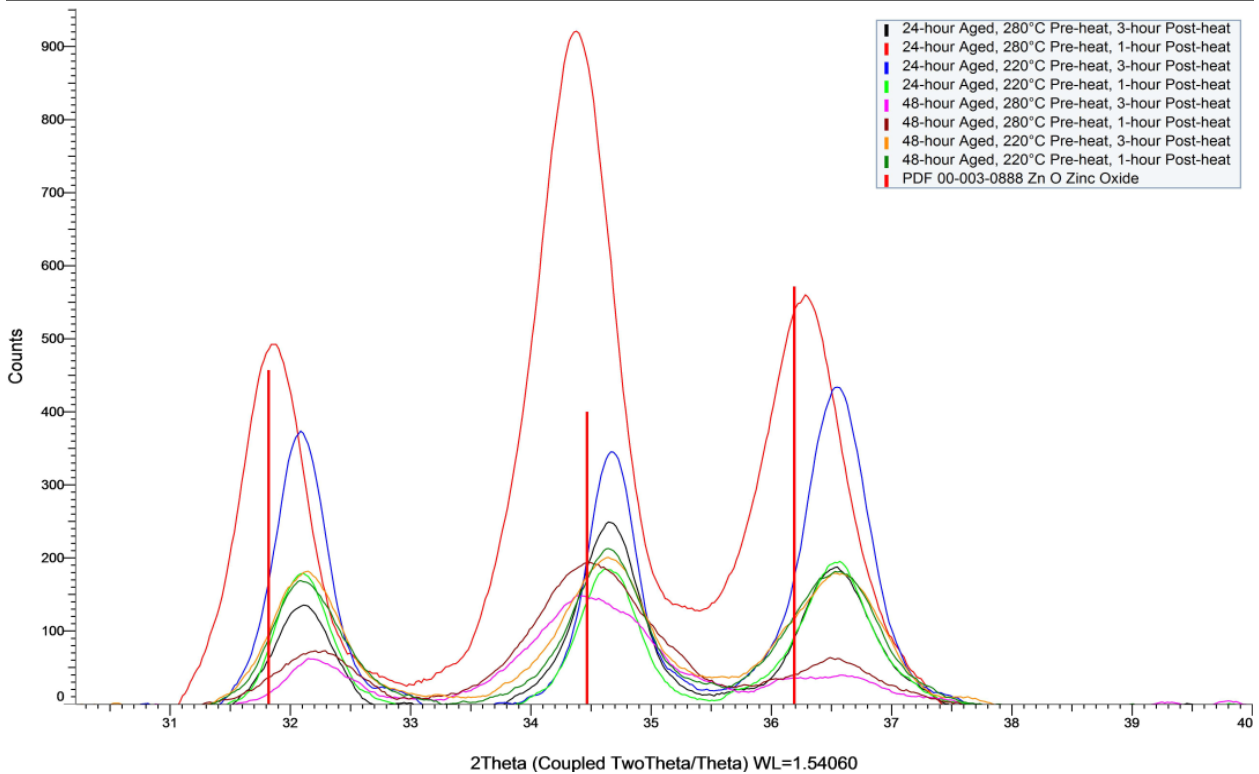
220°C Pre-heat Treatment



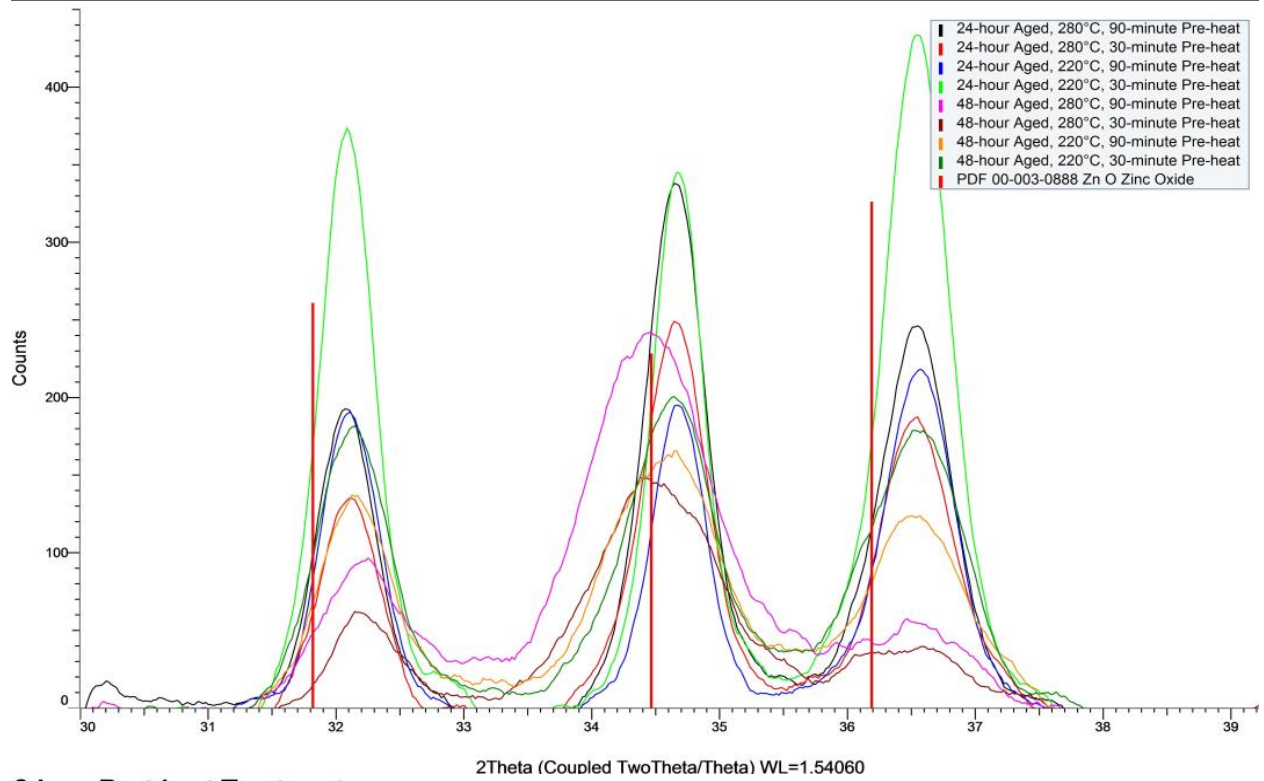
90-min Pre-heat Treatment



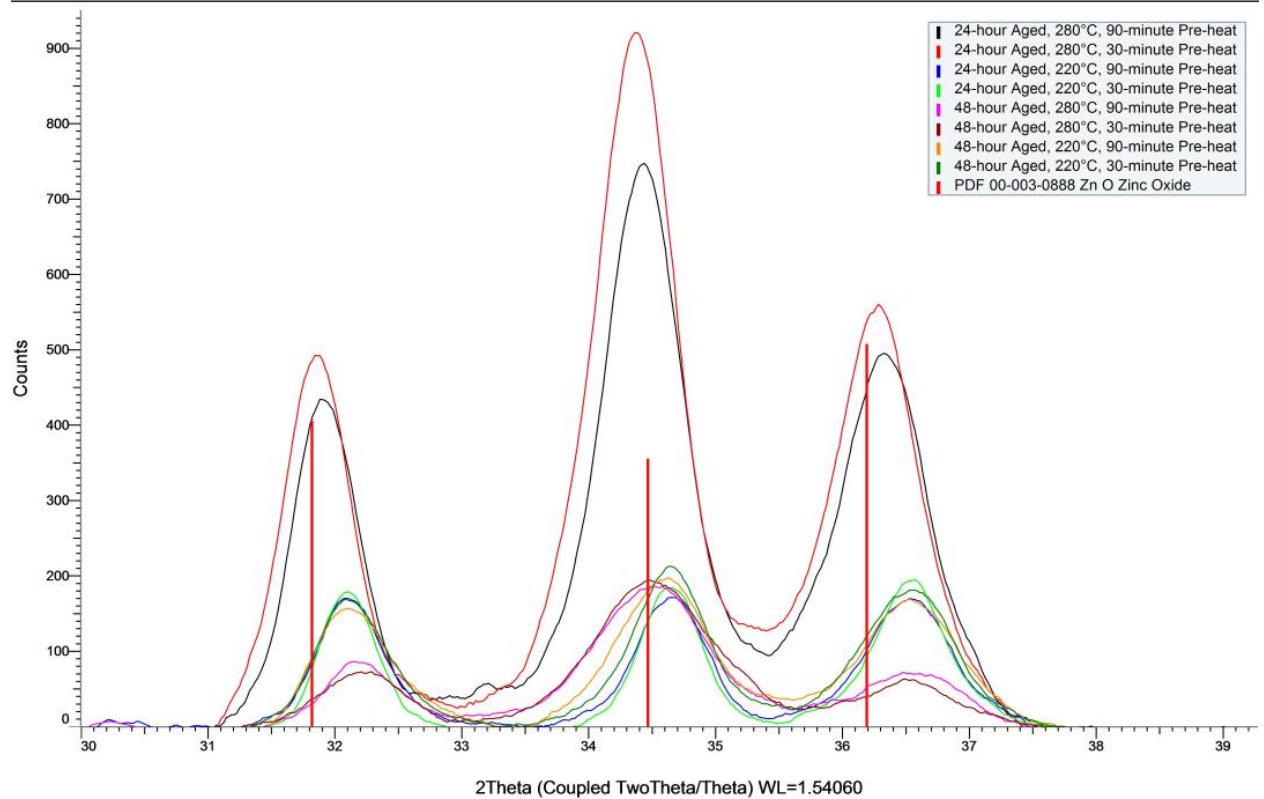
30-min Pre-heat Treatment



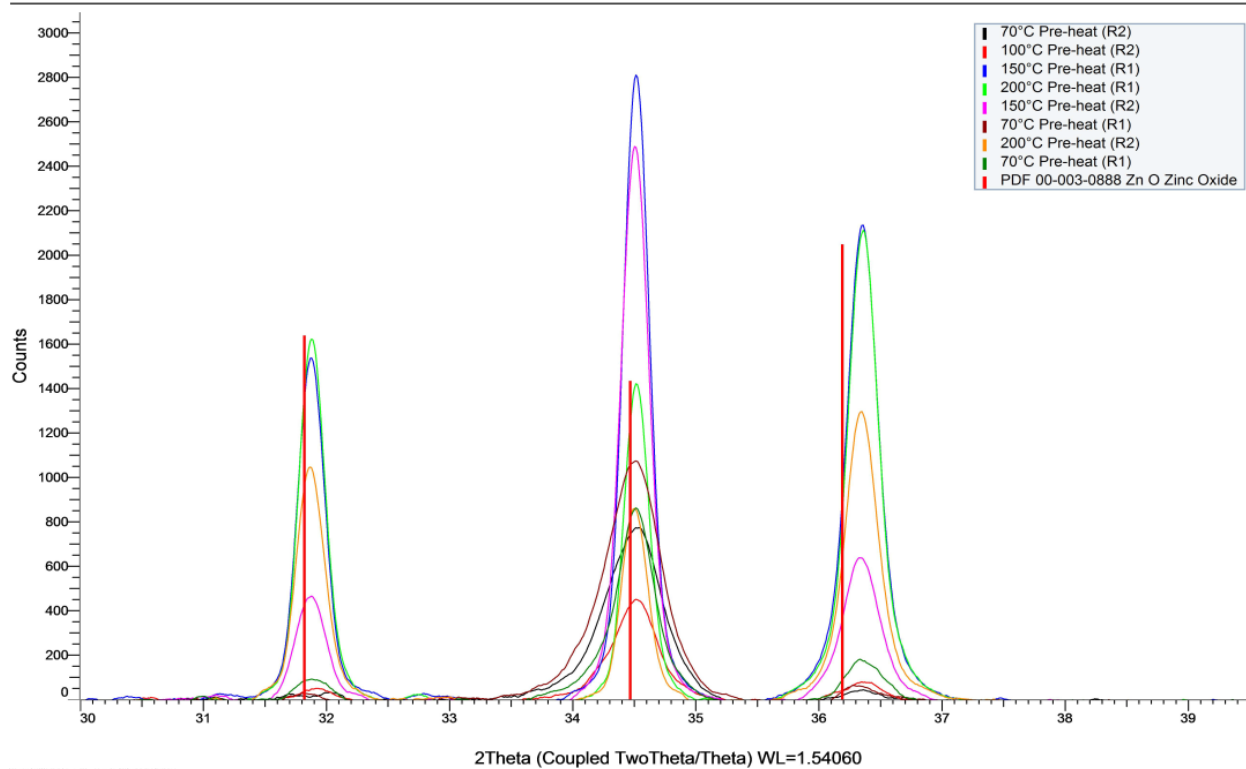
1-hour Post-heat Treatment



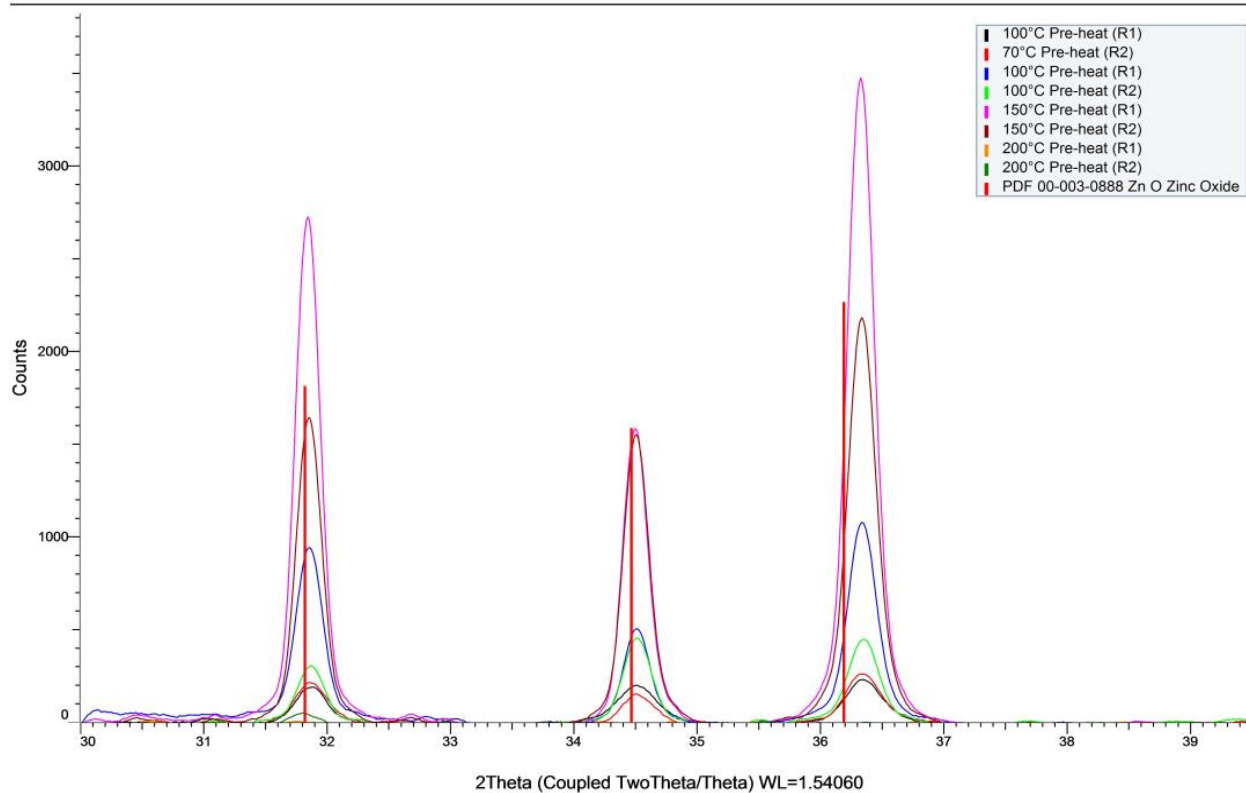
3-hour Post-heat Treatment



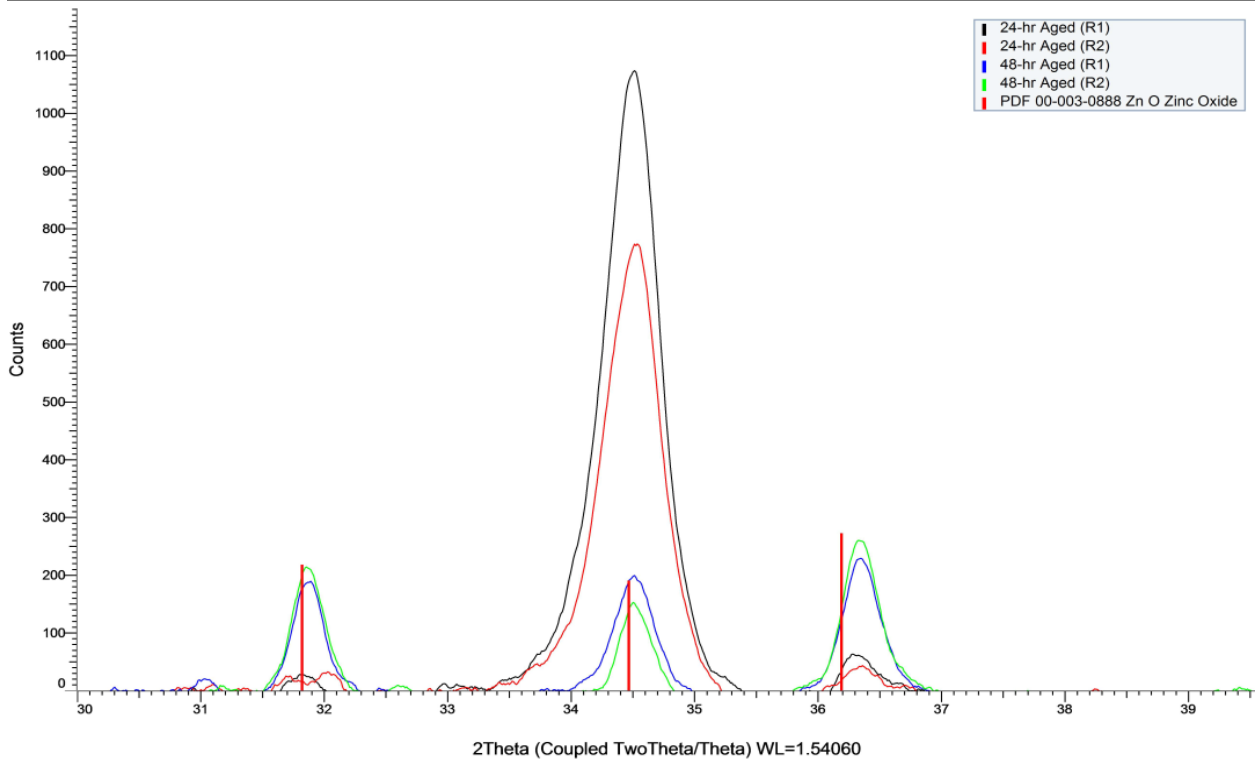
24-hour Aged



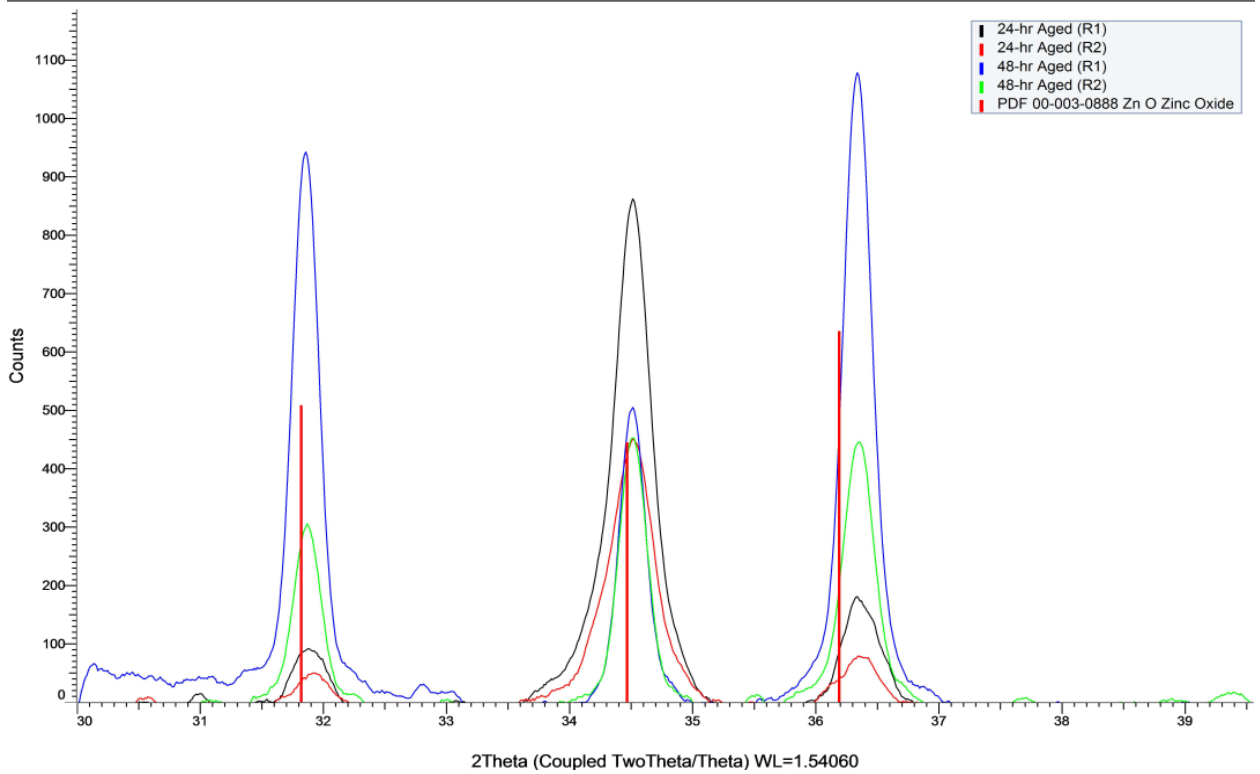
48-hour Aged



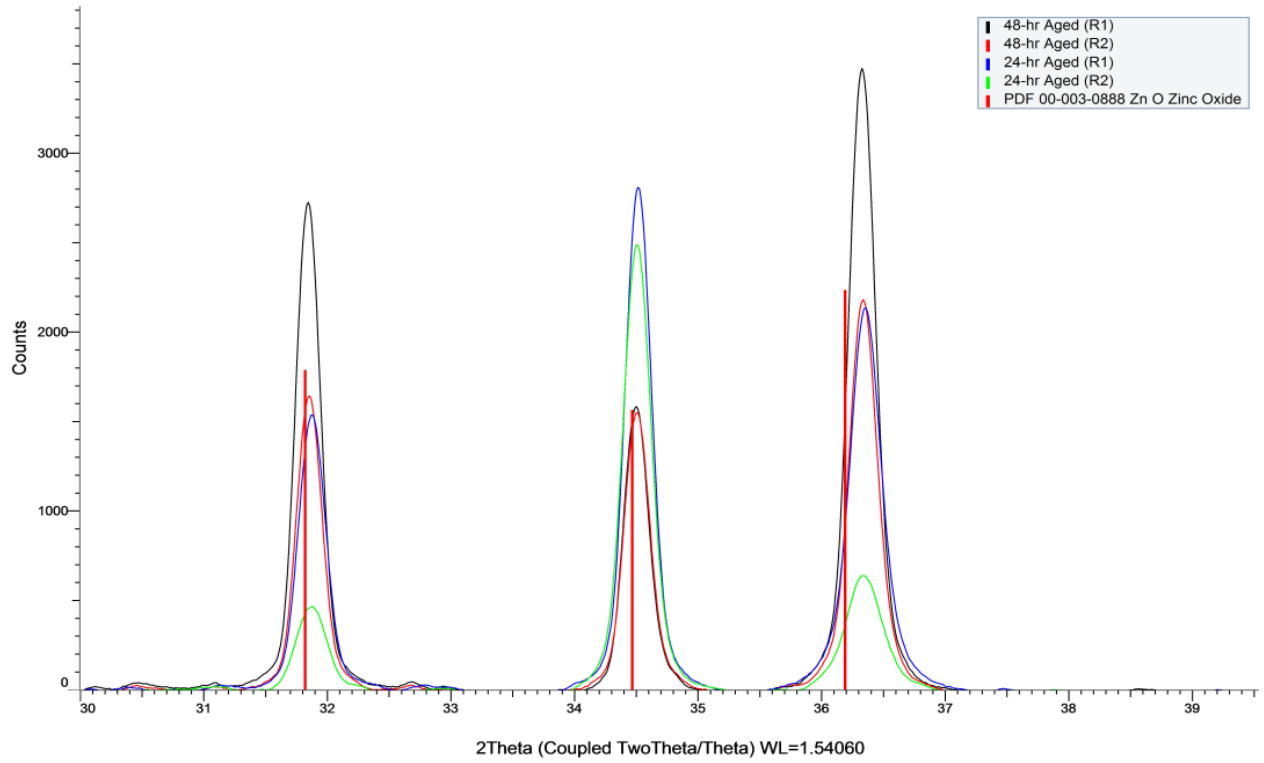
70°C Pre-heat Treatment



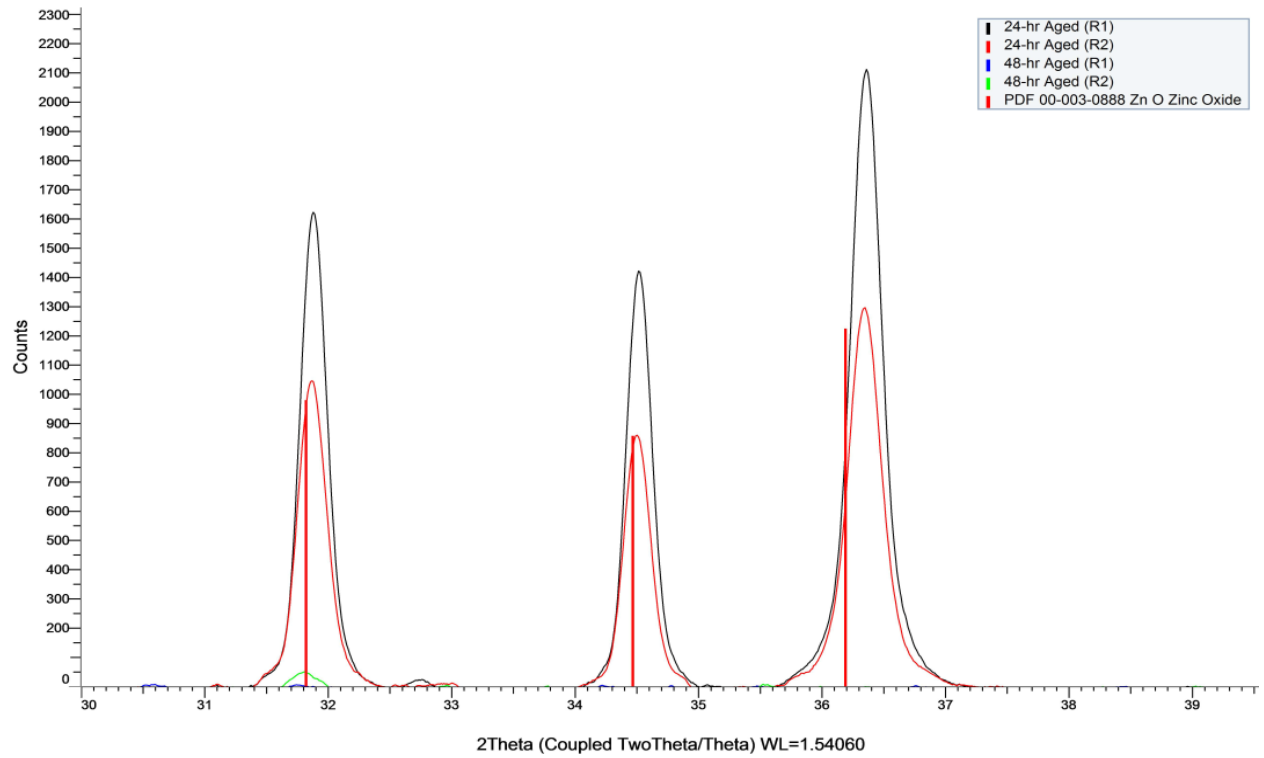
100°C Pre-heat Treatment



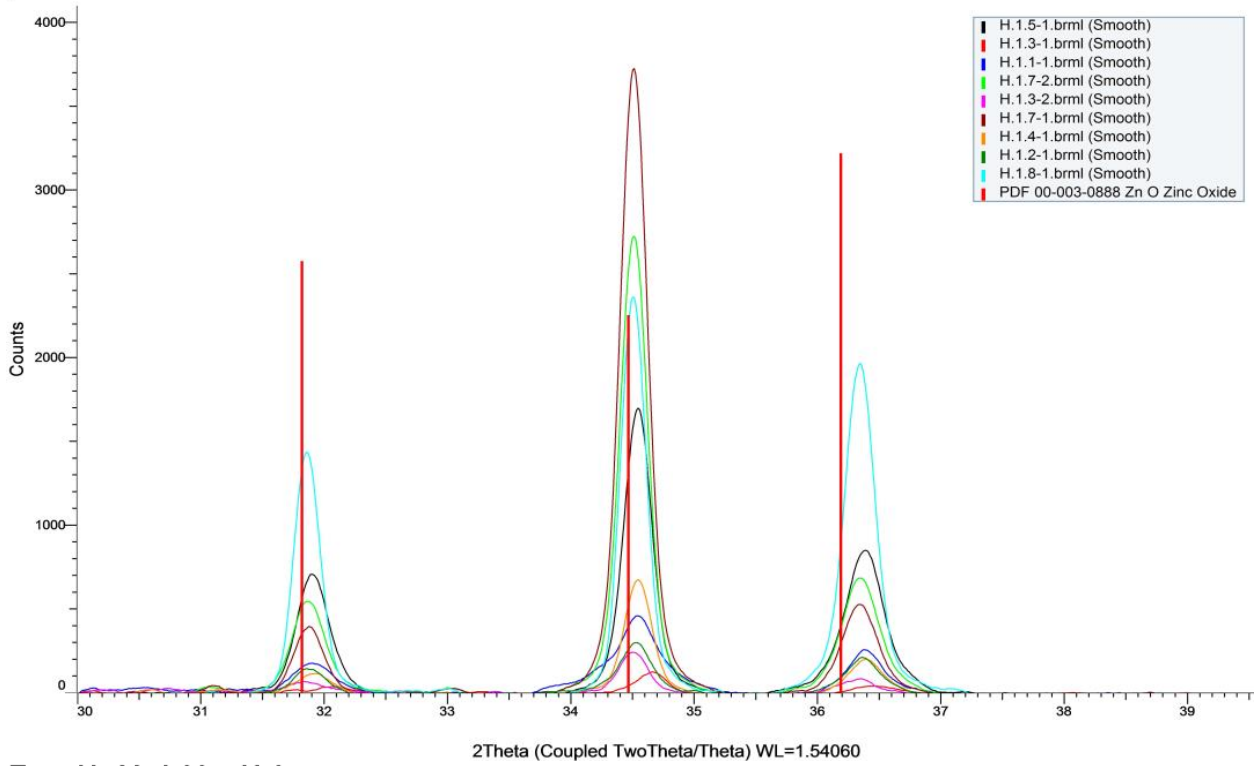
150°C Pre-heat Treatment



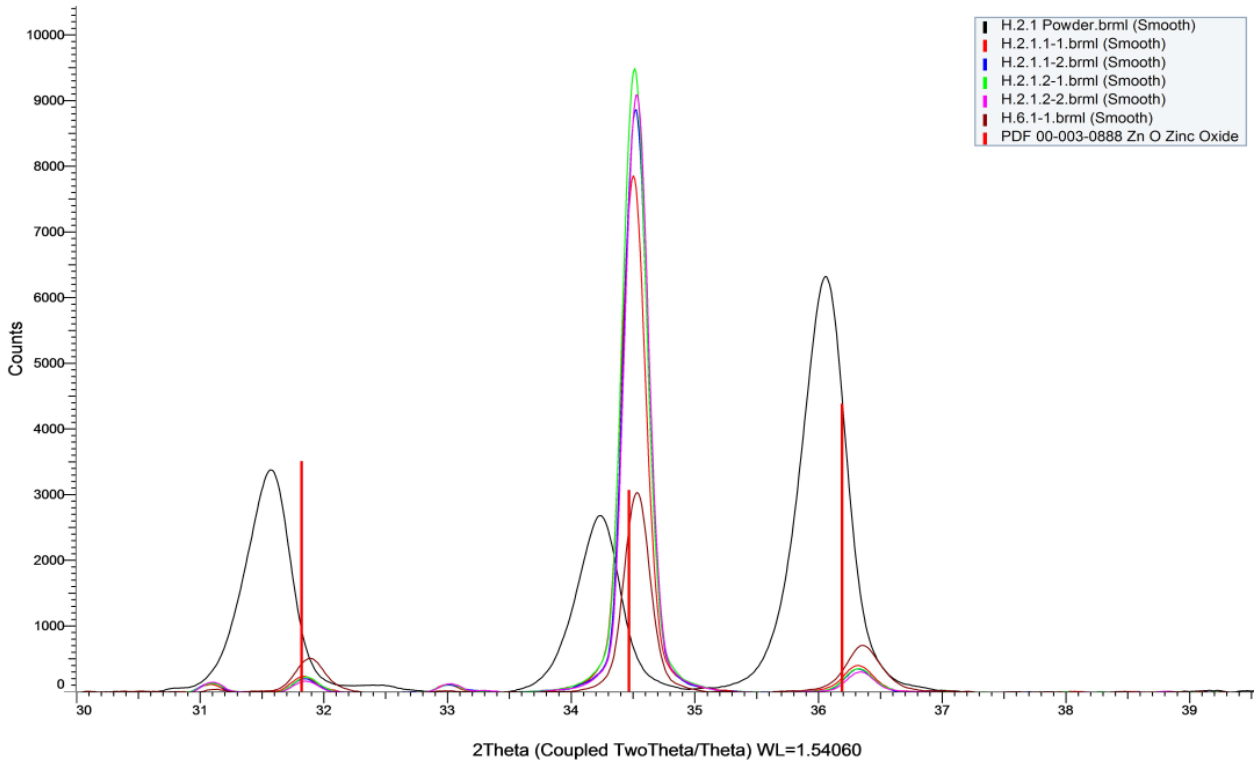
200°C Pre-heat Treatment



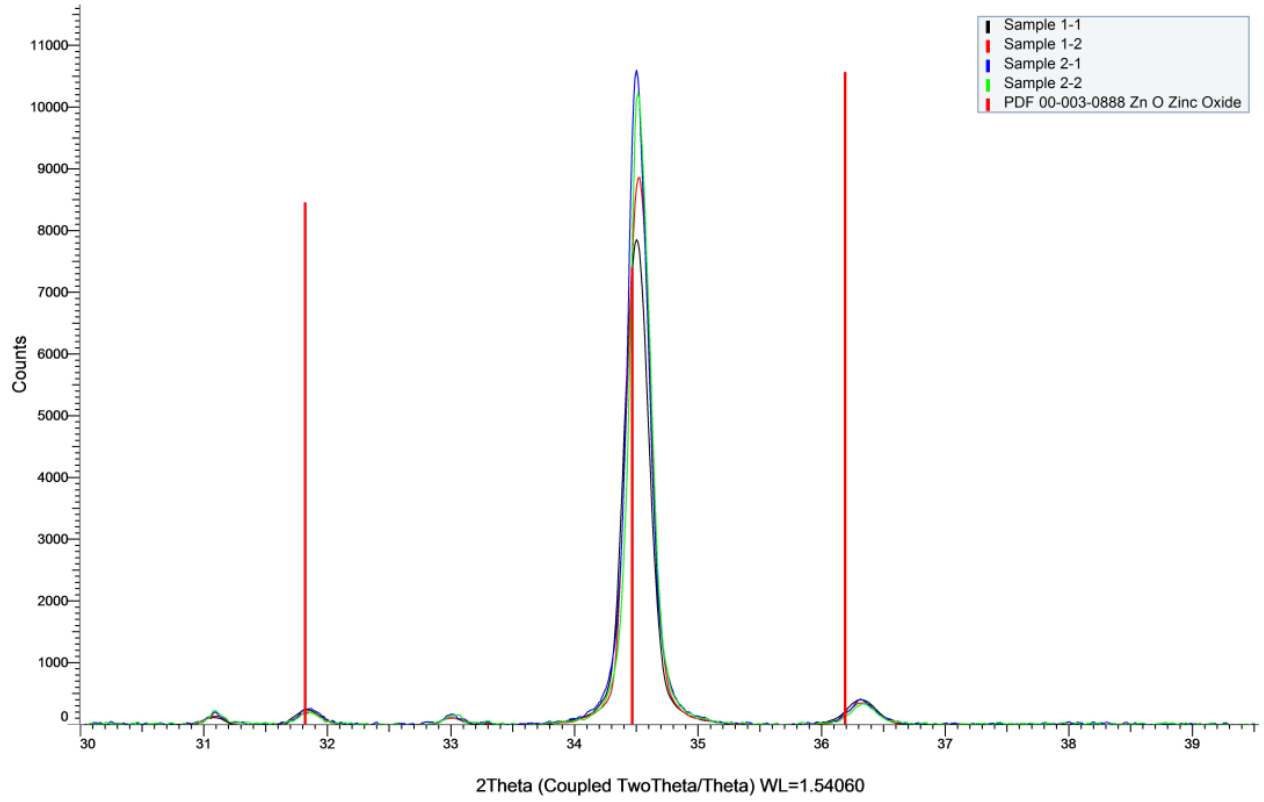
Expt. H - Variables Unknown



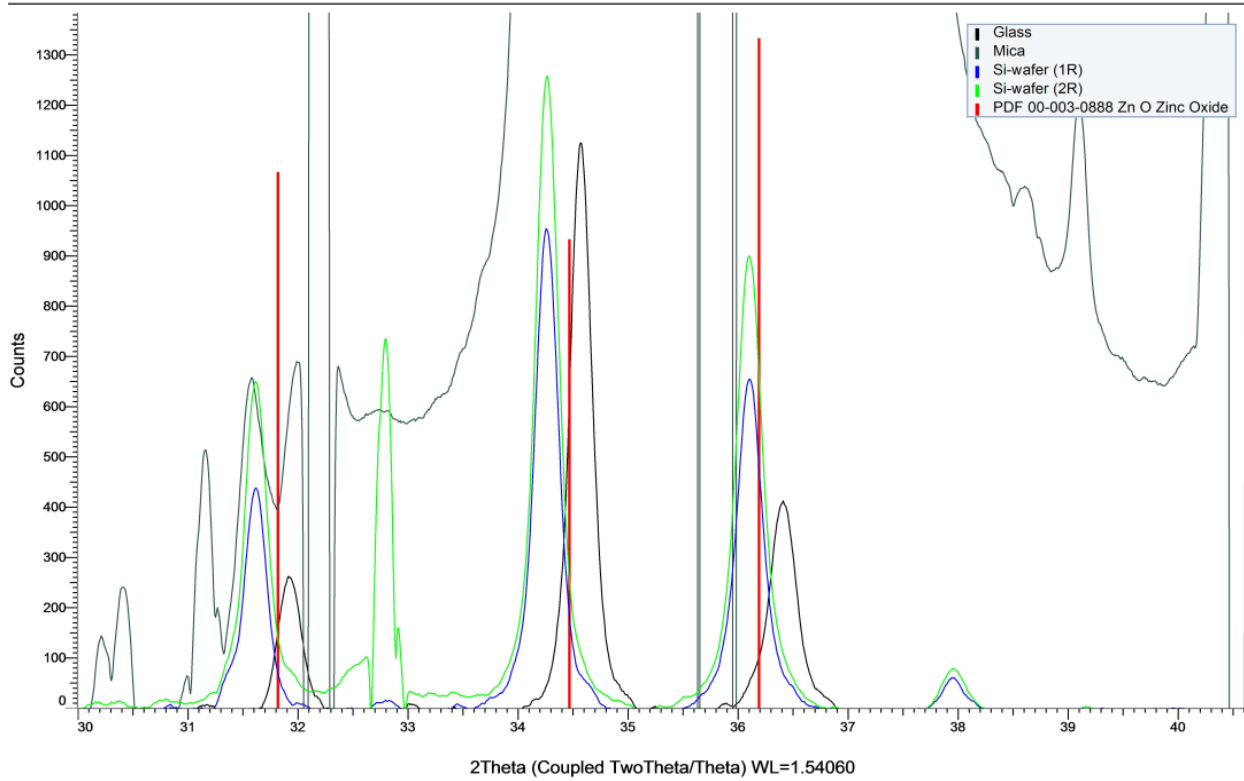
Expt. H - Variables Unknown



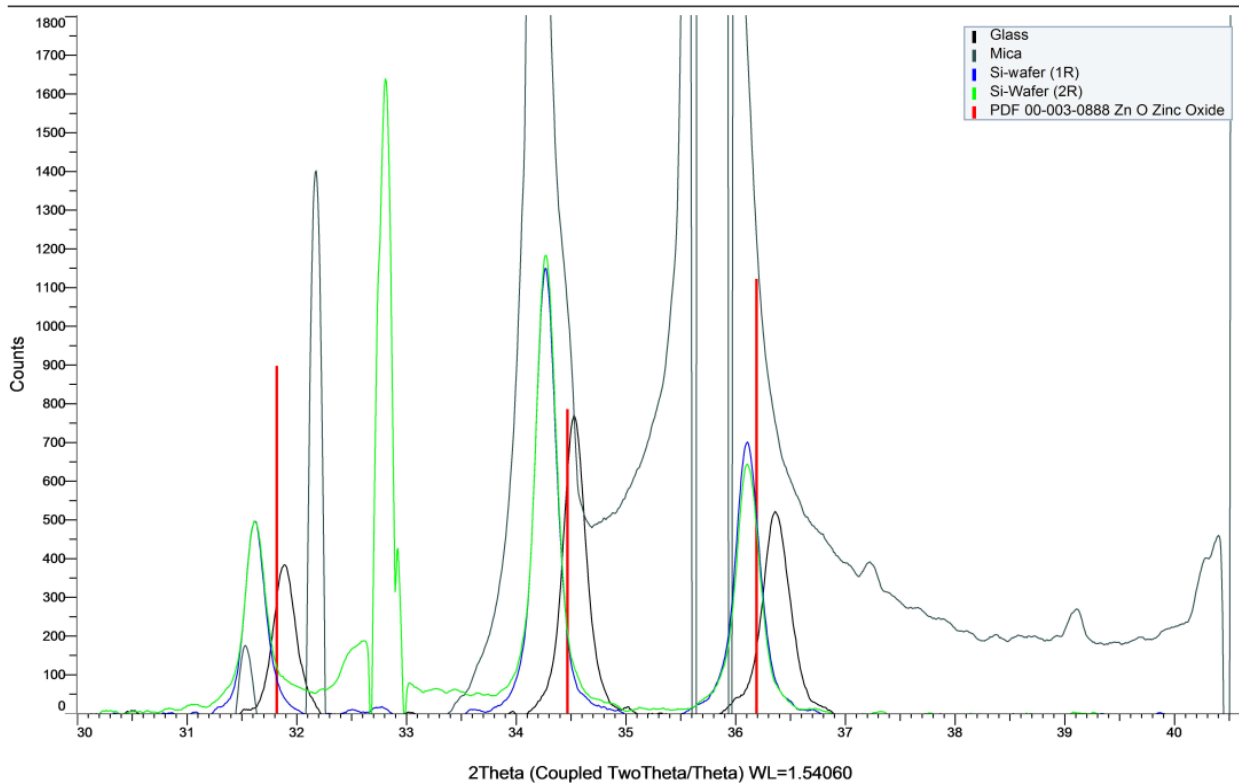
Expt. H



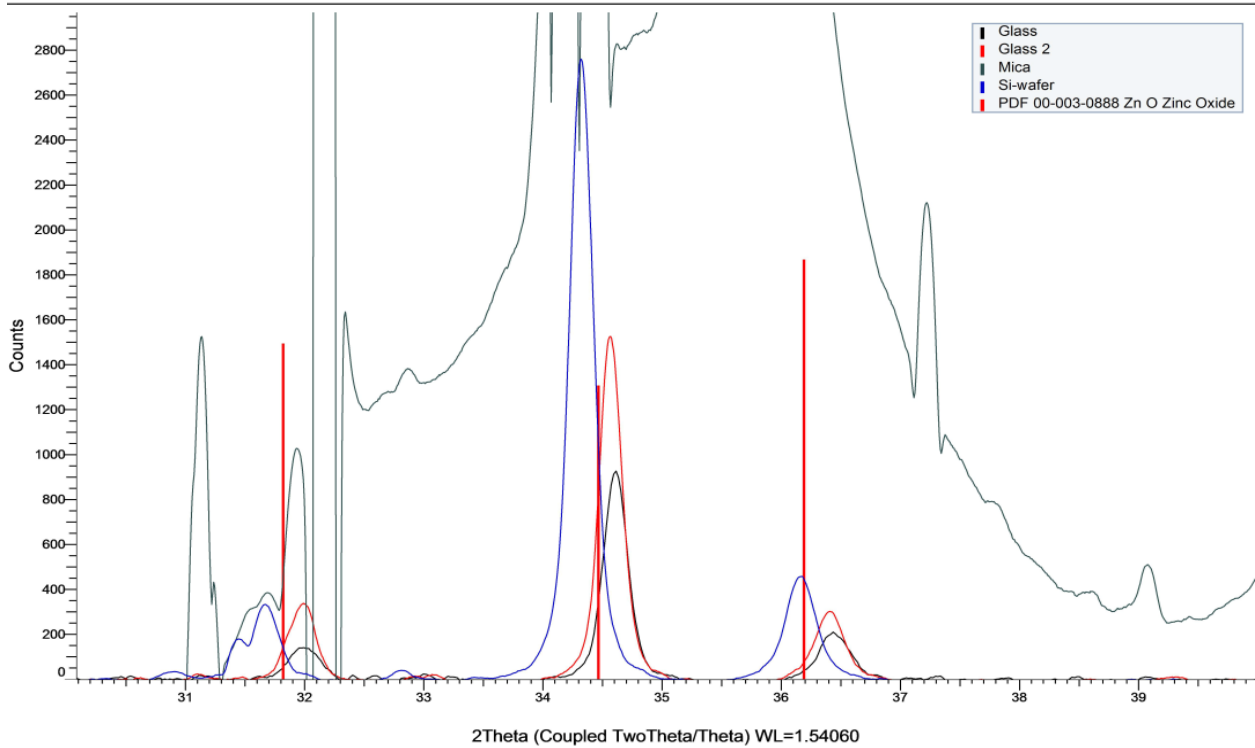
Undoped



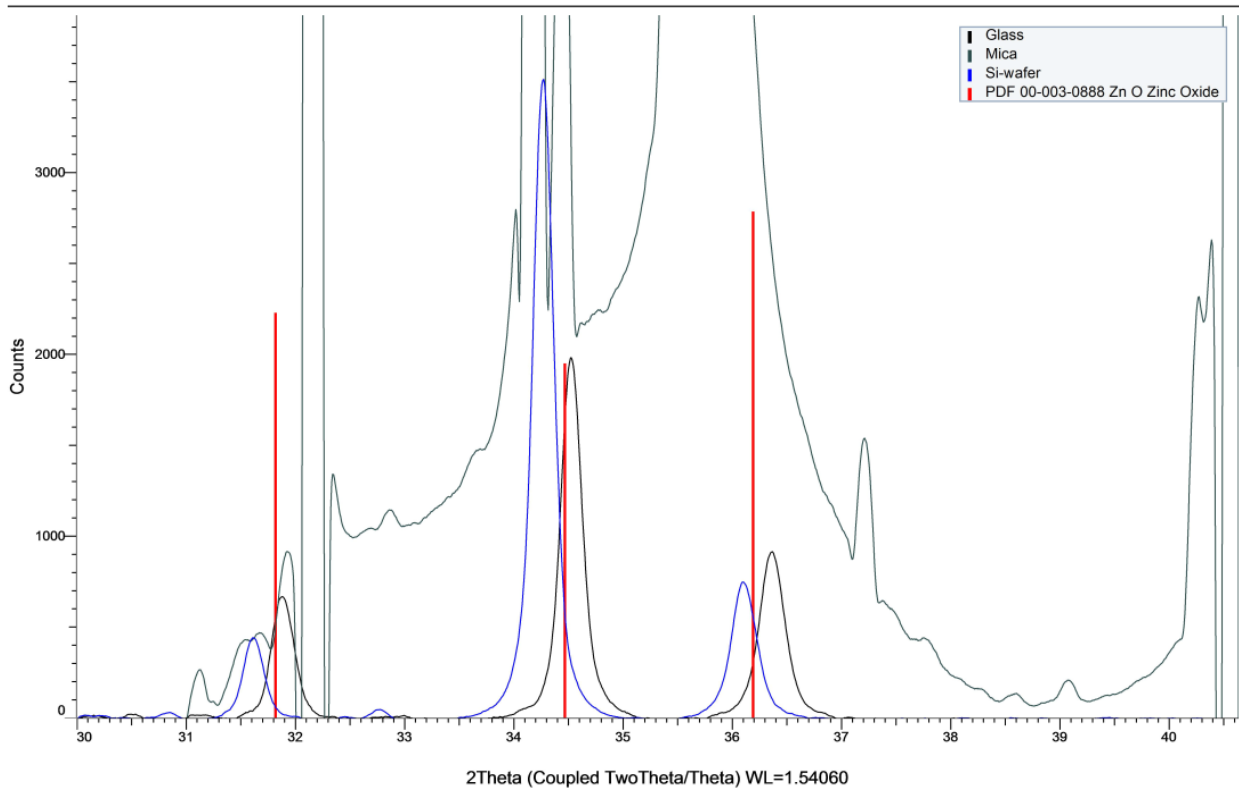
Silver-doped



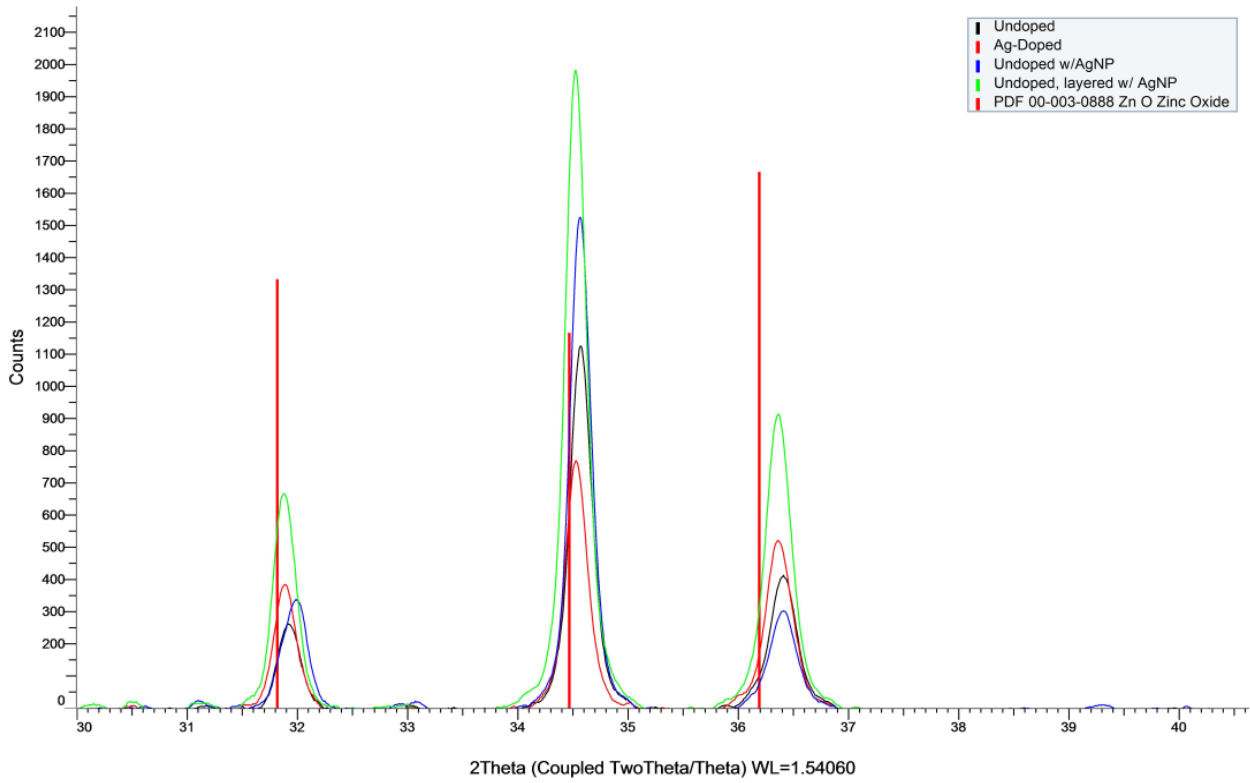
Undoped with AgNP in Sol



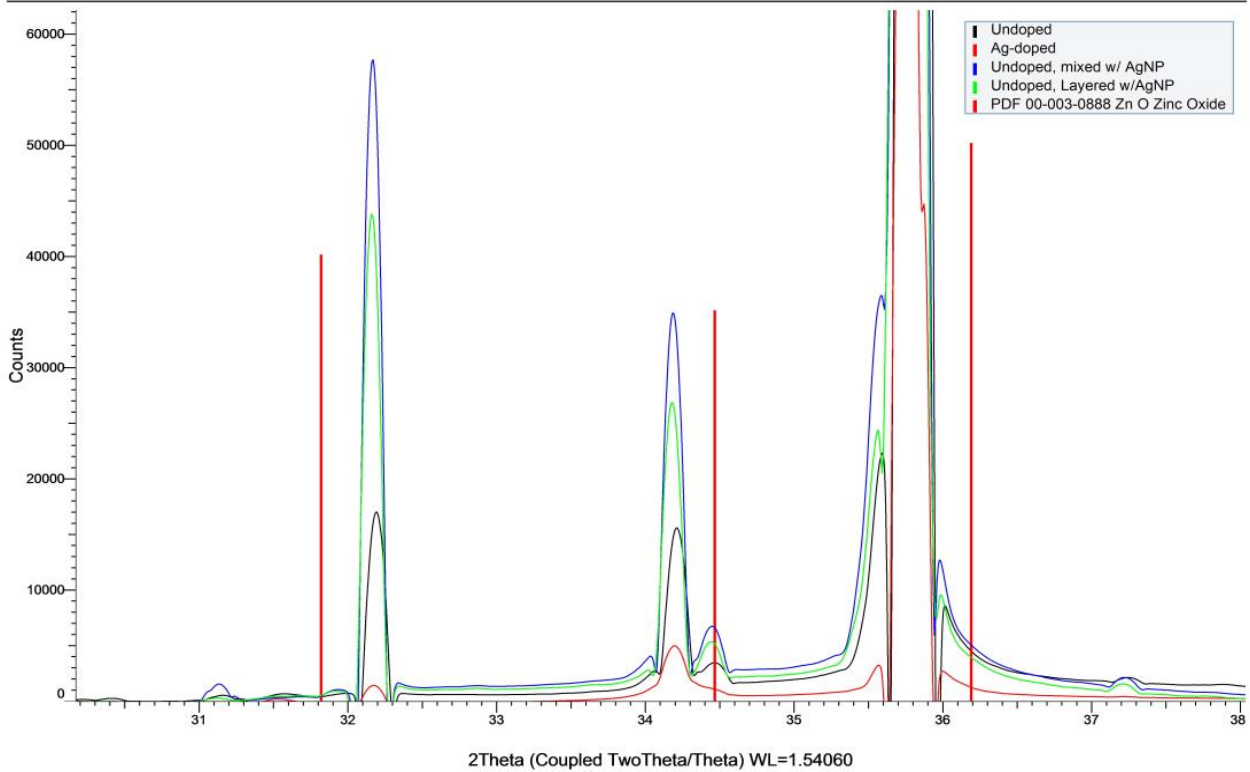
ZnO and AgNP Layering



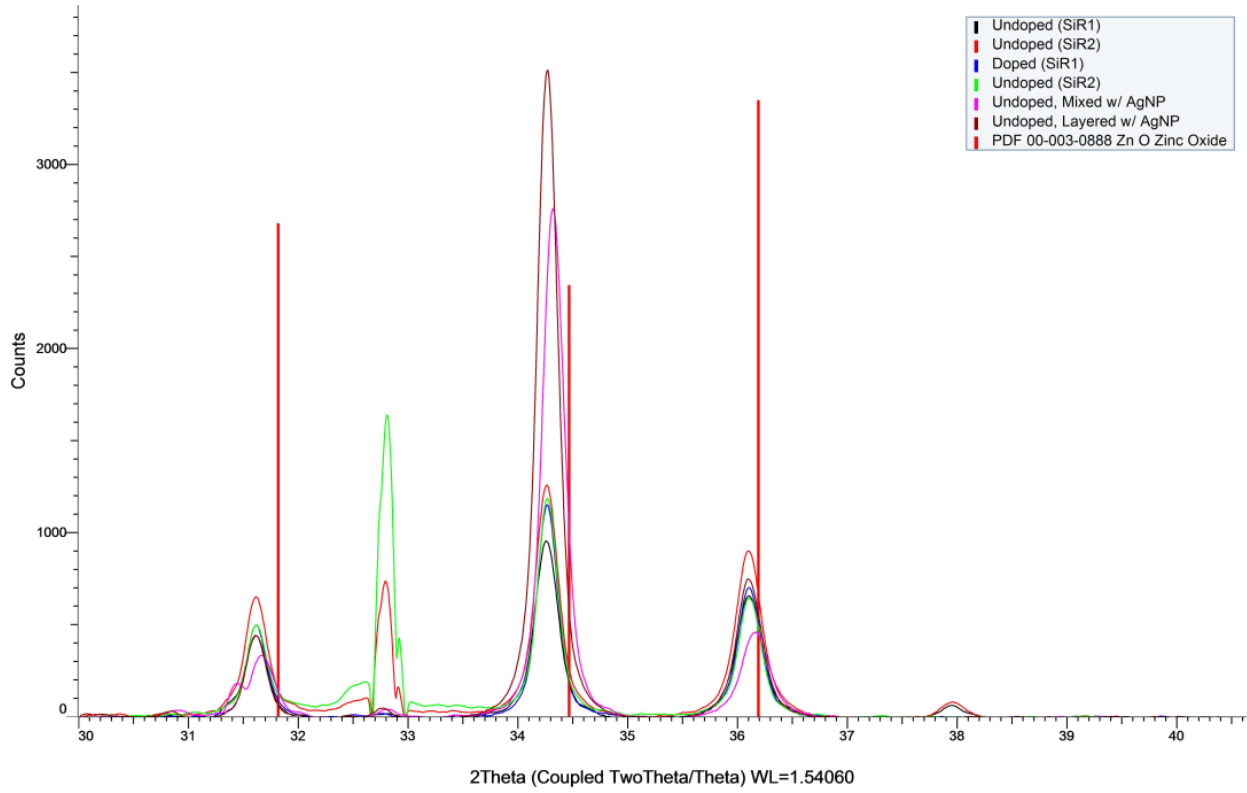
Soda-lime Glass Substrate



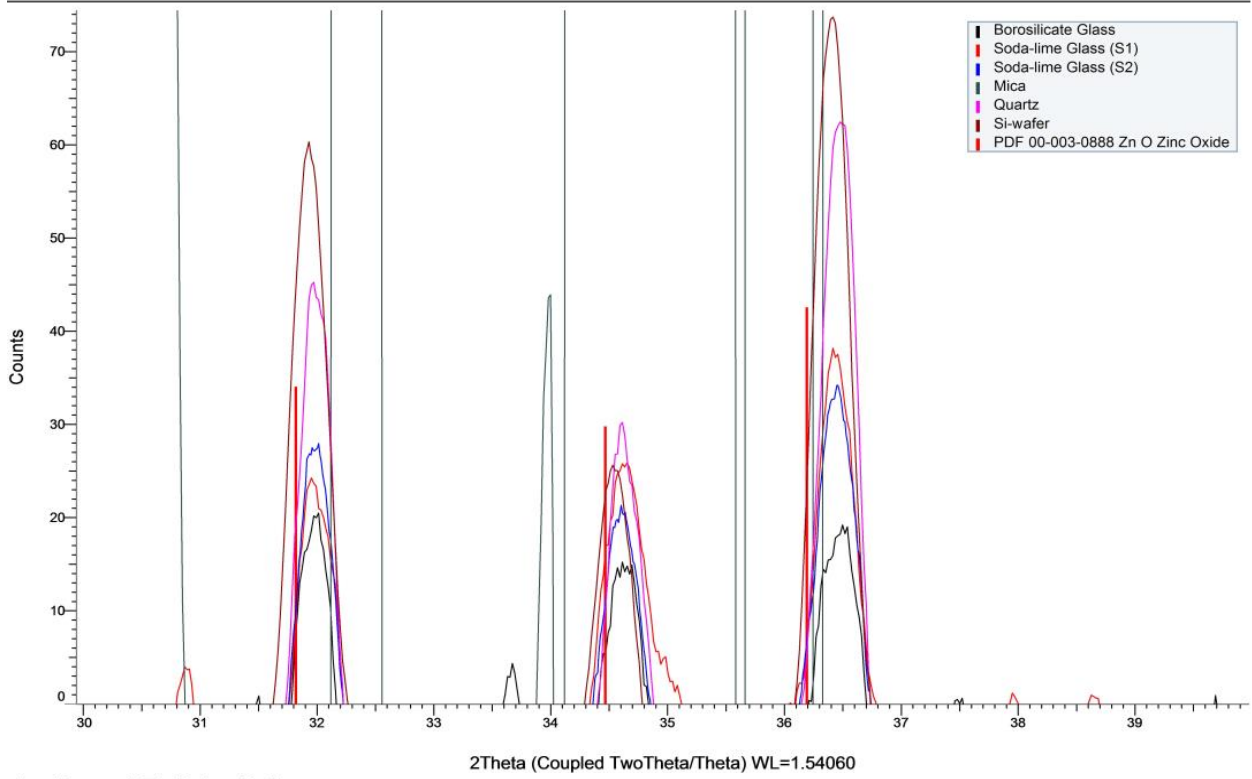
Mica Substrate



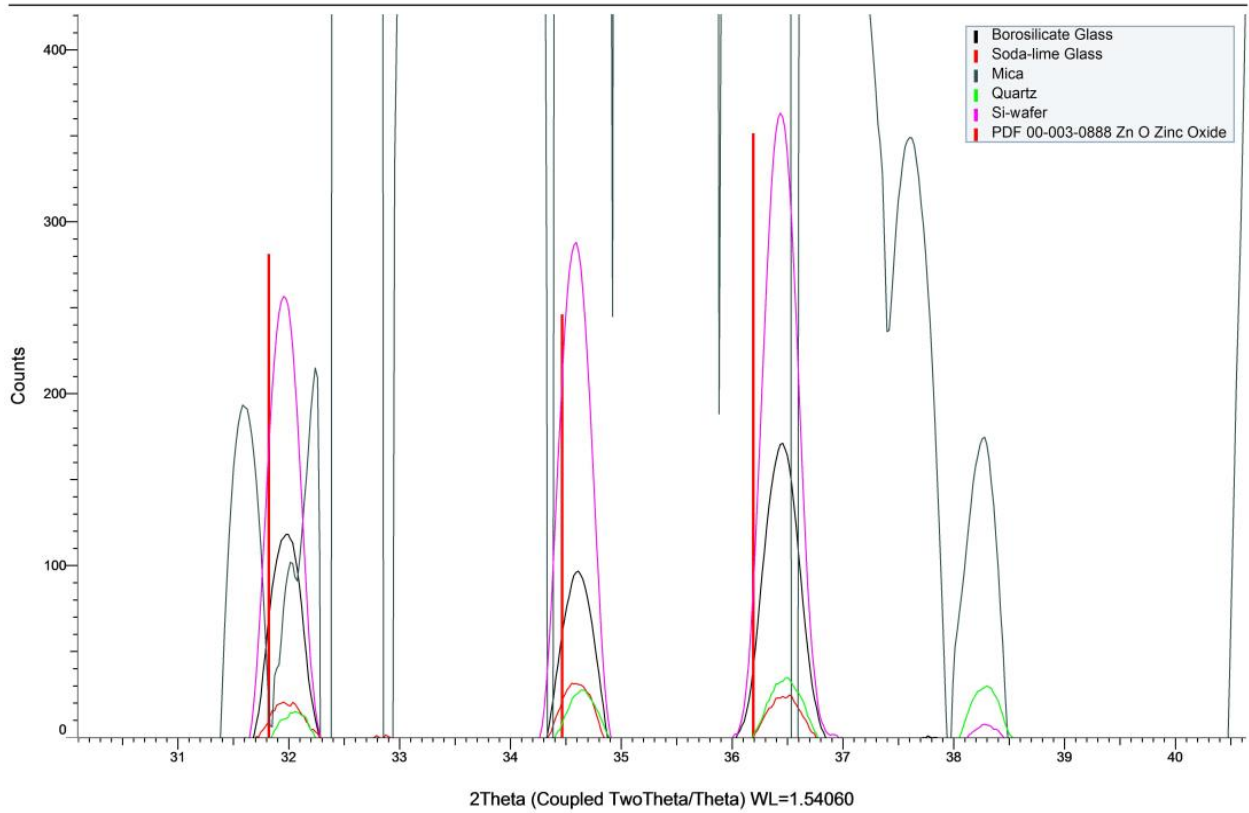
Si-wafer Substrate



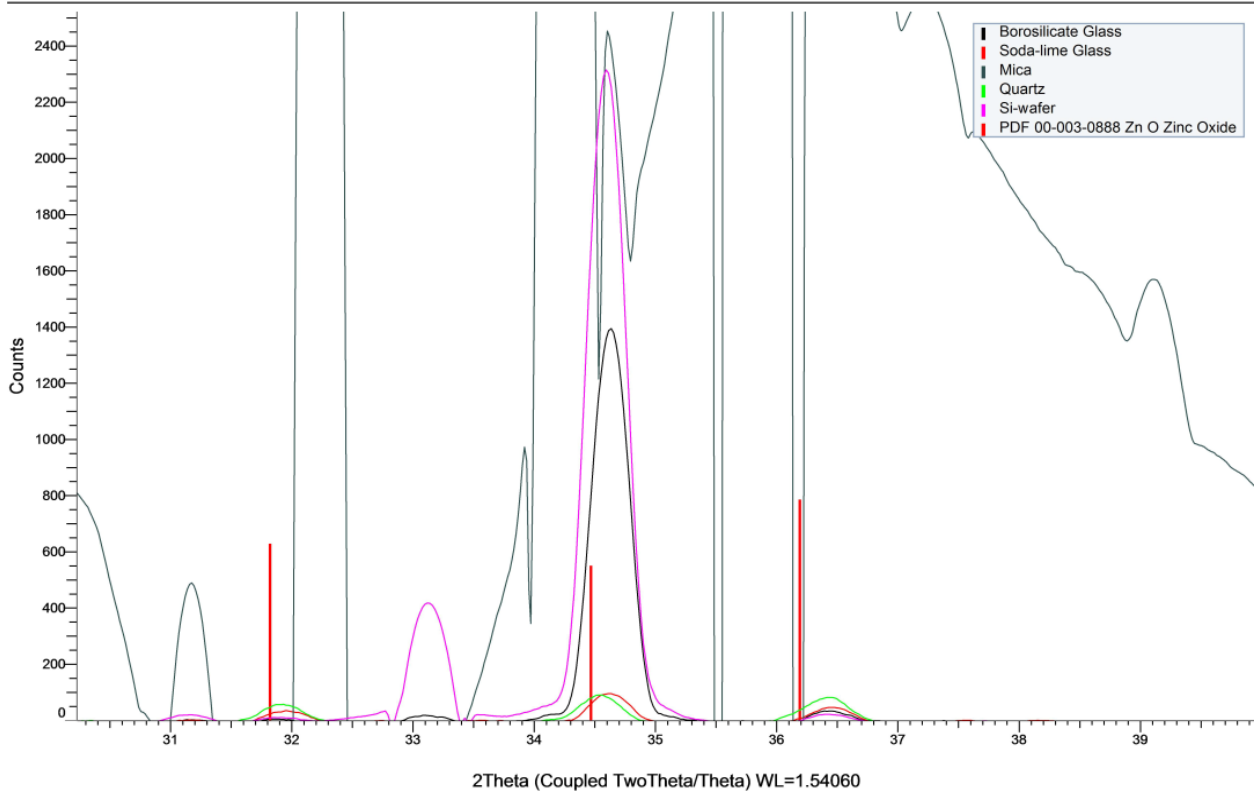
Undoped ZnO by Substrate



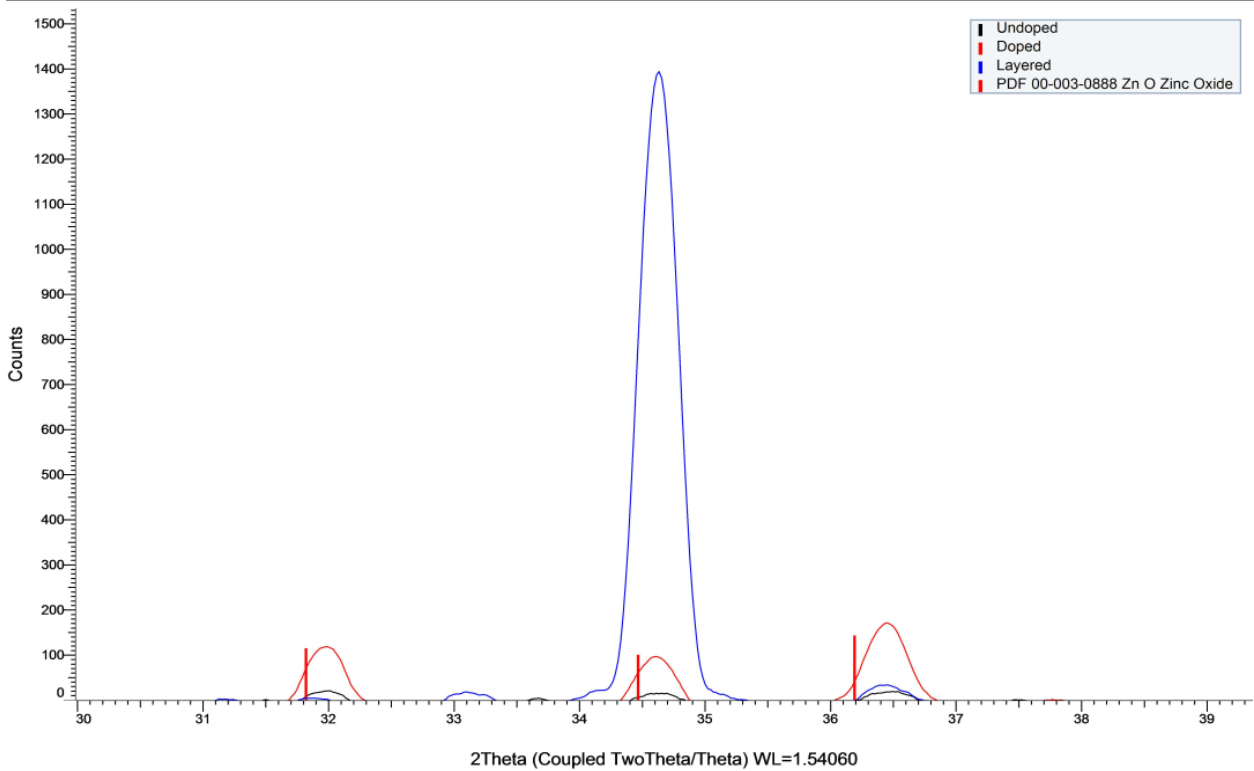
Ag-Doped ZnO by Substrate



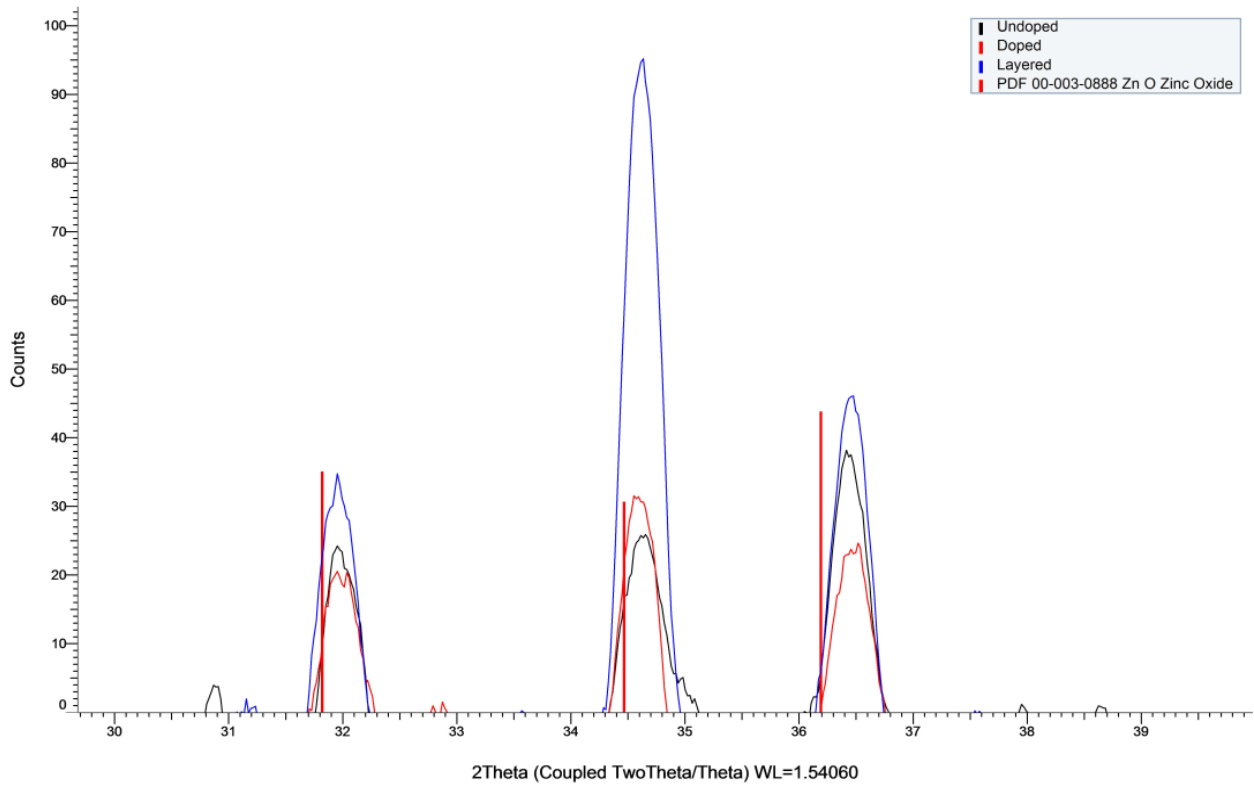
Undoped ZnO with Layered AgNP



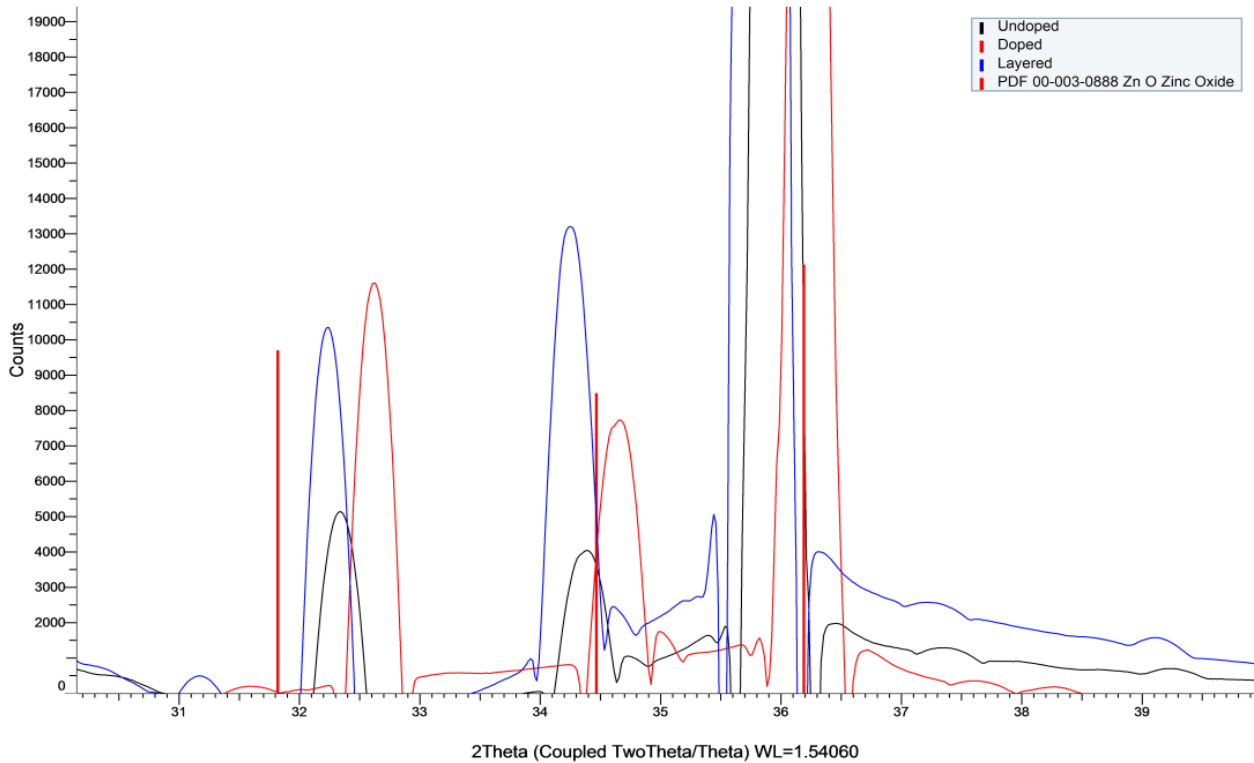
Borosilicate Glass Substrate



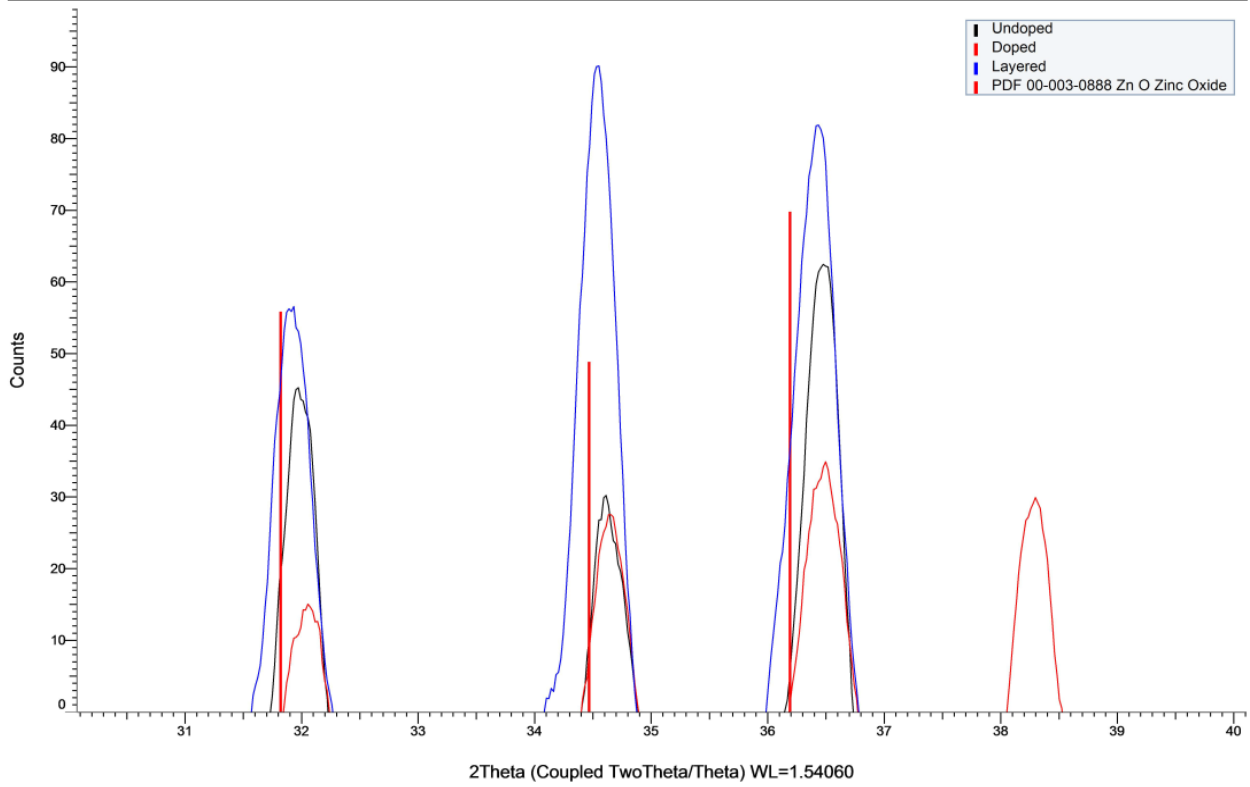
Soda-Lime Glass Substrate



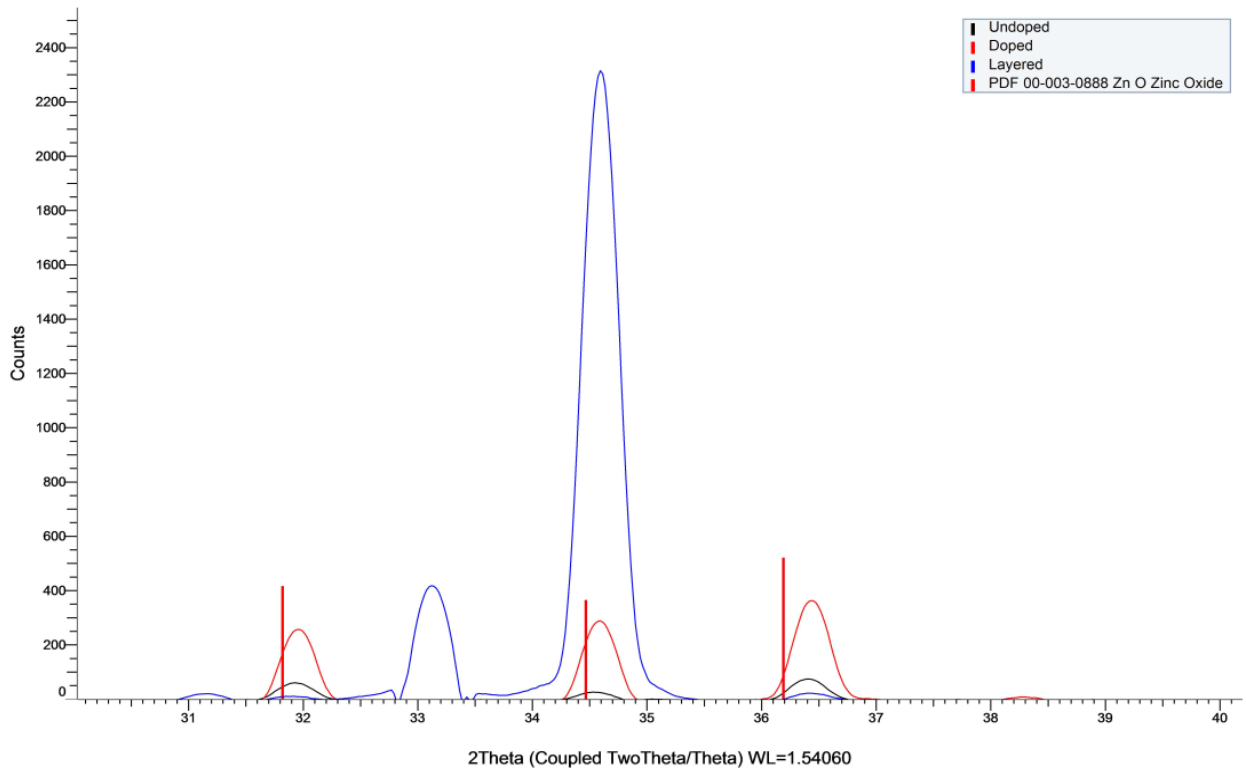
Mica Substrate



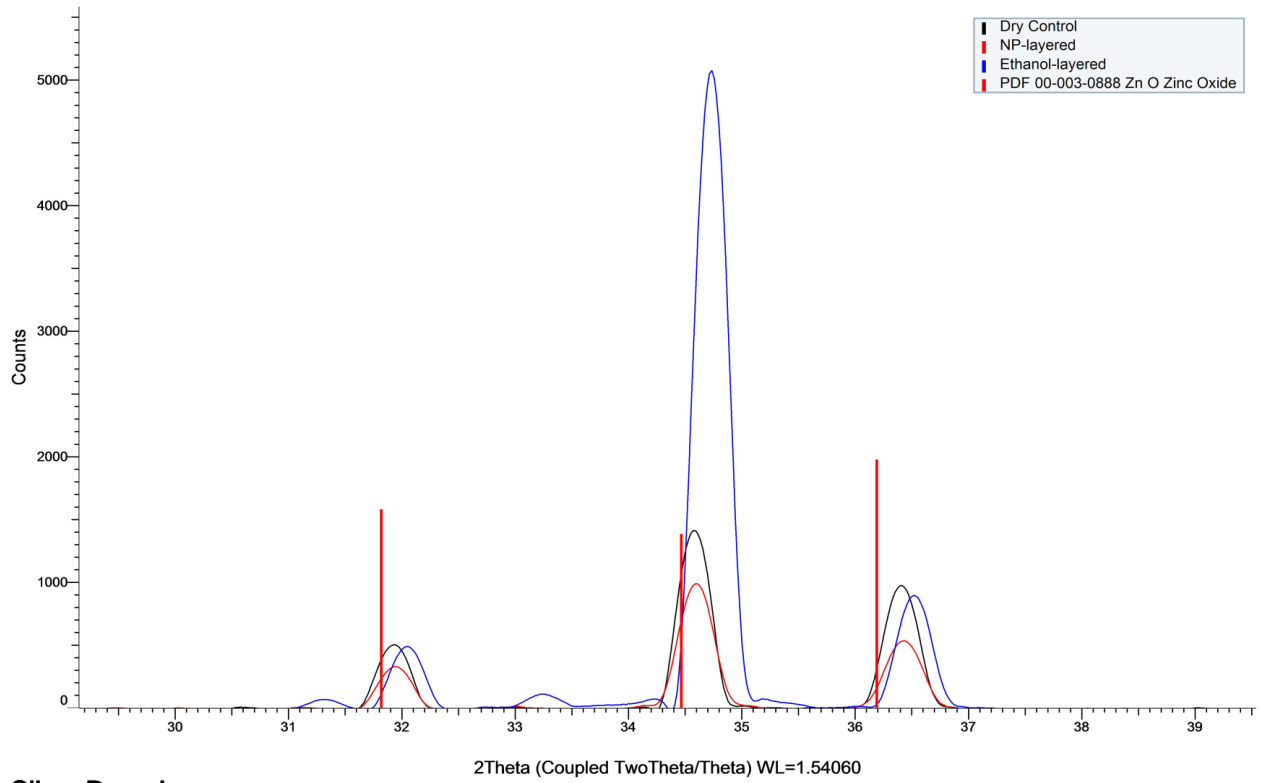
Quartz Substrate



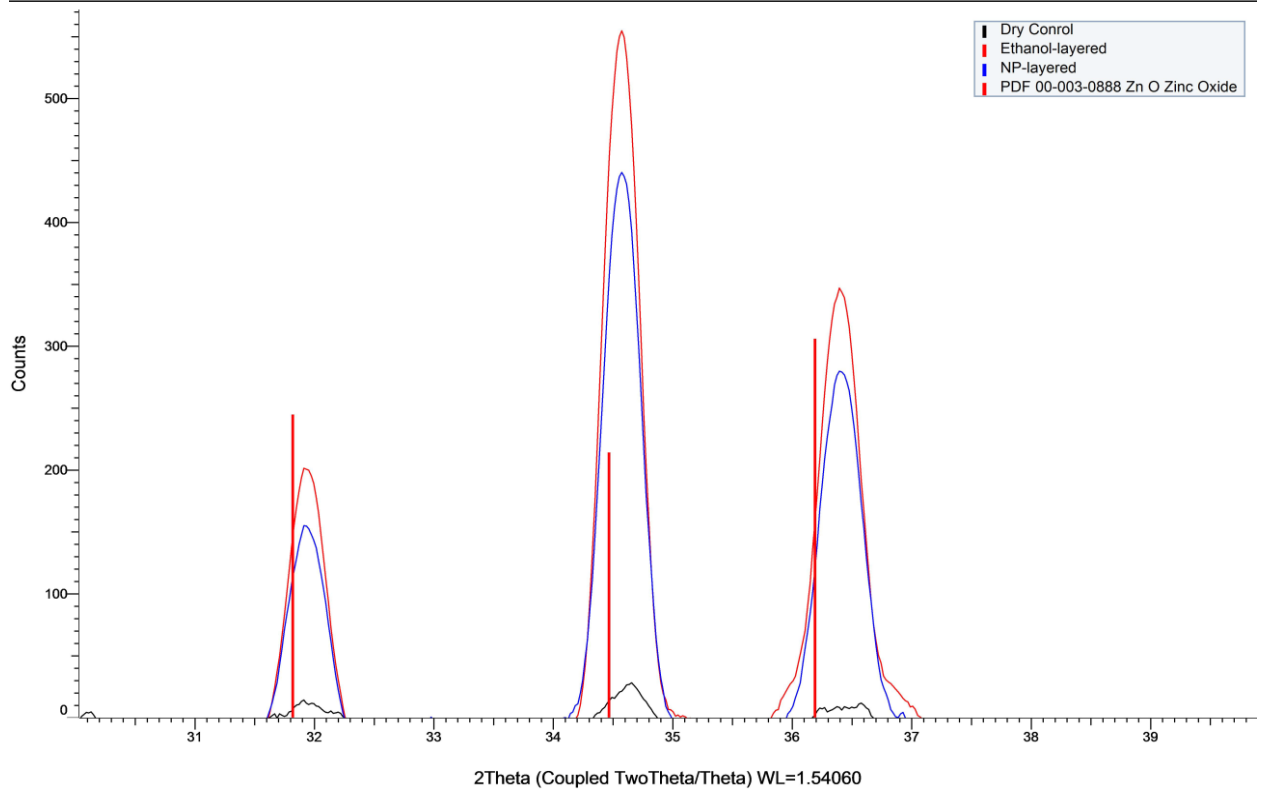
Si-wafer Substrate



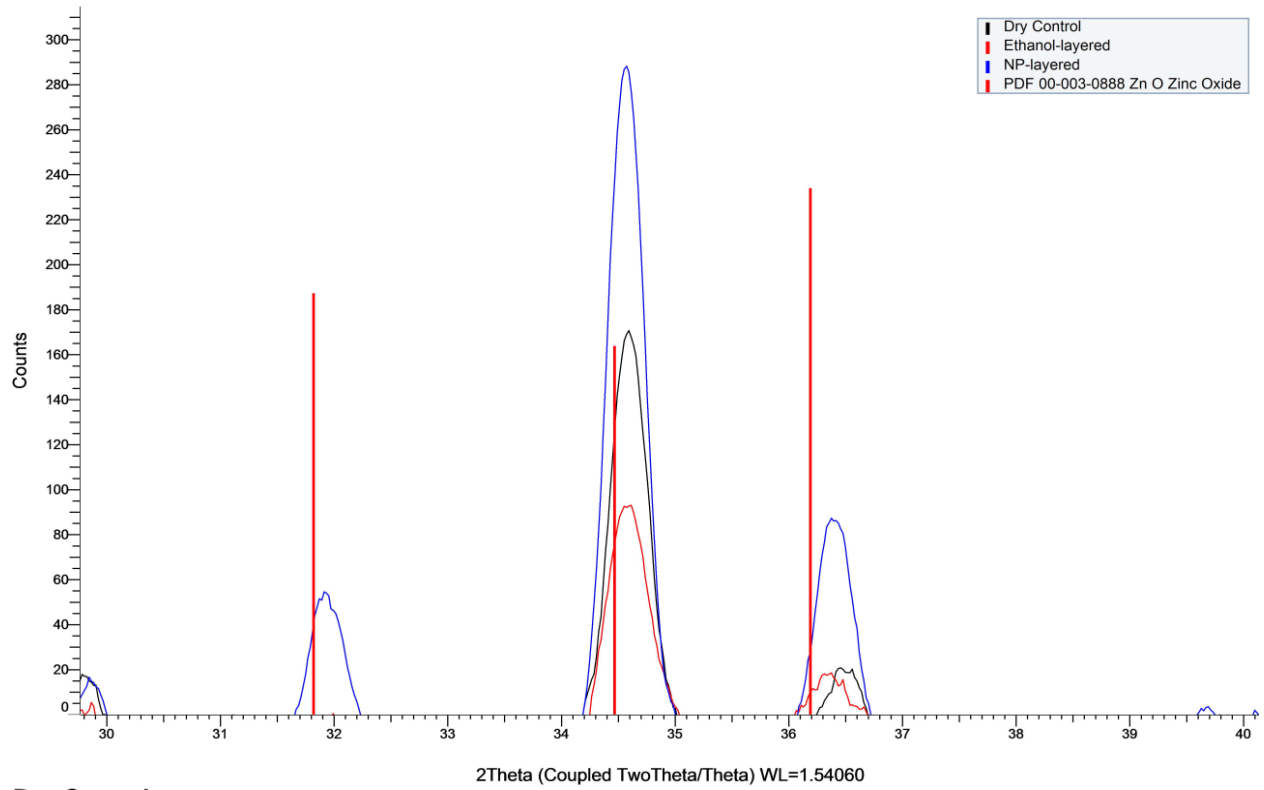
Undoped



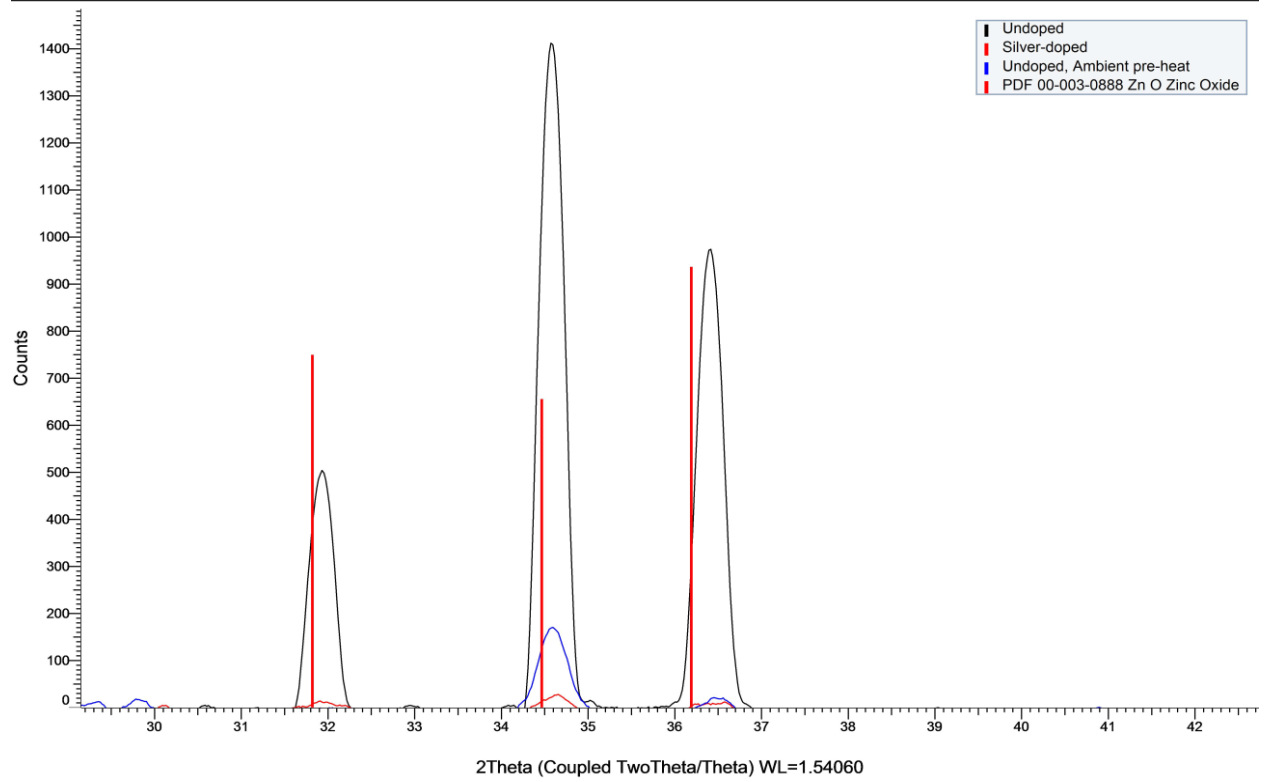
Silver Doped



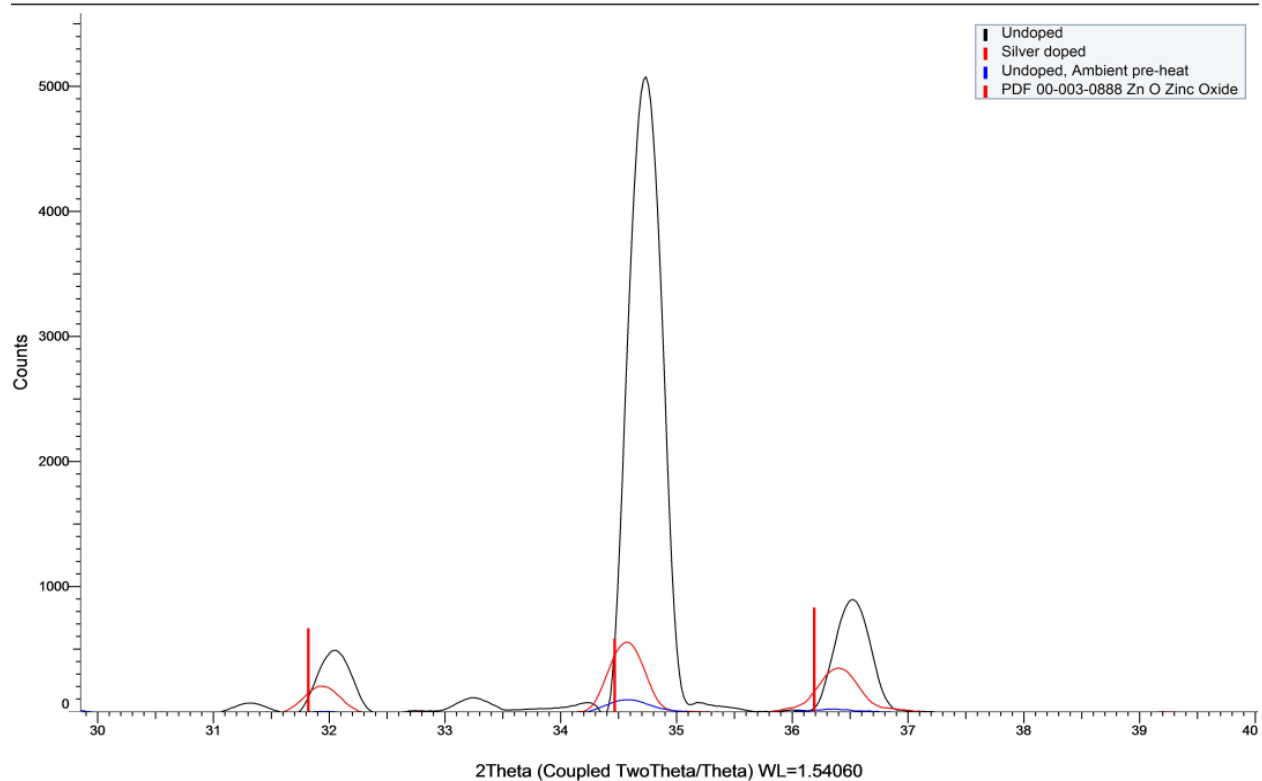
Undoped, Ambient pre-heat



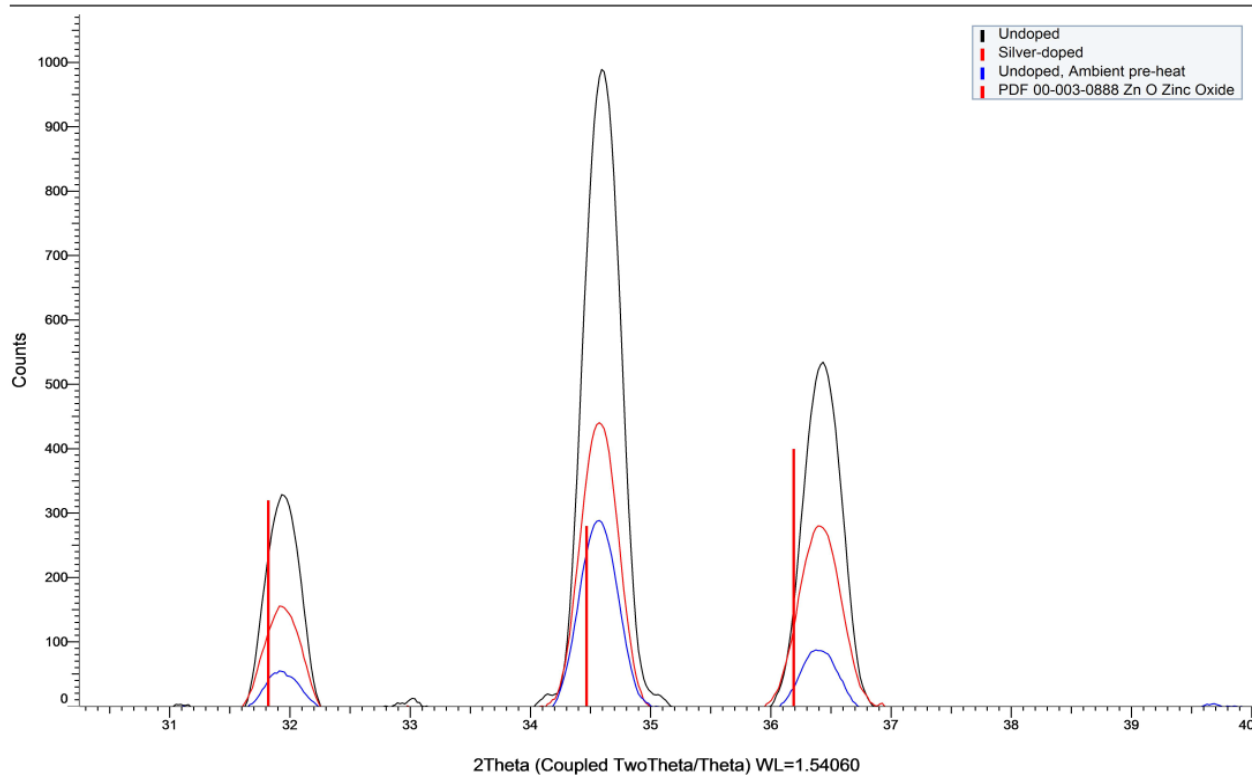
Dry Control



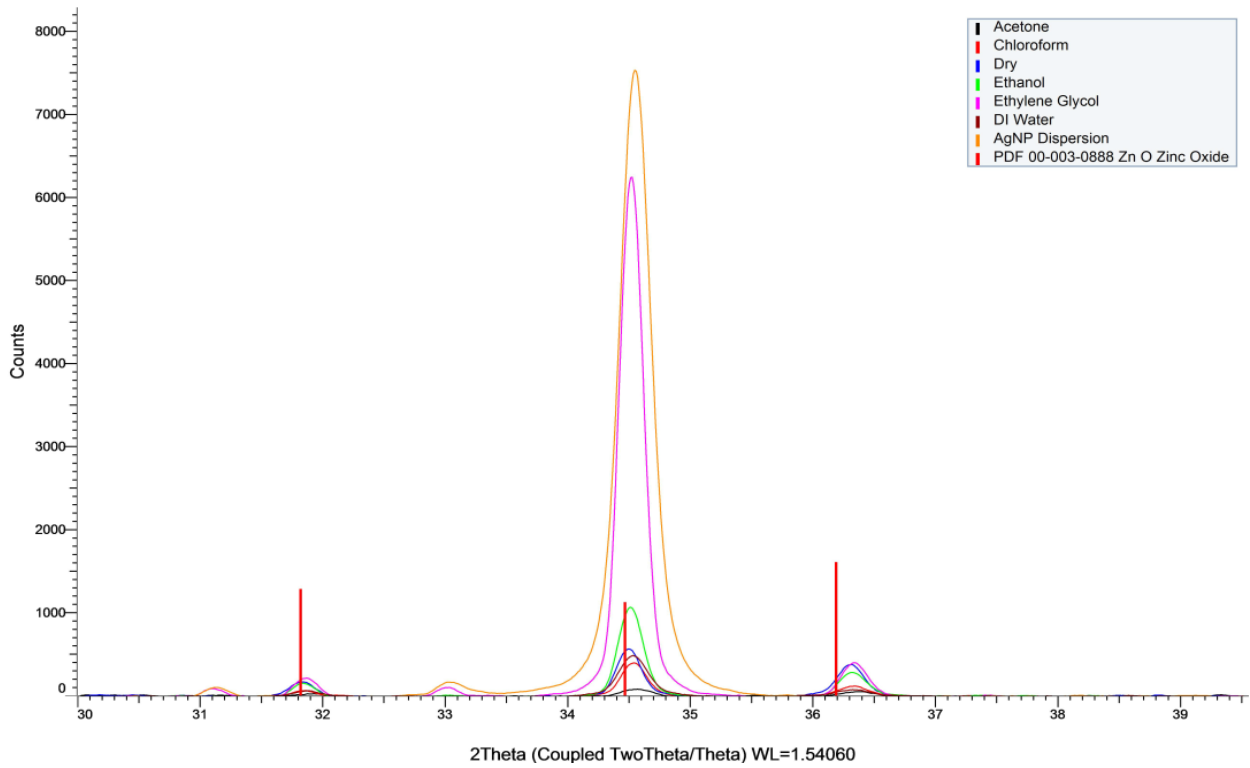
Ethanol-layered



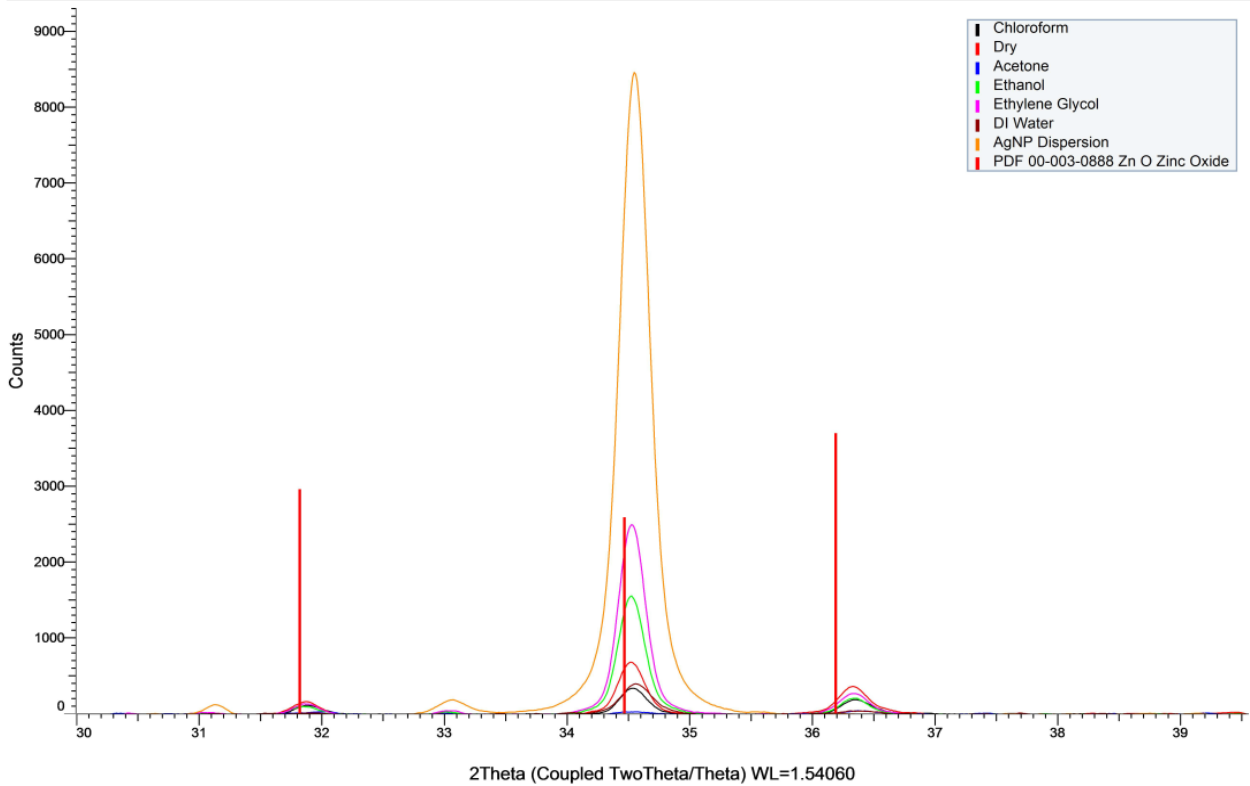
NP-layered



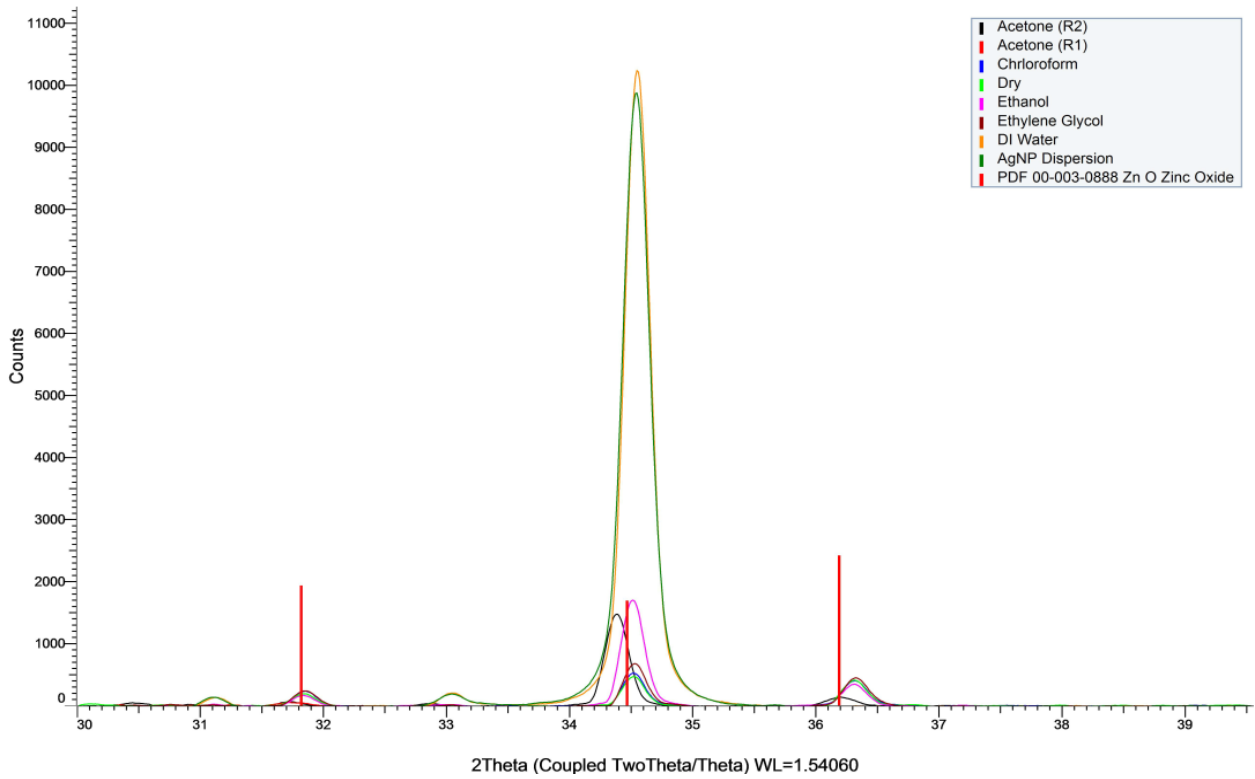
Undoped, Un-annealed



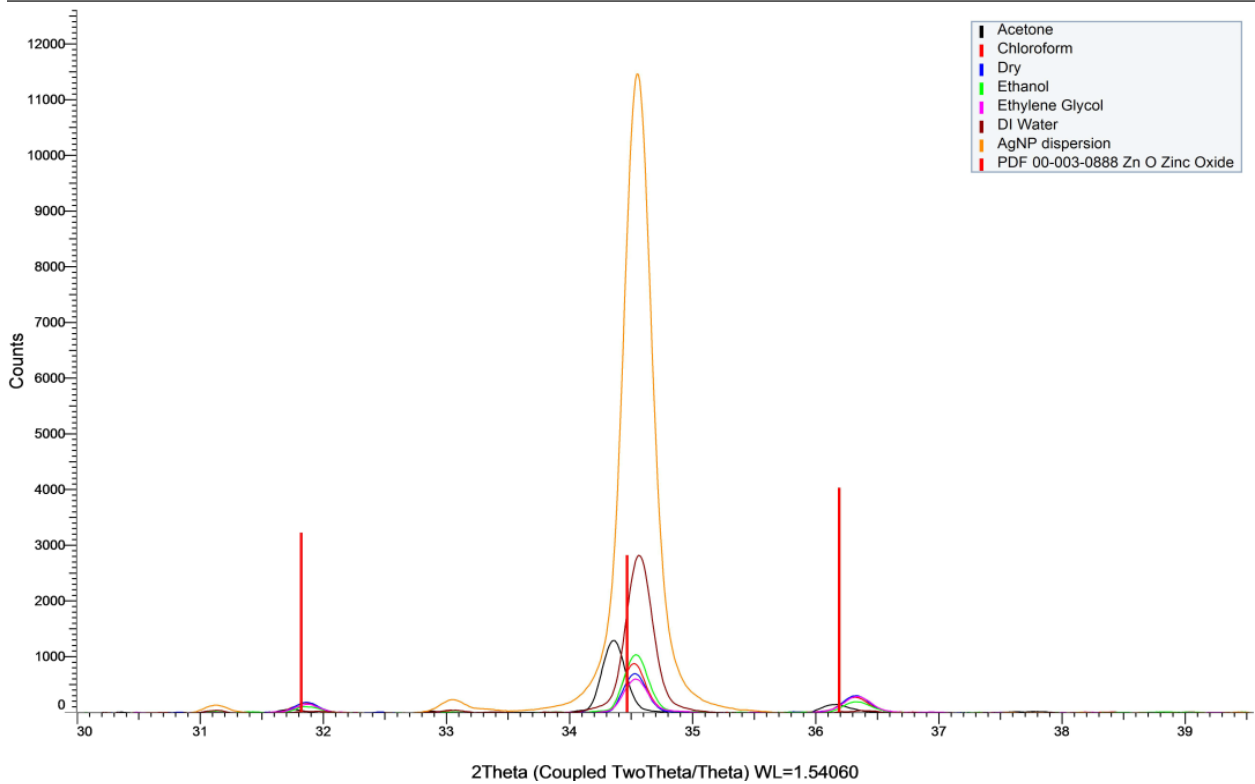
Silver-doped, Un-annealed



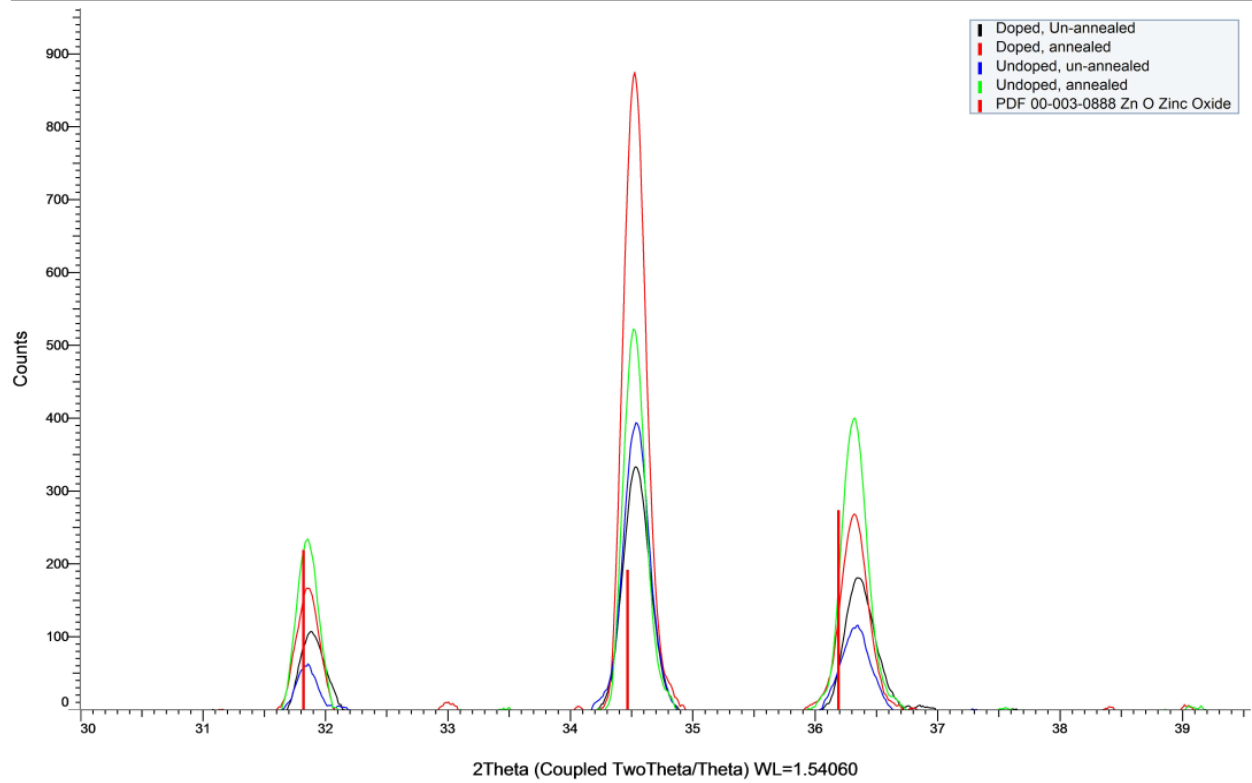
Undoped, Annealed



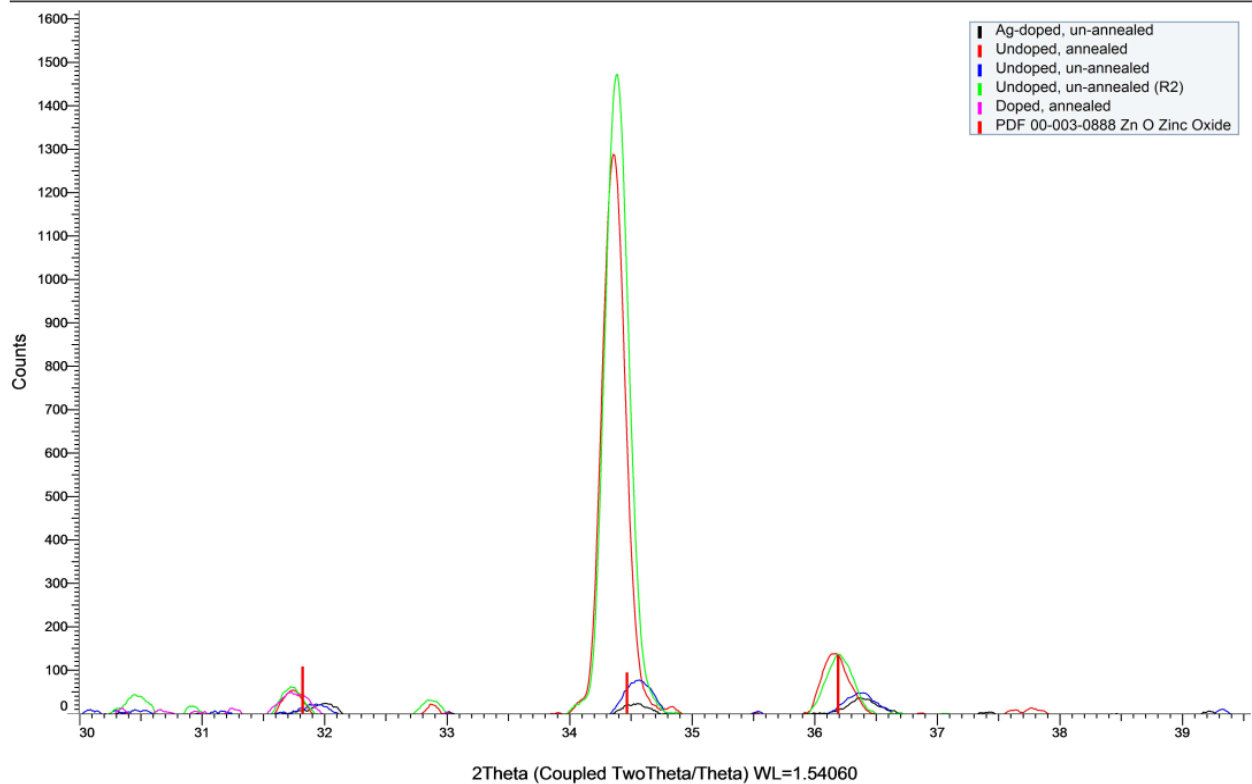
Doped, Annealed



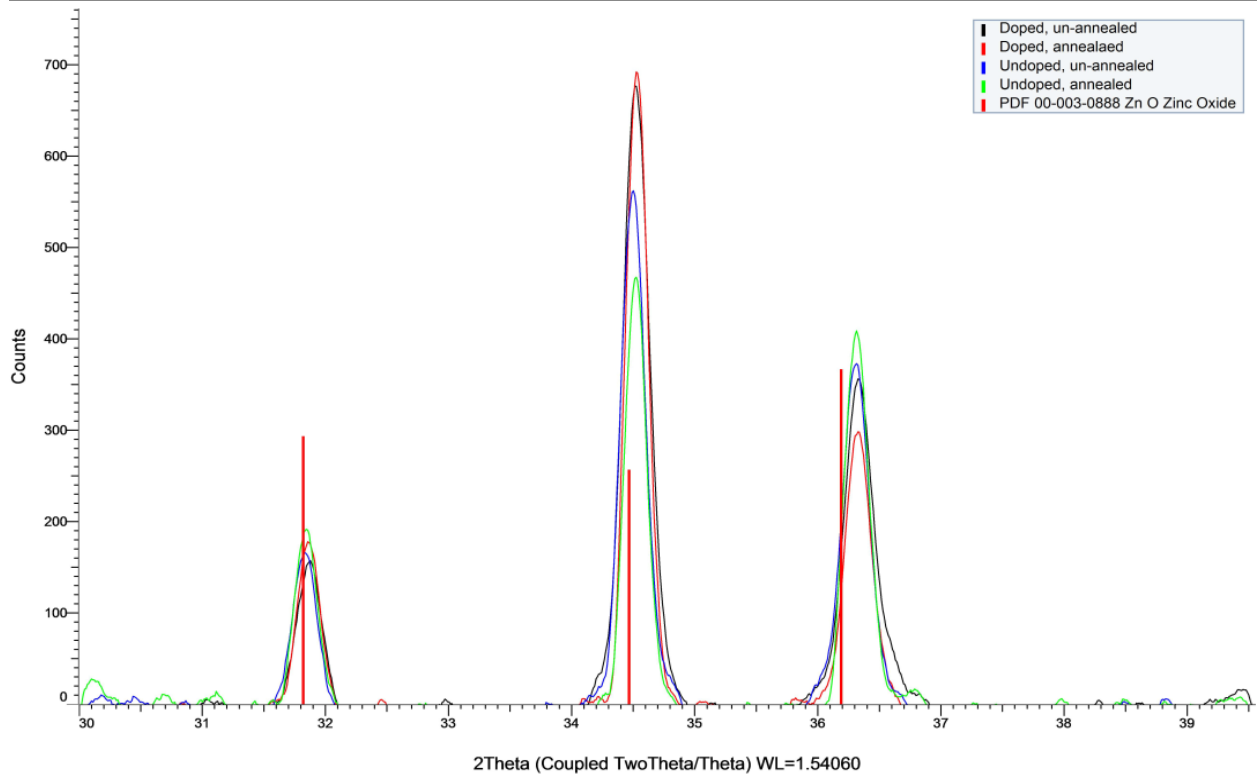
Chloroform-wetted



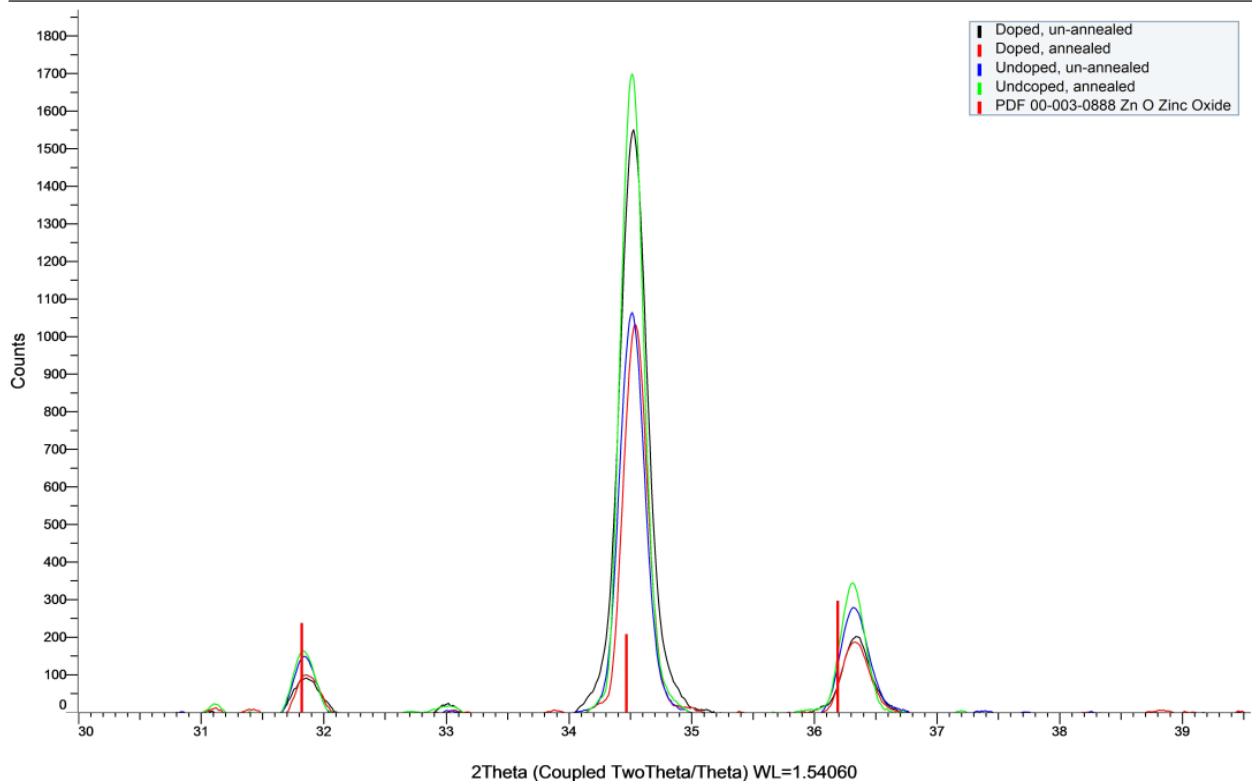
Acetone-wetted



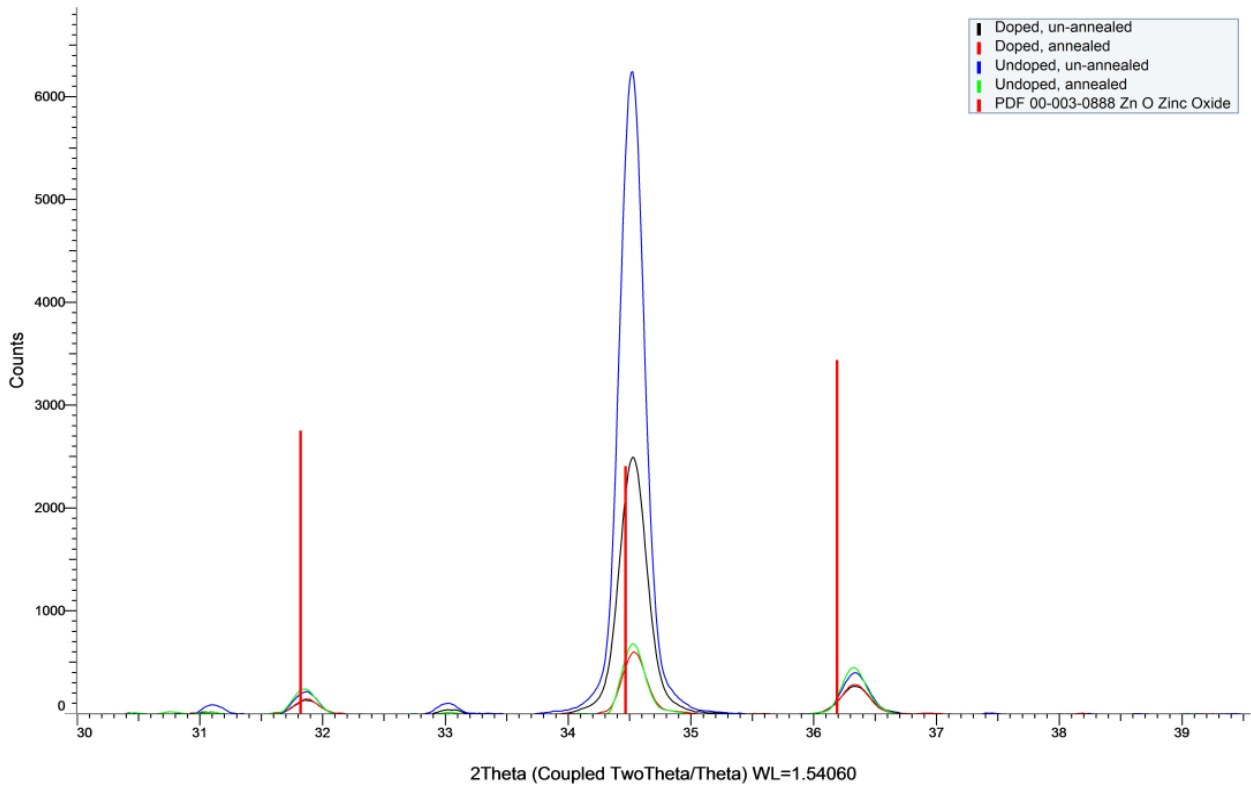
Dry (unwetted)



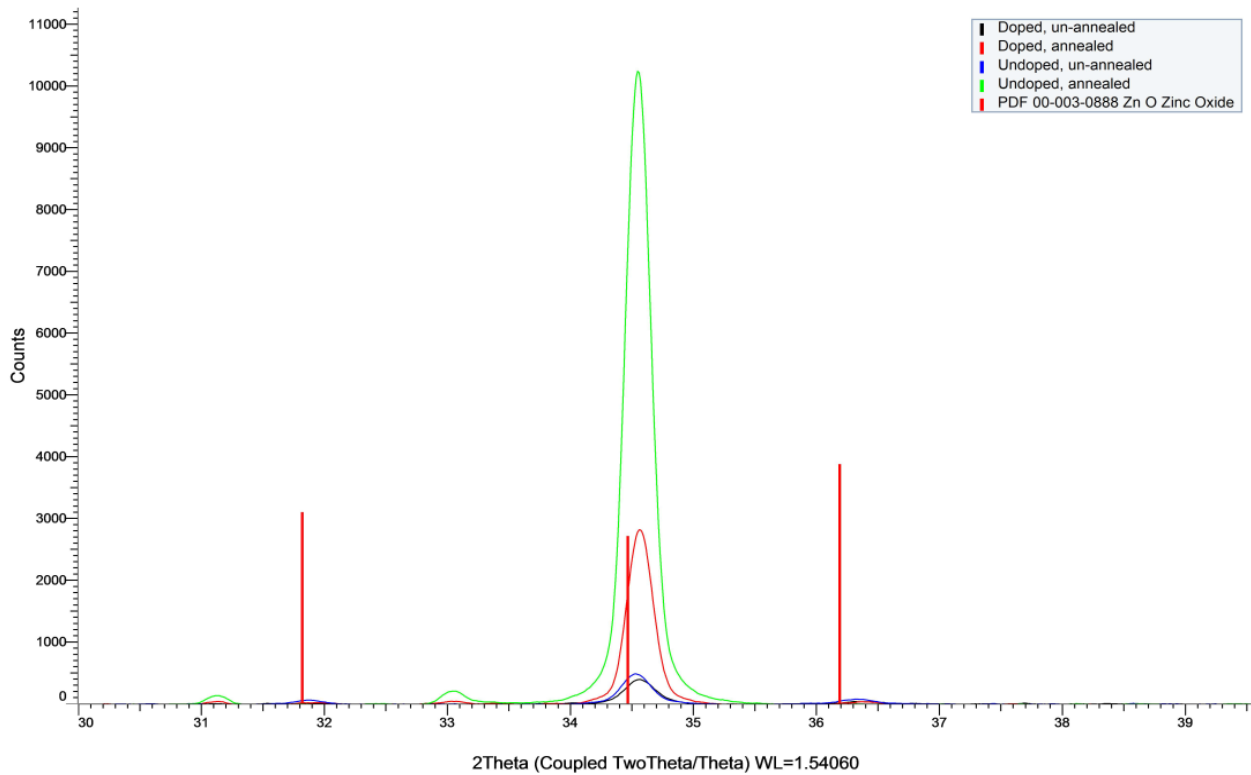
Ethanol-wetted



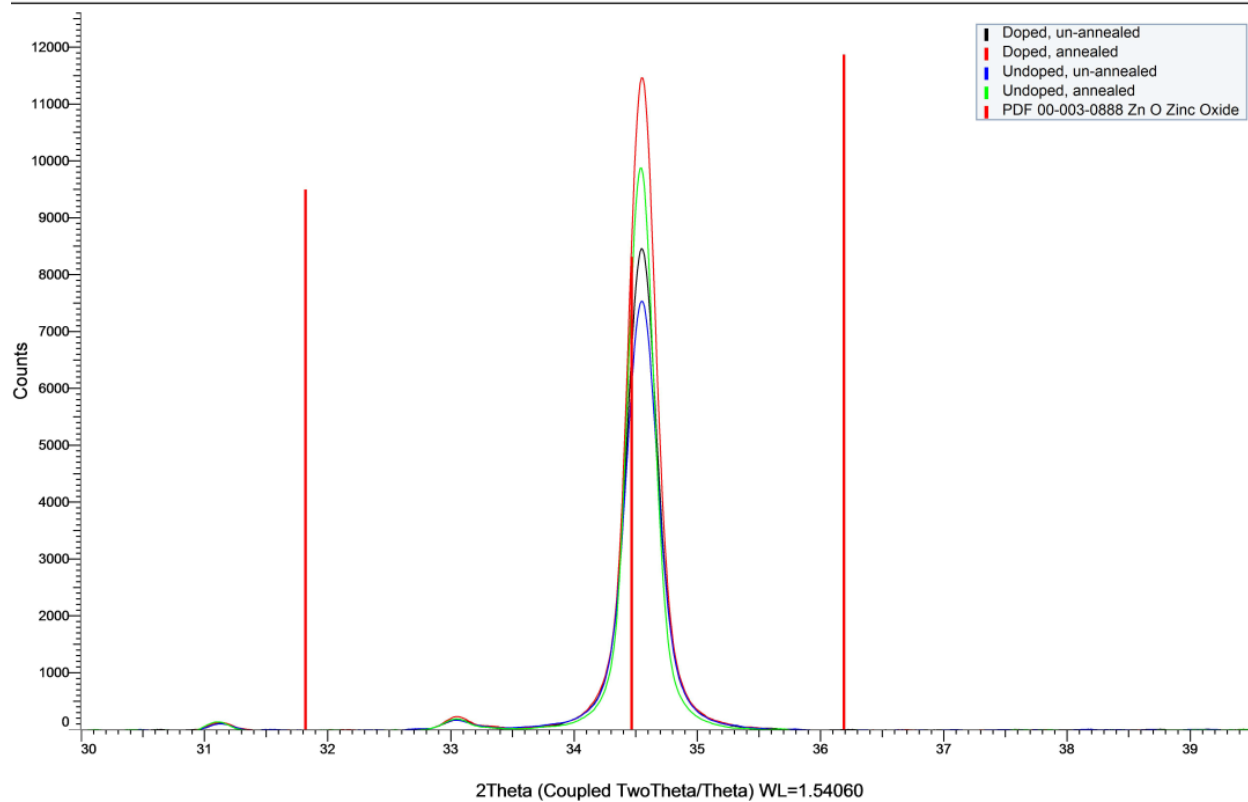
Ethylene Glycol - wetted



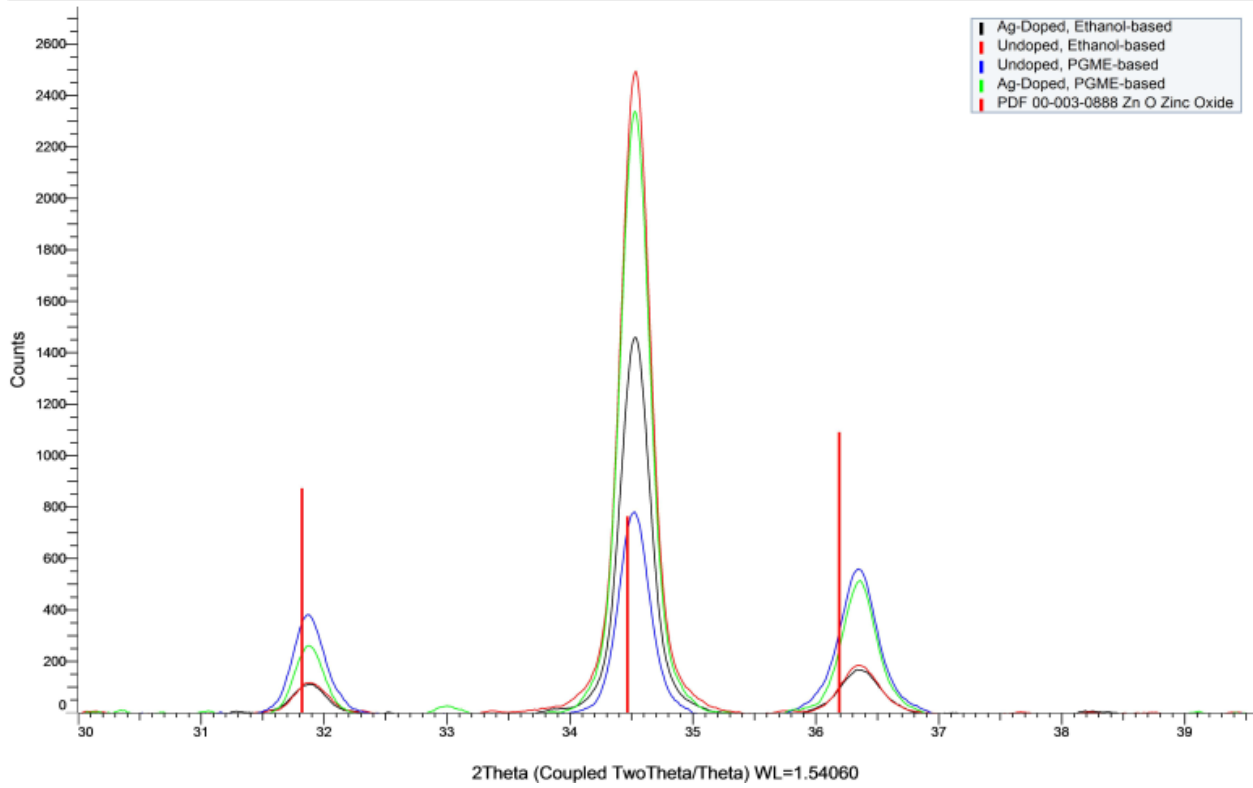
Water-wetted



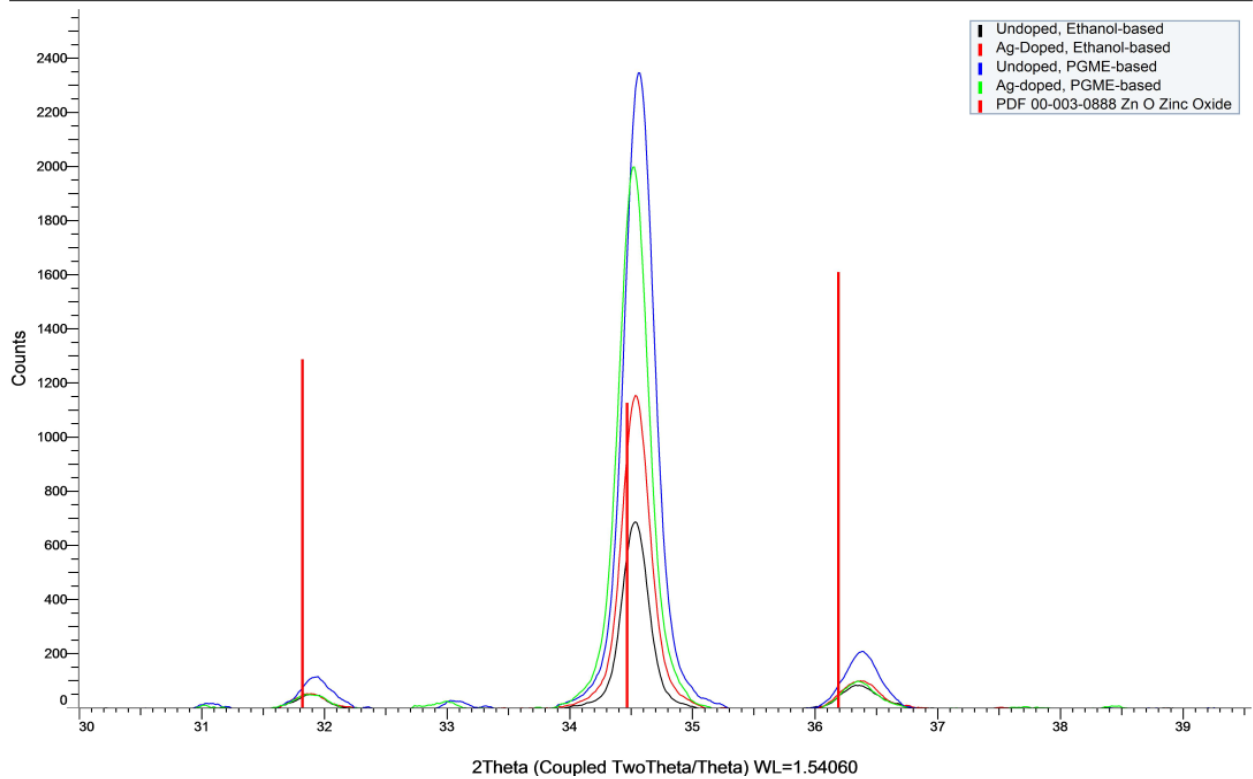
NP-wetted



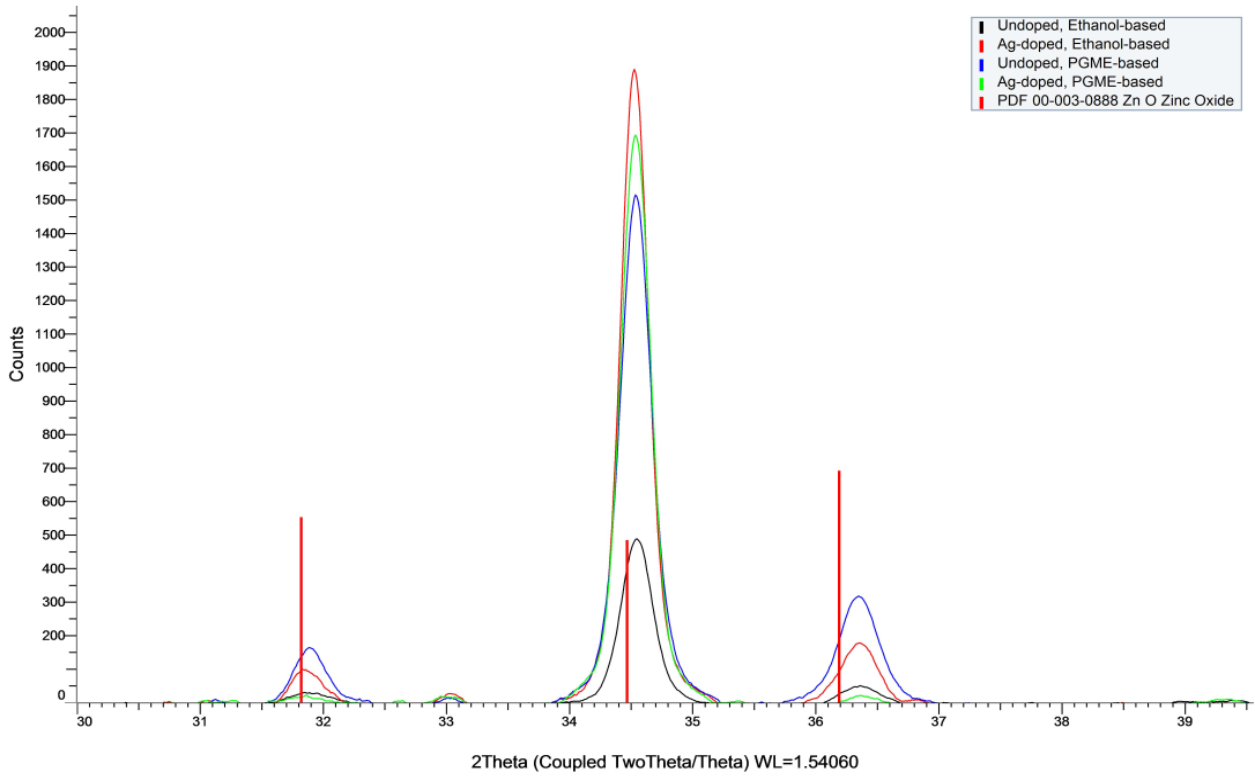
Dry (unwetted)



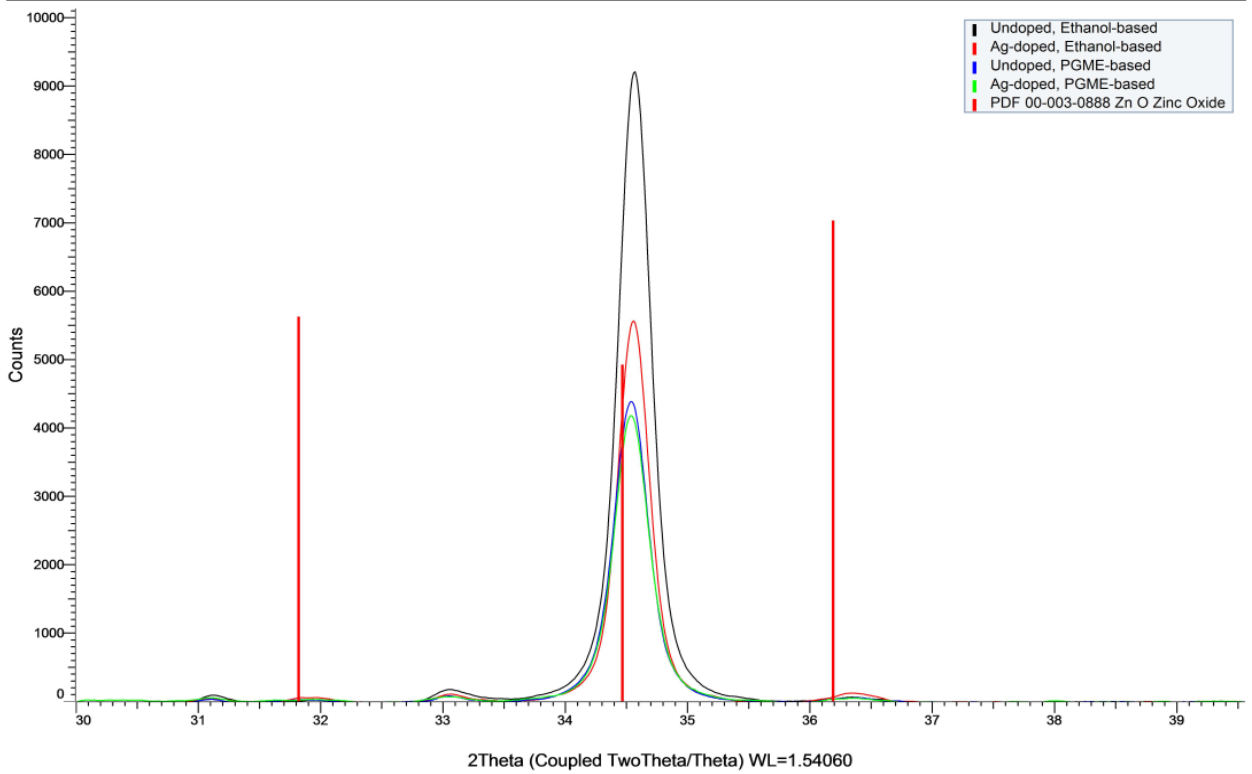
Ethanol-wetted



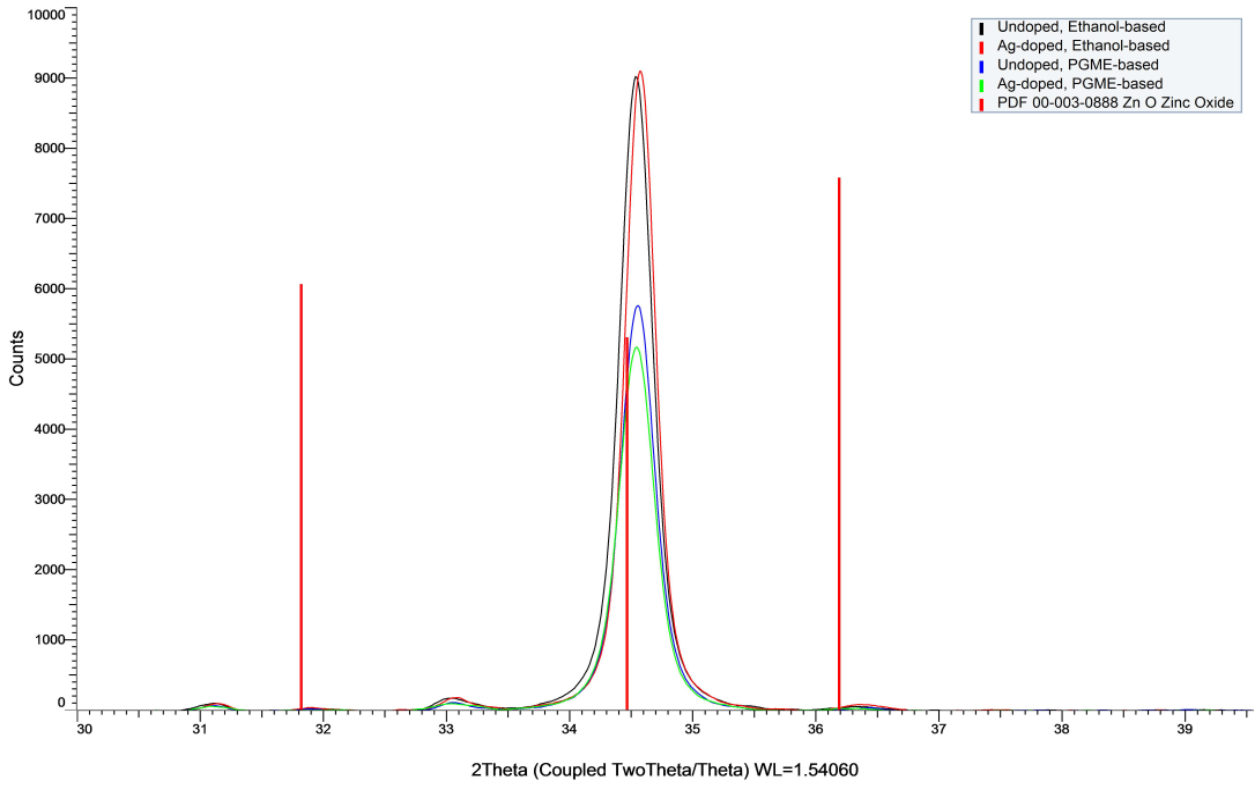
PGME-wetted



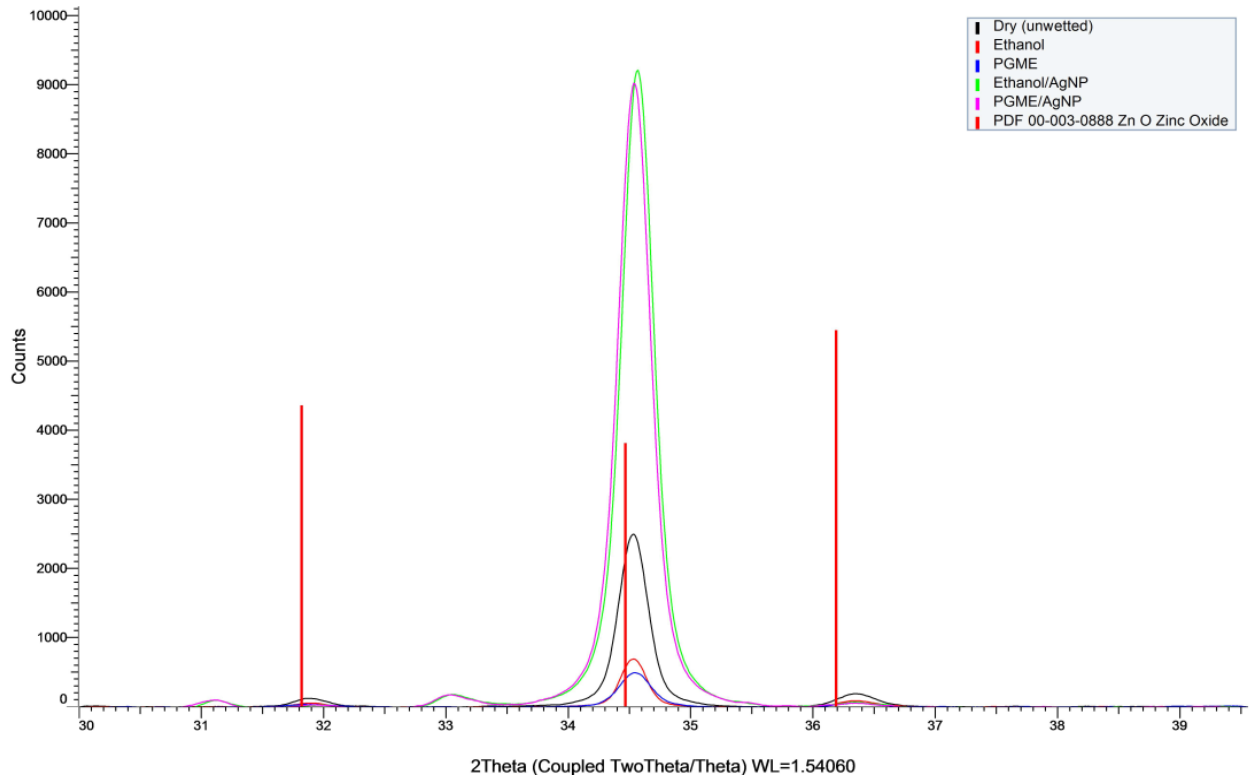
Ethanol/NP wetted



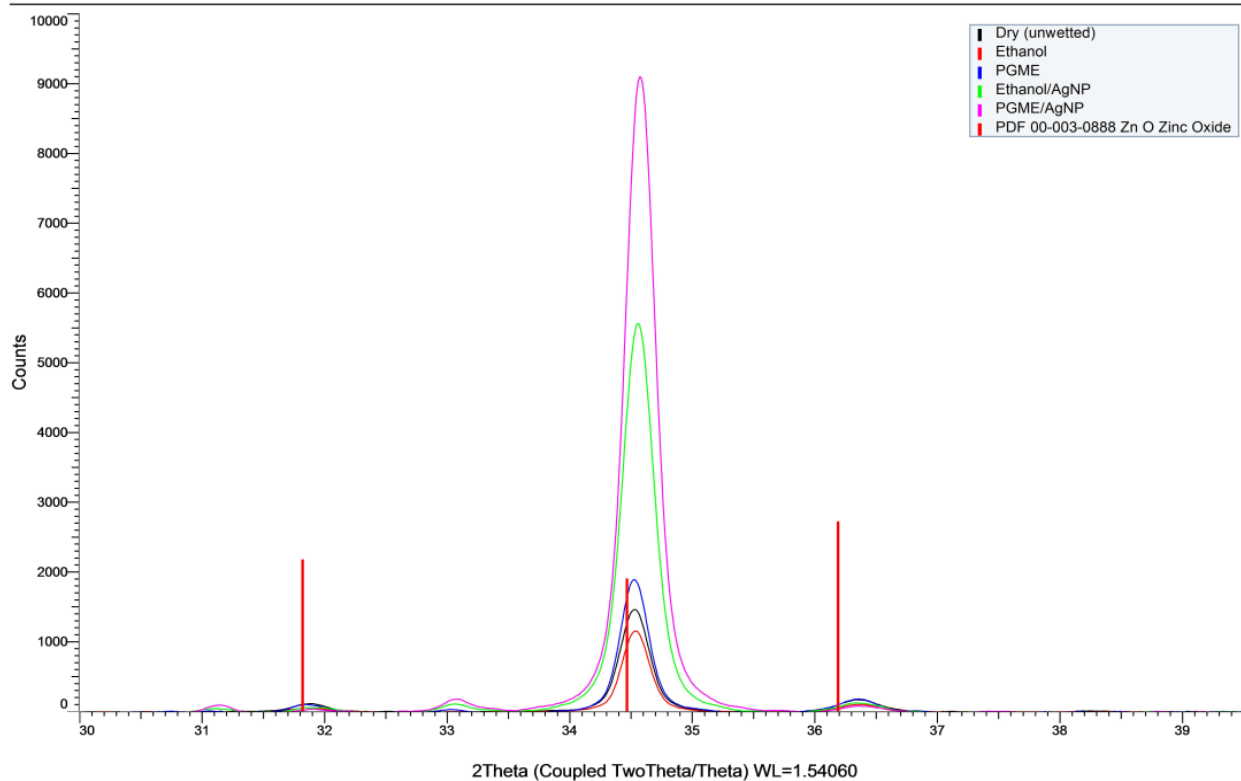
PGME/NP wetted



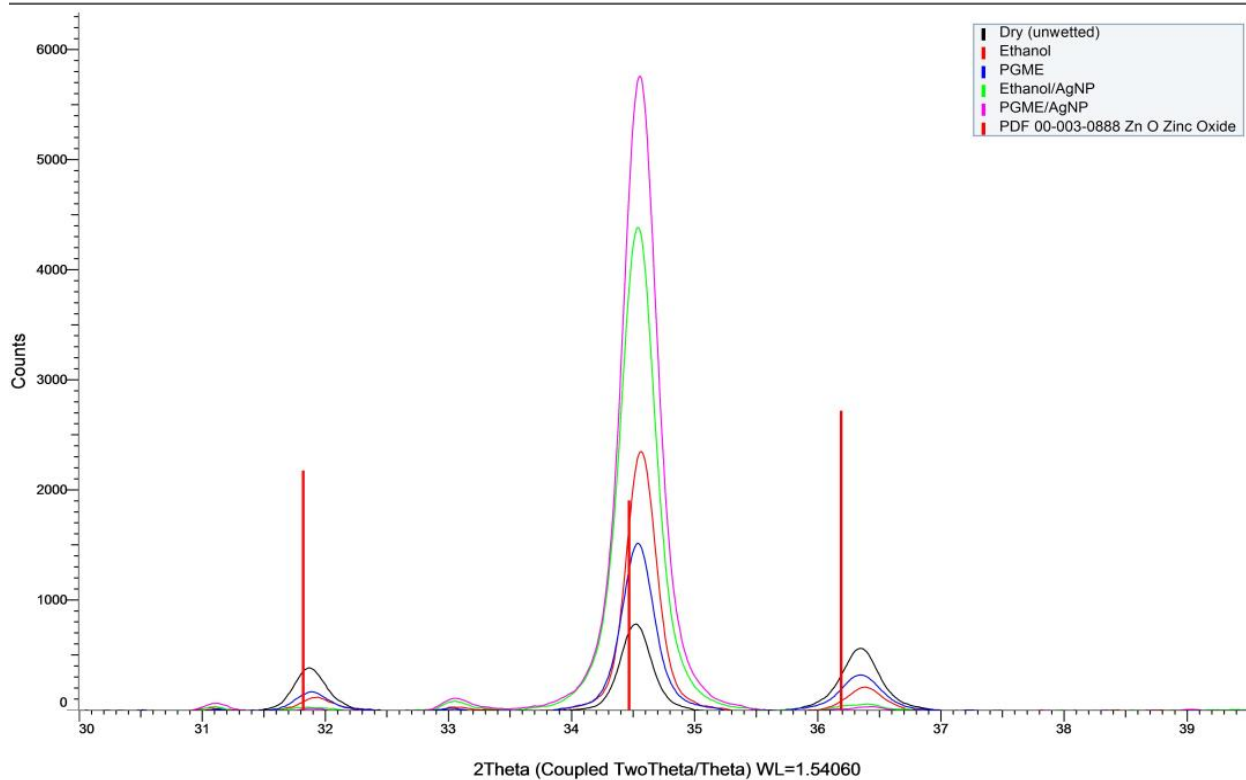
Undoped Ethanol-based



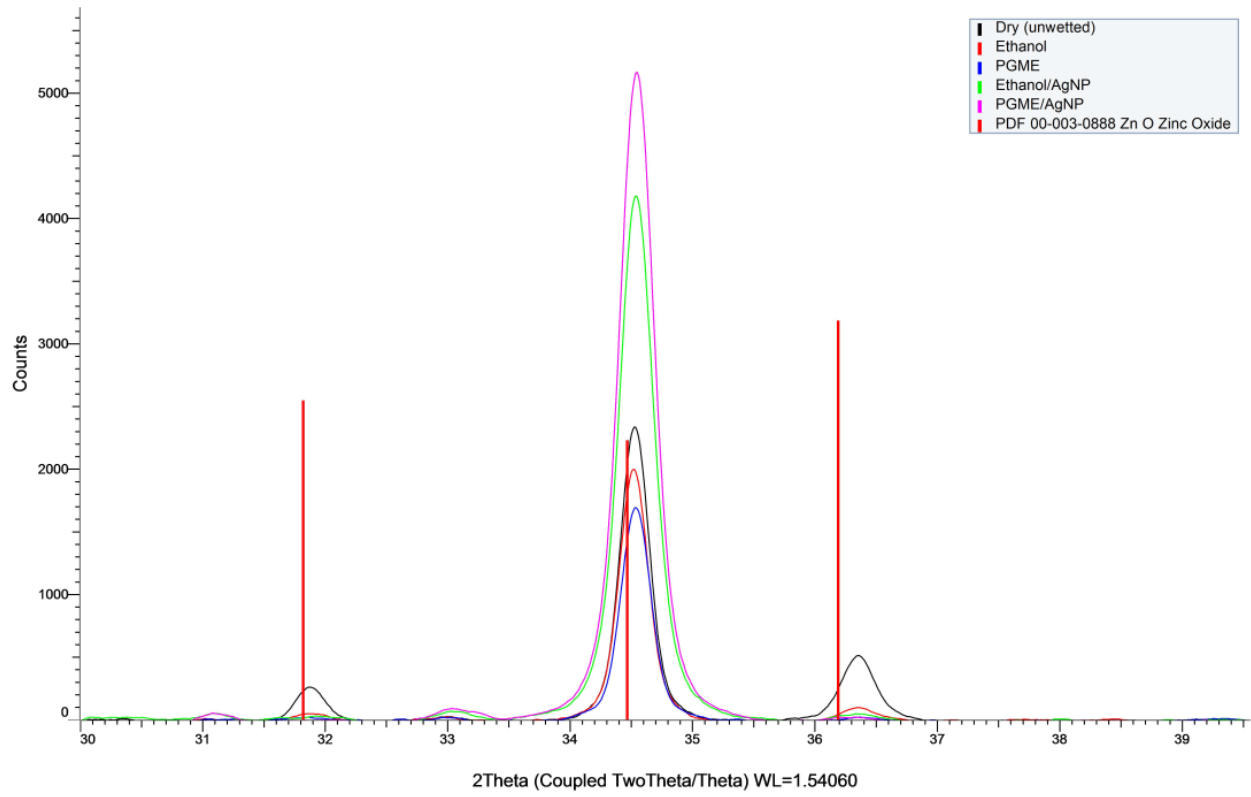
Ag-Doped Ethanol-based



Undoped PGME-based

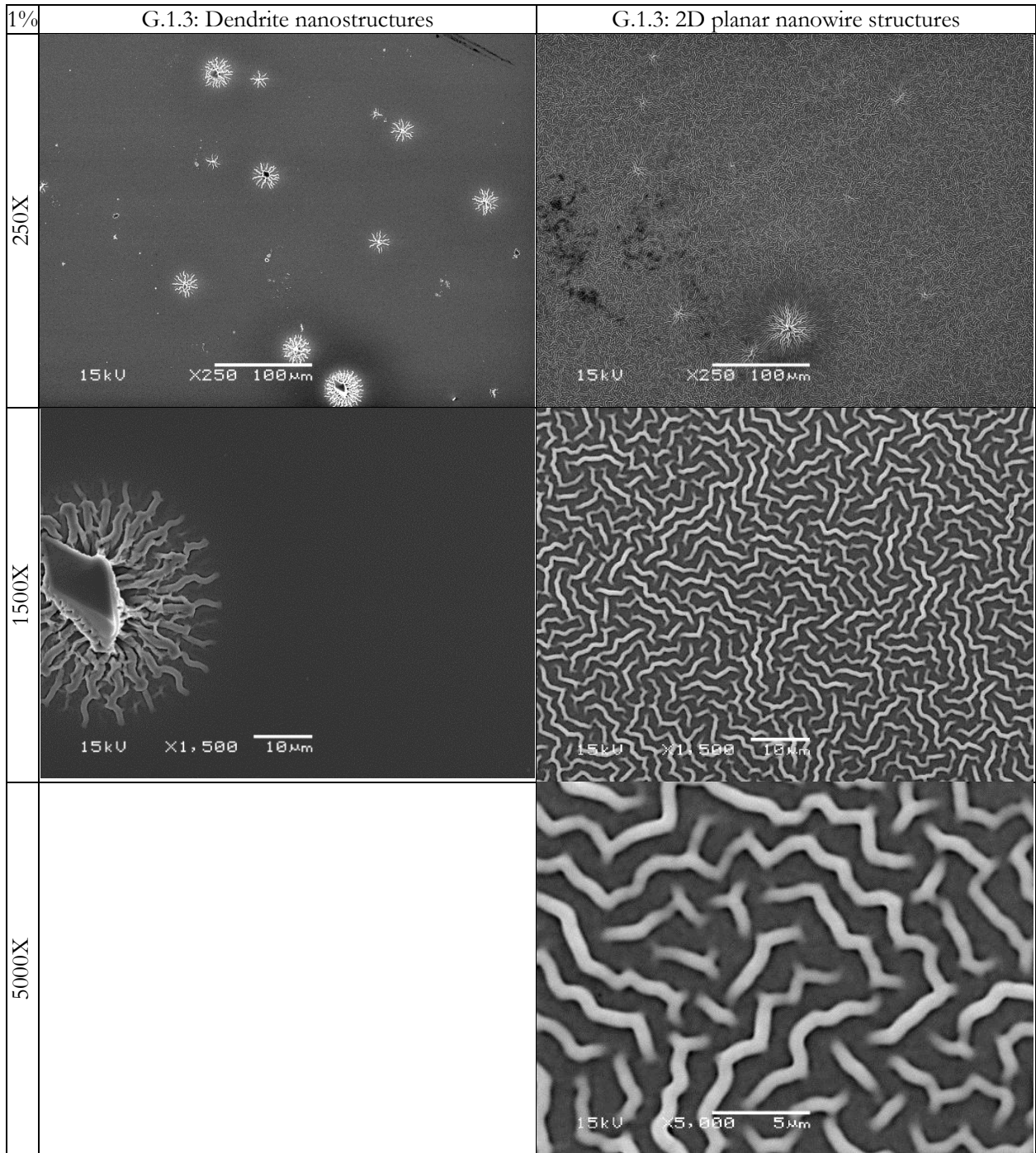


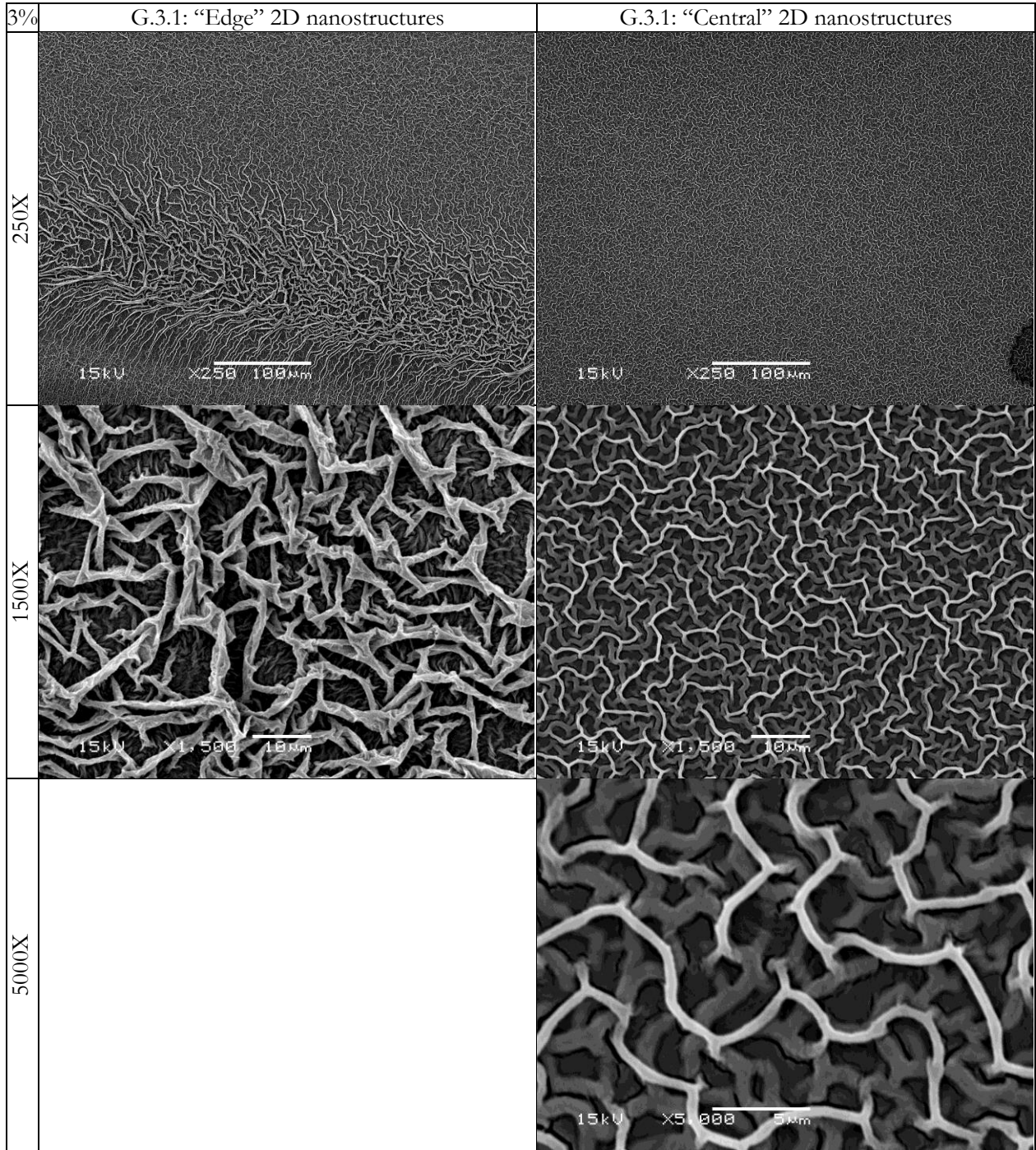
Ag-Doped PGME-based



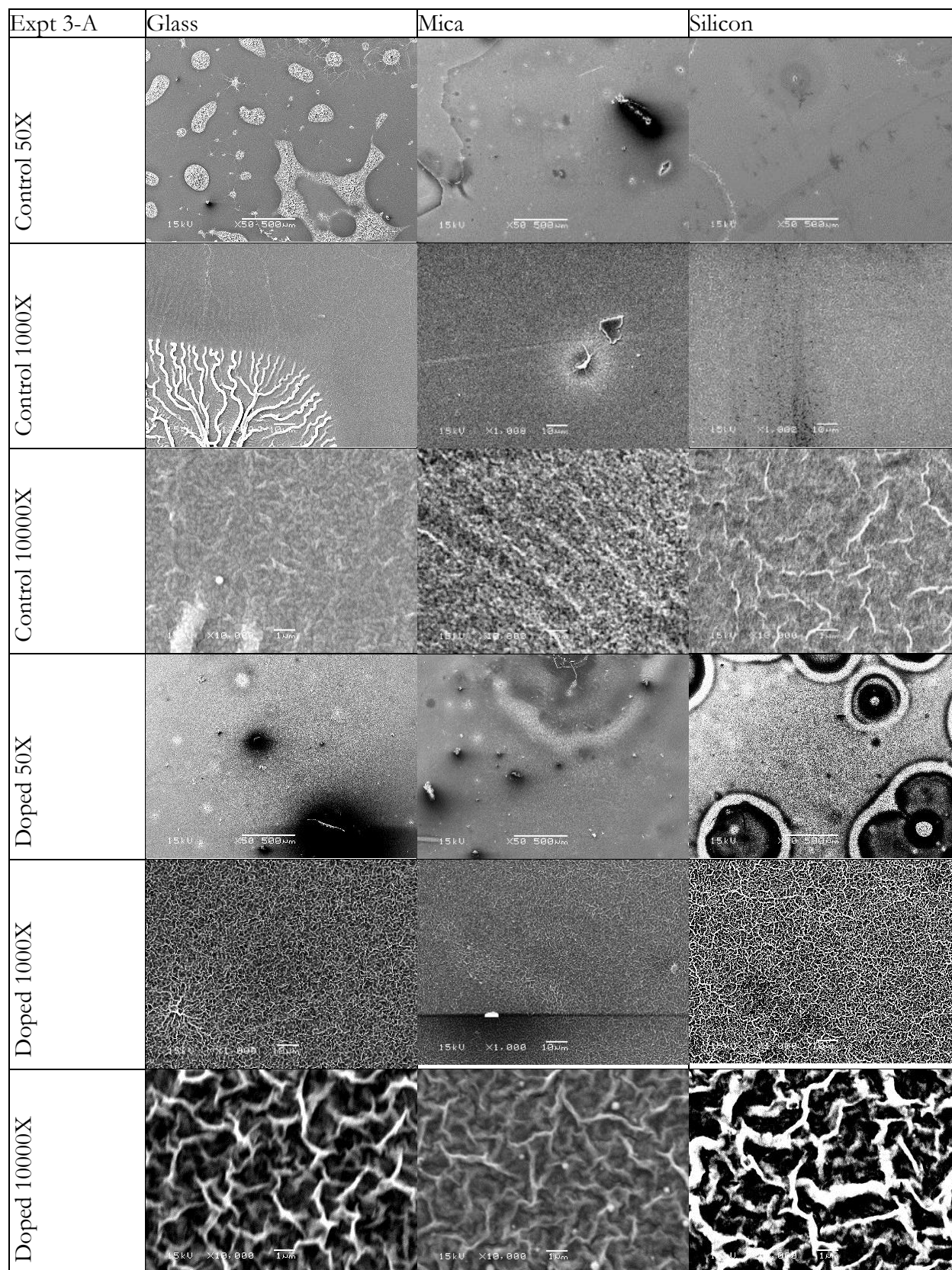
Appendix C: Microscopy

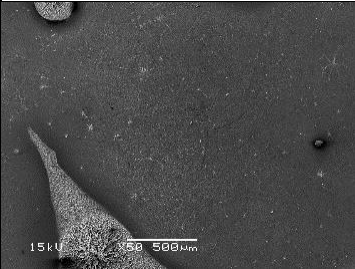
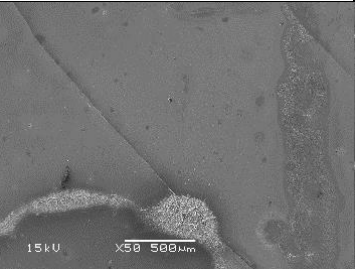
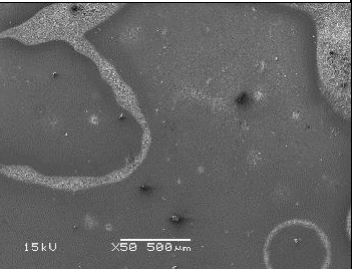
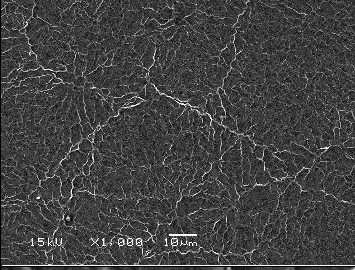
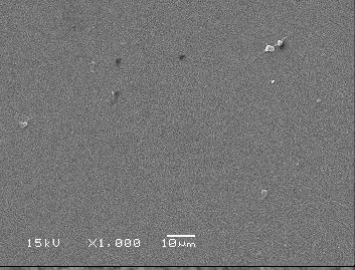
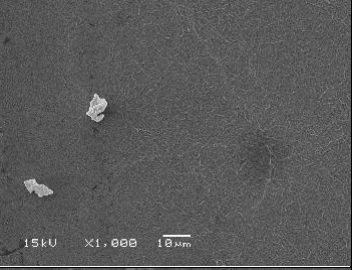
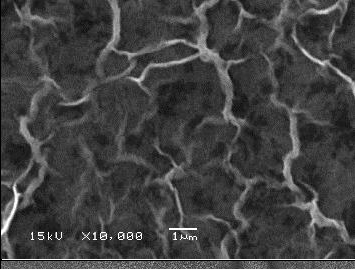
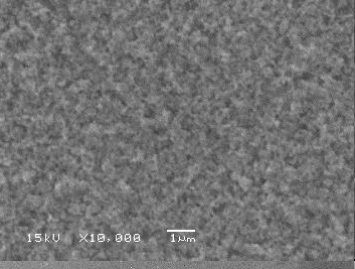
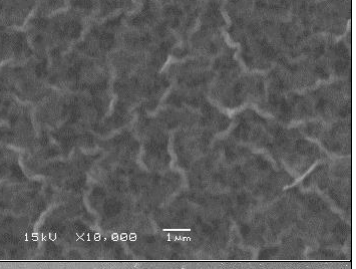
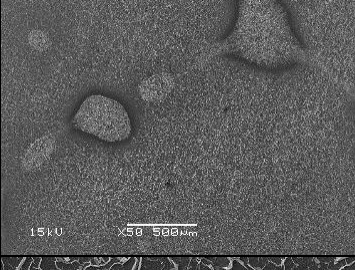
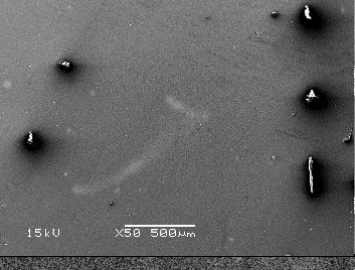
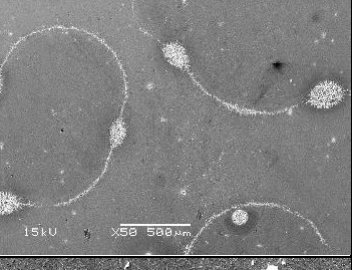
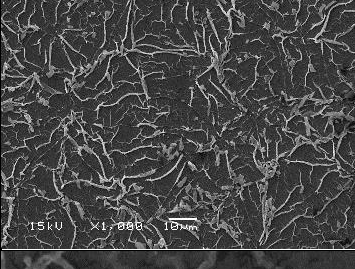
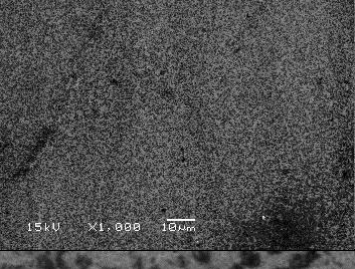
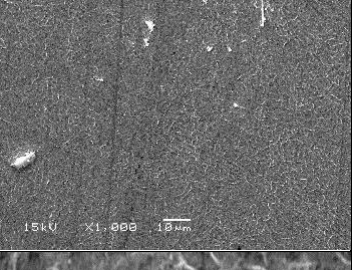
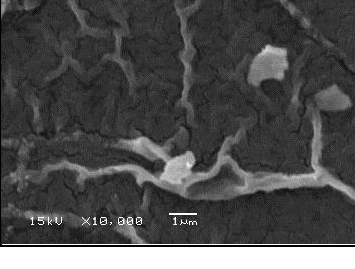
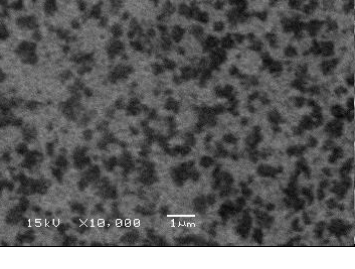
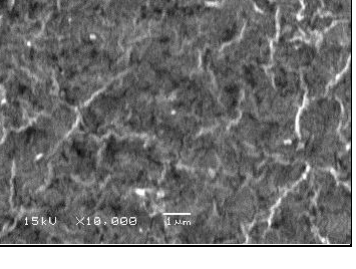
Appendix C-2DG: Experiment 2-DG



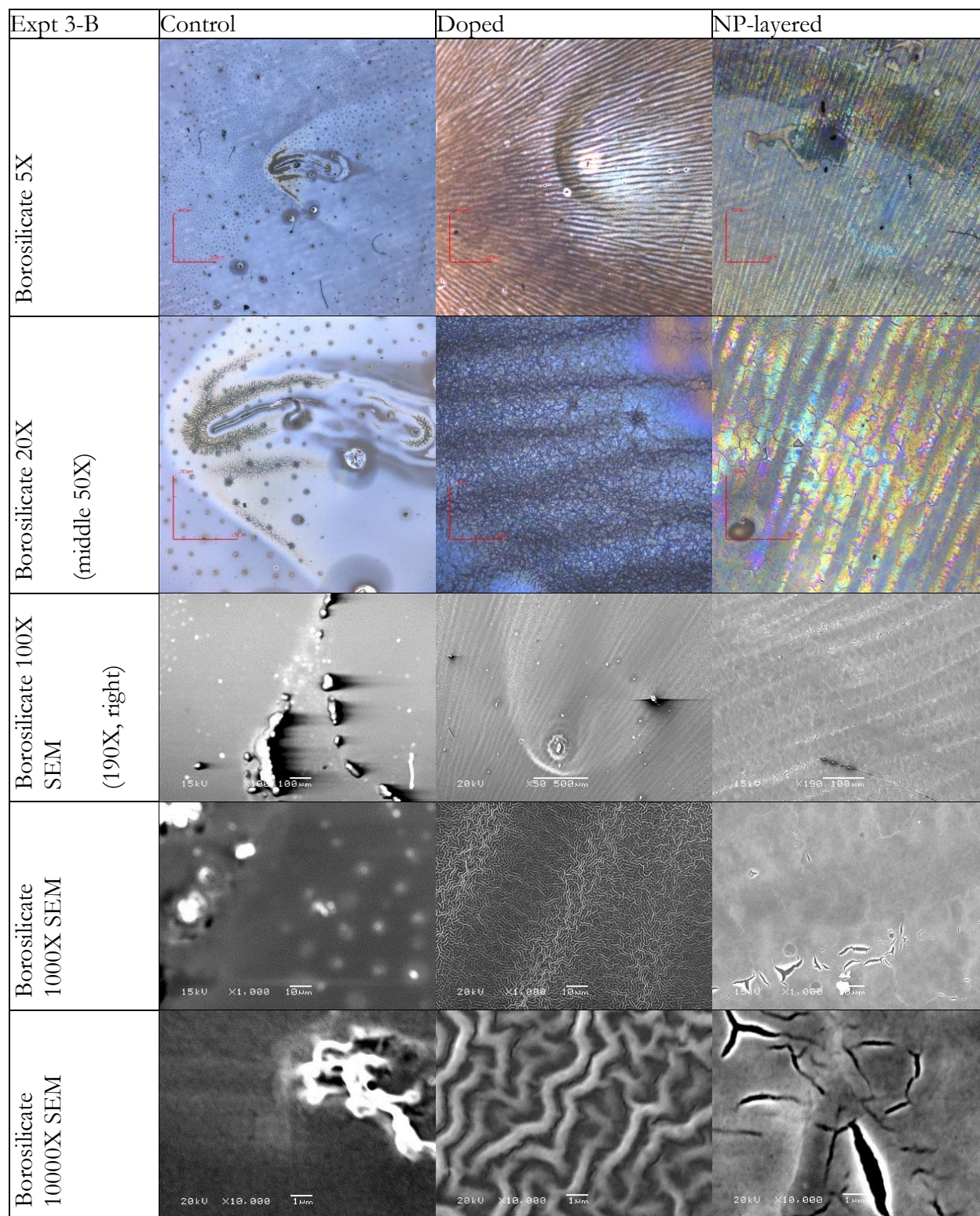


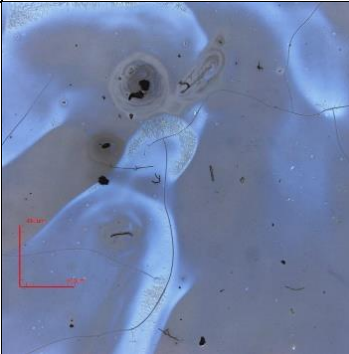
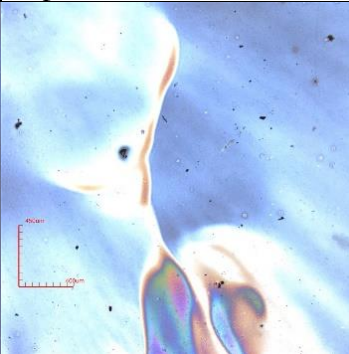
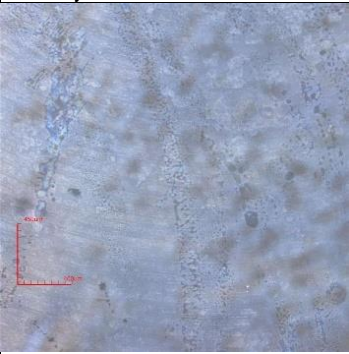
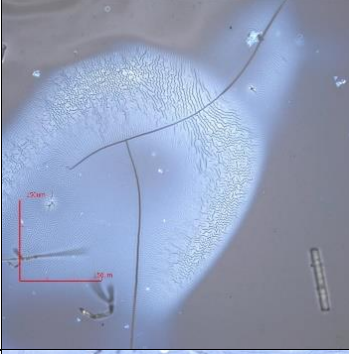
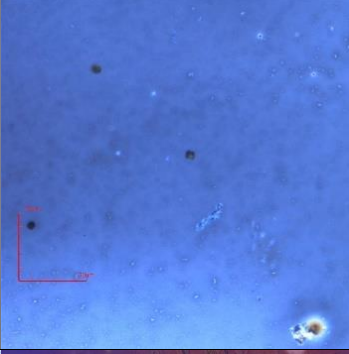
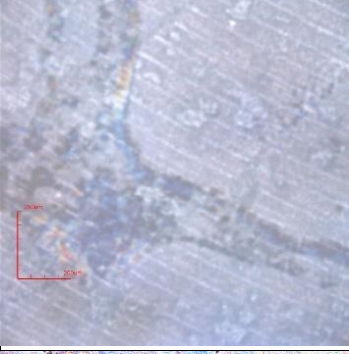
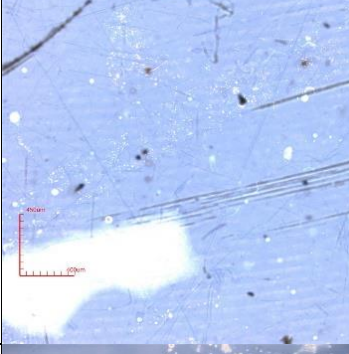
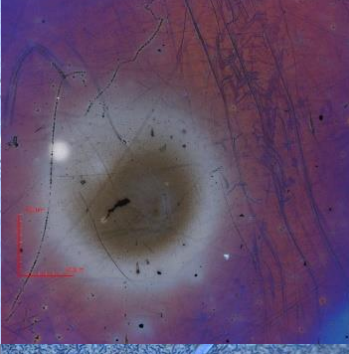
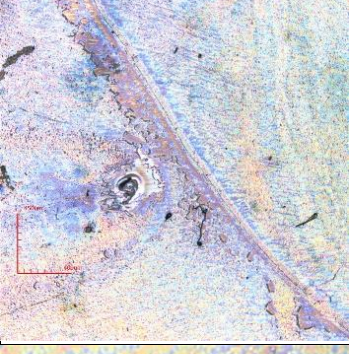
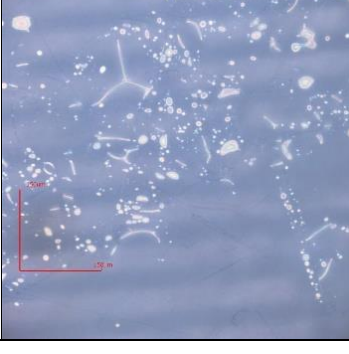
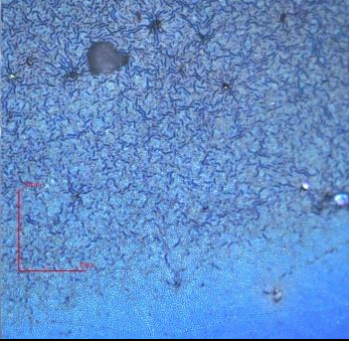
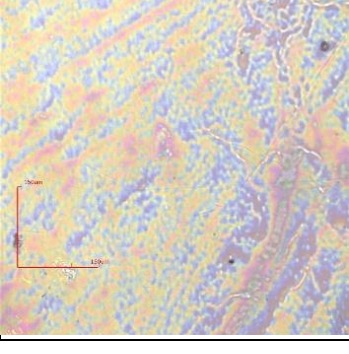
Appendix C-3A: Experiment 3-A



Expt 3-A	Glass	Mica	Silicon
AgNP Sol 50X			
AgNP Sol 1000X			
AgNP Sol 10000X			
NP Layered 50X			
NP Layered 1000X			
NP Layered 10000X			

Appendix C-3B: Experiment 3-B

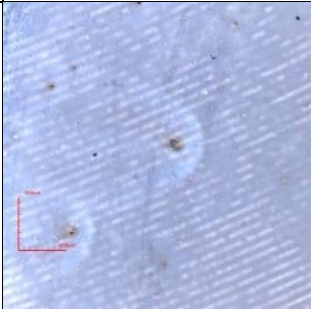

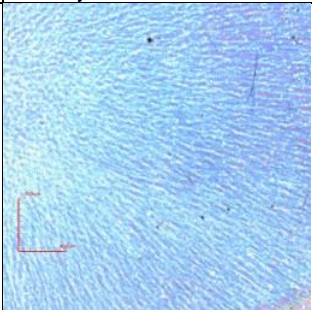
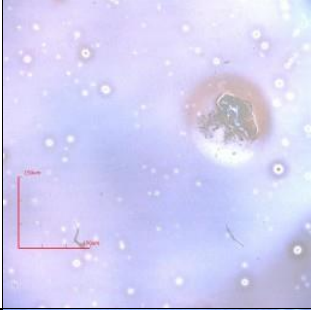
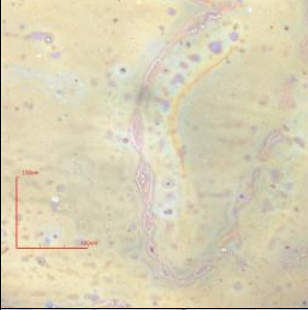
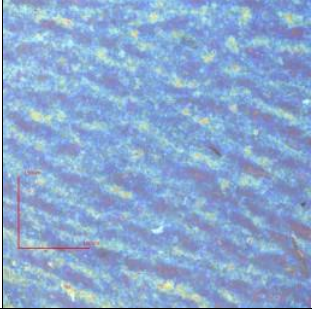
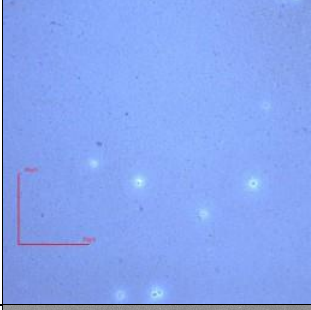
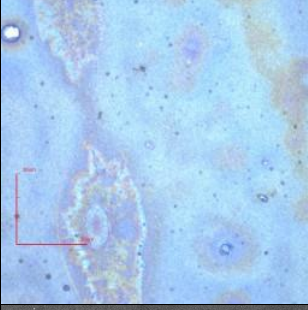
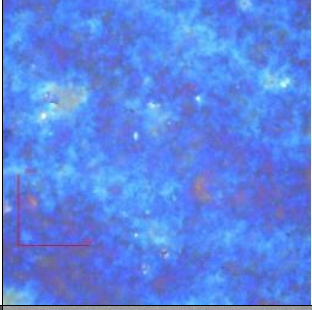
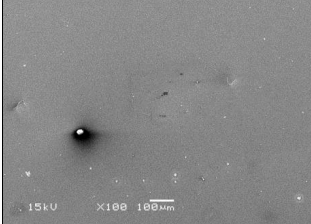
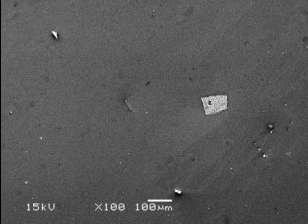
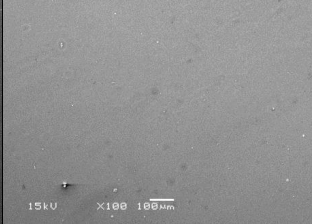

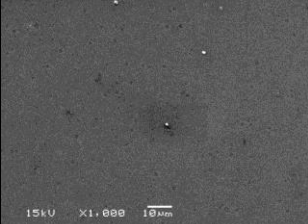
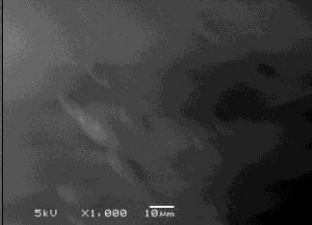
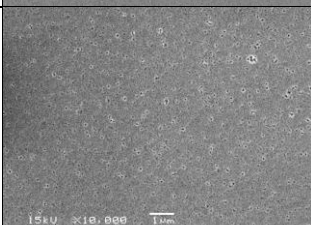

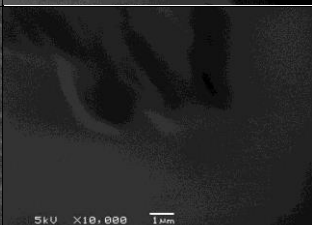


Expt B	Control	Doped	NP-layered
Glass 5X			
Glass (left, 20X) (middle, 50X) (right, 10X)			
Mica 5X			
Mica 20X (middle, 50X)			

Expt B	Control	Doped	NP-layered
Quartz 5X			
Quartz 20X (middle, 50X) (right, 50X)			
Silicon 10X (middle, 5X)			
Silicon (left, 100X) (middle, 20X) (right, 20X)			

Appendix C-3C: Experiment 3-C

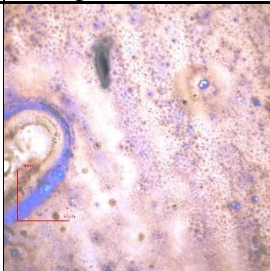
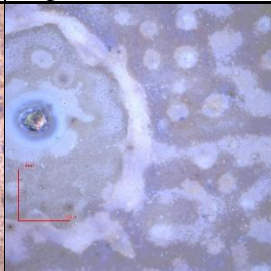
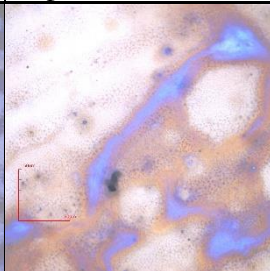
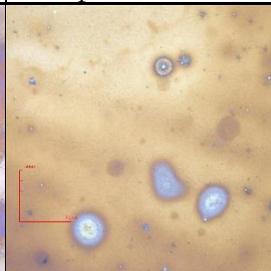
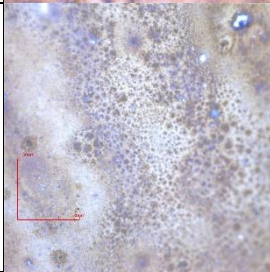
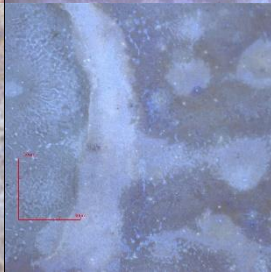
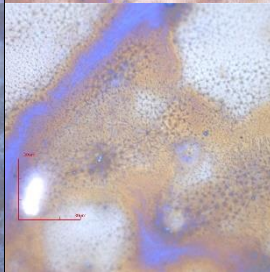
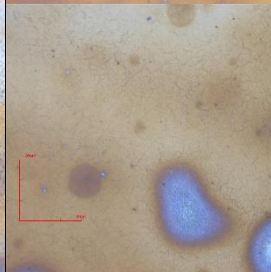
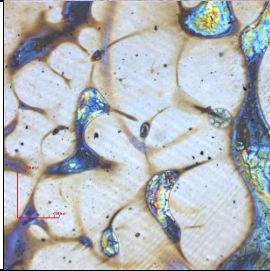
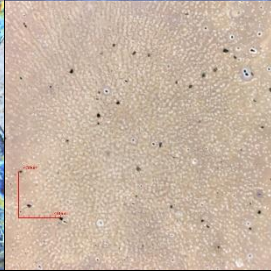
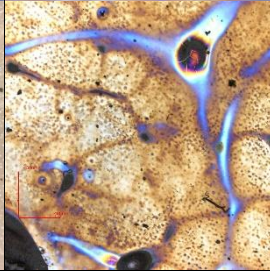
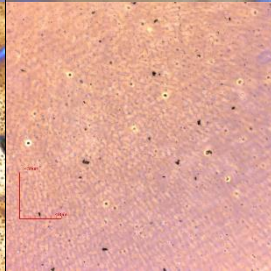
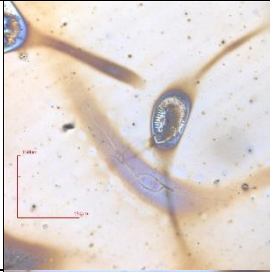
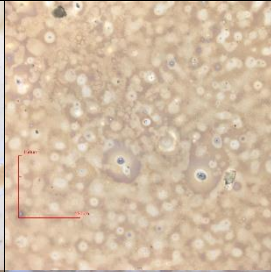
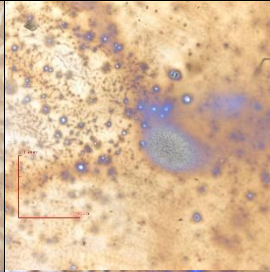
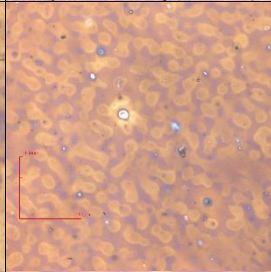

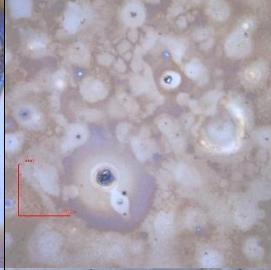
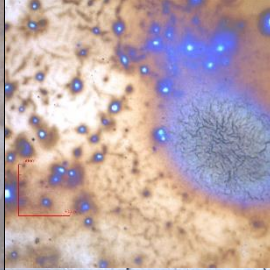
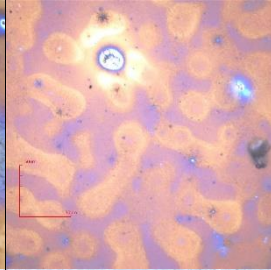
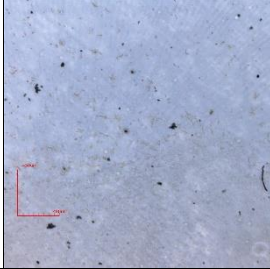
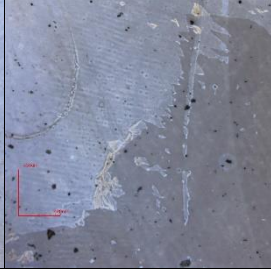
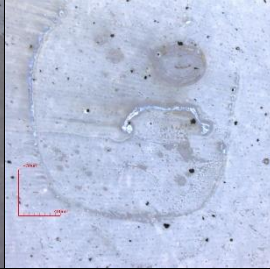
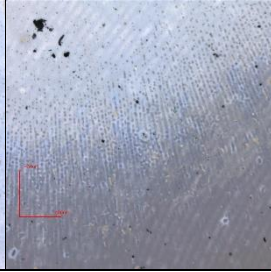
Expt 3-C	Control	Ethanol	NP-layered
Undoped 5X			
Undoped 20X			
Undoped 50X			
Undoped 100X SEM			
Undoped 1000X SEM			
Undoped 7-10KX SEM			

Expt 3-C	Control	Ethanol	NP-layered
Doped 5X			
Doped 20X			
Doped 100X			
Doped 100X SEM			
Doped 1000X SEM			
Doped 7-10KX SEM			

Appendix C-3D: Experiment 3-D

Expt D	Undoped	Doped	Doped Annealed	Undoped Annealed
Acetone 5X				
Acetone 20X (Right, 50X)				
Acetone 50X (Right, 100X)				
Chloroform 5X				
Chloroform 20X				
Chloroform 50X				

Expt D	Undoped	Doped	Doped Annealed	Undoped Annealed
Control 5X				
Control 20X				
Control 50X				
Control 100X				
Ethanol 5X				
Ethanol 20X				

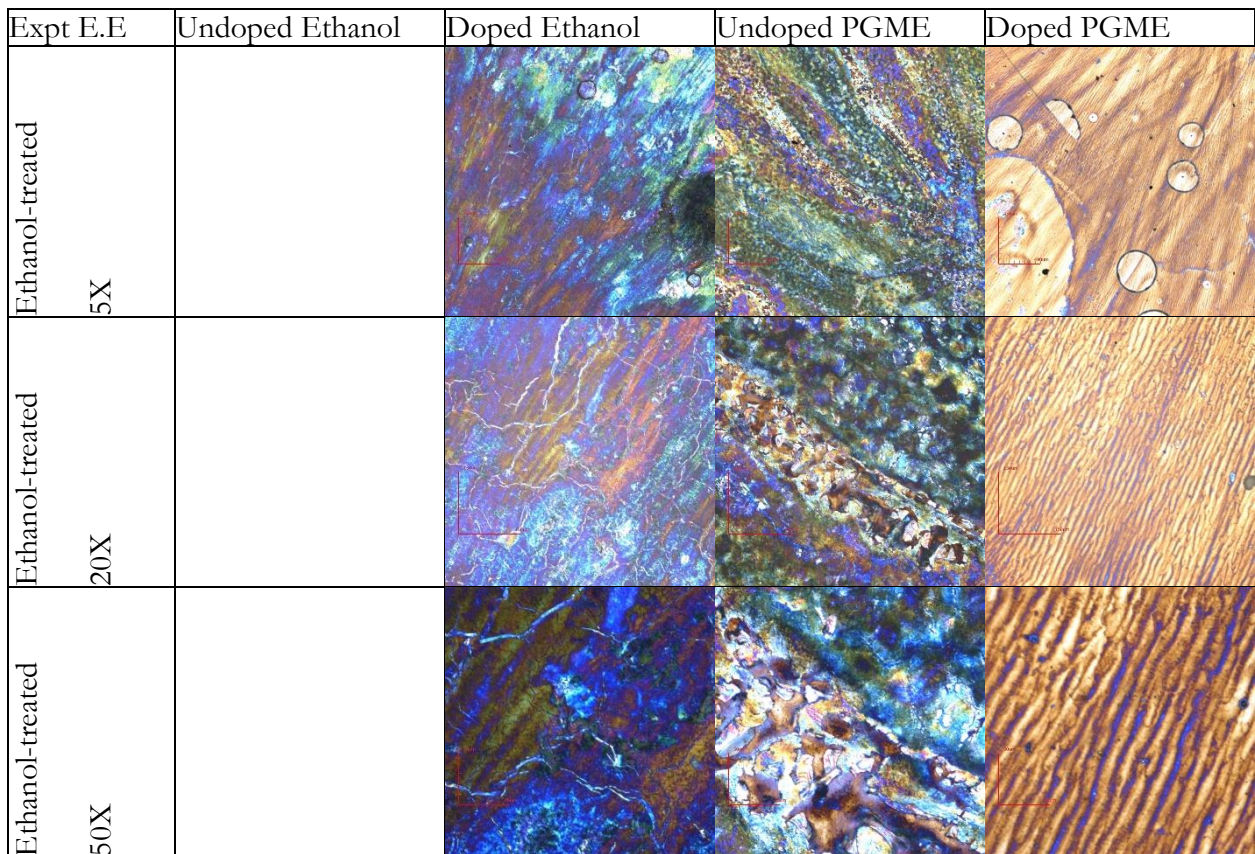
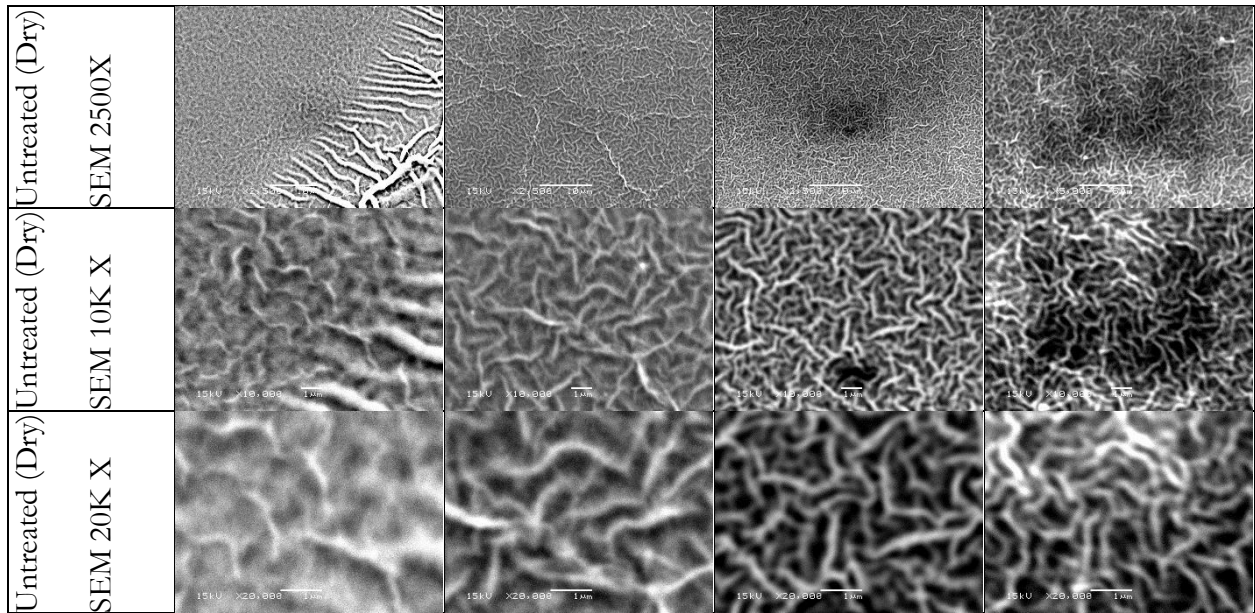
Expt D	Undoped	Doped	Doped Annealed	Undoped Annealed
Ethanol 50X				
Ethanol 100X				
Ethylene Glycol 5X				
Ethylene Glycol 20X				
Ethylene Glycol 50X				
DI Water 5X				

Expt D	Undoped	Doped	Doped Annealed	Undoped Annealed
DI Water 20X				
DI Water 50X				
Nanoparticles 5X				
Nanoparticles 20X				
Nanoparticles 50X				
Nanoparticles 100X SEM				

Expt D	Undoped	Doped	Doped Annealed	Undoped Annealed
Nanoparticles 250X SEM (Right, 500)				
Nanoparticles 1000X SEM				
Nanoparticles 2500X SEM				
Nanoparticles 10000X SEM				

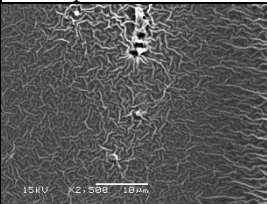
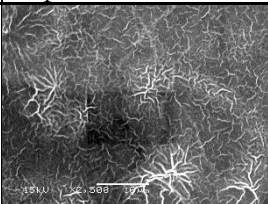
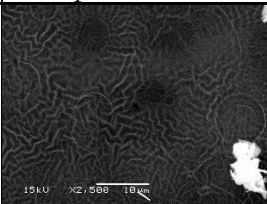
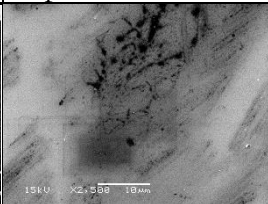
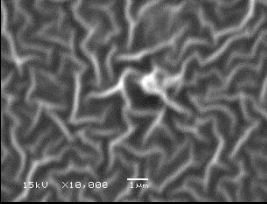
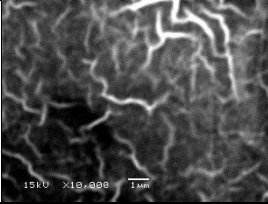
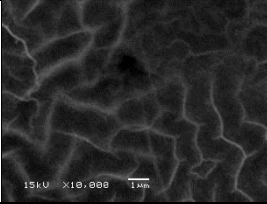
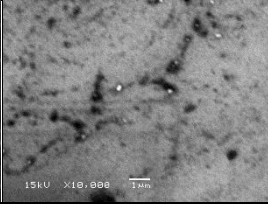
Appendix C-3E: Experiment 3-E

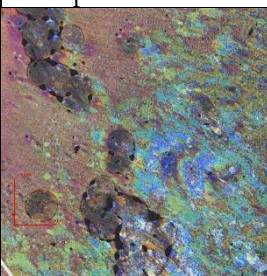
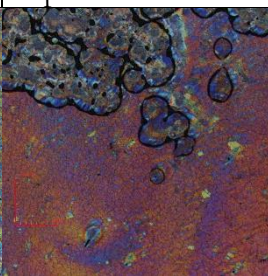
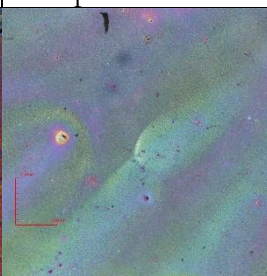
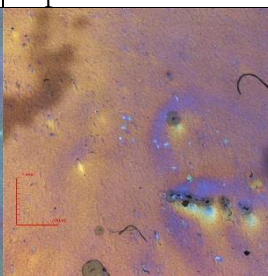
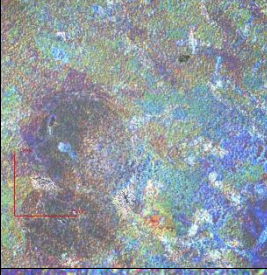
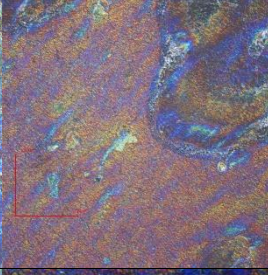
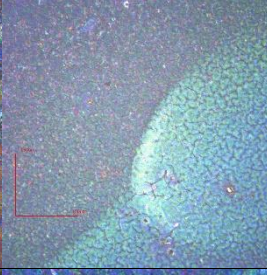
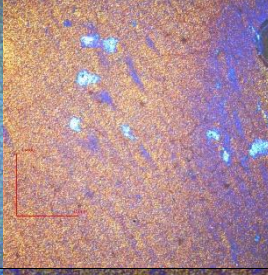
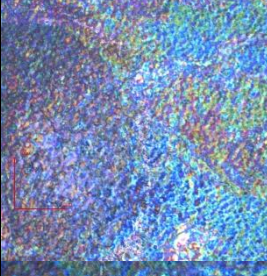
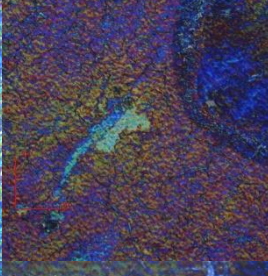
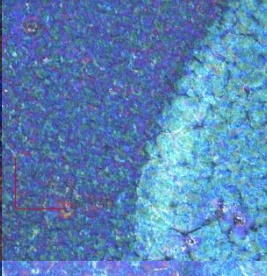
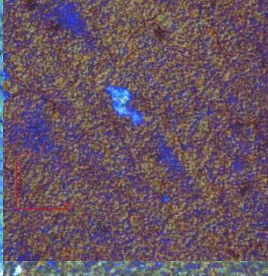
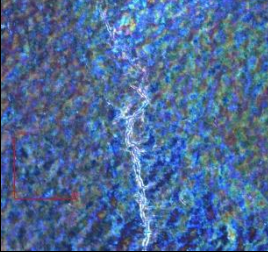
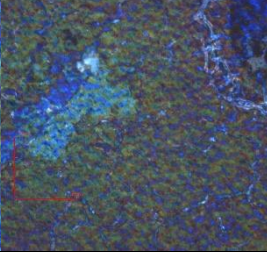
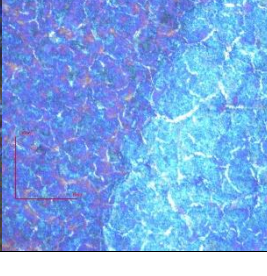
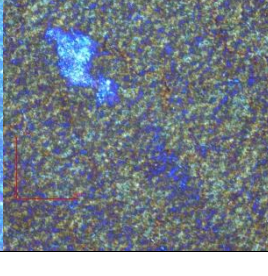
Expt E.D	Undoped Ethanol	Doped Ethanol	Undoped PGME	Doped PGME
Untreated (Dry) 5X				
Untreated (Dry) 20X				
Untreated (Dry) 50X				
Untreated (Dry) 100X				
Untreated (Dry) SEM 100X				
Untreated (Dry) SEM 1000X				



Expt E.E	Undoped Ethanol	Doped Ethanol	Undoped PGME	Doped PGME
Ethanol-treated 100X				
Ethanol-treated SEM 100X				
Ethanol-treated SEM 1000X				
Ethanol-treated SEM 2500X				
Ethanol-treated SEM 5K X				
Ethanol-treated SEM 10K X				

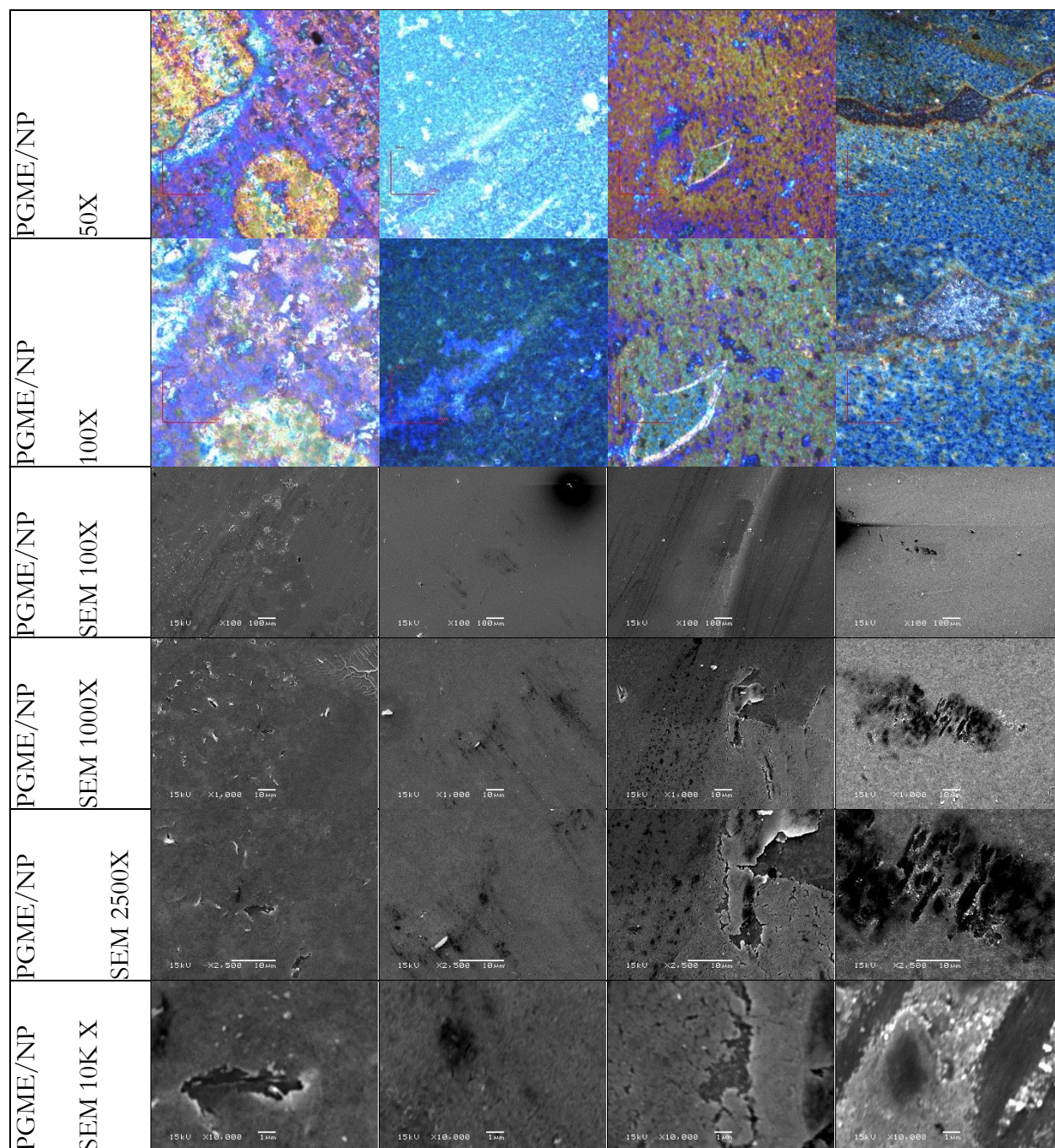
Expt E.G	Undoped Ethanol	Doped Ethanol	Undoped PGME	Doped PGME
PGME-Treated 5X				
PGME-Treated 20X				
PGME-Treated 50X				
PGME-Treated 100X				
PGME-Treated SEM 100X				
PGME-Treated SEM 1000X				

Expt E.G	Undoped Ethanol	Doped Ethanol	Undoped PGME	Doped PGME
PGME-Treated SEM 2500X				
PGME-Treated SEM 10K X				

Expt E.O	Undoped Ethanol	Doped Ethanol	Undoped PGME	Doped PGME
EtOH/NP 5X				
EtOH/NP 20X				
EtOH/NP 50X				
EtOH/NP 100X				

Expt E.O	Undoped Ethanol	Doped Ethanol	Undoped PGME	Doped PGME
EtOH/NP SEM 100X				
EtOH/NP				
EtOH/NP SEM 1000X				
EtOH/NP SEM 2500X				
EtOH/NP SEM 10K X				

Expt E.P	Undoped Ethanol	Doped Ethanol	Undoped PGME	Doped PGME
PGME/NP 5X				
PGME/NP 20X				



Appendix D: Degree of Preferential Orientation Calculation

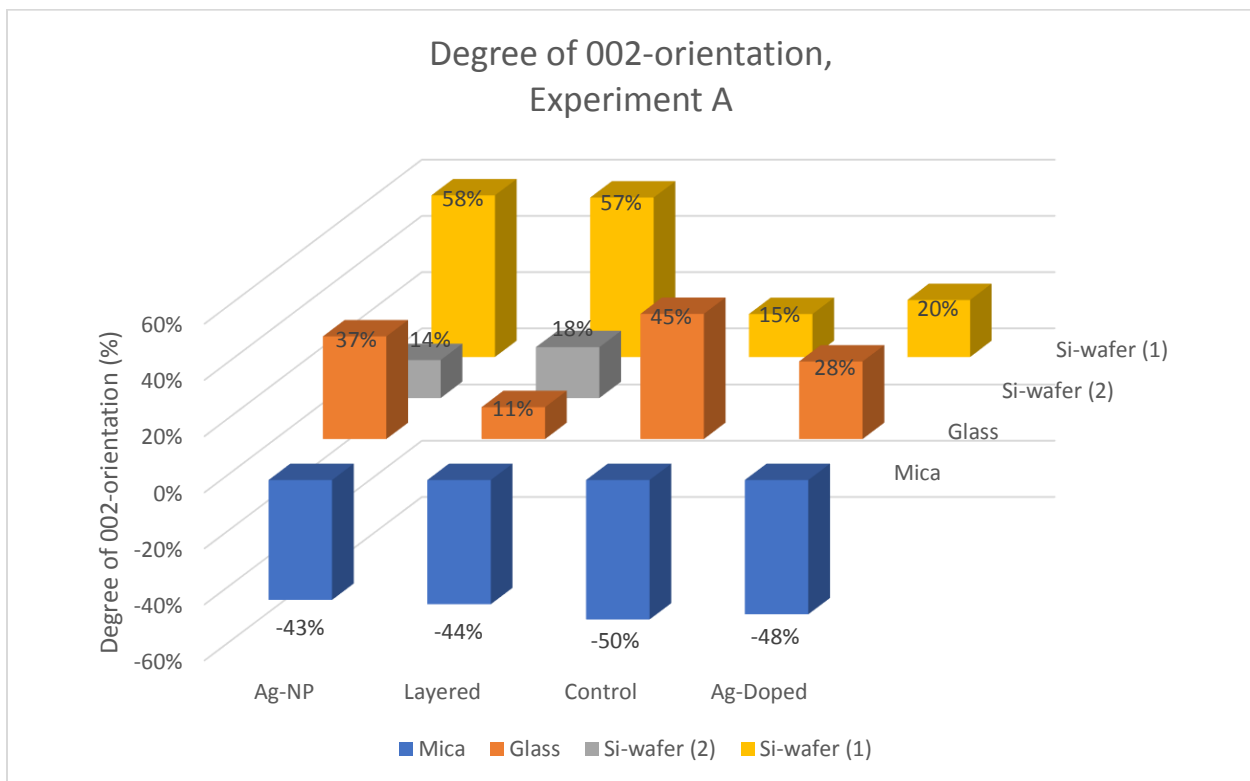
Calculation:

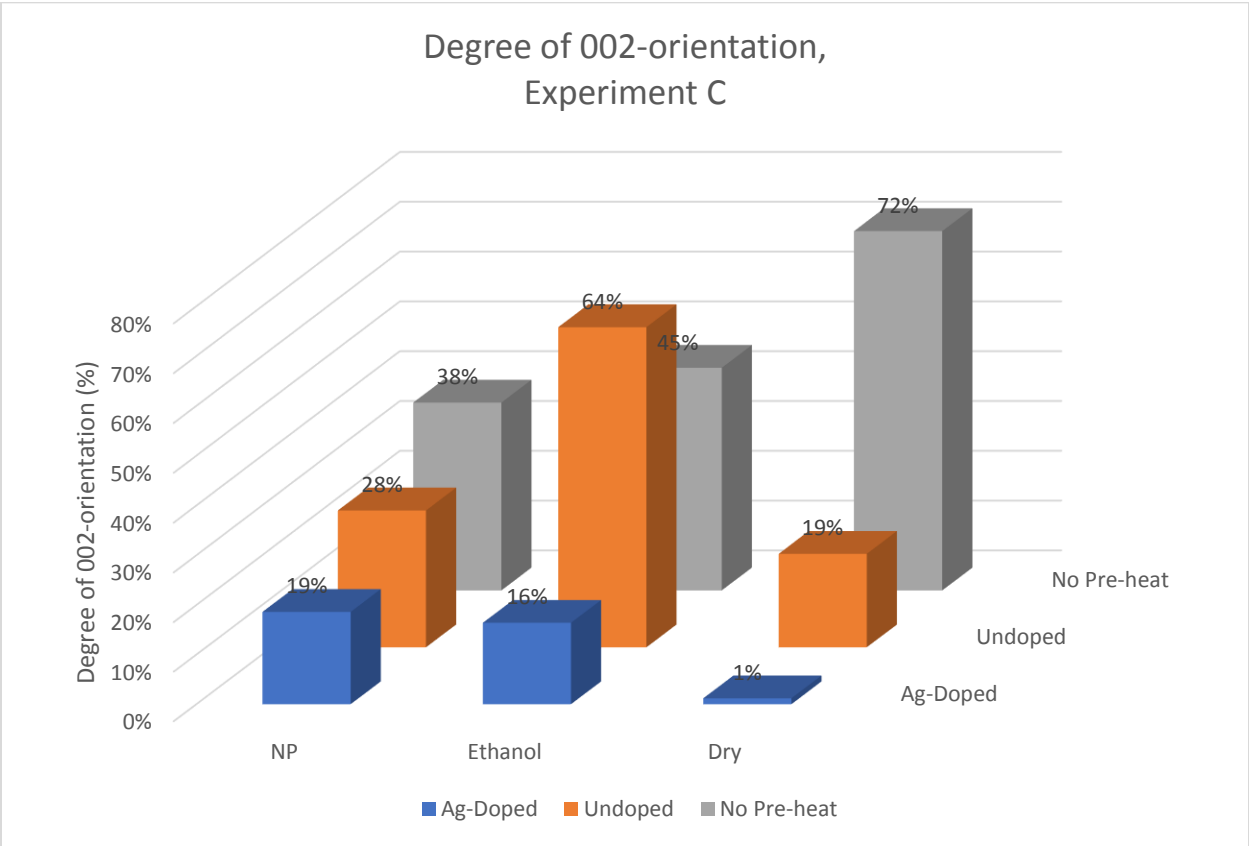
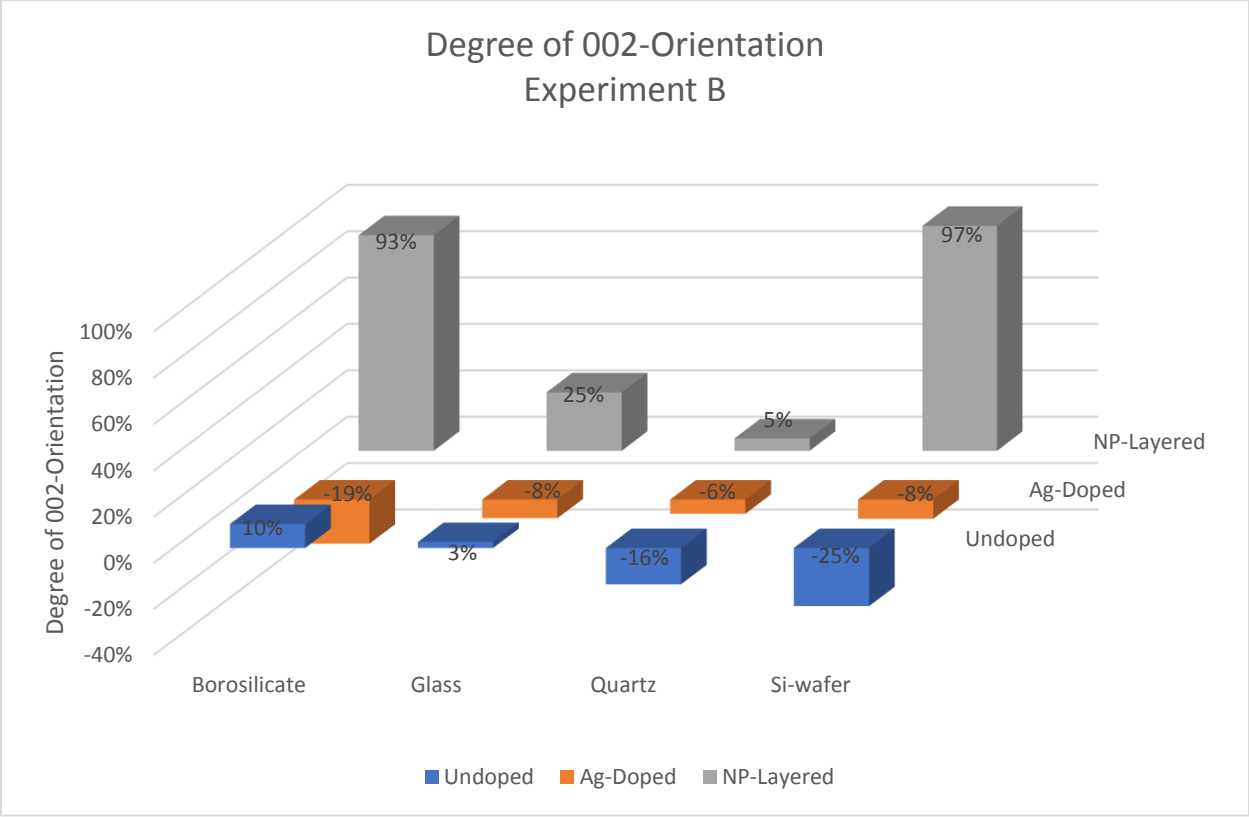
Sample	A_{100}	A_{002}	A_{101}	A_s	P_{002}	f_{002}
Standard	0.4522	0.7058	0.8326		0.354566	
A.1.G	0.7275	3.457	1.673	0.354566	0.590184	0.365052
A.2.G	1.203	2.398	2.004	0.354566	0.427832	0.113514
A.4.G	1.201	4.332	1.215	0.354566	0.641968	0.445284
A.5.G	1.999	5.751	3.046	0.354566	0.532697	0.275986
A.1.M	20.26	25.34	716.9	0.354566	0.033233	-0.49786
A.2.M	2.043	10.63	221.6	0.354566	0.045374	-0.47905
A.4.M	70.5	56.67	594.6	0.354566	0.078515	-0.4277
A.5.M	55.57	44.74	552.8	0.354566	0.068503	-0.44321
A.1.S1	1.407	3.154	2.396	0.354566	0.453356	0.15306
A.1.S2	1.929	4.046	3.183	0.354566	0.4418	0.135154
A.2.S2	1.174	3.197	2.213	0.354566	0.485571	0.202972
A.2.S1	1.401	3.361	2.369	0.354566	0.471322	0.180895
A.4.S	1.289	8.344	1.862	0.354566	0.725881	0.575294
A.5.S	1.31	10.35	2.699	0.354566	0.720802	0.567426
B.0.M	17.99	13.21	323.5	0.354566	0.037243	-0.49164
B.1.M	36.44	26.76	169	0.354566	0.115245	-0.37079
B.2.M	34.97	49.82	687.5	0.354566	0.064509	-0.4494
B.0.B	0.1017	0.2386	0.2256	0.354566	0.421629	0.103903
B.0.G	0.1782	0.2386	0.2256	0.354566	0.37142	0.026111
B.0.Q	0.1892	0.1711	0.3164	0.354566	0.252845	-0.1576
B.0.S	0.3405	0.1879	0.4514	0.354566	0.191774	-0.25222
B.1.B	0.5825	0.4458	0.9008	0.354566	0.231092	-0.1913
B.1.Q	0.1142	0.1588	0.2315	0.354566	0.314767	-0.06166
B.1.G	0.194	0.1636	0.1832	0.354566	0.302515	-0.08065
B.1.S	1.137	1.269	1.814	0.354566	0.300711	-0.08344
B.2.B	0.09155	6.369	0.2127	0.354566	0.954408	0.929361
B.2.G	0.2166	0.5083	0.2578	0.354566	0.517248	0.252051
B.2.Q	0.353	0.5052	0.4409	0.354566	0.388885	0.053171
B.2.S	0.06055	11.07	0.1584	0.354566	0.980605	0.96995
C.0.E	2.359	21.18	3.979	0.354566	0.769678	0.643152
C.0.D	2.202	5.891	4.284	0.354566	0.475963	0.188086
C.0.S	1.494	4.646	2.59	0.354566	0.532188	0.275197
C.1.D	0.1387	0.1472	0.1205	0.354566	0.362205	0.011834
C.1.E	0.9779	2.57	2.033	0.354566	0.460499	0.164126
C.1.S	0.7455	2.185	1.673	0.354566	0.474639	0.186034
C.2.E	0.08498	0.6517	0.2769	0.354566	0.642968	0.446835
C.2.S	0.4152	1.477	0.5779	0.354566	0.597951	0.377088

Sample	A ₁₀₀	A ₀₀₂	A ₁₀₁	A _s	P ₀₀₂	f ₀₀₂
C.2.D	0.03942	1.03	0.1865	0.354566	0.820116	0.721297
D.0.A	0.1213	0.264	0.2268	0.354566	0.431302	0.11889
D.0.C	0.2533	1.255	0.3794	0.354566	0.66483	0.480706
D.0.D	0.5101	1.867	1.27	0.354566	0.511914	0.243785
D.0.E	0.4071	3.21	0.9191	0.354566	0.707641	0.547034
D.0.G	0.6265	18.29	1.236	0.354566	0.90758	0.856809
D.0.H	0.2241	1.703	0.3169	0.354566	0.758913	0.626472
D.0.N	-0.08536	29.23	-0.09177	0.354566	1.006097	1.009446
D.1.A	0.2203	0.1868	0.1775	0.354566	0.319535	-0.05428
D.1.C	0.3714	1.069	0.6131	0.354566	0.520575	0.257204
D.1.D	0.5434	2.197	1.2	0.354566	0.557558	0.314504
D.1.E	0.3722	5.158	0.7485	0.354566	0.821508	0.723454
D.1.G	0.3802	8.165	0.9464	0.354566	0.860234	0.783455
D.1.H	0.1514	1.726	0.1526	0.354566	0.850246	0.76798
D.1.N	0.04504	31.7	-0.02049	0.354566	0.999226	0.998801
D.D.A	0.1659	3.386	0.4934	0.354566	0.837021	0.747489
D.D.C	0.5	2.317	0.8529	0.354566	0.631352	0.428837
D.D.D	0.5102	1.882	0.8907	0.354566	0.573274	0.338853
D.D.E	0.2124	2.8	0.6281	0.354566	0.769125	0.642295
D.D.G	0.4966	1.675	1.034	0.354566	0.522523	0.260223
D.D.H	0.1256	8.816	0.175	0.354566	0.967027	0.948914
D.D.N	0.01321	39.31	0.08638	0.354566	0.997473	0.996085
D.U.A	0.1885	4.018	0.4454	0.354566	0.863733	0.788875
D.U.C	0.6452	1.26	1.244	0.354566	0.400102	0.07055
D.U.D	0.52	1.23	1.223	0.354566	0.413724	0.091655
D.U.E	0.4273	4.348	0.9849	0.354566	0.754835	0.620154
D.U.G	0.7592	1.824	1.361	0.354566	0.462451	0.167151
D.U.H	-0.07685	31.68	-0.00316	0.354566	1.002532	1.003923
D.U.N	-0.05697	32.22	0.04455	0.354566	1.000386	1.000597
ED0	0.4964	9.013	0.7663	0.354566	0.877118	0.809613
EE0	0.213	2.278	0.3632	0.354566	0.798122	0.687221
EG0	0.1763	1.963	0.2171	0.354566	0.83305	0.741337
EO0	0.1719	37.14	0.3395	0.354566	0.986418	0.978956
EP0	0.1337	36.72	0.1597	0.354566	0.992073	0.987719
ED1	0.4227	5.348	0.474	0.354566	0.856406	0.777524
EE1	0.25	3.899	0.474	0.354566	0.843392	0.75736
EG1	0.4249	6.725	0.941	0.354566	0.831181	0.73844
EO1	0.3175	21.93	0.6883	0.354566	0.956147	0.932057
EP1	0.2057	34.25	0.3108	0.354566	0.985144	0.976983
ED2	1.448	2.995	2.527	0.354566	0.429699	0.116406
EE2	0.506	8.572	0.9744	0.354566	0.852732	0.77183

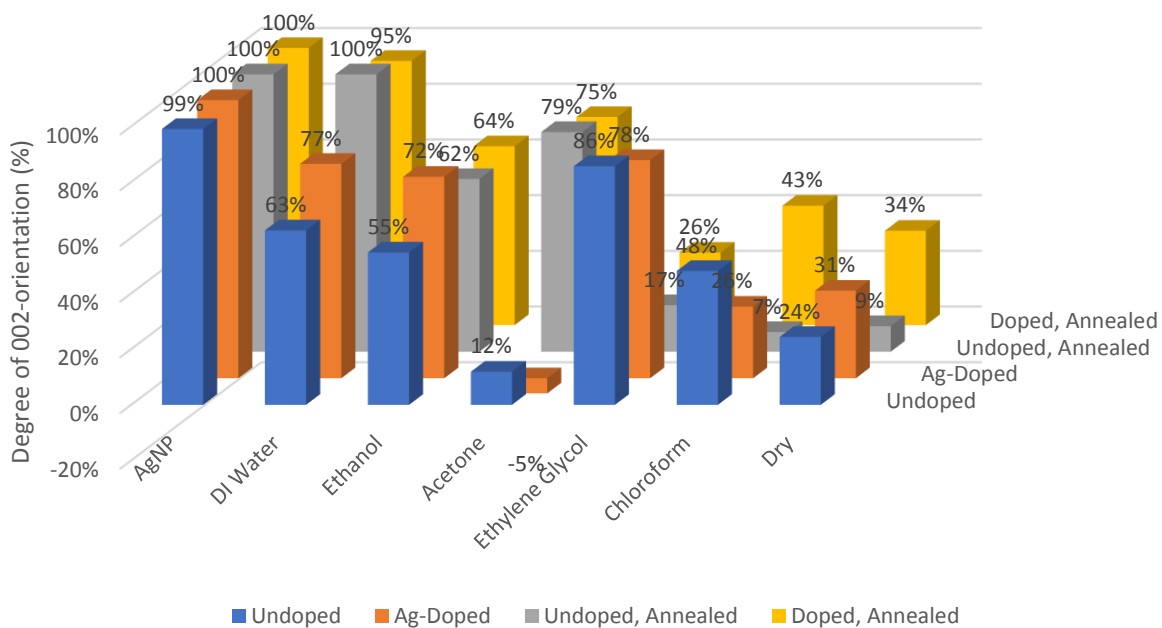
Sample	A_{100}	A_{002}	A_{101}	A_s	P_{002}	f_{002}
EG2	0.6748	5.932	1.53	0.354566	0.729034	0.580179
EO2	0.1713	18.95	0.3292	0.354566	0.974268	0.960132
EP2	0.0597	24.55	0.1997	0.354566	0.989544	0.9838
ED3	0.9286	8.349	2.176	0.354566	0.728941	0.580036
EE3	0.2765	7.392	0.4636	0.354566	0.90899	0.858994
EG3	0.1685	6.321	0.1147	0.354566	0.957118	0.933561
EO3	0.2364	18.04	0.3076	0.354566	0.970728	0.954647
EP3	0.09017	22.66	0.1694	0.354566	0.988675	0.982453

Graphs:

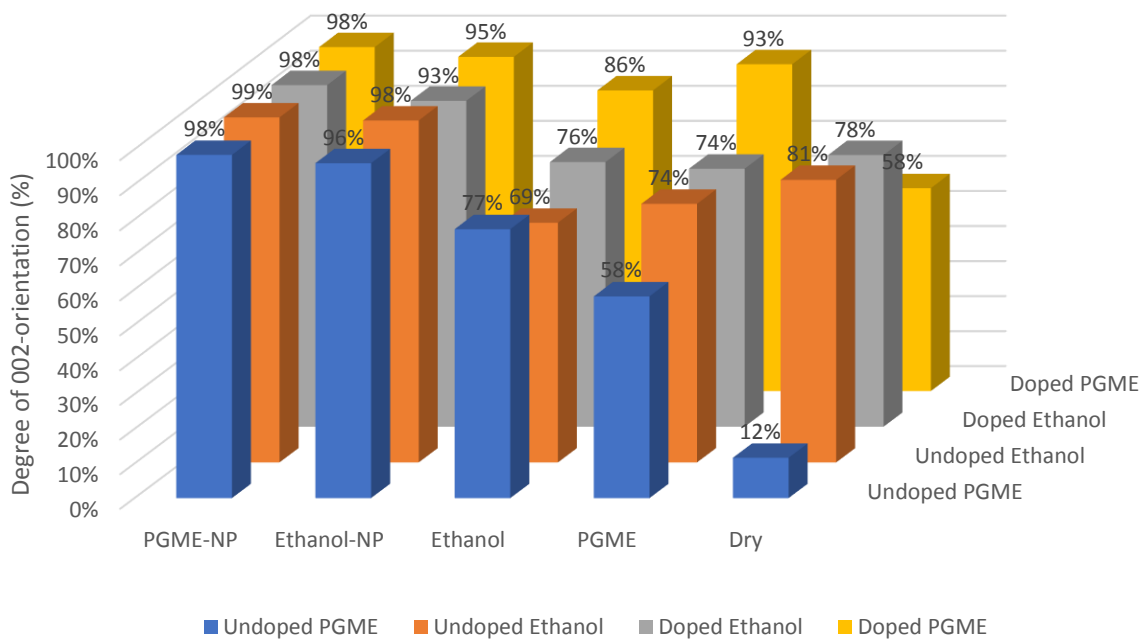




Degree of 002-orientation,
Experiment D

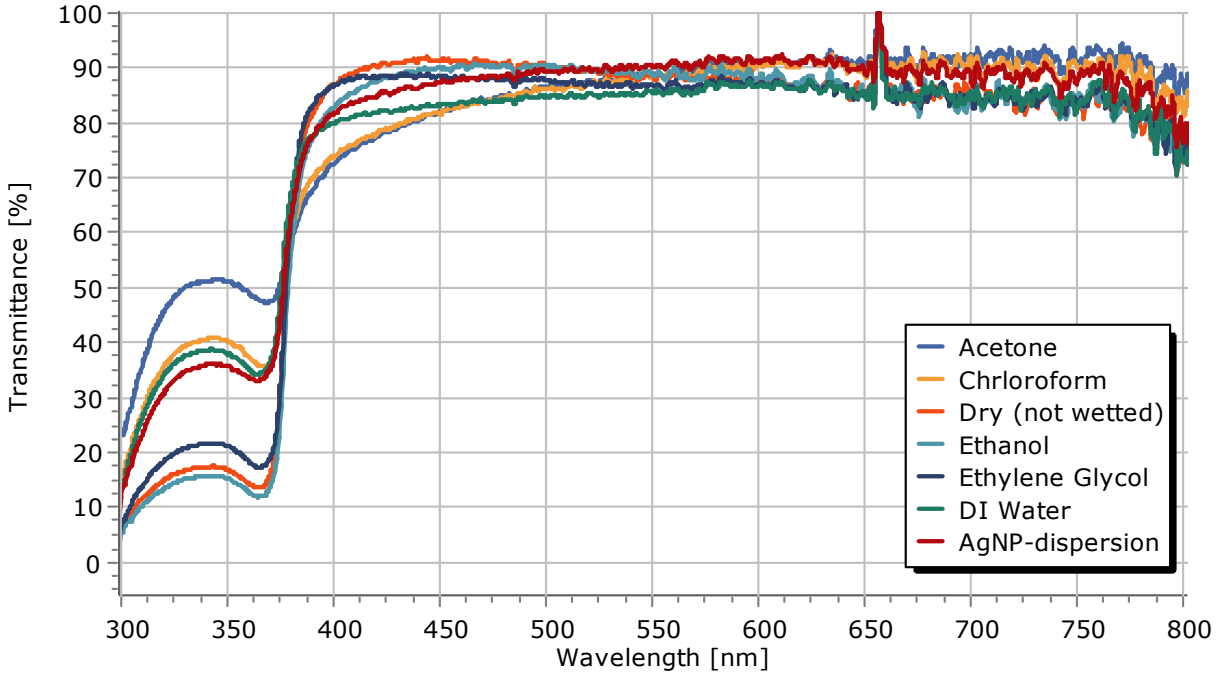


Degree of 002-orientation,
Experiment E

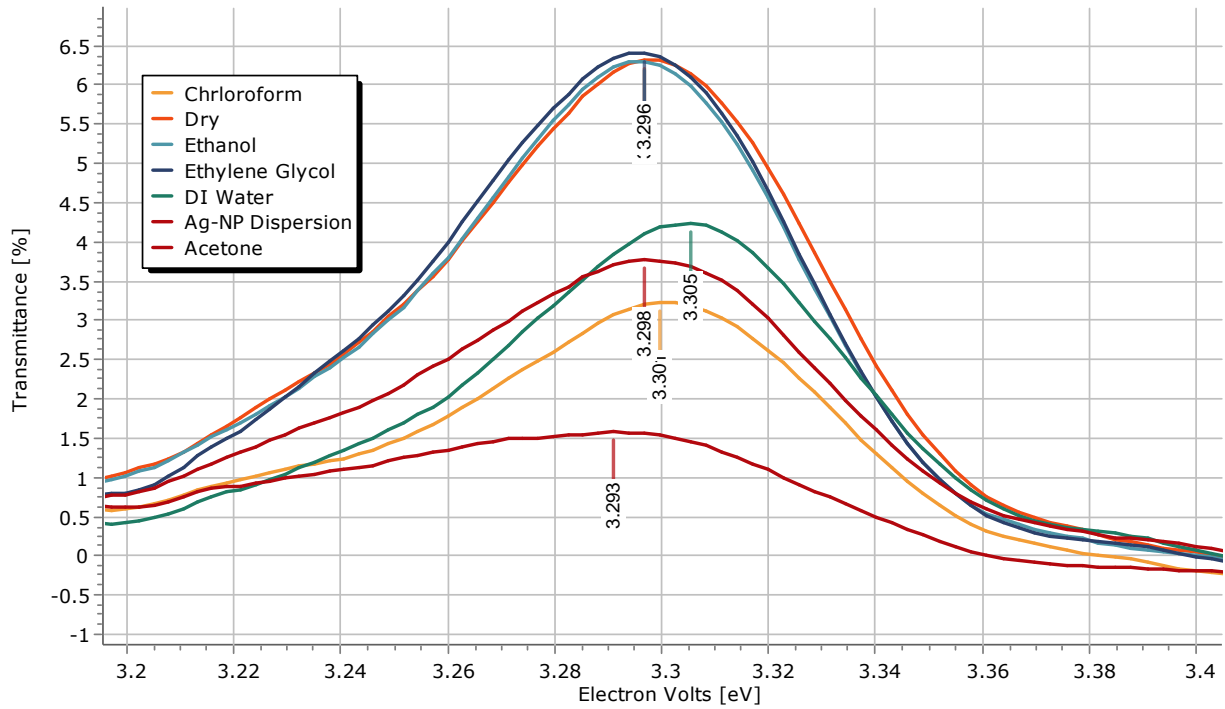


Appendix E: UV-Visual Spectroscopy

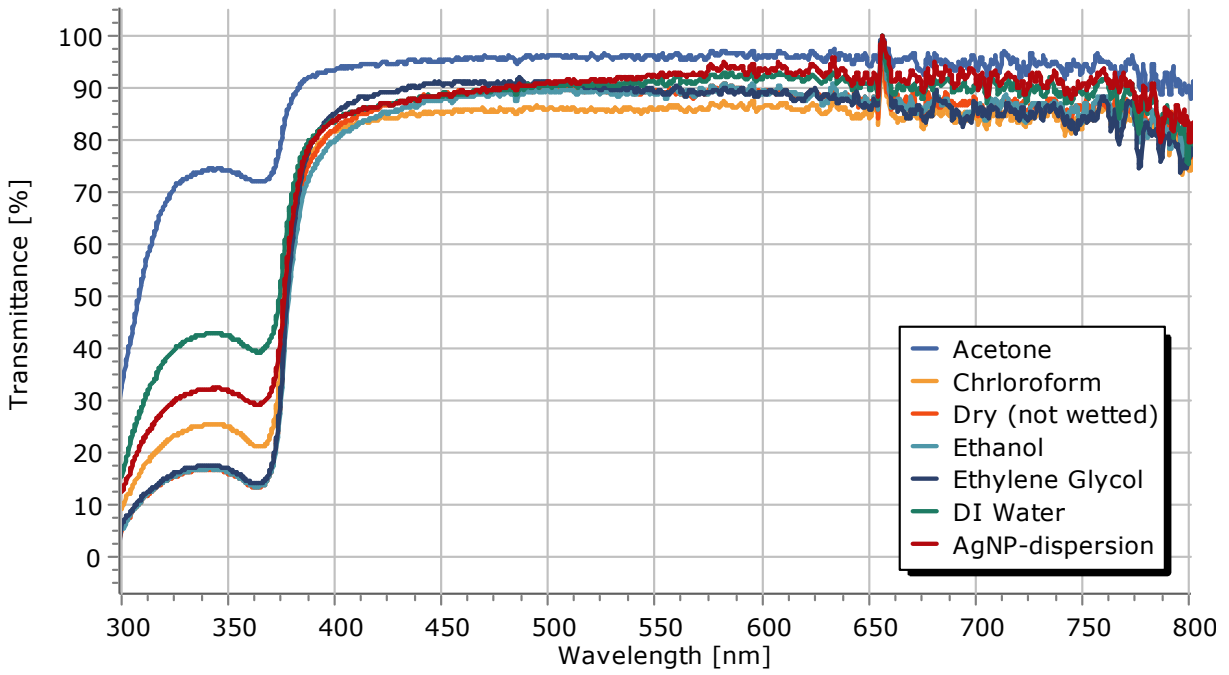
Experiment D: Undoped Spectra



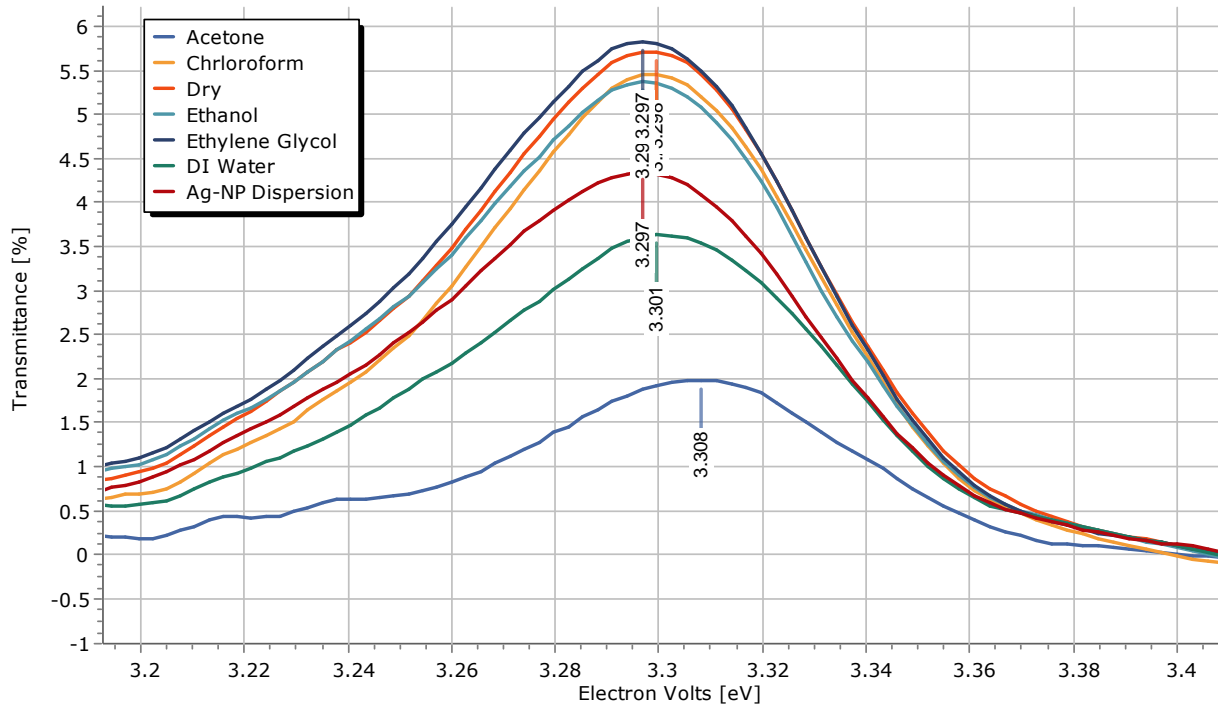
Experiment D: Undoped dT/dE:



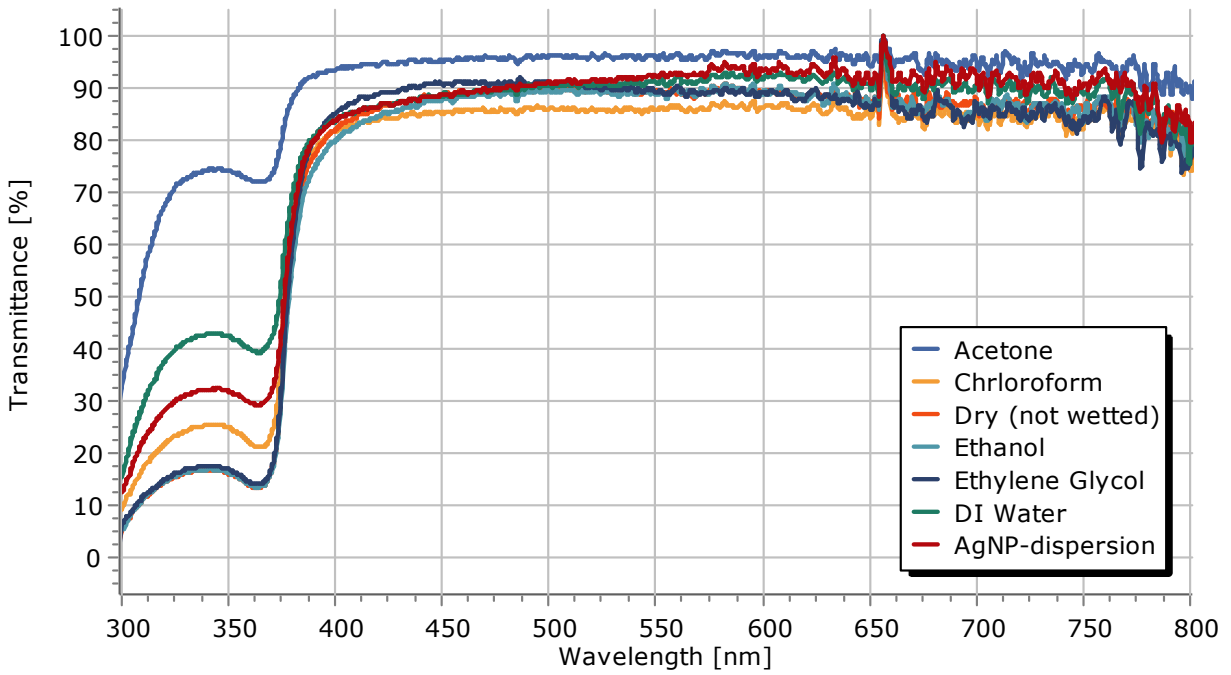
Experiment D: Ag-Doped



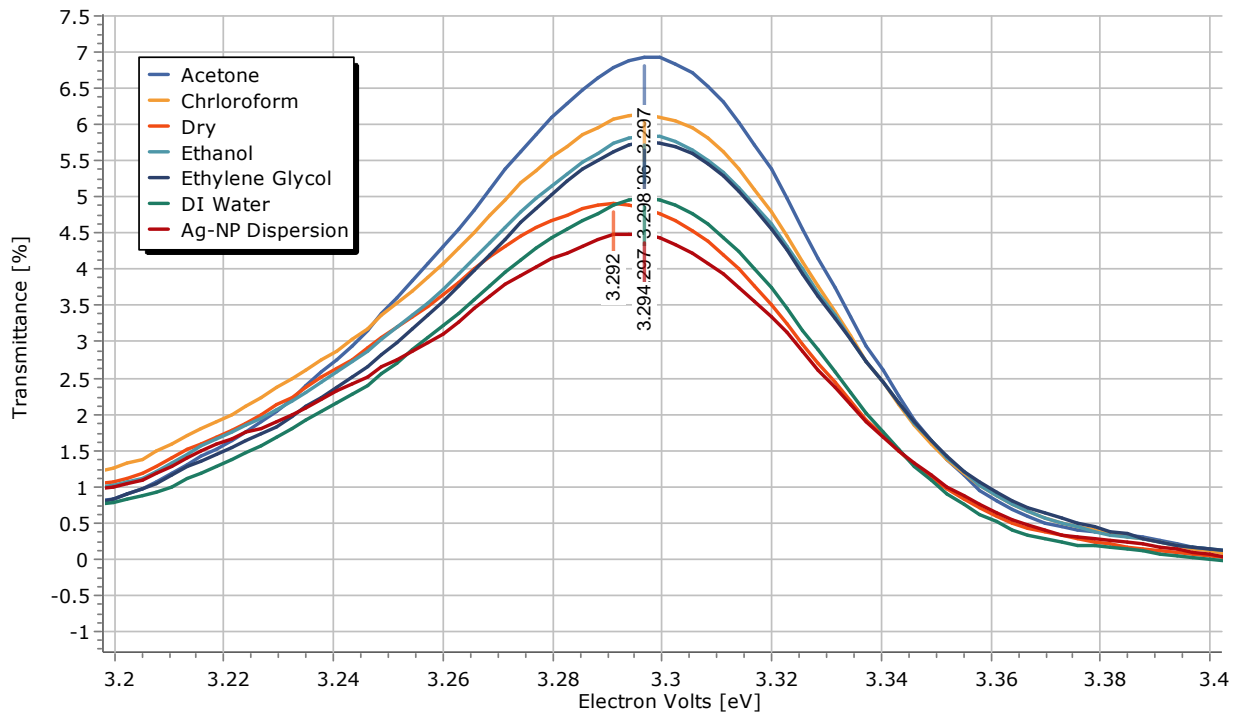
Experiment D: Ag-Doped dT/dE:



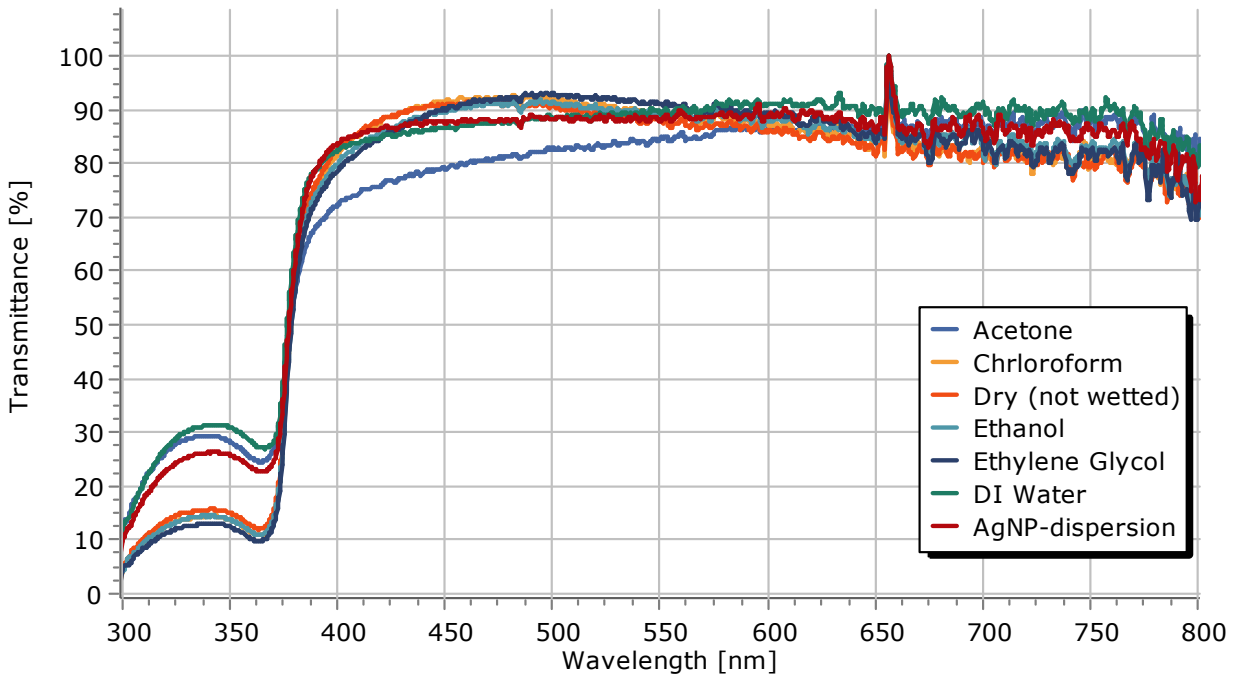
Experiment D: Doped, Annealed:



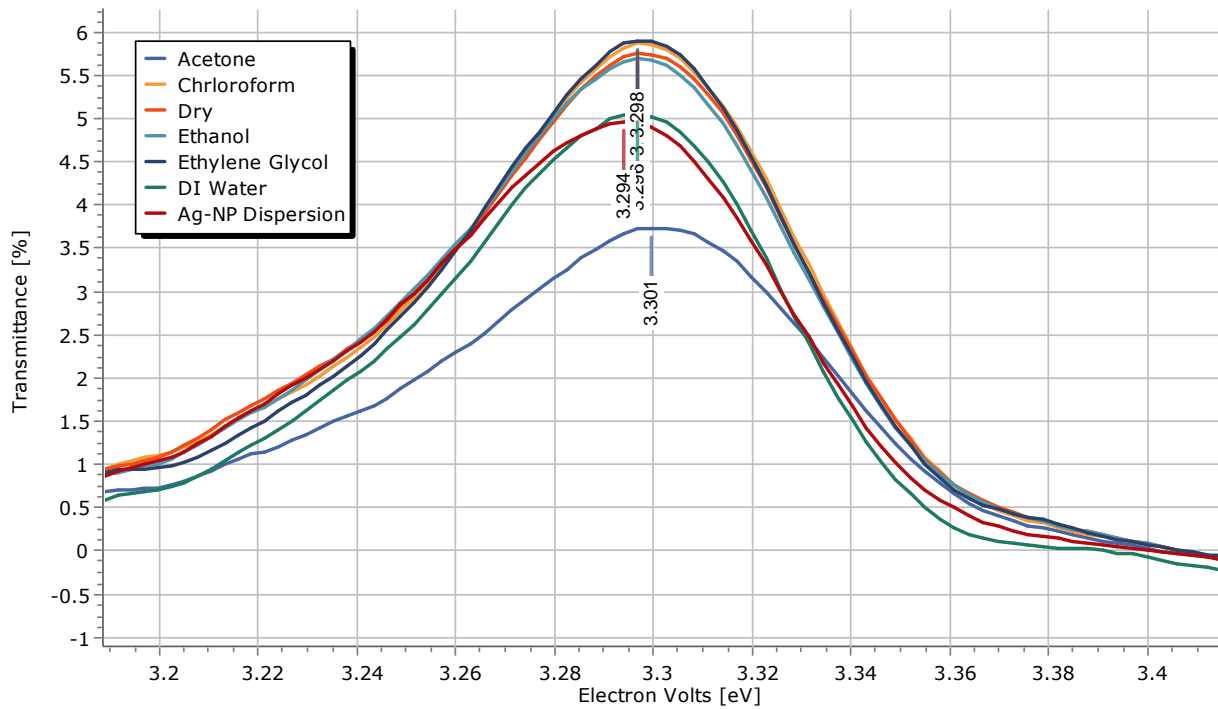
Experiment D: Doped, Annealed dT/dE:



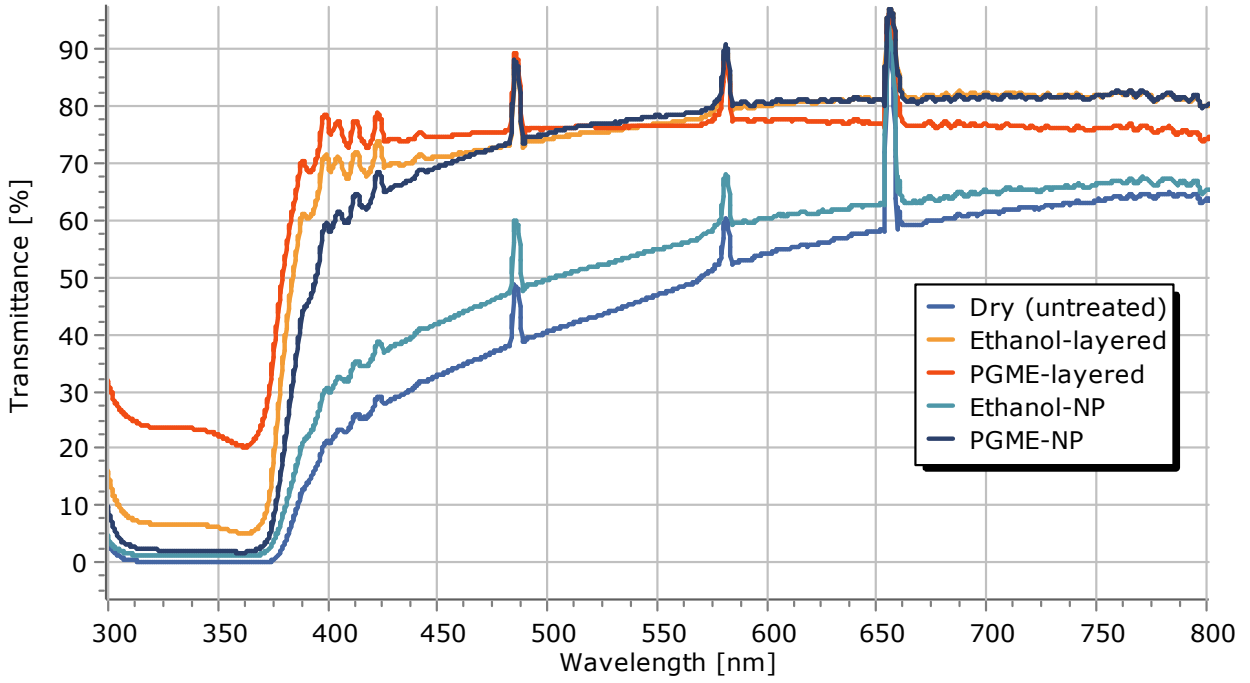
Experiment D: Undoped, Annealed



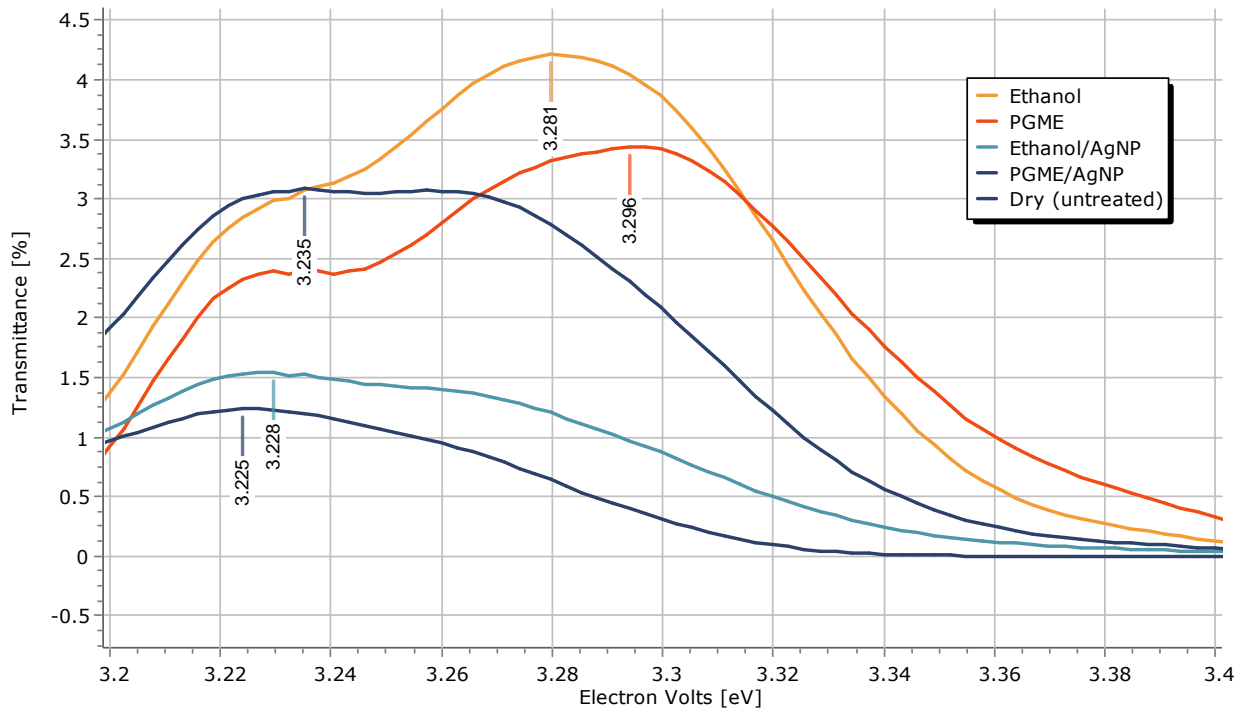
Experiment D: Undoped, Annealed dT/dE:



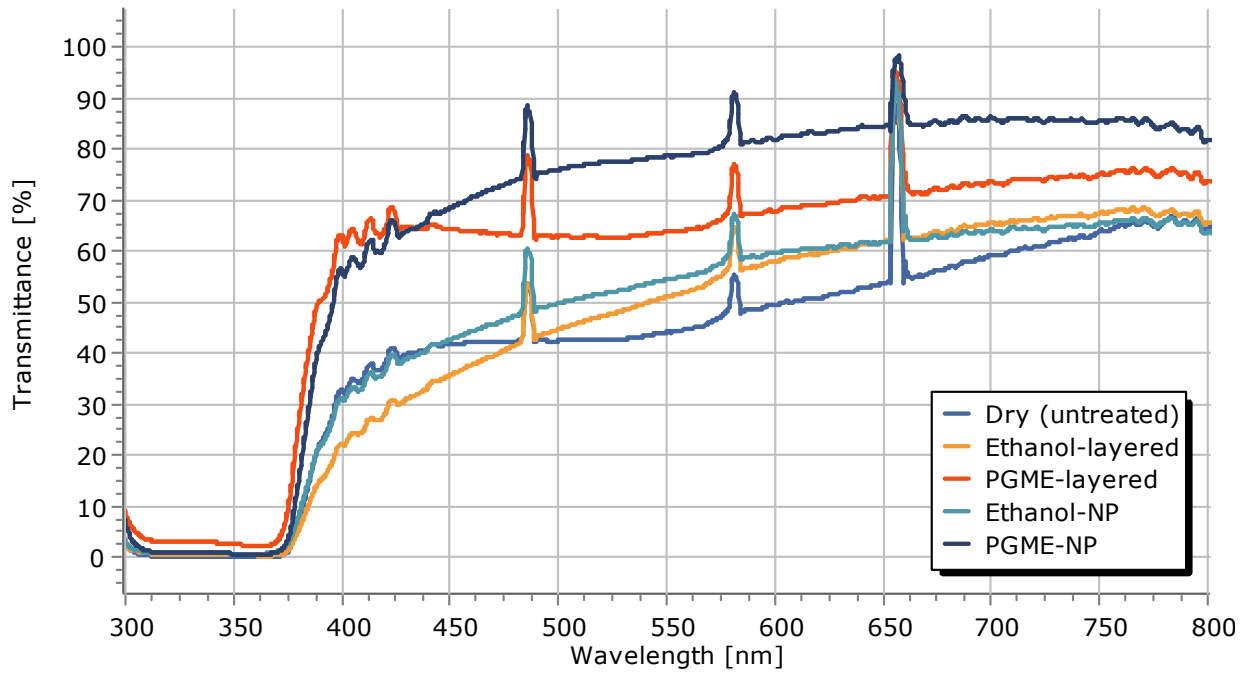
Experiment E: Undoped, Ethanol-based



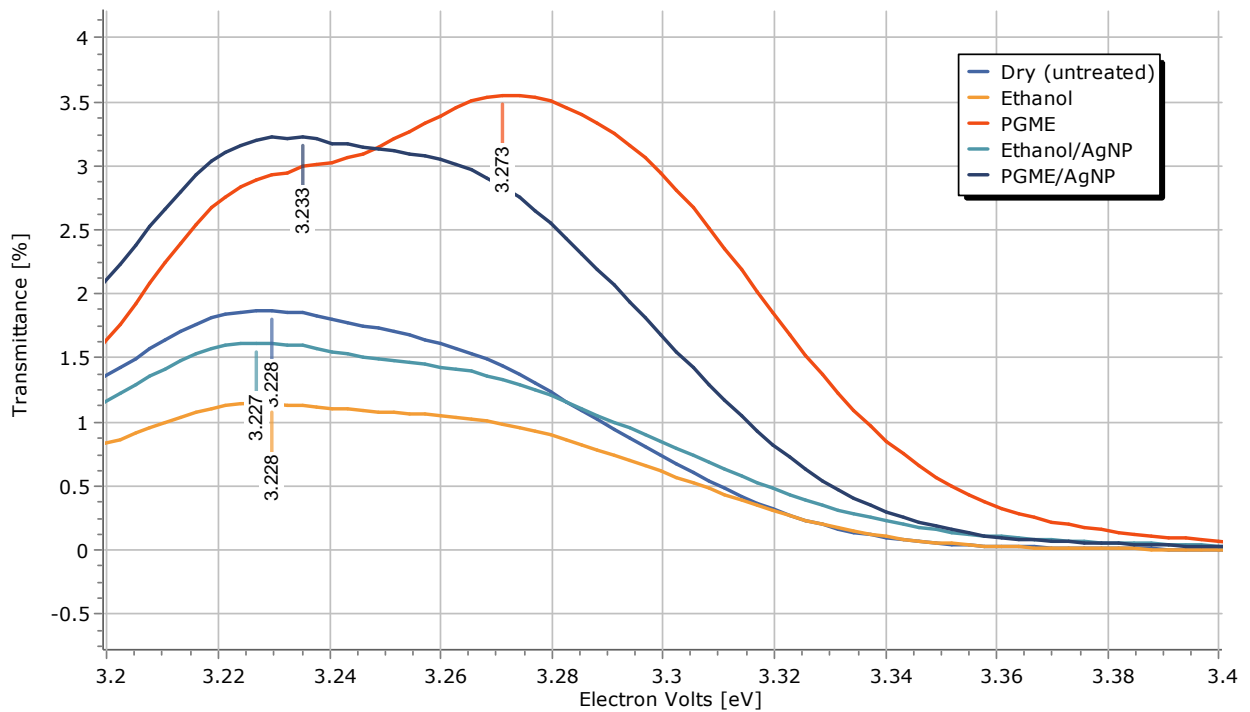
Experiment E: Undoped, Ethanol-based dT/dE:



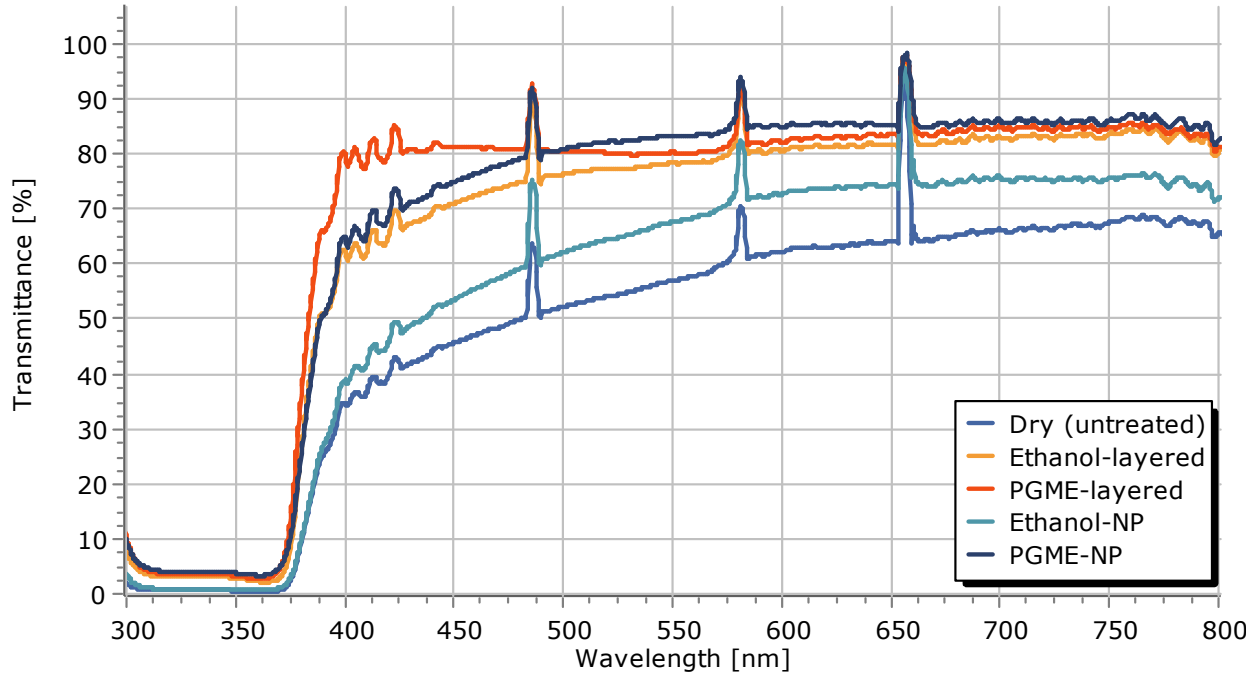
Experiment E: Doped, Ethanol-based



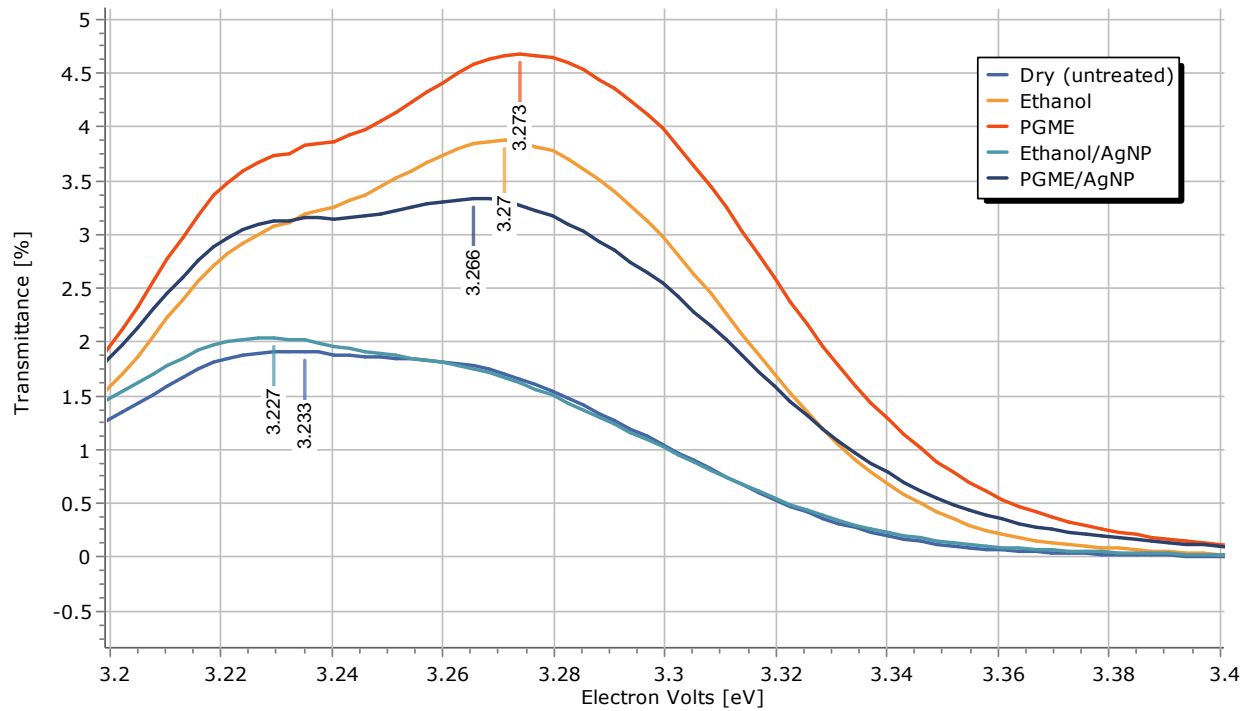
Experiment E: Doped, Ethanol-based dT/dE:



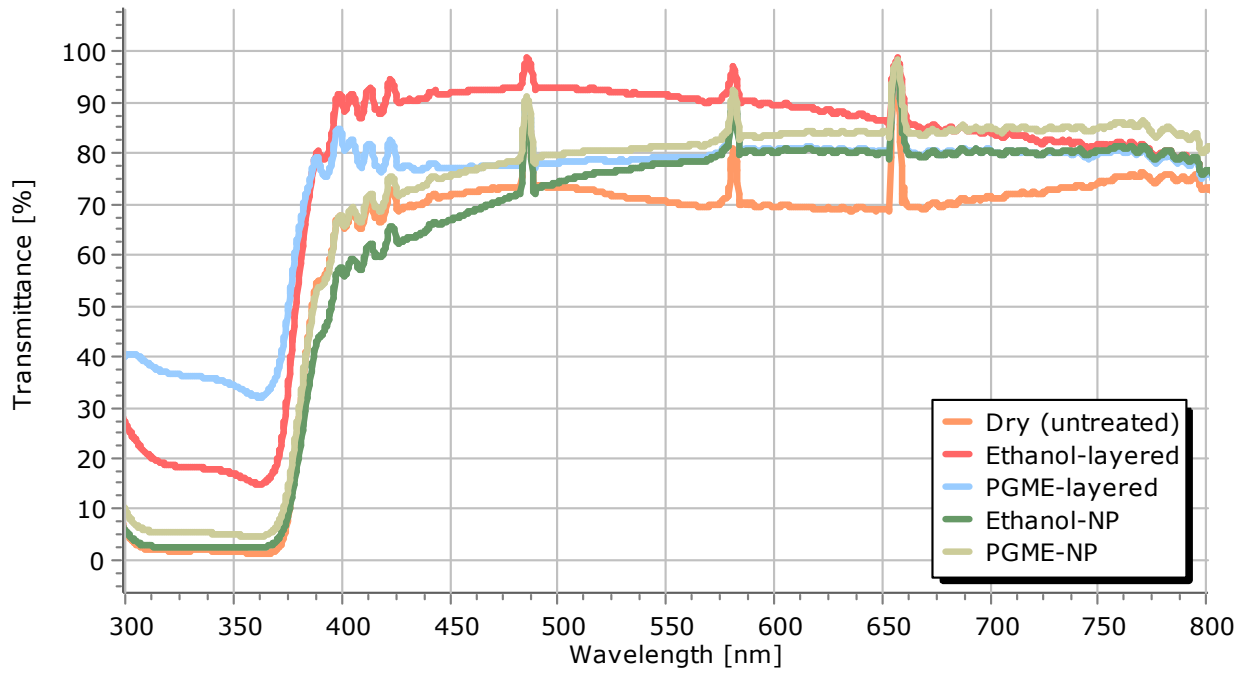
Experiment E: Undoped, PGME based:



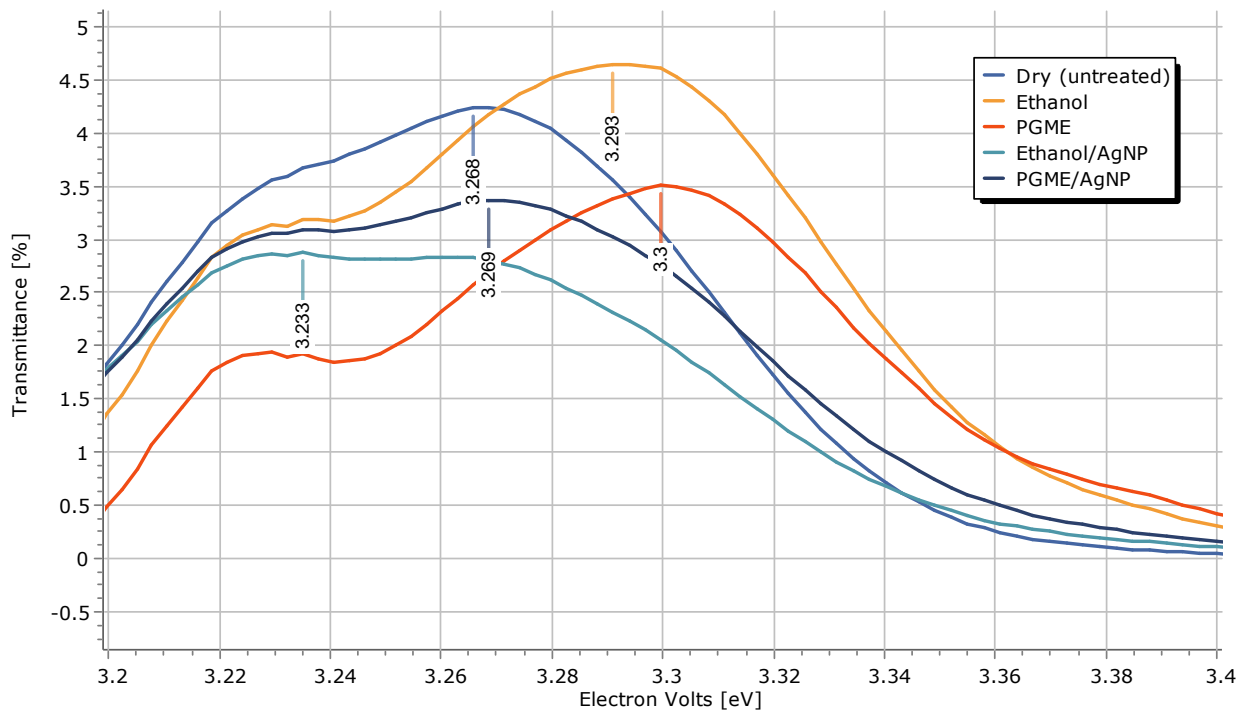
Experiment E: Undoped, PGME based dT/dE:



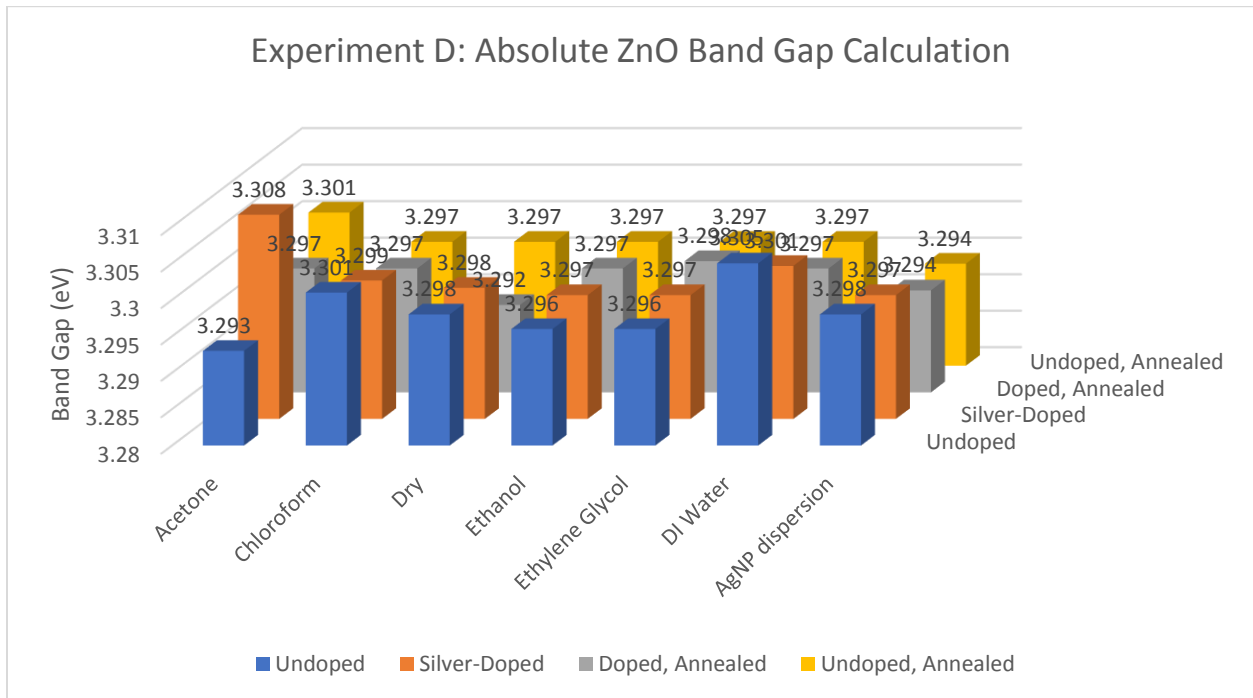
Experiment E: Doped, PGME-based



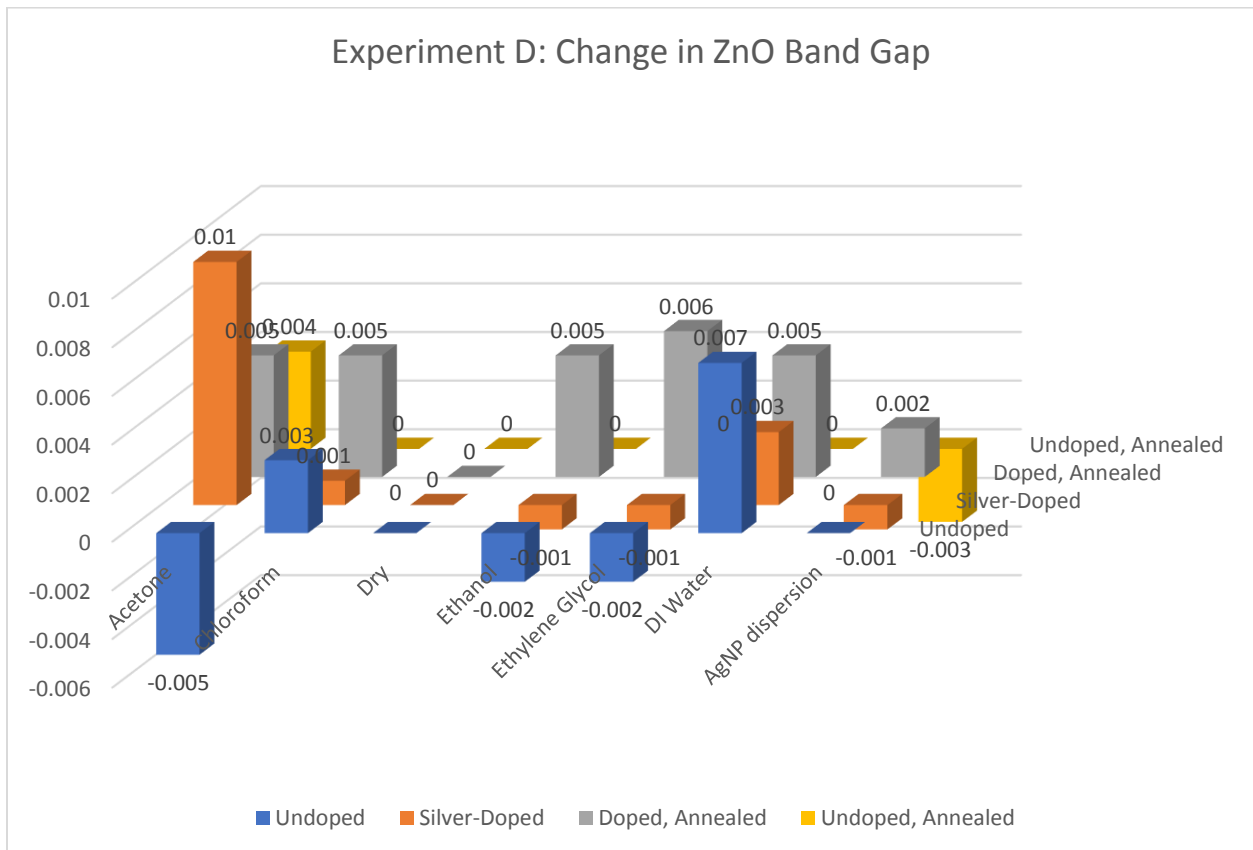
Experiment E: Doped, PGME-based dT/dE:



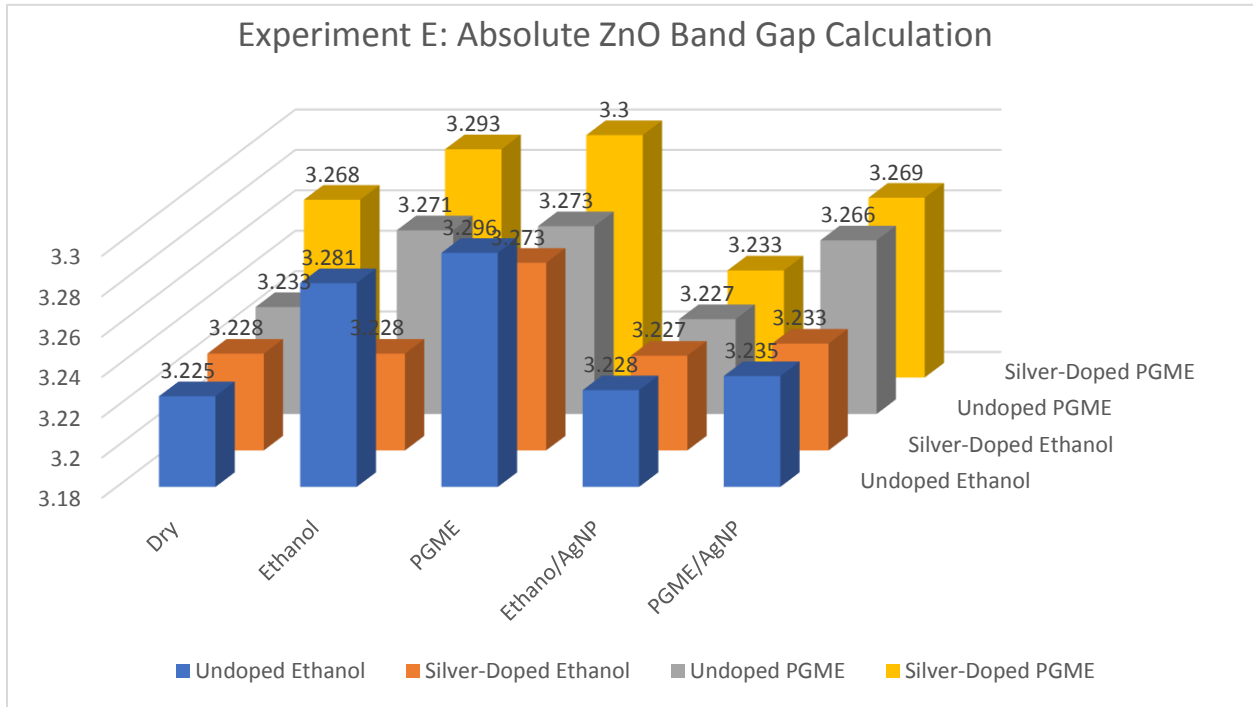
Experiment D: Calculated Band Gap by Solution and Treatment:



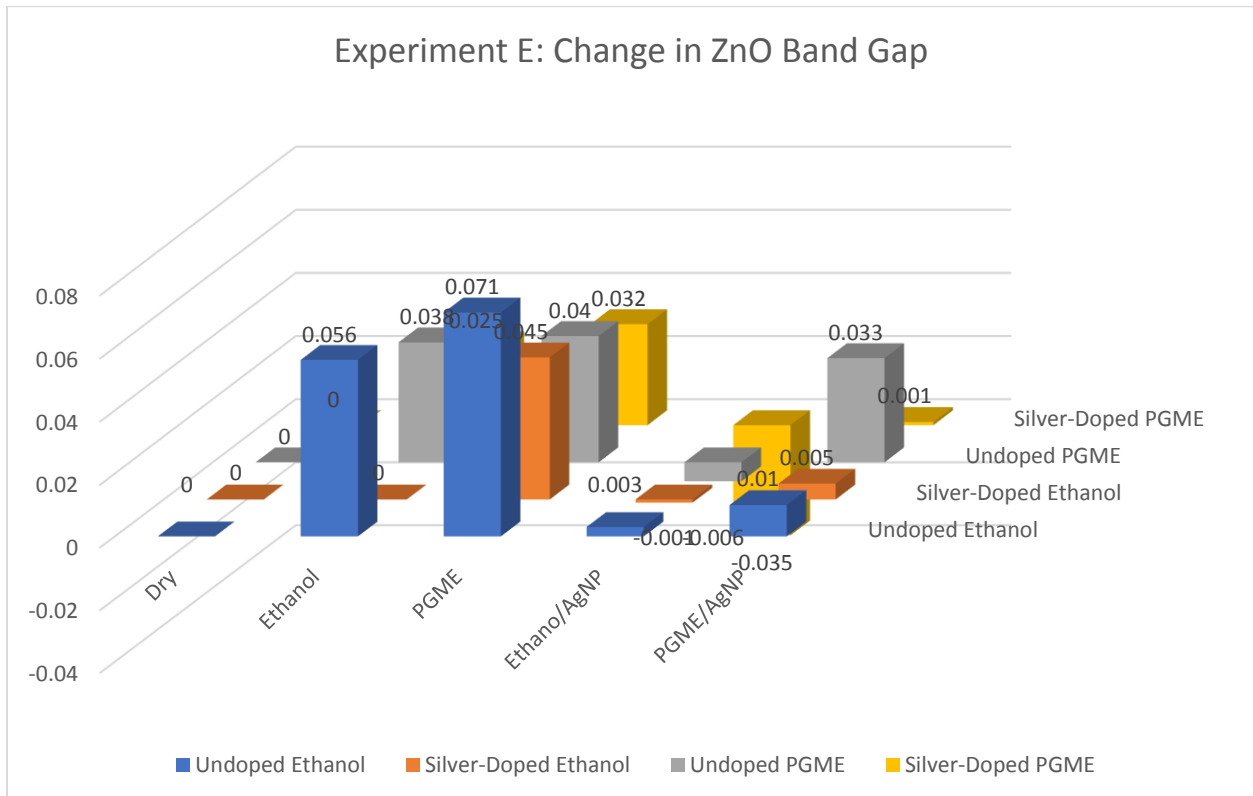
Experiment D: Change in Band Gap (compared to Untreated) by solution:



Experiment E: Calculated Band Gap by Solution and Treatment:



Experiment E: Change in Band Gap (compared to Untreated) by solution:



Appendix F: Chemicals Utilized

A variety of chemical compounds are utilized in the sol-gel synthesis process, including metallic precursor salts and various organic solvents. Shorthand abbreviations are used extensively throughout this work, and it is instructive that the reader be aware of the chemical structure and properties of these compounds. This table provides a key to the abbreviations used, their common names, organic “stick” structure, official IUPAC nomenclature and chemical formula, and a brief list of chemical properties of interest to this study.

Common Name	Abbreviation Used Herein	Structure	IUPAC Name, formula	Relevant Properties/Description
Ethanol	EtOH		Ethanol CH ₃ CH ₂ OH	Primary alcohol
Zinc Acetate Dihydrate	ZnAc		Zinc Acetate Dihydrate Zn(CH ₃ CO ₂) ₂ ·2H ₂ O	Organometallic salt
Silver Nitrate	AgNO ₃		Silver(I) nitrate	Soluble silver salt
DI Water	H ₂ O		Water H ₂ O	Deionized water suitable for solutions chemistry
Dimethyl Sulfoxide	DMSO		Dimethyl sulfoxide (CH ₃) ₂ SO	Polar, aprotic, highly miscible solvent
Chloroform	CHCl ₃		Trichloromethane CHCl ₃	Slightly polar, aprotic solvent
Propylene glycol methyl ether	PGME		1-Methoxypropan-2-ol C ₄ H ₁₀ O ₂	Polar, protic ether, secondary alcohol
Ethylene glycol methyl ether	EGME (also, 2-ME)		2-Methoxyethanol C ₃ H ₈ O ₂	Polar, protic Ether, Primary alcohol,
Ethanolamine, Monoethanolamine	EA, MEA		2-Aminoethan-1-ol C ₂ H ₇ NO	Primary amine, primary alcohol, weak base
Diethanolamine	DEA		2,2'-Iminodiethanol C ₄ H ₁₁ NO ₂	diol, secondary amine, weak base